
Synthesis and Crystallization Studies of Azobenzene Defect Polymers and Supramolecular Block Copolymers

Dissertation

zur Erlangung des
Doktorgrades der Naturwissenschaften (Dr. rer. nat.)

der

Naturwissenschaftlichen Fakultät II
Chemie, Physik und Mathematik

der Martin-Luther-Universität
Halle-Wittenberg

vorgelegt

von Herr Clement Appiah
geb. am 28.11.1985 in Berekum (Ghana)

Tag der öffentlichen Verteidigung: 20.März 2018

Gutachter: Prof. Dr. Wolfgang H. Binder

Prof. Dr. Michael Sommer

ACKNOWLEDGEMENT

Apart from personal efforts and steadfastness to work, constant inspiration and encouragement given by a number of individuals served as a driving force for the success of this thesis. Inspiration, guidance, direction, co-operation, all came in abundance and it seems almost an impossible task for me to acknowledge the same in adequate terms.

First of all, I take this opportunity to express my deep sense of gratitude and sincere thanks to my guide, lecturer and supervisor Prof. Dr. Wolfgang Binder, for his unflinching assistance, invaluable guidance and persistent encouragement. No words can express my sincere and deep sense of reverence to him. I am extremely indebted to him for the scientific attitude he has installed in me which will definitely stand in all my future endeavours.

I owe heartfelt thanks to Prof. Dr. Jörg Kreßler, my PhD mentor for the constant support and guidance throughout my PhD studies. I am extremely thankful to him for his suggestions and advices.

I will not fail to acknowledge the laudable contributions and guidance of Prof. Dr. Georg Woltersdorf for allowing me conduct all my UV-VIS measurements in his group and Prof. Dr. T. Thurn-Albrecht for allowing me conducts SAXS and WAXS measurements in his group. I am much grateful. Thank you.

Words are insufficient to express my gratefulness and indebtedness to the group members of AG Binder working group for their constant & unflinching cooperation. Their constant support has been instrumental in the smooth completion of this work.

All my family members in the persons of Vanessa Telong, Aldrich Telong Appiah, Mr. Joseph Ohene-Febiri, Gladys Nketia and Vida Gyinaa contributed significantly to bring yet another day like this in my life. They remain a constant source of strength throughout my educational career. I thank them for providing me the moral support and resources to finish this work.

Finally, I am thankful to the Almighty God for his blessings and guidance towards me in the success of this work.

To my family

TABLE OF CONTENT

ACKNOWLEDGEMENT.....	i
ABSTRACT.....	v
ABBREVIATIONS	vi
OUTLINE OF THE THESIS	1
1.0 INTRODUCTION	2
1.1 Crystallization in polymers	2
1.2 Crystallization in block copolymers.....	2
1.3 Crystallization of recurring defects in copolymers	6
1.3.1 Flory's exclusion theory of copolymer crystallization	7
1.3.2 Sanchez and Eby's inclusion/exclusion model	8
1.4 Exclusion crystallization in defect polymers	9
1.5 Inclusion crystallization in defect polymers	12
1.6 Synthesis and switching dynamics of photochromic polymers	15
1.6.1 Photo-responsive azobenzene chromophore	16
1.6.2 Synthetic methodologies for the design of azobenzene photochromes.....	18
1.6.3 Incorporation of azobenzene photochromes into polymers	19
1.7 Photo-physical relaxation dynamics of azobenzene monomers and polymers.	20
1.7.1 Photo-physical relaxation dynamic of azobenzene monomers	20
1.7.2 Photo-physical relaxation dynamic of azobenzene polymers.....	23
1.8 Stabilization of Cis-trans back relaxation of azobenzenes in the dark.....	24
2.0 SCOPE OF THESIS.....	27
2.1 Aim of the work.....	27

2.2 Concept.....	28
3.0 RESULTS AND DISCUSSION.....	31
3.1 Synthesis and characterization of new photoswitchable azobenzene-containing poly(ϵ -caprolactones).....	31
3.2 Synthesis of photoresponsive main-chain oligomers with azobenzene moieties via ADMET oligomerization and their micellization properties.....	46
3.3 Crystallization behavior of ADMET polyethylene containing azobenzene defects.....	64
3.4 Crystallization in segregated supramolecular pseudoblock copolymers.....	80
4.0 SUMMARY.....	94
5.0 REFERENCES.....	99
6.0 SUPPLEMENTARY INFORMATION.....	116
6.1 Synthesis and characterization of new photoswitchable azobenzene-containing poly(ϵ -caprolactones).....	116
6.2 Synthesis of photoresponsive main-chain oligomers with azobenzene moieties via ADMET oligomerization and their micellization properties.....	120
6.3 Crystallization behavior of ADMET polyethylene containing azobenzene defects.....	132
6.4 Crystallization in segregated supramolecular pseudoblock copolymers.....	135
7.0 CURRICULUM VITAE.....	142

ABSTRACT

Crystallization process in polymers is a more complex phenomenon that is associated with molecular reorganization at different time and length scales. The process is affected by several factors such as molecular weight, chain flexibility, chain defects, stereo-regularity and experimental conditions like temperature, pressure, nucleating agents, and stress. This in return affects the crystal growth and subsequently affects the morphology and thus, like the physical properties of the semi-crystalline polymer. The crystallization process becomes even more complicated when dealing with copolymers and block copolymers, as here the polymer melt is influenced by sequences of varying length, such as a second amorphous block introduced onto the crystallizable chain, branches or even defects. In this thesis the crystallization of polymers with precise defects, located within the melt crystal are addressed. Thus azobenzene polymers with an azo-group as defect were synthesized. Furthermore, supramolecular block copolymer comprised of a crystallizable poly(ϵ -caprolactone) (PCL)-block and an amorphous poly(styrene) (PS)-block were synthesized to study their crystallization from the melt or study their self-assembly in solution.

For the crystallization studies of the supramolecular block copolymers, different polymers were prepared via a combination of ring opening polymerization (synthesis of PCL) and atom transfer radical polymerization (synthesis of PS). The two homopolymers were connected to each other via triple hydrogen bond between thymine functionalized PCL and 2,4-diaminotriazine functionalized to the second PS-block. The purity of the synthesized samples was proven via NMR, MALDI TOF MS, IR, and GPC. The investigations of the crystallization studies via DSC and SAXS showed a strong decrease of the crystallization temperature and the rate of crystallization. Additionally, fractionated crystallization was observed in some of the PCL-PS block copolymers indicating a strong constraining effect.

Furthermore, the azobenzene functionalized polymers were obtained via the synthesis of PCL and subsequent modification via alkyne/azide click-reaction with azobenzene moieties. The synthesis via acyclic diene metathesis polymerization (ADMET) was also performed to obtain azobenzene-copolymers with precise azo defects, located within a polyethylene-like alkyl chain. The purity of the synthesized samples was proven via NMR, 2D-COSY NMR, MALDI-ToF MS, ESI-ToF MS, GPC, an online coupling of HPLC and GPC (2D-HPLC/GPC). Crystallization studies via DSC and WAXS for the ADMET azobenzene-copolymers showed that the azobenzene defects had a remarkable influence on the polymer melt morphology. Azobenzene units were included in the crystal phase, leading to a high melting point. Additionally, switching dynamics of the azobenzene-copolymers were investigated in solution. Trans to cis switching stability of the polymers were also investigated, proving that, fluorinated atoms on the azobenzene chromophore increased the lifetime of the switched cis structures with an estimated time constant of 164 min ($k = 1/\tau = 1.02 \times 10^{-4} \text{ s}^{-1}$).

ABBREVIATIONS

ATMS	Allyltrimethylsilane
Azo	Azobenzene
bipy	Bipyridine
calcd.	Calculated
CuAAC	Copper(I)-catalyzed alkyne–azide “click” cycloaddition
DCM	Dichloromethane
DIPEA	<i>N,N</i> -Diisopropylethylamine
DMA	<i>N,N</i> -Dimethylacetamide
DMF	<i>N,N</i> -Dimethylformamide
DMSO	Dimethyl sulfoxide
DSC	Differential scanning calorimetry
EA	Ethyl acetate
ESI	Electrospray ionization
FTIR spectroscopy	Fourier transform infrared spectroscopy
GPC	Gel permeation chromatography
IR	Infrared
MALDI	Matrix assisted laser desorption and ionization
MeOH	Methanol
MS	Mass spectrometry
NMR	Nuclear magnetic resonance
PCL	Poly(ϵ -caprolactone)
PDI	Polydispersity index
PS	Poly(styrene)
ROMP	Ring-opening metathesis polymerization
RT	Room temperature
SAXS	Small-angle X-ray scattering

SEM	Scanning electron microscopy
SN	Self nucleation
SSA	Successive self nucleation and annealing
TBTA	Tris[(1-benzyl-1 <i>H</i> -1,2,3-triazol-4-yl)methyl]amine
T_g	Glass transition temperature
TGA	Thermogravimetric analysis
THF	Tetrahydrofuran
TLC	Thin-layer chromatography
TMS	Trimethylsilyl
TOF	Time of flight
UPy	Ureidopyrimidone
UV	Ultraviolet
VIS	Visible light

IR-spectroscopy

w	Weak
m	Middle
s	Strong

NMR-spectroscopy

d	Doublet
dt	Doublet of a triplet
dd	Doublet of a doublet
m	Multiplet
qu	Quintet
s	Singlet
t	Triplet

OUTLINE OF THE THESIS

The **first** section of the thesis consists of a general introduction of concepts of block copolymers, copolymer crystallization, and synthesis of azobenzene photochromic molecules in polymers. This part focuses on the role of defects, amorphous block units on the crystalline lamellar structures of polymers and in defining their thermal stability. Starting from the very early investigations on copolymer crystallization, we will focus on the advancement of the crystallization studies by explaining some proposed models in copolymer crystallization, examples of included and excluded defect polymer systems and block copolymer crystallization studies in different polymeric systems. Additionally, focuses on the synthesis, switching dynamics and stability studies of azobenzene polymers will be discussed. We will consider some synthetic strategies employed for the synthesis of azobenzene polymers, their switching dynamics in solution and how to stabilize the cis structures upon switch.

In the **second** section, the aim and the synthetic concept will be explained elaborately. This chapter will cover the results obtained from the different publications related to crystalline-amorphous block copolymers and azobenzene functionalized polymers.

In the **third** section, we will be describing the details of the published results. This will discuss in details the crystallisation of the crystalline-amorphous block copolymer and azobenzene polymers.

In the **fourth** section, the overall conclusions of the thesis will be summarized.

The fifth section will contain all the supplementary data to give some information especially on the synthesis of the various compounds.

1.0 INTRODUCTION

1.1 Crystallization in polymers

Crystallization process in polymers is a complex phenomenon associated with molecular reorganization at different time and length scales [1]. Two separate stages, the emergence of small crystalline domains called primary nuclei, and their subsequent growth defines the crystallization process. The primary nucleus is a nanometer-sized structure which shape may be treated by equilibrium thermodynamics, while the growing crystals have very thin platelet shapes which must be kinetically controlled [1]. During crystallization, the polymer chains adopt either an extended or, what is more common, a chain-folded conformation, which are influenced by several internal and external factors such as molecular weight, chain architecture (e.g. linear, star, block copolymers), functional groups, chain flexibility, chain defects, stereo-regularity and experimental conditions like temperature, pressure, nucleating agents, and stress [1]. These factors have been shown in several investigated semi-crystalline polymers. Notable among these factors is the crystallization studies of star-shaped poly(ϵ -caprolactone)s, where the rate constant for the star-shaped polymers was observed to be lower than their linear counterparts within the same molecular weight range [2]. The higher the number of arms in the star-shaped polymer, the slower was the crystallization process. The presence of functional groups as well as their positions within polymer chains was also shown [3-6] to influence the crystallization process. Slow overall crystallization process and low melting temperatures were observed [4, 5]. Moreover, some compelling factors such as the linkage of several chemically different homopolymers to form block copolymers (BCP) have been shown to influence the crystallization process of semi-crystalline polymers. In contrast to the pure homopolymers the second blocks within the BCPs form "barriers" which restrict or allow the crystal growth process. As a result of the chemical heterogeneity in mostly formed block copolymers, nucleation as a primary step of the crystallization begins the crystallization process [4-6]. Two types of nucleation are known to exist; homogeneous and heterogeneous nucleation [6]. Homogeneous nucleation is often observed in strongly restricted systems such as polymer droplets, microphase-separated block copolymers (BCP) or polymers infiltrated in nanotubes [6]. In heterogeneous nucleation, the chain segments are deposited on foreign surfaces, e.g., dust or other impurities. Heterogeneous nucleation can be promoted by the addition of a nucleating agent. The nucleating agents (often organic compounds) can accelerate the onset of the crystallization and increase the crystallization temperature [4, 5].

1.2 Crystallization in block copolymers

Block copolymers are polymers that consist of two or more different monomeric blocks that are covalently linked to each other. The simplest architecture is the linear AB diblock copolymer, in which a homopolymer chain of monomers of type A is linked to a homopolymer chain of monomers of type B [7-10]. When studying block copolymer crystallization, mainly two cases can be distinguished; the first when one of the two components can crystallize, and the other remains amorphous (crystalline-amorphous), and the second when both components can crystallize (crystalline-crystalline) [11, 12]. The second case can be further broken down into at least two categories; one for the case that the two components have comparable glass transition temperatures and the other when the two glass transition temperatures are

far apart. Different factors influence the final three-dimensional structure of the block copolymer; this includes:

- Order-disorder transition temperature (T_{ODT})
- Glass transition temperature of the amorphous part (T_g)
- Crystallization temperature of the crystalline/semi-crystalline part (T_c)

Furthermore, depending on the relative values of the above-mentioned temperatures, different crystallization cases can be observed for the block copolymer. The final structure of the copolymer is thus a function of this relative order of temperature values, and in consequence, leads to the three distinct cases upon crystallization (Figure 1):

Case I: $T_{ODT} < T_c > T_g$. Crystallization occurs directly through the melt components, and phase separation leads to lamellar structures. Hard or soft confinement can be observed, depending on the relative order of the temperatures.

Case II: $T_{ODT} > T_c > T_g$. Crystallization occurs within sub-phases [micro domain], but in this case, it can also intrude into the rubbery phase of the second component, leading to breakout crystallization.

Case III: $T_{ODT} > T_g > T_c$. Crystallization occurs within segregated sub-phases of the strongly restricted amorphous component leading to confined crystallization.

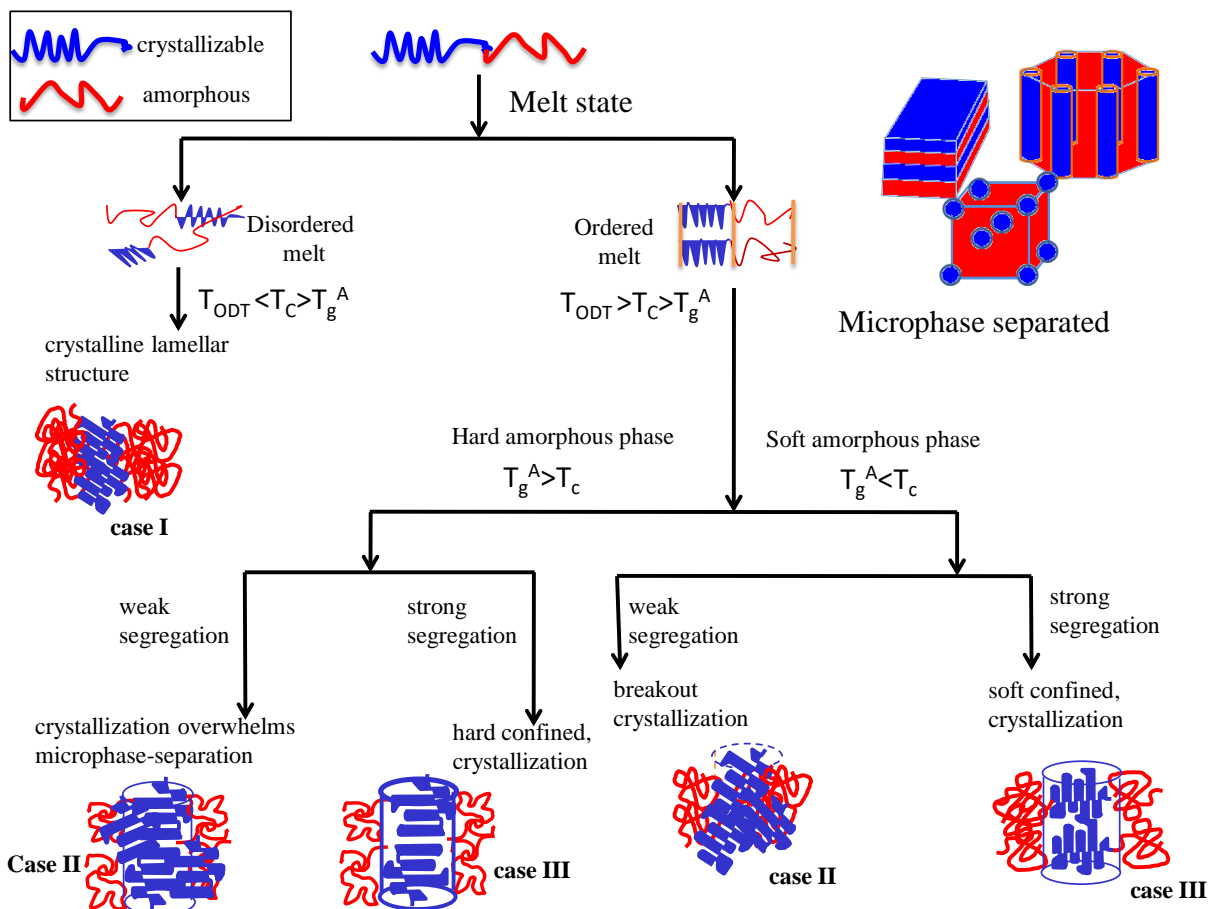


Figure 1. Block copolymer crystallization in different crystalline amorphous blocks.

In general, block copolymers having two or more immiscible segments exhibit different kinds of microphase morphologies depending on the relative volume fractions of the segments. In block copolymers, the morphology depends not only on the strength of the immiscibility (denoted by χN , where χ is the interaction parameter, and N is the total degree of polymerization) but also on whether the blocks are crystalline or amorphous [13]. When the χN parameter decreases (weak segregation limit, $\chi N < 10$), the crystals show “breakout-crystallization” (Figure 1, Case II) [14, 15] from the microphase-separated block copolymer. On the other hand, when the χN parameter increases (strong segregation limit, $\chi N \gg 10$), the crystalline order get confined (Figure 1, Case III) [16, 17] within the conventional block copolymer microphases such as inside lamellae, cylinders, and spheres (Figure 1) [18, 19]. In the general case that both blocks of the copolymer can crystallize (crystalline-crystalline), usually a more complicated phenomenon is observed. Investigations on such dual crystalline systems have shown that each component’s crystallization affects the other ones with well-characterized interactions [20]. When the two polymers have comparable melting temperatures, crystallization for both will occur almost simultaneously. On the other hand, when the melting temperatures are different, the first polymer to crystallize will yield a structure that could affect the second polymer’s crystallization [18, 19]. In some previous works [21-25] containing poly(ϵ -caprolactone) and poly(butadiene) block copolymers (PCL-PB), it was found that samples with lower molecular weights ($M_n \approx 10,000$ g/mol) and different ratios of PCL / PB were about 15 °C lower in their T_m values in comparison to their pure homopolymers and with different morphological structures upon changes in the block ratios, which indicated a strong difference in the crystallization behavior of the different block copolymers. Using synchrotron radiation SAXS studies, it was observed that the samples with 20 % PCL ratio showed crystallization directly from a disordered phase (Case I, Table 1, entry 1). However, upon increasing the PCL content to 36 % and 45 % (Table 1, entry 2), the samples had an ordered structure that was destroyed by precipitation during the crystallization process leading to breakout morphology (Case II) [23]. For high molecular weight samples ($M_n \approx 62000$ g/mol), no changes in the morphology were observed. It was shown that the crystallization took place within the block copolymer microdomains (Table 1, entry 3). Thus the energetic barrier to the destruction of the microphase was so large in the case of the high molecular weight PB-PCL that the microphase separation dominated the crystallization process, leading to confinement of the block copolymer microdomains (Case III) [26]. Several other selected block copolymer crystallization with the effect of the individual blocks on the crystallization parameters on the microphase-separated block copolymers are summarized in Table 1 below.

Table 1: Summary of the findings of the crystallization of block copolymers.

Entry	Materials	M_n [kg/mol]	Experimental findings
1 [23]	Poly(ϵ -caprolactone) PCL-b-PB	10	<ul style="list-style-type: none"> 20% PCL ratio, crystallization directly from a disordered phase (Case I)
2 [23]	Poly(ϵ -caprolactone-butadiene) PCL-b-PB	10	<ul style="list-style-type: none"> PCL content to 36% and 45%, ordered structures obtained. Destroyed by precipitation during the crystallization process breakout morphology (Case II)
3 [23] [26]	Poly(ϵ -caprolactone-butadiene) PCL-b-PB	62	<ul style="list-style-type: none"> no changes in the morphology Crystallization occurred within block copolymer microdomains. Confinement effect (case III)
4 [27]	Poly(ϵ -caprolactone-ethylene glycol) PCL-b-PEG	22	<ul style="list-style-type: none"> Isothermal crystallization of 20% w/w PEG. Similar crystallization rates to homopolymer for PCL chains. Slower crystallization rates for PEG in comparison to the homopolymer. (Case III)
5 [28, 29]	Poly(ϵ -caprolactone-ethylene glycol) PCL-b-PEG	14-43	<ul style="list-style-type: none"> PCL content 29-94% w/w. When PEG block was longer than PCL block, the PEG crystallized first, from the melt. Imperfect crystals formed (case II)
6 [30]	Poly(L-Lactide- ϵ -caprolactone) PLLA-b-PCL	24-29	<ul style="list-style-type: none"> Isothermal crystallization from a 44% and 60% PLLA miscible melt was investigated. PCL crystallized inside PLLA pre-crystallized spherulites. (Case III) For the 60% diblock, a transient microphase separated lamellar structure was identified (Case III)
7 [31, 32]	Poly(P-dioxanone- ϵ -caprolactone) PPDX-b-PCL	6-184	<ul style="list-style-type: none"> Under isothermal crystallization, PPDX was the first to crystallize. Higher temperatures supported the formation of granules whereas low temperatures favored the formation of banded spherulites. PPDX increased the crystallization rate of PCL [nucleation agent] (Case III)
8 [33, 34]	Poly(glycolic acid-valine-ethylene oxide-glycolic acid-valine) PGAv-b-PEO-b-PGAv	8-25	<ul style="list-style-type: none"> For PEO content of 37-59%, no crystallization occurred until -20°C. For compositions below 29% [PEO], no crystallization was observed. This phenomenon was attributed to the PGAv chains. The two blocks seemed to be immiscible for PEO contents lower than 29%
9 [35, 36]	PEO-b-PMMA	7-14	<ul style="list-style-type: none"> PEO's T_c, T_m, and X_c decrease with an increase in PMMA concentration in the range 0-61%. Fractionated crystallization was observed for PEO when its content was lower than 70% due to hindrance by PMMA. (Case II)
10 [37]	PB-b-PDMS PE-b-PDMS	28-128	<ul style="list-style-type: none"> PE crystals hindered PDMS crystallization when PDMS content was lower than 34%. This was not observed for amorphous PB. Crystallinity remains unaffected by PDMS content (Case III)

1.3 Crystallization of recurring defects in copolymers

Defects in polymer chains, irrespective of size and shape can affect the chemical microstructure of the polymer crystal, and subsequently affect the crystallization, thermal and mechanical properties of the polymer [38-41]. These defects include chain ends, comonomer units, coupling units, and stereo- or regio-defects. In crystalline polymers, depending on the size and nature of the defects, they are either excluded or included into the polymer crystal [42-47]. For example in poly(ethylene), PE crystals, it has been shown that, small groups such as halogens, oxygen, and the methyl branches can be partially incorporated into the orthorhombic poly(ethylene) lattice [48-50], while bigger branches such as propyl, styrene and vinyl acetate are excluded from the PE crystals [51-56]. When the defects are uniformly incorporated into the crystal lattice, leading to a defective crystal structure, it is termed as a uniform inclusion model, whereas in situations where they efficiently arrange themselves outside the crystal lamella, it is known as the exclusion model (Figure 2). Different theoretical model descriptions are used to explain these defects in copolymers. Notable among them is the model theory by Flory [57, 58], where the co-unit defects are completely excluded from the growing crystal. The model predicts a decrease in melting temperature with increasing comonomer content. This prediction has been verified experimentally by numerous studies on a variety of copolymers [49, 59].

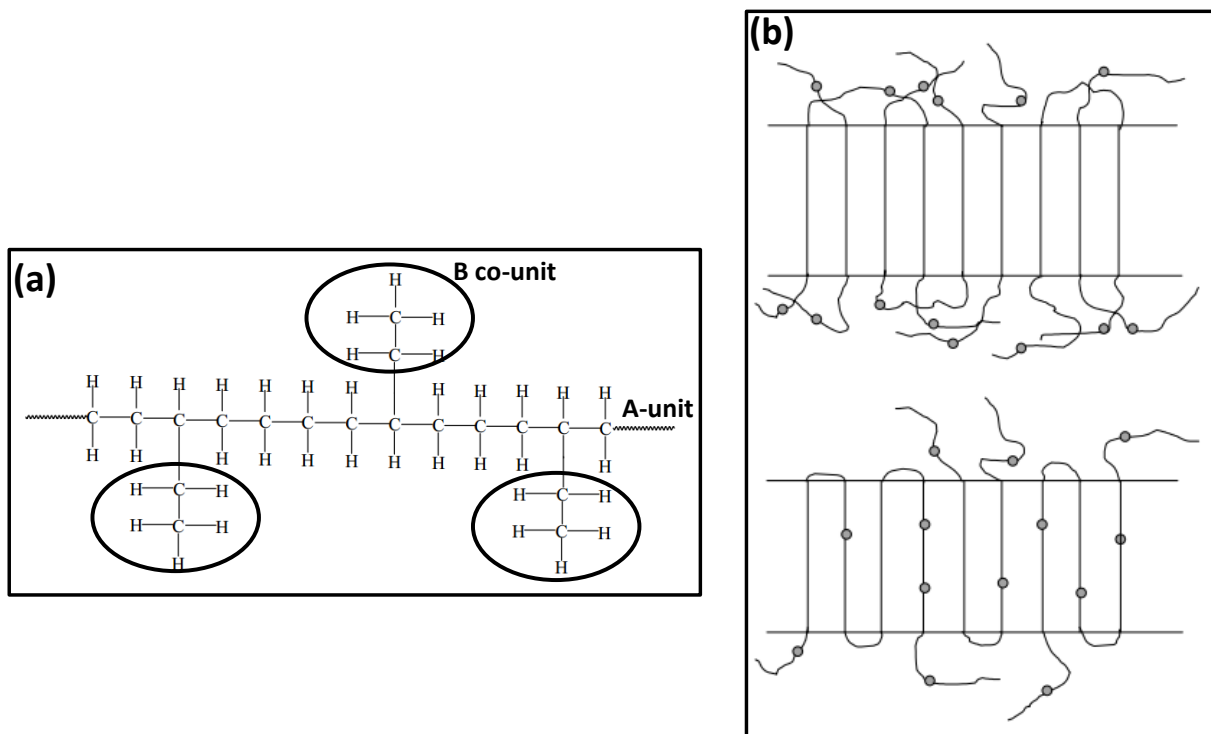


Figure 2. a) Structure of ethylene/1-butene copolymer. The ethylene co-units are shown in the circle, which are subsequently represented in Figure 2b as dots. b) Inclusion (down) and exclusion (top) models. The dots represent the co-units within the crystalline/amorphous A region. (Figure redrawn from reference [60]).

Also, the crystallization theory of defect polymers developed by Helfand and Lauritzen [61-64] on the kinetic theory for polymer crystallization recognizes the free energy costs of incorporating a co-unit into the crystal lattice. The theory rightly describes the inclusion of co-units not to only "modify the thermodynamic properties, but also profoundly affect the kinetic barriers to the crystal growth".

To obtain a comprehensive understanding of the findings of this thesis, a detailed review on some of the theories in exclusion and inclusion defects in crystalline polymers are considered in the proceeding pages.

1.3.1 Flory's exclusion theory of copolymer crystallization [57, 58]

Flory's exclusion theory assumes the co-units B as defects that are completely excluded from the crystallites formed by the A units. The model assumes all the sequence of the crystalline lattice to be composed of A units. The ability of A units to crystallize is dependent on a limiting sequence length, ξ . If ξ is larger than a critical value, ξ^* at equilibrium, crystallization takes place. However, if ξ is smaller than the critical value, ξ^* , crystallization will not happen at all. At high temperatures, crystallizable units of length ξ larger than ξ^* crystallize to form thick crystallites, while at lower crystallization temperatures, thinner crystal formation occurs. The ξ^* expression according to Flory is given by:

$$\xi^* = \left[\ln \left(\frac{D \cdot X_A}{P} \right) + 2 \ln \left(\frac{1-P}{1-e^{-\theta}} \right) \right] \left[\frac{-1}{\theta + \ln p} \right] \dots \dots \dots (1)$$

Where D is the crystal surface free energy effects, p is a probability that unit A is succeeded by unit A regardless of the preceding units, and X_A is the mole fraction of crystallizable A units. That is, for a random copolymer $p = X_A$, for a block copolymer $p > X_A$ and an alternating copolymer $p < X_A$, θ is a measure of the undercooling. This can be expressed in terms of the heat of fusion per unit (ΔH_u) and the melting temperature of the pure polymer (T_m°) as shown in equation (y)

$$\theta = \left(\frac{\Delta H_u}{R} \right) \left(\frac{1}{T} - \frac{1}{T_m^\circ} \right) \dots \dots \dots (y)$$

The melting point depression, T_m according to Flory is also defined as:

$$\frac{1}{T_m} - \frac{1}{T_m^\circ} = - \left(\frac{R}{\Delta H_u} \right) \ln p \dots \dots \dots (2)$$

Where R is a gas constant, T_m° is the melting point of the pure polymer, ΔH_u is the heat of fusion per unit. It is implicit in Equation (7) that the melting temperature is independent of the chemical nature of co-unit B. The same is true of the degree of crystallinity: the universal decrease in crystallinity due to copolymerization is solely a function of the amount of units B and not of their chemical nature.

The theory description by Flory to some extent has been experimentally verified in many investigations [51]; however, there seem to be some major discrepancies in the theory that were not tackled. For example, the melting point depression calculated using Flory's expression is invariably smaller than that observed experimentally for most investigated statistical copolymers [60]. Also, the heats of fusion

calculated for a homopolymer from Flory's analysis of copolymers are much lower than those measured experimentally by methods such as depression in melting point of the homopolymer by a diluent [60].

1.3.2 Sanchez and Eby's inclusion/exclusion model [60]

Sanchez and Eby's [60] model is one of the most elaborate and concise descriptions to exclusion and inclusion defects polymers. The model describes the kinetic determination of the crystalline morphology. It also shows that the inclusion of defects in a crystal leads to a thermodynamically more stable system. In the inclusion model, the depression of the crystal melting point is due to the decrease in the heat of fusion. Conversely, in the exclusion model, the melting point depression is due to an increase in the entropy of fusion. Under isothermal conditions, the Sanchez-Eby theory predicts an increase in the lamellar thickness with the concentration of defect units, for both the inclusion and exclusion models. The model adopts a statistical copolymer comprised of crystallizable A units and B co-units (defect). According to the model, a random copolymer must lie between two extremes (Figure 2b) (a) uniform inclusion, where the crystalline phase is a composition of both A and B units; the B co-units produce defects in the crystalline A lattice and (b) those of co-unit exclusion: where the crystalline phase is composed of entirely of A units and is in metastable equilibrium with a mixed amorphous phase A units and the non-crystallizable B co-units [60]. An expression for the free energy of crystallization of the copolymer, ΔG , is derived based on the condition that a real copolymer crystal is formed under kinetic conditions which determine the actual concentration of B co-units in the crystal [60].

$$\Delta G = \Delta G^\circ - RT \left\{ \frac{\varepsilon X_c}{RT} + (1 - X_c) \ln \left[\frac{1 - X_c}{1 - X} \right] + X_c \ln \left[\frac{X_c}{X} \right] \right\} \dots \dots \dots (3)$$

where; ΔG° = the free energy of crystallization of the homopolymer
 ε = the excess free energy of a defect (due to the presence of a B co-unit in the crystal lattice)
 X_c = the concentration of co-units in the crystal, and
 X = the overall composition of co-units in the copolymer.

For uniform inclusion of the co-units, $X_c = X$,

While for exclusion of the co-units, $X_c = 0$.

At equilibrium, the co-unit concentration, X_{eq} is determined as shown in equation (4)

$$X_{eq} = \frac{X e^{-\varepsilon/RT}}{1 - X + X e^{-\varepsilon/RT}} \dots \dots \dots (4)$$

At equilibrium, when we consider $\Delta G = 0$ and use the relation shown in equation (x), a new equation (5) can be formulated by combining equations (3) and (4).

$$\Delta G^\circ = \Delta H_f^\circ \left(1 - \frac{T}{T_m} \right) \dots \dots \dots (x)$$

$$\frac{1}{T_m} - \frac{1}{T_m} = - \frac{R}{\Delta H_f^\circ} \left\{ \frac{\varepsilon X_c}{RT_m} + (1 - X_c) \ln \left[\frac{1 - X_c}{1 - X} \right] + X_c \ln \left[\frac{X_c}{X} \right] \right\} \dots \dots \dots (5)$$

Where ΔH_f° = the heat of fusion of the homopolymer,

T_m° = the equilibrium melting temperature of the homopolymers and

T_m = melting point depression for the copolymer

For the case of uniform inclusion, $X_c = X$, the melting point depression can be calculated as shown in equation (6). Thus, the melting temperature depression is principally an enthalpic effect due to the presence of defects in the crystal lattice. The depression of the crystal melting point is due to the decrease in the heat of fusion.

$$T_m = T_m^\circ \left(1 - \frac{\varepsilon R}{\Delta H_f^\circ} X \right) \dots \dots \dots (6)$$

On the other hand, the complete exclusion of co-units from the crystal lattice, $X_c = 0$, results in equation (7). This describes the entropic effect arising from the necessity for sequential ordering of the chains during crystallization. The melting point depression is due to an increase in the entropy of fusion.

$$\frac{1}{T_m} = \frac{1}{T_m^\circ} + \frac{R}{\Delta H_f} \ln \left(\frac{1}{1-X} \right) \dots \dots \dots (7)$$

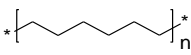
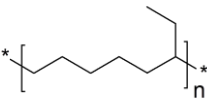
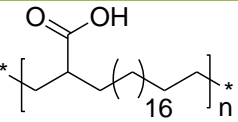
1.4 Exclusion crystallization in defect polymers

In the exclusion defect polymers, defects like branches, errors in tacticity or hetero-monomers are expelled to the amorphous phase and subsequently influence the crystallization process. Thus, it is possible to control the crystal properties like the degree of crystallization or lamellae thickness by adjusting the macromolecular architecture during the polymerization process. Polymerization processes will usually yield more or fewer irregularities, which are randomly distributed along the polymer chain. The type, nature, and density of the defects in the polymer chain will then determine the crystallization properties of the polymer [65]. In many synthesized exclusion defect polymers, thin crystal morphology within the polymer microstructure is mainly reported upon exclusion of the defects from the growing crystal lamella [60, 66-68]. An example can be seen in ADMET polyethylenes with n-hexyl branches at every 21st backbone carbon excluded from the crystalline lamella [66]. Thin crystal morphological structures were observed upon crystallization of this copolymer [66]. TEM images, SAXS and WAXD measurements showed that the polymers were made up of extremely narrow lamella thickness distributions with an average lamella thickness of approximately 26 Å. Further analysis revealed the average lamella thickness to be precise the distance between the n-hexyl branches along the polymer backbone and confirmed the exclusion of the n-hexyl branches from the crystalline lamella (Table 2, Entry 1). Upon modifying the defect type with stereo-irregular carboxylic acid groups [69], an uncommonly reported crystal structure for ADMET polymers, multilayer adjacent re-entry crystals, where the polymer chains make hairpin turns near each functional group was observed (Table 2, Entry 2). These multilayer chain-folded structures have however been demonstrated in other synthetic polymers like in polyesters containing alkyl segments in the polymer backbone with precisely defined lengths, where short poly(ethylene glycol) (PEG) chains are grafted to the polymer near each ester group [13, 70]. The same crystal morphology was also shown for ADMET PEs with organic nanoparticles [55] of defined shape and size as shown in table 2, entry 3.

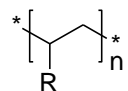
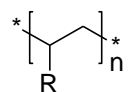
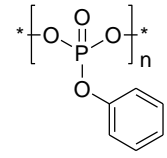
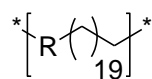
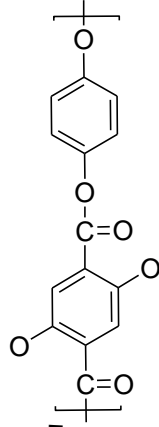
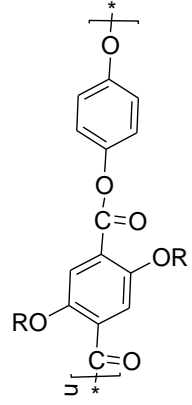
Other characteristic behaviors identified in excluded defect polymers upon crystallization are the insignificant or no change in the thermodynamic properties e.g. the heat of fusion and enthalpy of fusion of the polymer crystals [71-73] when compared to their corresponding polymers without defects. In a Ziegler-Natta propylene-ethylene copolymers with ethylene content up to 11% studies, the authors reported an apparently no observed change in the normalized heat of fusion or the unit cell dimensions as a function of comonomer content upon exclusion of the ethylene defects from the crystalline lamella [74] (Table 2, entry 4), indicating that the exclusion of the defects to the amorphous region did not affect the thermodynamic properties of the copolymer. Several other investigations (Table 1, entry 5-6) studied on propylene-ethylene copolymers [71-73] in the same ethylene concentration range as that of (Table 2, entry 4) revealed nearly the same effect on the normalized heat of fusion upon exclusion or partial inclusion of the defect in the crystal lamellae. However, a small decrease in the normalized enthalpy of fusion with an increase in ethylene content and a slight expansion of the unit cell were noticeable for the investigated copolymers measured for propylene homopolymer and propylene-ethylene copolymers [75-77].

Moreover, consequential decreases in the crystallization parameters like melting temperature upon exclusion of defects from the crystalline lamellae have been shown for most reported defect polymers [71-73]. Exemplified effect is shown in the investigations on various copolymers including fractions of ethylene/1-butene, ethylene/octene, ethylene/vinylacetate, ethylene/propylene, hydrogenated polybutadienes and diazoalkanes using dilatometry measurements [71-73]. All the copolymers except those containing methyl side groups were shown to be represented by a single curve on the T_m vs. comonomer content plot [51]. The methyl group-containing copolymers displayed higher T_m 's suggesting inclusion into the crystal lattice on an equilibrium basis, while the bigger sized defect copolymers showed lower T_m 's, suggesting exclusion from the crystal lattice (Table 2, entry 7-8). A similar investigation was reported for ortho-substituted phenylene units as defects in the main chain of series of polyethylenes. TGA, DSC, WAXD, and SAXS were utilized for analysis to reveal a remarkable depression of the melting temperature (T_m) upon exclusion of the ortho-substituted phenylene units from the crystal phase [68] (Table 2, entry 9). Some further experimental results from selected examples of model systems on exclusion crystallization in defect polymers are listed in Table 2 (entries 10-14).

Table 2. Exclusion defect crystallization in copolymers and their representative structural defects

Entry	Type of defect	Copolymer structure	Experimental findings
1 [66]			<ul style="list-style-type: none"> Narrow lamella thickness distribution polymers with average lamella thickness of approximately 26 Å. Exclusion of n-hexyl branch from the crystalline lamella leading to thin crystal morphology.
2 [69]	—COOH		<ul style="list-style-type: none"> Multilayer adjacent re-entry crystals formed Polymer chains make hairpin turns near each functional group.

3 [55]	—COOH	$* \left[\text{CH}_2 \text{---} \underset{\text{COOH}}{\text{CH}} \text{---} (\text{CH}_2)_{40} \text{---} \text{CH}_2 \right]_n *$	<ul style="list-style-type: none"> • COOH groups form layers on the nanocrystal surface, to self-stabilize the nanocrystals. • Nanocrystal thickness directly determined by the length of the long chain methylene spacer between the functional groups.
4 [74]	—CH ₂ CH ₃	$* \left[\text{CH}_2 \text{---} \underset{\text{R}}{\text{CH}} \text{---} \text{CH}_2 \text{---} \text{CH}_2 \right]_n *$	<ul style="list-style-type: none"> • Neither the normalized heat of fusion nor the unit cell dimensions changed as a function of comonomer content.
5 [71-73]	$\text{R} = \begin{matrix} \text{---CH}_2\text{CH}_3 \\ \text{---CH}_2\text{CH}_2\text{CH}_3 \\ \text{H}_3\text{C---C---CH}_3 \\ \\ \text{---} \end{matrix}$	$* \left[\text{CH}_2 \text{---} \underset{\text{R}}{\text{CH}} \text{---} \text{CH}_2 \right]_n *$	<ul style="list-style-type: none"> • A similar report to entry 4 for the studies on random ethylene/α-olefin copolymers. • No changes in the heat of fusion or the unit cell dimensions as a function of comonomer content.
6 [75-77]	—CH ₂ CH ₃	$* \left[\text{CH}_2 \text{---} \underset{\text{R}}{\text{CH}} \text{---} \text{CH}_2 \text{---} \text{CH}_2 \right]_n *$	<ul style="list-style-type: none"> • A decrease in the normalized enthalpy of fusion with increasing ethylene content. • Expansion of the unit cell along the <i>b</i> direction for propylene homopolymer and propylene-ethylene copolymers.
7 [51]	$\text{R} = \begin{matrix} \text{---C=C---H}_2\text{---CH}_3 \\ \quad \\ \text{H} \quad \text{H} \\ \text{---} \end{matrix}$ 	$* \left[\text{CH}_2 \text{---} \underset{\text{R}}{\text{CH}} \text{---} \text{CH}_2 \right]_n *$	<ul style="list-style-type: none"> • All copolymers except methyl side group copolymers showed single curve on the T_m vs. comonomer content plot, indicating exclusion of the branches from the crystal lattice. • Included methyl side group copolymers displayed higher T_m's on an equilibrium basis.
8 [52, 78]	$\text{R} = \begin{matrix} \text{---C=C---H}_2\text{---CH}_3 \\ \quad \\ \text{H} \quad \text{H} \\ \text{---} \end{matrix}$ 	$* \left[\text{CH}_2 \text{---} \underset{\text{R}}{\text{CH}} \text{---} \text{CH}_2 \right]_n *$	<ul style="list-style-type: none"> • Follow-up investigation to entry 8. • The investigations showed that deviations from the single curve in entry 8 are as a result of differences in sequence distribution, and not the chemical nature of the comonomer.
9 [68]		$* \left[\text{---} \underset{\text{O}}{\text{C}} \text{---} (\text{C}_6\text{H}_4)_{20} \text{---} \underset{\text{O}}{\text{C}} \text{---} \right]_n *$	<ul style="list-style-type: none"> • Substitution position in the arylene units influenced the chain stacking and the location of the arylene groups in the solid phase. • Exclusion of the ortho-substituted phenylene units from the crystal phase, leading to a low melting temperature (T_m).
10 [79]	$\text{R} = \begin{matrix} \text{---C=CH}_2 \\ \\ \text{H} \\ \text{---} \end{matrix}$ $m = 1, 3, 5$	$* \left[\text{CH}_2 \text{---} \underset{\text{R}}{\text{CH}} \text{---} \text{CH}_2 \right]_n *$	<ul style="list-style-type: none"> • Rate of comonomer co-crystallization estimated as PB > PE > PH = PO for comonomer contents < 13 mol% and PE > PH > PO for > 13 mol% comonomer contents. • A rejection model especially the 1-octene units from the crystals was reported.

<p>11 [52, 80-82]</p> $R = \begin{array}{c} \text{---C=CH}_2 \\ \\ \text{H} \end{array}$ 	<ul style="list-style-type: none"> • Short spin-lattice relaxation of copolymers, showing concentration of branches in a single mobile and disordered phase. • Chemical oxidation study showed accessibility of the branches to the oxidizing agent, while the crystalline core was not, implying the branches location to the disordered amorphous phase.
<p>12 [52, 83]</p> $R = \begin{array}{c} \text{---C=CH}_2 \\ \\ \text{H} \end{array}$ 	<ul style="list-style-type: none"> • A significant interfacial region with a thickness in the range of ~20-40 Å for rejection of the co-units from the crystal lattice. • Increasing the thickness with increasing comonomer content up to M_n of 100,000 g/mol.
<p>13 [84]</p>  $R = \begin{array}{c} * \left[\text{O} \begin{array}{c} \text{O} \\ \\ \text{P} \\ \\ \text{O} \end{array} \text{O} \right]_n \\ \\ \text{CH}_3 \end{array}$  $* \left[\text{C} \begin{array}{c} \text{H}_2 \\ \\ \text{---} \end{array} \left(\text{C} \begin{array}{c} \text{H}_2 \\ \\ \text{---} \end{array} \right)_3 \text{C} \begin{array}{c} \text{H}_2 \\ \\ \text{---} \end{array} \right]_n$	<ul style="list-style-type: none"> • Melting temperature as low as 14 °C reported for butyl side chain defects, while an increase in T_m of 30 °C and 50 °C showed for much bulkier phosphate and phosphonate defects. • Incorporated groups (inclusion or exclusion) was based on the conformation, structure, and geometry of the defects.
<p>14 [85]</p>  <p style="text-align: center;">R = 6-12 alkyl units</p> 	<ul style="list-style-type: none"> • Polyethylene-like glass transitions α_{PE} observed for these polymers using dynamic mechanical data analysis. • The alkyl nanodomain size was the most critical factor determining the α_{PE} dynamics of the methylene units.

1.5 Inclusion crystallization in defect polymers

In the case of inclusion defect crystallization, the functional or amorphous groups are mainly small enough to be embedded inside the crystalline regions. The groups arrange into layers to optimize their packing. Upon crystallization of the inclusion defect polymers, different characteristic properties are observed; for example, many observed crystal structure morphologies for inclusion defect polymers are those of the extended-chain crystals [86, 87]. Aliphatic polyamides (nylons) are classical examples of precise polymers that form extended-chain layered crystallites [86, 87]. In ADMET polyethylenes with precise chlorine substitution on every 15th backbone carbon (Table 3, entry 1), a polymorphism of crystal structures was reported, all of which were of the extended-chain variety [88]. Under fast crystallization kinetics, the chains assemble in an all-trans planar packing with a layered chlorine distribution. Extended-chain crystal structures have also been shown in methyl [89], and sulfone [90] group defected polymers. Also, reports on a triazole ring based point defect at the middle of a PEO chain revealed a single type of

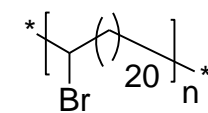
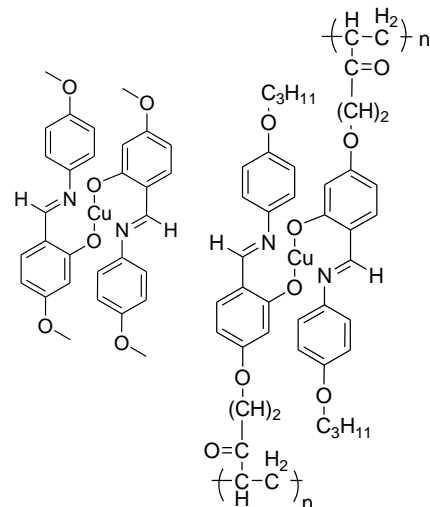
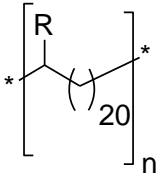
lamella crystal after cooling to $T = 0\text{ }^{\circ}\text{C}$ [91]. An extended chain crystal structure model was generated for the packing of the polymers (Table 3, entry 2).

Furthermore, the influence of the crystallinity as a result of defect inclusion in the crystalline lattice of copolymers has been reported using several different copolymers [40, 92]. Notable example is shown in the investigations of a series of copolymers composed of bromotrifluoroethylene (BTFE) [92], where upon using Fourier transformed infrared spectroscopy, DSC, dielectric spectroscopy and WAXD analysis revealed that, for small amounts of BTFE (<2 mol%), the co-unit (BTFE) was dispersed primarily as single defects and minimally affected the crystallinity and the chain conformation distributions (Table 3, entry 3). As the BTFE content further increased and the prevalence of BTFE monomer runs increased, there was found to be a substantial drop in the crystallinity and the crystallite size along with the inhibiting of the all-trans chain conformation [92]. Similar studies were conducted on series of 11 different ADMET polymers with varying defect sizes [40]. Thermal characterization of the polymers via DSC confirmed the precise nature of the ADMET polymers by displaying sharp and well-defined endothermic transitions. Methyl and ethyl branches were included in the unit cell, which resulted in a decrease in the degree of crystallinity of the ADMET polyethylene compared to an unbranched ADMET polyethylene standard. WAXS investigations revealed a loss of the crystal structure upon incorporation of the precisely placed branches into the unit cell, resulting in a shift of the unit cell from orthorhombic to triclinic crystal structure (Table 3, entry 4).

Moreover, a decrease in the equilibrium melting temperature as a result of the co-units incorporation into the crystalline lattice has been characterized by inclusion defect polymers upon crystallization [50, 68]. An example of this effect is shown in the investigations of an incorporation of random propylene and butane defects in ethylene-propylene and ethylene/1-butene crystallizable random copolymers [50], where a decrease in the equilibrium melting temperature, T_m° and a change in the surface free energy, σ_e upon inclusion of the copolymer in the crystal lattice was revealed. The annealing behavior and thermodynamics of fusion of the solution-grown single crystals of the ethylene-propylene and ethylene/1-butene crystallizable random copolymers were examined in comparison with linear polyethylene crystallized from the melt and dilute solution. Correlation of the quantities such as long spacing, annealing temperature, and apparent enthalpy of fusion, led to the conclusion that the single crystal aggregates were involved in a morphological transformation during the process of annealing. Both classes of polymers showed a lowering in T_m° with the increasing number of side groups, though the effect was more pronounced in the ethylene-propylene copolymers. Some additional investigations on melting point decrement upon incorporation of defects in the crystal lamella are shown crystallization of arylene ether defect units in the main chain of series of polyethylenes (Table 3, entry 5) [68] and other selected results in table 3, entry 11.

Table 3. Inclusion defect crystallization in copolymers and their representative structural defects

Entry	Type of defect	Copolymer structure	Experimental findings
1 [88]	-Cl		<ul style="list-style-type: none"> Extended-chain crystals. Fast crystallization kinetics; chains assemble in an all-trans planar packing. Slow crystallization rates favor herringbone-like non-planar structure.
2 [91]			<ul style="list-style-type: none"> A single type of lamella crystal; an extended chain crystal structure model at T = 0 °C.
3 [92]	-Br		<ul style="list-style-type: none"> Bromotrifluoroethylene, BTFE (<2 mol%) dispersed as single defects; minimally affected the crystallinity and the chain conformation distributions. Increased BTFE content implies a drop in crystallinity and crystallite size.
4 [40]	R = methyl, ethyl, iso-propyl, sec-butyl, cyclohexyl, adamantyl		<ul style="list-style-type: none"> Methyl and ethyl branches included in the unit cell. A decrease in melting point and degrees of crystallinity. Loss of crystal structure upon defect incorporation with a resultant shift of the unit cell from orthorhombic to a triclinic crystal structure.
5 [68]			<ul style="list-style-type: none"> para-substituted phenylene units were excluded from the crystal phase leading to a lowering T_m. meta-substituted phenylene units could be partially included into the crystal, resulting in mixed crystal structures and an intermediate T_m
6 [93]			<ul style="list-style-type: none"> 42 % of the ethylene units included in the propylene crystal for copolymers with ethylene concentration of 0.8-7.5 mol%. A decrease in the normalized heat of fusion with ethylene inclusion in the polypropylene crystal.
7 [94]	-Cl		<ul style="list-style-type: none"> Folding and packing of the chain segments rendered strains in the lattice to destabilize the orthorhombic unit cell. Restricted of crystallinity from 80 to ~30 %, and crystal thickness from ~180 to 90 Å with increasing Cl content. Trans-trans crystal packing conformations observed at Cl level > ~10 mol %.
8 [95]	R = methyl, ethyl		<ul style="list-style-type: none"> Shift of the two strong scattering peaks to 21.1° and 23.0°, corresponding to (110) (d= 4.19 Å) and (200) (d= 3.87 Å) reflection planes with lattice parameters a = 7.74 Å and b = 5.00 Å as result of methyl branch inclusion in the crystal lattice. An expansion of the unit cell by 4.6% and 1.4% along the a- and b-axes proved the distortion in the orthorhombic unit cell.

<p>9 [96]</p> <p>-Br</p>		<ul style="list-style-type: none"> • Four crystalline forms obtained for the uniaxially oriented specimens of the polyethylene-like polymer. • Unoriented samples were difficult to obtain a chain conformation and chain packing mode.
<p>10 [97]</p>		<ul style="list-style-type: none"> • Introduction of copper atoms (5-65 mol%) resulted into cross-linked polymeric chains. • Enantiotropic smectic A and smectic C mesophases of the original polyacrylate disrupted due to the statistical incorporation of the copper (II) ions. • Restriction of motion of the copper complex around the long molecular axis upon incorporation of the copper (II) ions.
<p>11 [40]</p> <p>R = methyl, ethyl, propyl, butyl, pentyl, hexyl, iso-propyl, sec-butyl, tert-butyl, cyclohexyl, adamantyl</p>		<ul style="list-style-type: none"> • Methyl and ethyl branches included in the unit cell, with a resultant decrease in the melting point and degrees of crystallinity. • WAXS investigations revealed loss of the crystal structure upon incorporation of the precisely placed branches into the unit cell. • Crystal structure lost its symmetry with the unit cell shifting from orthorhombic to triclinic crystal structure.

1.6 Synthesis and switching dynamics of photochromic polymers

Organic photochromic molecules known in photo-control polymers include azobenzenes, stilbenes, benzoimine, spiropyranes, fulgides, diarylethenes and chromenes (Figure 3) [98]. Among these, azobenzenes, stilbenes and benzoimines stands out to be three of the most important photochromic molecules widely investigated. Three different classes of photochromic processes are shown upon illumination of these molecules: *trans-cis-trans* isomerisations, photo-induced ring closing reactions and photo-tautomerism [99, 100]. Depending on the thermal stability of the photogenerated isomers, these photochromic molecules can be divided into two main categories: P-type (photochemically reversible type); these do not transform to their initial isomer even upon heating at higher temperatures; an example includes the fulgides and the diarylethenes. T-type (thermally reversible type); the photogenerated isomers thermally revert to their initial form (e.g., azobenzenes, stilbenes, benzoimine and spiropyranes).

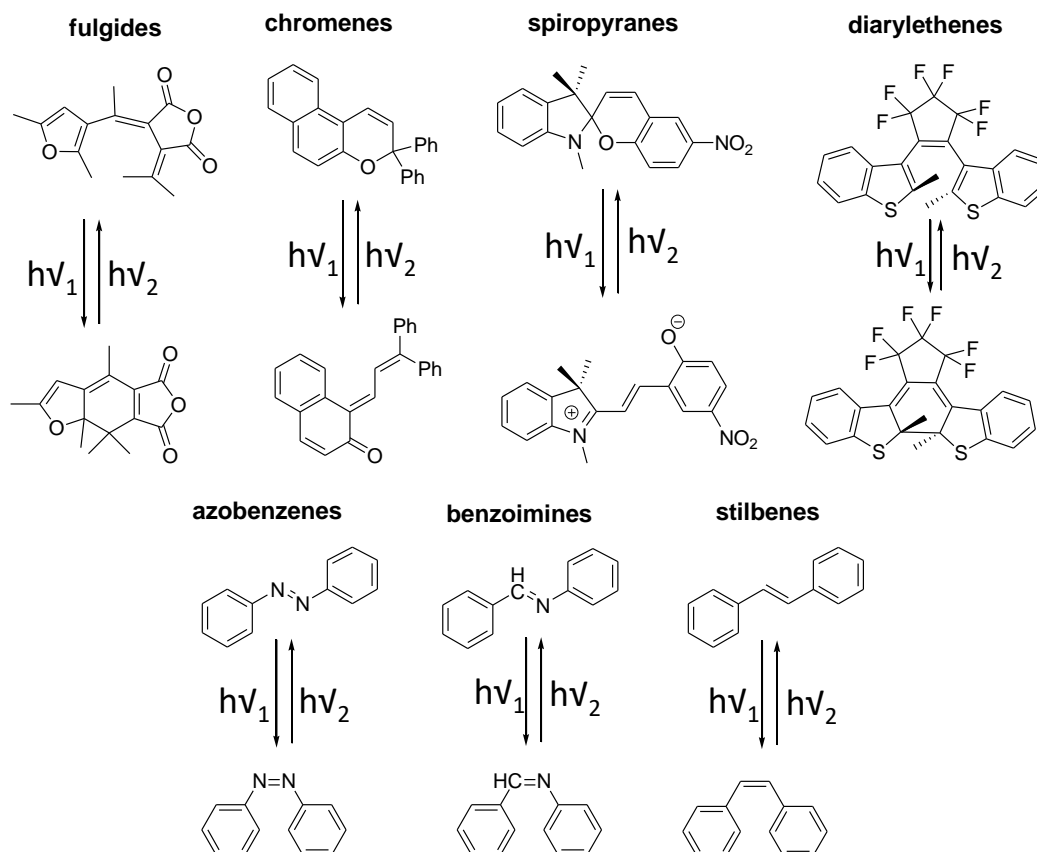


Figure 3. Selection of organic photochromic molecules known in photochemistry and their photochromic reactions (Figure redrawn from citation [98]).

1.6.1 Photo-responsive azobenzene chromophore

Azobenzenes are versatile molecules with two phenyl rings separated by an azo ($-\text{N}=\text{N}-$) bond. Azobenzenes are usually absorbing light in the blue region, and therefore the vast majority of azobenzenes exhibit a yellow, orange or red colour. They have two isomeric states: a thermally stable *trans* configuration, and a metastable *cis* form. This chromophore was described for the first time in 1834 [101], and in 1937 Hartley [102] revealed an interesting property of the molecule, i.e. the reversible photochemical E-Z isomerisation. Under irradiation, the E (*trans*) azobenzene is converted to the Z (*cis*) form, which thermally reverts to the more stable *trans* on a timescale dictated by the molecule's particular substitution pattern [103].

The mechanism of the photoisomerization process is a fundamental subject in azobenzenes. Two pathways have been accepted until now [100]. It is accepted that the photoirradiation step from *trans* to *cis* has a rotational pathway and/or an inversion pathway, whereas the heating step from *cis* to *trans* has an inversion pathway (Figure 4) [100].

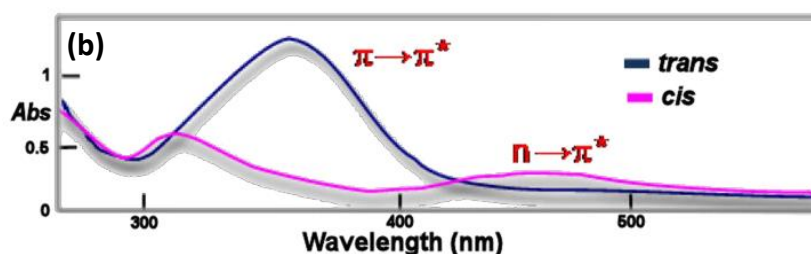
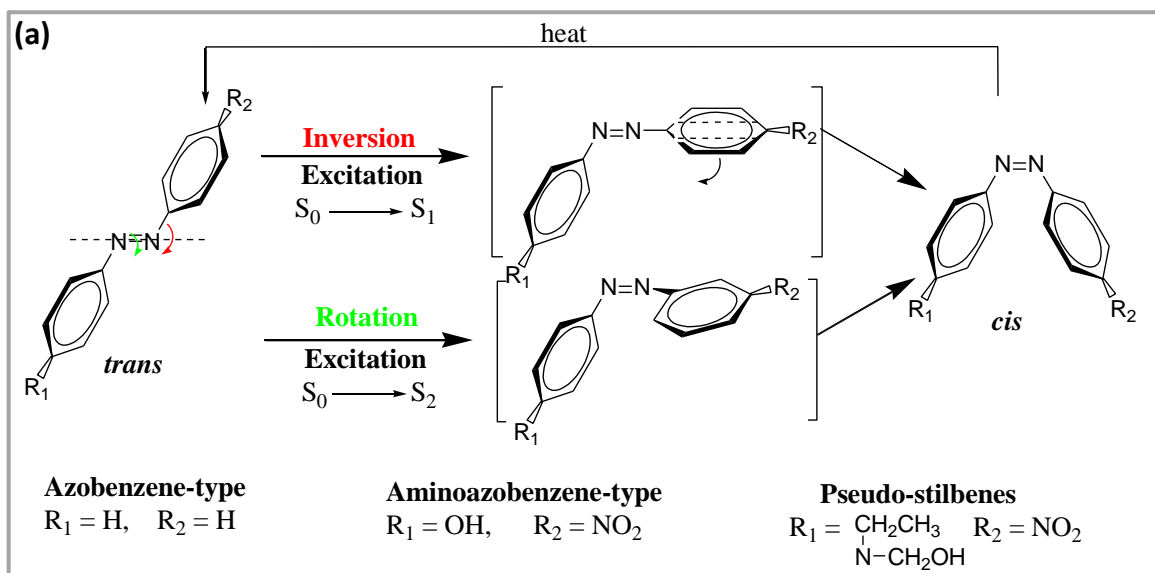


Figure 4. (a) Mechanistic isomerization pathway from *trans*- to *cis*-azobenzene and vice versa showing representative structures of azobenzene-type, aminoazobenzene-type and pseudo-stilbenes chromophores (b) UV-absorption spectra of an azobenzene-type chromophore showing the $\pi\text{-}\pi^*$ and $n\text{-}\pi^*$ transition bands (Figure redrawn from citation [104]).

Azobenzene chromophore can be divided into 3 types [105]: azobenzene-type molecules, which are the unsubstituted azobenzenes; aminoazobenzene-type molecules, which are ortho- or para-substituted with an electron-donating group; and pseudo-stilbenes, which are substituted at the 4 and 4' positions with an electron-donating and an electron-withdrawing group (such as an amino and a nitro group).

Aminoazobenzene groups are characterized by their close proximity of the $n\text{-}\pi^*$ states and the $\pi\text{-}\pi^*$ states. Absorption bands in these azobenzenes are very sensitive to solvent polarity, as the azo group in an aminoazobenzene will interact with hydrogen bonding solvents more readily than the amino group [105, 106].

The pseudo-stilbene class of azobenzenes shows a contraposed electron-withdrawing and -donating groups that create a highly asymmetric electron distribution within the conjugated system [107, 108]. They are basically characterized by a low-lying $\pi\text{-}\pi^*$ state. Rearrangement of the electronic states of azobenzene can result in the formation of a pseudo-stilbene; thus by raising the energy of the $n\text{-}\pi^*$ state, via protonation of the azobenzene, or by lowering the $\pi\text{-}\pi^*$ state of the azobenzene via substitution with electron donating or accepting groups [109].

1.6.2 Synthetic methodologies for the design of azobenzene photochromes

Incorporation of azobenzene into polymers starts with the design and synthesis of the azobenzene photochromic monomers. Many efforts have been subjected towards the synthesis of azobenzene monomers, not only in the yields but also with the efficiency and the final structure of the purified product. Two main methods have been used in the synthesis of azobenzene photochromes [100]: i.e. (i) creation of an azo bond by coupling of two identical or non-identical aromatic compounds [110-125]; and (ii) creation of an azo bond by oxidation of hydrazo compounds [126-129] or by reduction of azoxybenzene derivatives [130-133]. These two methods, in consequence, have led to the evolvement of two different classes of azobenzene derivatives: the symmetric and the dissymmetric azobenzenes (Figure 5).

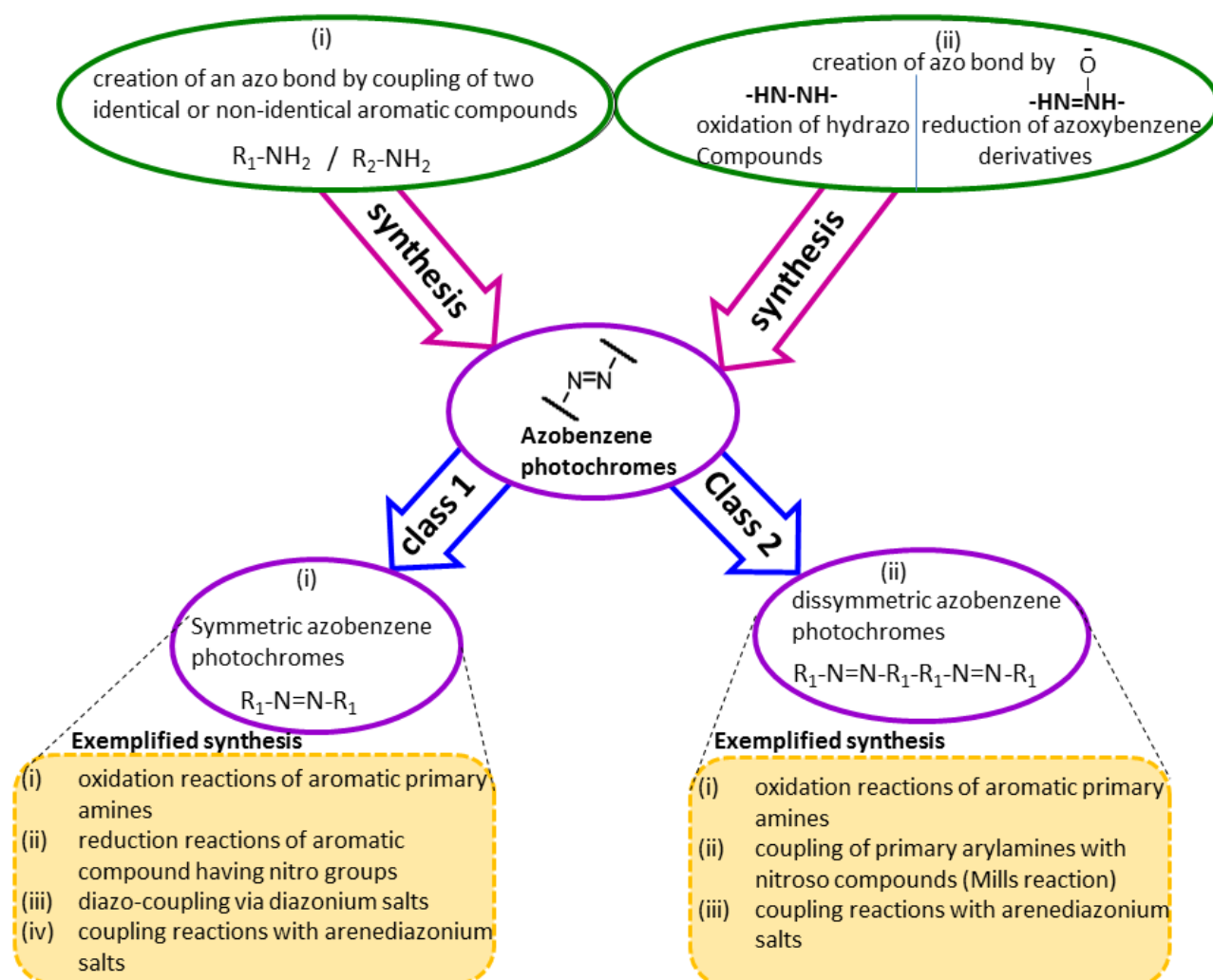


Figure 5. Schematic representation of the synthesis of the symmetric and the dissymmetric azobenzenes

Synthesis of the symmetric azobenzene derivatives is effected by (i) oxidation reactions of aromatic primary amines [112, 134-138]; (ii) reduction reactions of aromatic compound having nitro groups [117, 139-142]; (iii) diazo-coupling via diazonium salts [121, 143-153]; and (iv) coupling reactions with arenediazonium salts [154, 155], while the synthesis of the dissymmetric azobenzene derivatives is effected by (i) oxidation reactions of aromatic primary amines [113]; (ii) coupling of primary arylamines with nitroso compounds (Mills reaction) [122, 156-165]; and (iii) coupling reactions with arenediazonium salts [154-155, 166]. A notable example among these synthetic strategies is the synthesis of a sterically

hindered [3+3] cycloalkyne dimer linked via an azo bond [112] using oxidative coupling method in the presence of MnO_2 in benzene. Yields of about 64 % were obtained, with switching dynamics of the system proving a stable *cis* isomer that formed polymeric aggregates by nonpolar π - π interactions. Furthermore, upon using the diazo coupling of *p*-nitrobenzenediazonium tetraborate with calyx[4]arene in the presence of pyridine and THF, the synthesis of arene cone bis-azobenzene derivative was achieved [121, 150]. Yields of about 42 % were reported for the synthesized monomers.

1.6.3 Incorporation of azobenzene photochromes into polymers

Incorporating the developed azobenzene photochromes into polymers regardless of the efficiency and final structure of the product, are carried out through two main approaches: i.e. starting from an azobenzene monomer with defined structure and then (i) covalently introducing the polymer chain via different synthetic routes or (ii) non-covalently binding the polymer chains via ionic, dipole-dipole interactions or through the formation of inclusion complexes. Both of these methods have advantages or disadvantages, but in general, they have a lot in common with regards to their synthesis. Depending on the application, one can decide whether to compromise the desired features of the intended material by the use of either of the two methods. Synthesizing azobenzene polymers via covalent binding of polymer chains to azo groups are subsequently achieved in either of the two approaches: (a) polymerization of the monomeric azobenzene chromophores or (b) post-modification of the functional groups of an already synthesized polymer with an azo-monomer (Figure 6). Polymerization of the monomeric chromophores in general can undergo almost all type of polymerization reactions, such as free radical polymerization [167-170], Michael addition polymerization [171], atom transfer radical polymerization (ATRP) [172-174], polycondensation reactions [175, 176], reversible addition-fragmentation chain transfer polymerization (RAFT) [177, 178], and acyclic diene metathesis polymerization (ADMET) [179, 180]. This technique is a very popular approach which provides a variety of novel azobenzene polymers with well-defined structures due to the possibility of the initial design of the azobenzene monomer. However, the post-modification strategy also presents an interesting means of tuning the polymeric properties with the azobenzene chromophore. Thus, the post-modification strategy provides the opportunity to tune an already known polymer with defined structure and particular properties for the intended application. But the quantitative conversion of the functional groups in such reactions can be quite a challenge. These different synthetic strategies have been exploited in the development of many azobenzene-functionalized polymers, including hyperbranched azo-polymers [180], dendritic macromolecular azo-polymers [181] and precise ADMET azo-polymers [179].

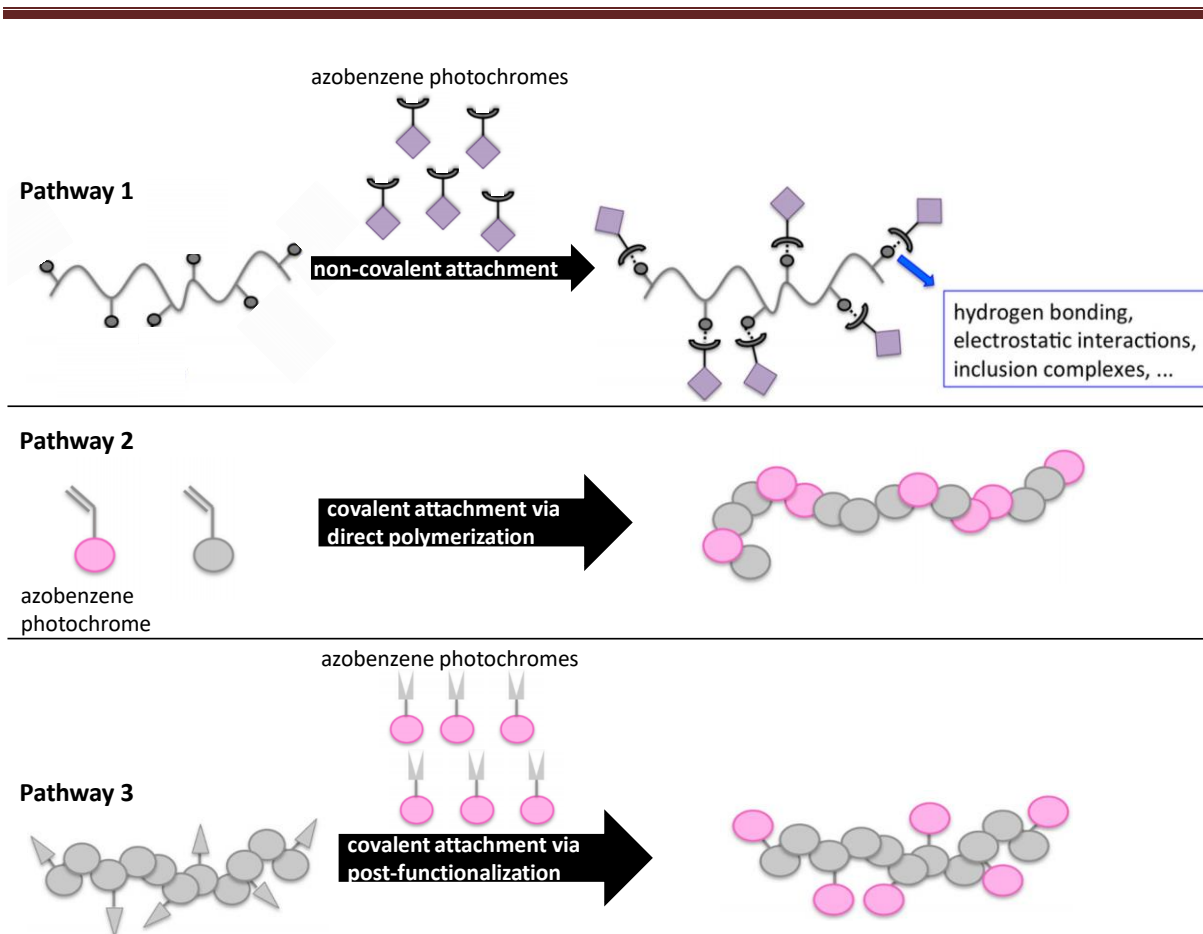


Figure 6. Different synthetic pathways to incorporate azobenzene photochromes into polymer chains; Pathway 1: non-covalent attachment, Pathway 2: covalent attachment via direct polymerization and Pathway 3: covalent attachment via post-functionalization.

1.7 Photo-physical relaxation dynamics of azobenzene monomers and polymers.

1.7.1 Photo-physical relaxation dynamics of azobenzene monomers

Photo-physical relaxation dynamics of azobenzene compounds are studied from the main spectral features of the weak long wavelength absorption band (dominated by the *cis*-form azobenzene) and the short wavelength absorption band (dominated by the *trans*-form azobenzene) [181-183]. Activation energy barrier between the *cis* and *trans* conformation is around 50 kJ mol^{-1} [105]. For *cis* azobenzene in benzene solution, molar absorption coefficient, ϵ of $404 \text{ mol}^{-1} \text{ dm}^3 \text{ cm}^{-1}$ for the $n\text{-}\pi^*$ transition at 449 nm, and $1250 \text{ mol}^{-1} \text{ dm}^3 \text{ cm}^{-1}$ at 440 nm for the *trans*-form are shown [184]. The molar absorption coefficient for the $\pi\text{-}\pi^*$ transition of this azobenzene type is around $22000 \text{ mol}^{-1} \text{ dm}^3 \text{ cm}^{-1}$. Excitation into the $\pi\text{-}\pi^*$ absorption of the *trans*-form results in the population of the *cis* isomer with a quantum yield of about 0.4, while excitation into the $n\text{-}\pi^*$ transition of the *cis* form at approximately 450 nm populates the *trans* isomer with a quantum yield of about 0.25 [184]. Lifetimes of the *cis* state are typically on the order of hours, minutes, and seconds, for azobenzenes, aminoazobenzenes, and pseudo-stilbenes, respectively [185, 186]. Energy barrier for thermal isomerisation is on the order of 90 kJ/mol [185, 186].

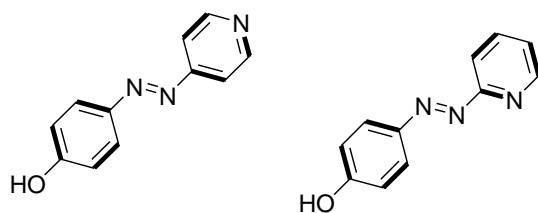
In general, the photo-physical relaxation dynamics in azobenzene monomers can be influenced by several factors. These factors can be internal, such as substituents on the azobenzene chromophores, chemical structure effect, electron withdrawing and donating groups on the chromophore or external factors which

results from the procedure used for the studies e.g. solvent effect and temperature. Some notable internal/external effect influences are shown in the studies of different azophenol derivatives [187] (Table 4 entry 1), where upon using different solvent systems in the photo-relaxation process, different isomerisation times were obtained for the same azo molecule. Mono- para- and di-substituted azophenols were investigated, where both mono- and para-substituted azophenols exhibited fast thermal isomerisation kinetics in ethanol at 298 K with relaxation times of 205 and 306 ms, respectively. The relaxation times for these two azocompounds remarkably increased in toluene by four orders of magnitude up to 31 and 28 min, respectively. The para-di-substituted azophenol also showed a similar behaviour: relaxation time of 33 min and 306 ms in toluene and ethanol was respectively reported. Moreover, the chemical structure of the azobenzene photochrome was also shown to affect the photo-physical relaxation of the azo-monomers [188]. A change in the substitution pattern (e.g. ortho-, meta- and para- substitution) of the groups on the aromatic benzene ring affected the photo-physical relaxation of the monomers. Thus the photo-relaxations of an ortho-methyl hydroxy-substituted azopyridinium salt and para-methyl hydroxy-substituted azopyridinium salts showed relaxation times of 150 μ s and 33 μ s respectively. This showed that a change in the chemical only from an ortho to para arrangement of the substituents on the aromatic benzene ring had a significant influence on the relaxation dynamics of the azo-monomer. Table 4 shows some other selected factors on the photo-relaxation of the azobenzene monomers.

Table 4: The influence of internal/external factors on the photo-relaxations of azobenzene monomers.

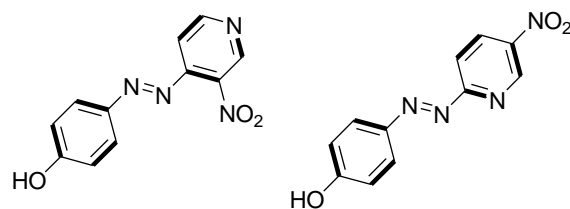
Factors influencing the photo-relaxation dynamics		Reference
1) Solvent effects on photo-relaxation of different azophenol derivatives		[189]
Ethanol	$\tau = 205$ ms	$\tau = 306$ ms
Toluene	$\tau = 31$ min	$\tau = 28$ min
		$\tau = 265$ ms
		$\tau = 33$ min
2) Chemical structure effect on on photo-relaxation of azopyridinium salts in ethanol		[188]
	$\tau = 150$ μ s	$\tau = 150$ μ s

3) Ortho- and para-pyridine substitution effect on photo-relaxation in ethanol and ethanol/phenol solvent mixute [188]



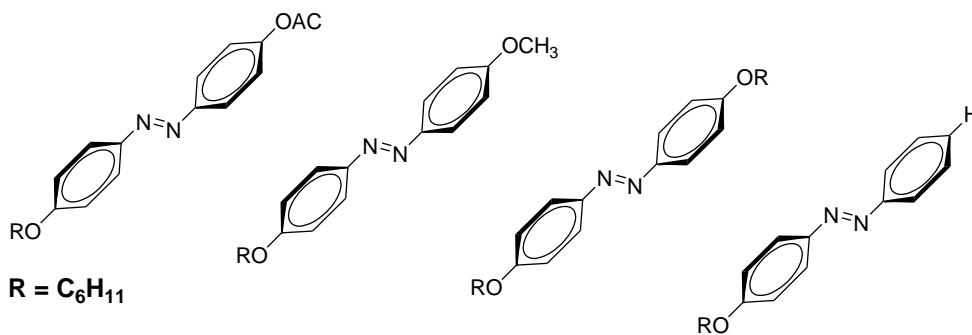
Ethanol	$\tau = 14 \text{ ms}$	$\tau = 49 \text{ ms}$
Ethanol + PhOH	$\tau = 1.4 \text{ ms}$	$\tau = 11 \text{ ms}$

4) Ortho- and para-pyridine substitution with additional electron withdrawing effect on photo-relaxation in ethanol and ethanol/phenol solvent mixute [188]



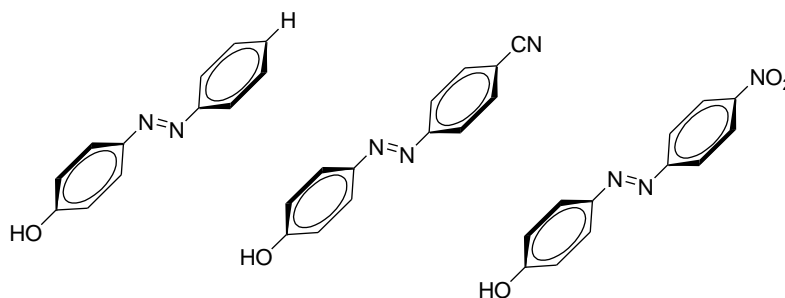
Ethanol	$\tau = 1.4 \text{ ms}$	$\tau = 2.9 \text{ ms}$
Ethanol + PhOH	$\tau = 644 \text{ }\mu\text{s}$	$\tau = 1.1 \text{ ms}$

5) Chemical structure effect on on photo-relaxation of different azoderivatives in ethanol [189]



$\tau = 49 \text{ h}$	$\tau = 13 \text{ h}$	$\tau = 12 \text{ h}$	$\tau = 70 \text{ h}$
-----------------------	-----------------------	-----------------------	-----------------------

6) Electron-withdrawing effects on photo-relaxation of different azophenol derivatives in ethanol [188]



$\tau = 205 \text{ ms}$	$\tau = 27 \text{ ms}$	$\tau = 4.6 \text{ ms}$
-------------------------	------------------------	-------------------------

1.7.2 Photo-physical relaxation dynamics of azobenzene polymers

The photo-physical relaxation dynamics of azobenzene polymers, in general, have been reported for polymers having several alkyl branched chains, aryl rings and liquid crystals [190, 191]. Upon incorporating azobenzene photochromes into these polymers, different noticeable characteristic properties result. For example, polymers possessing azo backbone groups are identified to have a rate constant of about 10^{-8} s^{-1} for the *trans-cis* isomerisation [192] in solution, which usually increases in the solid state. It must be pointed out that aromatic azo compounds, in contrast to aliphatic azo compounds, are rather stable with respect to photochemical decomposition. The quantum yield for decomposition of azobenzene incorporated into polymers is estimated to be less than 10^{-3} [192-194].

Azo polymers in dilute solutions are also shown [195-198] to behave similarly to low molecular weight azo monomers. An example is shown in the synthesis and photochemical investigations of a series of polyaromatic ureas with pyridine moieties [196, 197]. Absorption maxima at approximately 400 nm and ϵ value of $6.43 \times 10^4 \text{ mol}^{-1} \text{ dm}^3 \text{ cm}^{-1}$ were exhibited by these compounds. The reported activation energies for the *cis-trans* thermal isomerisation of the polymers suggested similar energy barriers to lower molecular weight monomer and polymer analogs. No difference in the activation energies among the different azo-polyureas and the azo monomers were observed. Similar results have been obtained from the studies of the rate of photo-isomerization of highly diluted polymers and their low molecular weight analogs [199-201].

Other interesting properties observed upon incorporation of the azobenzene chromophores into polymers are the changes that result in their geometry [202-204]. For example, the introduction of azobenzene photochromes into the main chain of poly(para-phenylene) backbones, led to changes in the shape of the azo-polymer upon irradiation [205]. The embedded photoswitches acted as hinges, which upon light-induced isomerization led to reversible shrinking and stretching of the polymer backbone. Thus, rigid poly(para-phenylene)s displayed large twist angles along its polyaromatic backbone leading to an 86 % overall *cis* content. Also, the introduction of azobenzene photochromes into the core of spherical dendrimers [206] was reported to result into (quasi)isotropic nano-objects that displayed significant changes in the hydrodynamic volume upon photoirradiation. Moreover, changes in the shape and aggregate size of photoresponsive azo-micelles were also shown [207-211] to result in a photo-induced deformation of the azo-polymeric aggregates leading to clustering effect of the micellar particles [211].

Furthermore, some properties like structural changes [205, 212, 213], solubility changes [214-216], crystallization [204, 217], photoswitchable phase changes [218], and phase separation (or reversal of phase separation) [219] have been observed in many azobenzene incorporated polymers. Also, significant changes in the thermal properties such as the glass-transition temperature (T_g) have been photochemically modulated, causing photoinduced solid-to-liquid transitions [220] and changes in the porosity by the photoisomerization [221].

1.8 Stabilization of *cis-trans* back relaxation of azobenzenes in the dark

Obtaining a bistable *cis/trans* isomers of azobenzene compounds is of significant interest to most researchers, as these allow their application not only in material sciences but also in life sciences, particularly in the field of photopharmacology (the development of drugs that can be activated by light and possibly auto-deactivate over time [222, 223]), and for the control of neuronal activities [224]. *Cis-trans* back conversion in azobenzenes is a photoreaction process that causes the rearrangement of the electronic and the nuclear structure of the molecule without any bond breaking [98]. If the *cis-to-trans* back reaction is induced by visible-light excitation instead of thermal reactions, the formation of phenyl radicals may occur and dediazotation can be observed [225]. This has been shown in the photodecomposition of aliphatic azo compounds [226-229] investigated in both liquid and gas phase, where the major products derived were methyl and substituted methyl radicals and a molecule of nitrogen. Stabilization of the thermal *cis-to-trans* back reaction of azobenzenes has been investigated and established [177, 230, 231] to depend on the chemical architecture of the system; that is the chromophore type [232-234], the type of attachment of groups (polymers, molecules) to the chromophore, glass transition temperature (T_g) and crystallinity of the components attached [177, 230, 231]. Thus, stabilization of the switched *cis* isomer is accomplished mainly by the design of the chromophore used in the photoirradiation process.

Introduction of steric effects like macrocyclic strains [99, 233, 235-244] in azobenzenophanes is one standard strategy employed in stabilizing the *cis* isomer. Very high steric strains in some instances are shown to an extent of even compensating the sterical demand of the *cis*-isomer, which then becomes the thermally most stable isomer. Examples of this steric effect influence on the *cis*-isomer are shown in the photoswitching studies of azobenzenophane, 5,6-dihydrodibenzo[1,2]diazocine bridged by ethylene linker in the ortho position (Figure 7) [240]. The *cis*-isomer after the switch became the thermally most stable form due to the high distortion in the *trans*-isomer. A thermal lifetime of up to 15 h was reported for the *cis*-form (Table 5, entry 2), with switching efficiency of about 90 % of the *cis*-form to *trans*-form using blue light at $\lambda \approx 370$ -400 nm.

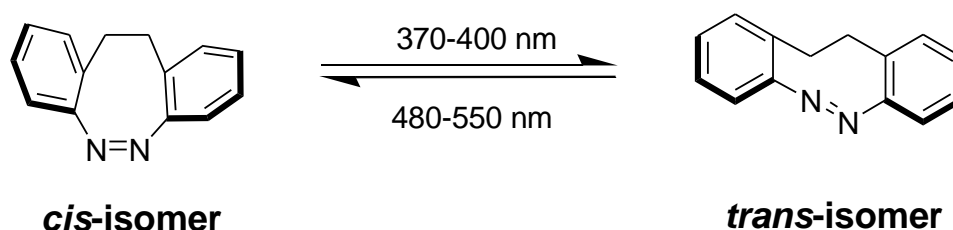


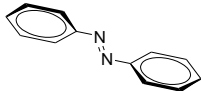
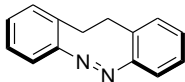
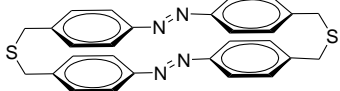
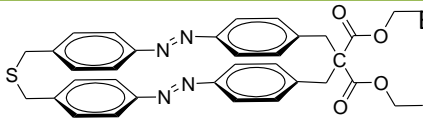
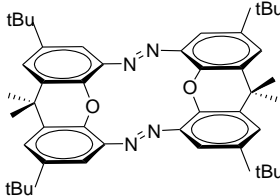
Figure 7. Thermally most stable *cis*-form of azobenzenophane (Figure redrawn from citation [240]).

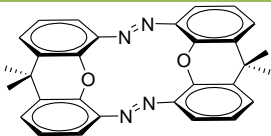
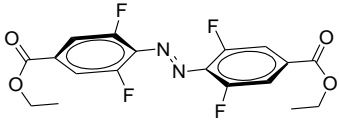
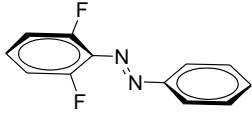
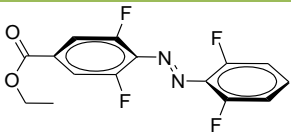
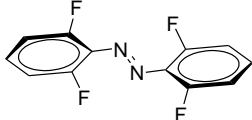
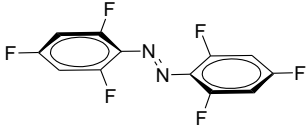
Another interesting example of steric effect stabilization of azobenzenes is also found in the investigations of macrocyclic azobenzenes [99], where a change in the structure of the azobenzenophanes had a strong influence on the stability and photochromism of the synthesized chromophores (Table 5, entry 3-4). Two macrocycle azobenzenophanes with different tethers were prepared; one macrocycle bridged by two thioether tethers and the other modified macrocycle consisting of malonic acid ester containing a C_3 linker and one thioether linker. The unmodified macrocycle showed shorter *cis* half-life (within days),

whiles the modified macrocycle showed half-life of over one year. A nearly 100 % photochemical *trans* to *cis* conversion was achieved upon irradiation at 366 nm. With this complete photochemical conversion and high stability of both isomers, the system was suitable and satisfied the requirements for optical storage devices. Moreover, photoinduced molecular hinges [233, 236, 241] where the (*trans*, *trans*)-isomer showed a flat geometry, with the (*cis*, *cis*)-isomer showing a bent structure with an angle of 112° was also shown to stabilize the *cis* isomer upon switching (Table 5, entries 5-6). The bent (*cis*, *cis*)-isomer was found to be exceptionally stable with a lifetime of 6.4 years. The lifetime of the intermediate mixed isomer (*trans*, *cis*)-isomer was however found to be only 2.73 min as a result of the high distortion between mixed (*trans*, *cis*) conformers.

Stabilization of the *cis*-isomer via electronic effects is one other strategy employed in recent times to obtain *cis*-isomers with longer lifetimes. Half-lives of about two years for the *cis*-isomer has been measured at room temperature for some F₄-azobenzenes [109, 205, 212, 213, 245]. Many experimentalists [109, 205, 212, 213, 245] have utilized this chromophore in several materials and life science applications to proof the *cis*-isomers of the F-azobenzenes to stabilize from hours to days depending on the attached functional groups to the chromophore and the number of the F-atoms on the chromophore. The higher the number of the F-atoms, the more stabilized the *cis*-isomer observed (Table 5, entries 7-11). A pure unmodified azobenzene (Table 5, entry 1) was reported to have a *cis* half-life of 4 h, which was observed to increase to 25 h upon introducing only two fluorine atoms on the aromatic benzene ring (Table 5, entry 8). The stabilization effect even increased further from 92 h to 95 h after introducing four and six fluorine atoms respectively, proving a strong influence by fluorine electrons on the stabilization of the generated *cis*-isomer.

Table 5. Thermal half-lives ($t_{1/2}$) of the *cis*-isomers of different stabilized azobenzenes.

Entry	Azobenzene structure	Solvent and wavelength for <i>trans</i> -to- <i>cis</i> conversion	Half-life ($t_{1/2}$) <i>cis</i> -form
1 [245]		MeCN, $\lambda = 365$ nm	4 h
2 [240]		n-hexane, $\lambda = 480$ -550 nm	15 h
3 [99]		Benzene, $\lambda = 365$ nm	5 days
4 [99]		Benzene, $\lambda = 365$ nm	1 year
5 [236, 241]		Chloroform, $\lambda = 366$ nm	>14 days

6 [233]		Toluene, $\lambda = 366 \text{ nm}$	6.4 years
7 [205, 212, 213, 245]		MeCN, $\lambda > 500 \text{ nm}$	15 h
8 [205, 212, 213, 245]		MeCN, $\lambda > 500 \text{ nm}$	25 h
9 [205, 212, 213, 245]		MeCN, $\lambda > 500 \text{ nm}$	30 h
10 [205, 212, 213, 245]		MeCN, $\lambda > 500 \text{ nm}$	92 h
11 [205, 212, 213, 245]		MeCN, $\lambda > 500 \text{ nm}$	95 h

2.0 SCOPE OF THESIS

2.1 Aim of the work

The overall aim of this work is to investigate crystallization in designed homo- and copolymers. To this endeavour, various azobenzene functionalized copolymers, and supramolecular block copolymers were designed and synthesized for the purpose of crystallization studies. In general, the introduction of an organic molecule or another polymer to a crystalline polymer is expected to have a high impact on the crystallization behavior. This effect will be critically looked at in this thesis, focusing on the final crystal structural inclusion, and morphology in block copolymers. The thesis is also targeted at understanding the switching dynamics of reversible *cis-trans* isomerisation of azobenzene polymers in solution and in the solid state.

For the crystallization studies two different types of polymers, azobenzene copolymers, and supramolecular block copolymers, with distinctive molecular weights are aimed to be synthesized. Azobenzenes are selected as the constituent co-units to react with a polymer to explore the role of the reversible *cis-trans* isomerisation of the final functionalized polymers in solution and in the solid state. Different synthetic methods and conditions are required to achieve the designed products in an efficient process. An elaborative characterization of the products will be performed via spectroscopic methods. Once the accuracy of the structures is confirmed, further investigations can be conducted to monitor their thermal behavior as well as other physical properties (photoswitching, relaxation).

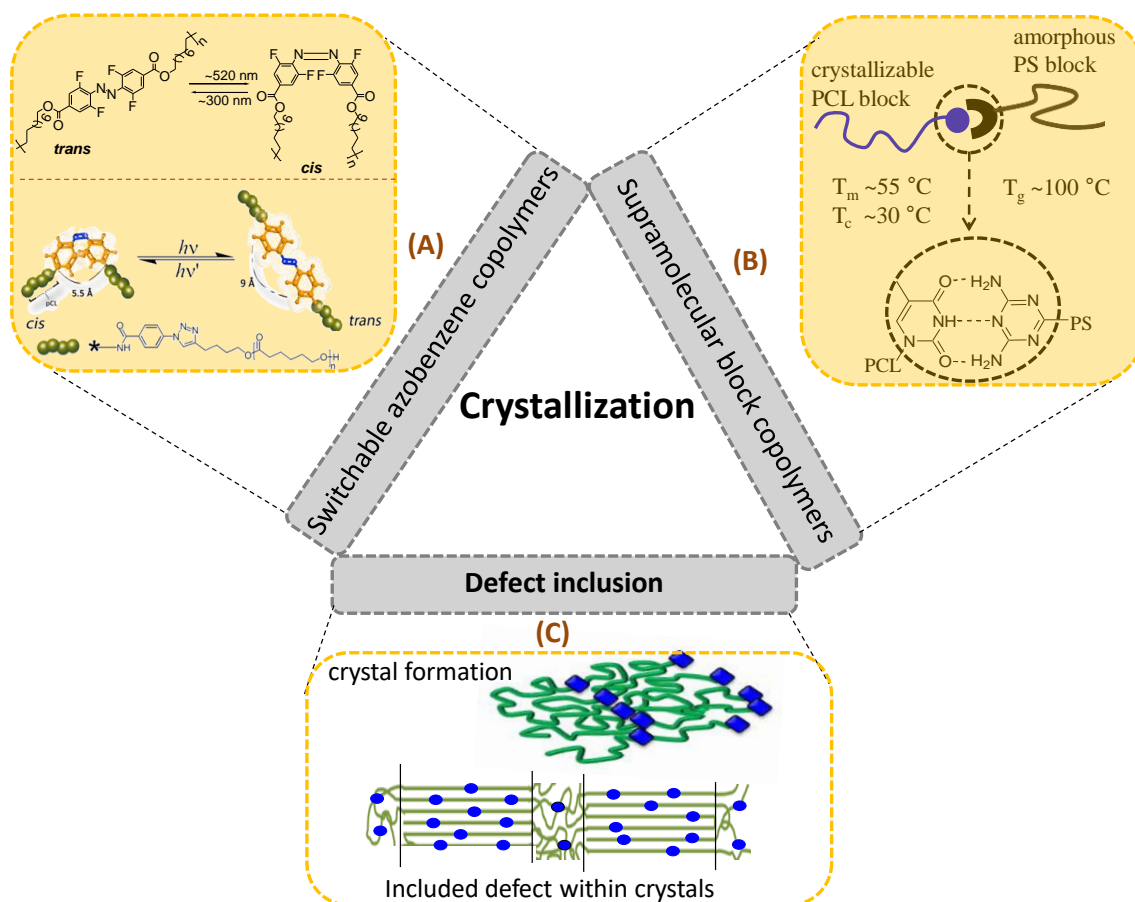


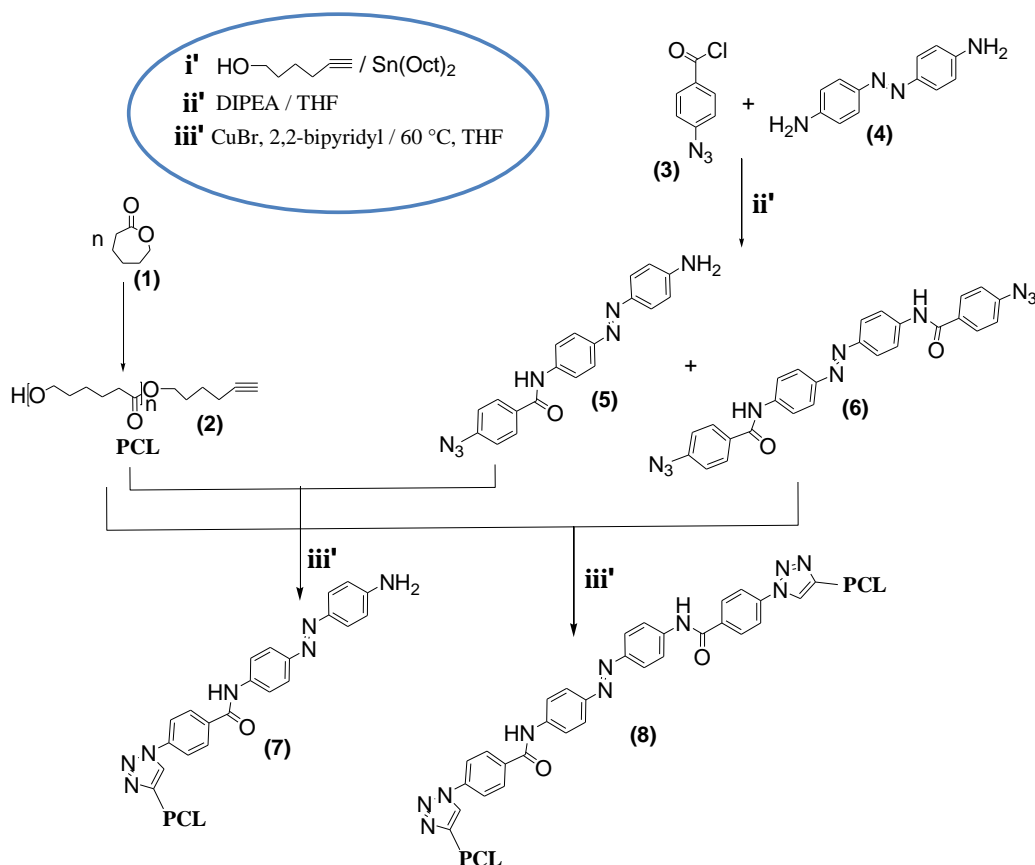
Figure 8. Schematic representations of the structure of the designed azobenzene copolymers (A), supramolecular block copolymers (B), and defect inclusion of designed azobenzene polymers (C)

Also, the supramolecular combination of one crystallizable (PCL) and one amorphous (PS) block, reversibly bound together, is an entirely new system with attractive mechano-physical properties. The special feature of this system is that due to the very high glass transition temperature of poly(styrene) (PS, $T_g \approx 100\text{ }^\circ\text{C}$) this block is considered as hard barrier, which should serve as a restrictive block on the PCL crystallization.

2.2 Concept

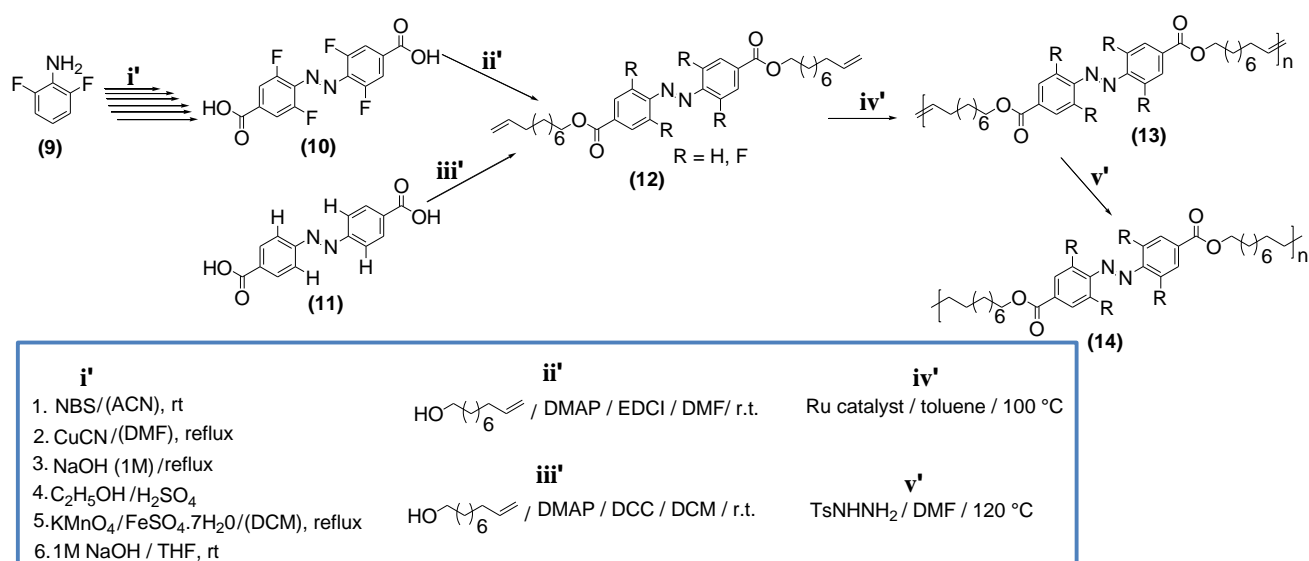
As already described in the aim, the thesis encompasses the design and synthesis of azobenzene-functionalized copolymers and supramolecular block copolymers that will be used for crystallization studies. For this purpose reminiscent poly(ethylene) (obtained from ADMET polymerization), poly(ϵ -caprolactone) (from ROP), and poly(styrene) (from ATRP) with different molecular weights were chosen as polymers for the crystallization studies. The synthetic concept of this research consists of two main parts: synthesis of azobenzene copolymers; poly(ϵ -caprolactone)-based azobenzenes, precision ADMET poly(ethylene)-based azobenzenes and synthesis of supramolecular block copolymers; poly(ϵ -caprolactone)-b- poly(styrene).

Part 1: synthesis of azobenzene copolymers; poly(ϵ -caprolactone)-based azobenzenes and precision ADMET poly(ethylene)-based azobenzenes



Scheme 2.1: General pathway toward the synthesis of the designed poly(ϵ -caprolactone)-based azobenzenes

Scheme 2.1 illustrates the possibility through which a post-functionalization of a polymer (**2**) with azobenzene chromophores (**5**, **6**) can be achieved via “azide-alkyne click chemistry,” resulting in the azobenzene copolymers (**7** and **8**).

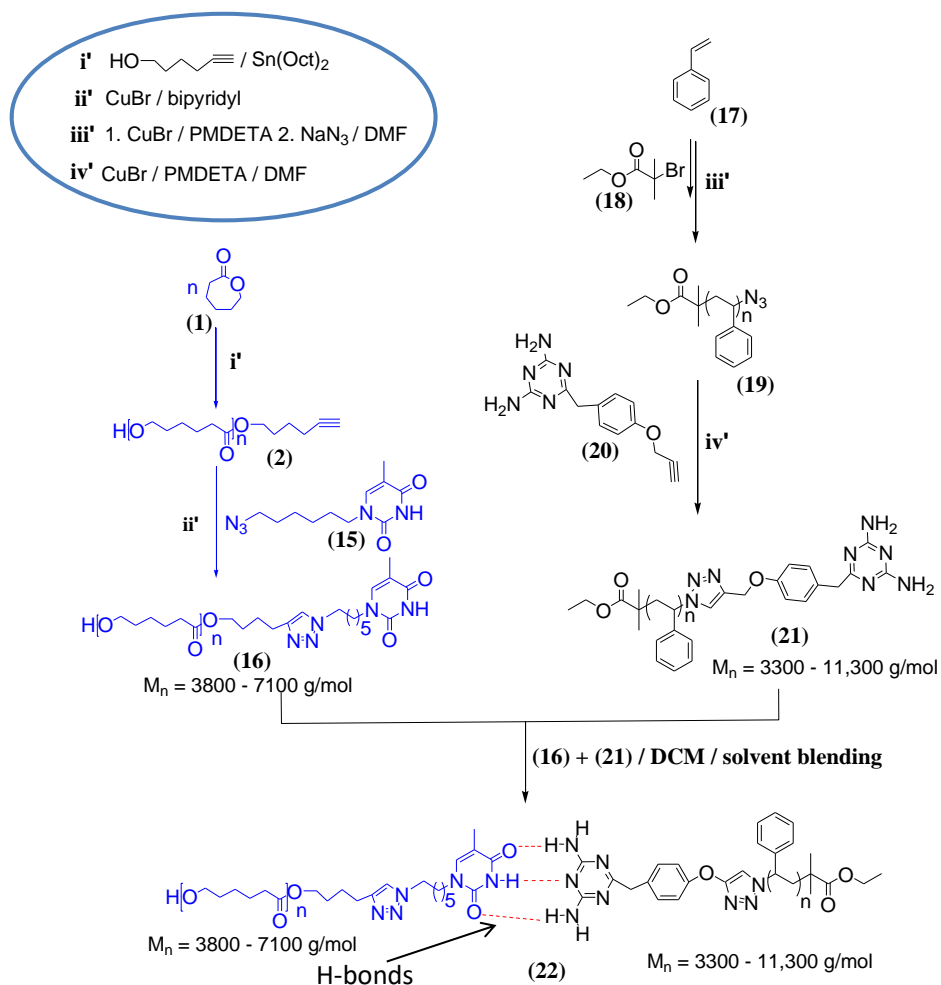


Scheme 2.2: General pathway toward the synthesis of the designed precision ADMET poly(ethylene)-based azobenzenes

Scheme 2.2 illustrates the proposed pathway for designing a polymer with an expected sharper recycling of the cis/trans isomerisation of the azobenzene units. Azobenzene copolymers (**14**) were obtained following the direct polymerization of a symmetric α,ω -azobenzene diene (**12**) via ADMET, to obtain polymers with precisely placed azobenzene moieties in the olefin chains of the polymer (**13**). The ADMET approach circumvents the random nature of branching in polyethylene with the elimination of chain transfer processes. Importantly, the design of the symmetrical α,ω -azobenzene diene monomer obviates the ethylene comonomer reactivity ratio problems and ensures the precise placement of defects (azobenzenes) along the polymer chain. Preparations of unsaturated copolymers, where both the identity of the defect and its position are known without equivocation, are achieved via this approach. Subsequent hydrogenation of the copolymers with *p*-toluenesulfonylhydrazide should yield fully saturated azobenzene copolymers (**14**) that will be used for the crystallization studies.

The results of this part of the thesis can be found in the first to third section of the Result and Discussion part dealing with the “Click chemistry” promoted post-functionalization of a polymer unto an azobenzene chromophore unit (Appiah, C.; Siefertmann, K. R.; Jorewitz, M.; Barqawi, H.; Binder, W. H., RSC Adv. 2016, 6 (8), 6358-6367), direct polymerization approach of a symmetric α,ω -azobenzene dienes (Appiah, C.; Woltersdorf, G.; Binder, W. H., Polym. Chem. 2017, 8, 2752-2763) and crystallization studies of the precisely placed azobenzene copolymers (Appiah, C.; Woltersdorf, G.; Pérez-Camargo R. A.; Müller A. J.; Binder, W. H., Eur. Polym. J. 2017, *accepted*).

Part 2: synthesis of supramolecular block copolymers; poly(ϵ -caprolactone)-*b*- poly(styrene)



Scheme 2.3. General pathway toward the synthesis of the designed of supramolecular block copolymers; poly(ϵ -caprolactone)-*b*- poly(styrene)

Supramolecular block copolymers having one amorphous block (PS) and one semi-crystalline block (PCL) were synthesized for the purpose of studying the crystallization behavior of the semi-crystalline PCL polymer. As depicted in Scheme 2.3, to obtain such supramolecular block copolymers it was necessary to insert an alkyne moiety to the selected PCL chains, which was carried out via the design of the initiator in the polymerization reaction (**i'**) to yield polymers with alkyne moieties. Meanwhile, the amorphous PS block was synthesized via ATRP and functionalized with sodium azide to obtain an azido-functionalized PS-block (**19**). All synthesized products were characterized by means of NMR spectroscopy. The accuracy of the structures was proven via MALDI-ToF Ms measurements. The synthesized polymers were subsequently modified with different organic compounds (thymine (**15**) and 2,4-diaminotriazine (**20**) via azide/alkyne click reactions (**ii'** and **iv'**). A solvent blending of the two functionalized polymers at room temperature yielded the supramolecular block copolymers (**22**). Furthermore, the supramolecular block copolymers were subjected to SAXS, POM and DSC measurements to study their crystallization behaviors. The results of this part of the thesis can also be found in the fourth section of the Result and Discussion part dealing with supramolecular hydrogen bonding interactions between the PCL and PS blocks (Appiah, C.; Akbarzadeh, J.; Peterlik, H.; Binder, W. H., Eur. Polym. J. 2015, 64 (0), 138-146).

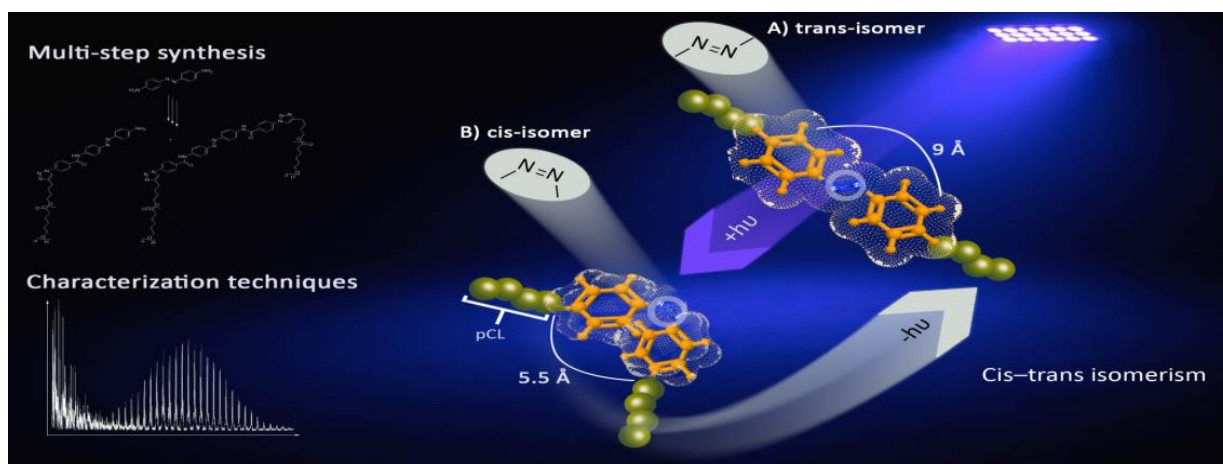
3.0 RESULTS AND DISCUSSION

3.1 Synthesis and Characterization of new Photoswitchable Azobenzene-containing poly(ϵ -caprolactones).

Appiah Clement^a, Katrin R. Siefermann^b, Marcel Jorewitz^b, Haitham Barqawi^a, and Wolfgang H. Binder^{*a}

^aInstitute of Chemistry, Chair of Macromolecular Chemistry, Faculty of Natural Science II (Chemistry, Physics and Mathematics), Martin-Luther University Halle-Wittenberg, Halle (Saale) D-06120, Germany.

^bLeibniz-Institute of Surface Modification, Permoserstrasse 15, Leipzig, Germany.



RSC Adv., 2016, 6, 6358

Abstract: A novel and efficient strategy in obtaining series of mono- and bi-armed azobenzene-containing poly(ϵ -caprolactone)s is described, starting from a commercially available azobenzene dye via azide/alkyne-"click"-reactions. The attachment of alkyne-telechelic poly(ϵ -caprolactone)s (1 kDa and 3 kDa), followed by chromatographic separation allowed the attachment of either one or two PCL-chains to either side of the azobenzene-dye. The resulting mono- and bi-armed photo-switchable polymers are fully characterized by 2D-NMR techniques and show a high thermal stability. In particular, liquid chromatography at critical conditions (LCCC) coupled to ESI-TOF allowed to prove presence of either one or two polymer chains affixed onto the central azobenzene dye.

Introduction

Polymeric based molecular switches have recently attracted much interest due to their wide range of applications ranging from nanomedicine such as affinity separations, enzyme recovery and drug delivery [1,2] to industrial applications including storage [3] and communication elements in optical devices [4]. The output of such a photoresponsive polymeric materials

mainly depends on a complex interplay between the chromophores [5] (e.g. an azobenzene dye), the morphology of the polymeric network (amorphous, semicrystalline and liquid crystalline) [3a], the thermomechanical properties of the material (glassy or rubbery state modulus), and the molecular geometry of the sample [6]. Thus, e.g. reversible solubility of azobenzene polymers [7] or reversible contractions of

thin films [8] (see also e.g. the work of Eisenbach [9] and Blair [10]) have been reported, stressing the importance of photochemically switchable polymers. The photoresponsive properties of azobenzene-containing polymers are based on the photo-induced fast and reversible isomerization between *trans*- and *cis*-isomers of the azobenzene moiety upon exposure to UV or visible light, which can trigger significant changes in the physicochemical properties of the corresponding polymeric materials [11-13]. Similar to C=C double bonds, the azobenzenes display two geometric isomers (*cis* and *trans*) around the N=N double bond [14], where the *trans* isomer is the more stable isomer. Isomerization to the *cis*-isomer is accomplished upon irradiation at a wavelength of ~320-350 nm. Due to the reversibility of this reaction, the *trans*-isomer can be easily recovered by irradiating the *cis*-isomer at a wavelength of 400-450 nm or via pure thermal relaxation [14]. These two photochemical reactions usually occur on picoseconds scales, while the thermal relaxation from *cis*- to *trans*-isomer is much slower (milliseconds to days) [15-17]. It is important to mention that after the photo-isomerization process, characteristic changes in the physical properties of the two isomers affect the molecular geometry and the dipole moment of the dye [15, 16]. Thus the attachment of polymeric chains onto the azobenzene in consequence leads to additional effects of the optoelectronic and relaxation properties of the dye [18, 19] often influenced by the value of the chemical linkage between the azo-dye and the polymer chain [19]. It has been demonstrated that the linkage between the azo chromophore and the polymer backbone can restrict both, the molecular mechanical properties and the motion of the azo-groups [20]: polymers linked via a rigid attachment to the azo chromophore can confine both, the chromophore's motion and its subsequent re-orientation, but also can induce an increased stability of the formed *cis*-isomer after the light has been turned off [20]. A large number of publications has been dealing

with the influence of the polymeric chains on the physicochemical properties of the azo moiety [21-23], such as an elongation of the *cis*-lifetime [24, 25]. Lamarre and Sung [25] have studied the physical ageing and molecular motion of azochromophoric labels attached to the main chain poly(urethane)s, showing a lifetime of 4 days after switching to the *cis*-form. Furthermore, the conformational strain of macrocyclic azo compounds has also been used to lock the *cis* form for days [24, 26]. Intermolecular interactions, such as hydrogen bonds to generate cyclic structures can also lead to largely increased lifetimes of the *cis*-form of up to ~40 days [27].

Several synthetic strategies have so far been reported in obtaining azobenzene polymers either via the direct polymerization of a monovinyl azo monomer [28, 29], or via a postfunctionalization of a polymer onto an azo-dye [2b, 30]. Based on this methodology both, side-chain [31] and main-chain [32] azobenzene polymers have been prepared, resulting in different architectures like block- [32,33], brush- [34, 35], star- [36] and dendritic- [37-39] polymers. Besides a direct polymerization of suitable monomers, the subsequent attachment of azobenzenes onto polymer matrices [40, 41] or the covalent attachment of polymers onto azobenzenes [42, 43] has been reported. Despite the many reported methodologies, not always the expected polymers were obtained [44-46], often due to some setbacks in their preparation and purification.

We hereby report an efficient strategy in preparing a series of azobenzene containing poly(ϵ -caprolactone)s by chemical modification of a commercially available azobenzene dye into poly(ϵ -caprolactone) backbone with different molecular weights (see Fig. 1). The chemical separations and purification of the resulting azobenzene polymers are described in details.

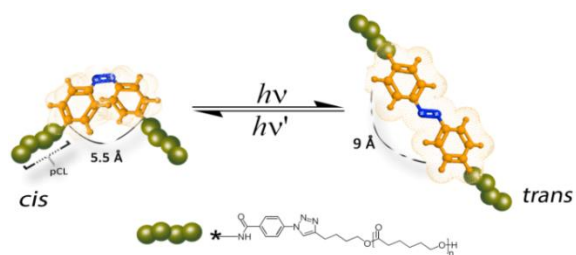


Figure 1. Isomerization of azobenzene polymers

Experimental

Materials

All chemicals used for the synthesis were purchased from Sigma-Aldrich and CHEMOS chemicals. ϵ -Caprolactone was stirred and distilled over calcium hydride (100 °C, 10 mbar). Tin(II)-2-ethylhexanoate and 5-hexyn-1-ol were also purified via the distillation procedures in the literature [47, 48]. Cu(I)Br was stirred for 2 days in acetic acid/anhydride, washed with dry diethyl ether several times, and dried *in vacuo* under an argon atmosphere. *N,N*-Diisopropylethylamine (DIPEA), *N,N*-dicyclohexylcarbodiimide (DCC), *N,N*-dimethylamino-4-pyridine (DMAP) and 2,2'-bipyridine were used without further purification. Tetrahydrofuran (THF) was predried over sodium hydroxide (NaOH) for several days followed by heating over sodium/benzophenone and final distillation under an argon atmosphere before use.

Measurements

NMR spectroscopy was recorded on a Varian Gemini 2000 FT-NMR spectrometer (400 MHz). Chloroform (99.8 atom % D) and dimethyl sulfoxide-d₆ (99.9 atom % D) were used as solvents, using MestrecC software version 4.7.0.0 for the FIDs analysis. Chemical shifts (δ) were recorded in parts per million (ppm) and referenced to residual protonated solvent (CDCl₃: 7.26 ppm (¹H), 77.0 ppm (¹³C), (CD₃)₂SO: 2.54 ppm (¹H), 39.52 ppm (¹³C); coupling constants (J) are given in Hertz (Hz) using standard abbreviations (s = singlet, d = doublet, t = triplet, m = multiplet).

GPC measurements were conducted on a Viscotek GPCmax VE 2001 with a Styragel linear column GMHHR. THF was used as a carrier solvent at 1 mL/min at room temperature. The sample concentration was approximately 3 mg/mL. Poly(styrene) standards (in the range of 1050-1,870,000 g/mol) were used for conventional external calibration, using a Waters RI 3580 refractive index detector at 35 °C.

FTIR spectra were recorded with a Bruker Vertex70MIR spectrometer using an ATR Golden Gate unit with a diamond crystal. The scan number was 32 scans per spectrum with a resolution of 2 cm⁻¹.

MALDI-TOF-MS was done on a Bruker Autoflex III Smartbeam using a nitrogen laser source ($\lambda = 337$ nm) in reflection and linear modes. The polymer samples were dissolved in THF at a concentration of 20 mg/mL; 1,8,9-anthracenetriol in THF (20 mg/mL) was used as matrix material; sodium trifluoroacetate (NaTFA) in THF (20 mg/mL) was used as salt. The solutions of the polymer, the matrix, and the salt were mixed in a volume ratio of 100:20:2 and 2 μ L of this mixture were spotted on the MALDI target plate. The instrument was calibrated with a poly(ethylene glycol) standard ($M_p = 2000$ g/mol) using a quadratic calibration method.

ESI-TOF MS measurements were carried out on a Bruker Daltonics microgel time-of-flight LC-MS system. Spectra were recorded in a positive mode with an accelerator voltage of 4.5 kV, a transfer line with 190 °C and a scan range of 50-7000 m/z at the spectral rate of 1 Hz. The spectra were processed on Bruker Daltonics ESI compass 1.3 for microTOF (Data Analysis 4.0). Samples were prepared by dissolving 1-5 mg of the respective compound in 1 ml mixture of THF/methanol (92/8).

HPLC measurements were performed on Elite LaChrom HPLC, Hitachi VWR, equipped with an autosampler, a quaternary gradient pump, a degasser, a diode array detector (UV-DAD) operating at 190 – 900 nm and a column oven with temperature control (temperature = 20 °C). Temperatures were maintained constant (± 0.2 °C) throughout all experiments, and the injected sample

volume was 30 μ L. Liquid chromatography at critical conditions (LCCC) was carried out on a non polar reversed-phase Atlantis-RP C18 column, 100 \AA , 5 μ m, dimension 4.6 \times 250 mm; methanol/DCM = 8/92 was used as the mobile phase with a flow rate of 0.30 mL/min. The DAD signals were recorded on EZchrom Elite software version 3.3.2 SP2 with an operating wavelength from 190 to 900 nm at a sampling width of 200 ms to obtain sufficient data points across peaks.

Synthesis of alkyne-functionalized PCL (PCL-alkyne).

Alkyne-functionalized PCL was prepared via coordination insertion ring opening polymerization (ROP) using ϵ -caprolactone as a monomer, 5-hexyn-1-ol as an initiator, and tin(II) 2-ethylhexanoate ($\text{Sn}(\text{Oct})_2$) as a catalyst according to the literature^[246]. Briefly, a Schlenk flask was carefully dried by heating (500 $^\circ\text{C}$), purged with argon, cooled down, charged with the initiator 5-hexyn-1-ol (55 μ L, 5.0×10^{-4} mol), adding the catalyst tin (II) 2-ethylhexanoate (6.0×10^{-6} mol, 2 μ L), and a solvent mixture of 3 mL toluene and 1 mL THF. This mixture was stirred at room temperature for 30 min to promote the complex formation between catalyst and initiator. Afterward, the solution was treated with ϵ -caprolactone (3 mL, 0.026 mol) and stirred at 110 $^\circ\text{C}$ for 3h. Finally, the product was dissolved in dry DCM (10mL) and precipitated into cold methanol (150 mL), filtered off and dried under vacuum overnight.

$^1\text{H-NMR}$ (400 MHz, CDCl_3 , δ , ppm, PCL-alkyne3, DP = 29): 4.04 (t, 59H, J = 6.7 Hz), 3.63 (t, 2H, J = 6.5 Hz), 2.28 (t, 59H, J = 6.7 Hz), 1.94 (t, 1H, J = 2.6 Hz), 1.65 (m, 118H), 1.38 (m, 59H). $^{13}\text{C-NMR}$ (100 MHz, CDCl_3 , δ , ppm, PCL-alkyne3): 173.4, 64.1, 34.1, 28.3, 25.5, 24.4.

Synthesis of 4-(azidobenzamido)-4'-(amino)azobenzene (2) and 4,4'-bis(benzamido) azobenzene (3)

To a solution of 4,4'-bis(amino)azobenzene (1) (1 mol eq.) and DIPEA (2.2 mol eq.) in THF at 0 $^\circ\text{C}$ was added 4-azidobenzoyl chloride (3 mol eq.) dissolved in THF. The mixture was stirred for 30 min, and finally warmed to

room temperature with constant stirring for 24 h. The obtained crude product was filtered and purified via column chromatography (DCM / ETOAc 3:1, Rf values: 4,4'-bis(benzamido) azobenzene = 0.82, 4-(azidobenzamido)-4'-(amino)azobenzene = 0.61).

Alternatively [49] into a dried and nitrogen purged flask was added a solution of 4-azidobenzoic acid (2 mol eq.) and DCC (1 mol equiv.) in THF (5 ml). The mixture was stirred for 6 h at 0 $^\circ\text{C}$ to form bis-azidobenzoic anhydride. In a second dried round bottom flask a solution of 4,4'-bis(amino)azobenzene (1 mol equiv.) and DMAP (0.5 mol equiv.) in THF (5 ml) were added. The two solutions were then mixed and stirred at room temperature for 48 h. The obtained crude product was purified in a similar fashion as the previous method.

$^1\text{H-NMR}$ (400 MHz, DMSO, δ , ppm, 2): 10.42, (s, 1H), 8.04 (d, 2H, J = 8.03 Hz), 7.93 (d, 2H, J = 8.23 Hz), 7.76 (d, 2H, J = 8.30 Hz), 7.63 (d, 2H, J = 8.81 Hz), 7.28 (d, 2H, J = 8.02 Hz), 6.66 (d, 2H, J = 8.12 Hz), 6.00 (s, 2H). $^{13}\text{C-NMR}$ (100 MHz, DMSO, δ , ppm, 2): 165.0, 152.9, 148.8, 143.3, 140.8, 131.6, 130.2, 125.3, 122.8, 120.9, 119.5, 113.9.

$^1\text{H-NMR}$ (400 MHz, DMSO, δ , ppm, 3): 12.95, (s, 2H), 7.95 (d, 8H, J = 8.35 Hz), 7.20 (d, 4H, J = 8.48 Hz), 5.58 (d, 4H, J = 8.03 Hz). $^{13}\text{C-NMR}$ (100 MHz, DMSO, δ , ppm, 3): 207.0, 157.1, 131.6, 119.5.

IR (cm^{-1} , 3): 3385.8, 3074.8, 2989.9, 2811.2, 2703.9, 2407.8, 2119.8, 1649.9, 1601.9, 1420.5, 1345.1, 1313.2, 1180.0, 1129.4, 1098.1, 1067.9, 1037.7, 930.6, 851.2, 822.5, 773.8, 689.5, 570.5.

Synthesis of 4-(poly(ϵ -caprolactone)-benzamido)-4'-(amino)azobenzene (polymer-1a and polymer-1b) and 4,4'-bis (poly (ϵ -caprolactone)-benzamido)azobenzene (polymer-2a and polymer-2b)

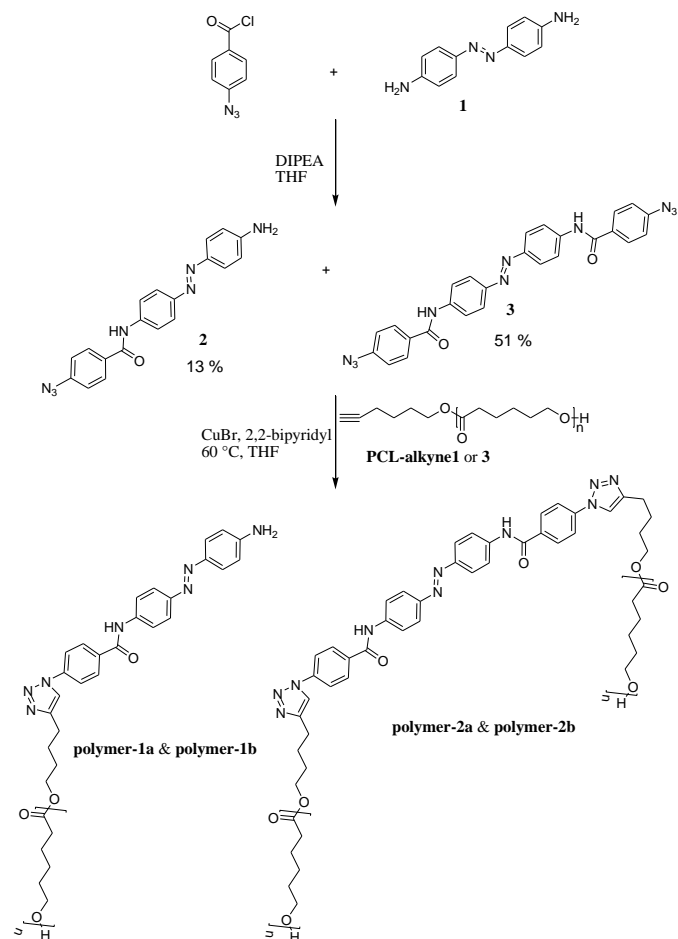
The functionalization of PCL with 4-(azidobenzamido)-4'-(amino)azobenzene and 4,4'-bis(benzamido) azobenzene was conducted via an azide/alkyne click-reaction, using 2,2'-bipyridine as base and $\text{Cu}(\text{I})\text{Br}$ as a catalyst. The reaction was accomplished in a one-necked flask carefully dried and purged with argon. Alkyne-

functionalized PCL (**PCL-alkyne**) (1 mol equiv) and azide-functionalized azobenzene dyes (4 mol equiv.) were dissolved in 6 mL of dry THF, then a solution of 2,2'-bipyridyl (20 mol equiv) in dry THF (2 mL) was added via a syringe and the mixture was degassed with argon for 30 min to remove oxygen. Subsequently, a catalytic amount of Cu(I)Br (1 mol equiv) was weighed into the flask. The flask was closed with a septum, and the mixture was degassed again with argon for another 30 min. The reaction proceeded for 24 h by stirring at 80 °C. Afterwards, the reaction mixture was cooled down to room temperature and the product was purified by chromatography via a silica gel packed column (ethyl acetate:DCM 1:3). The crude product was dissolved in 10 mL of DCM, slowly added into methanol (200 mL) and left overnight for complete precipitation. The precipitation step was repeated two more times to completely remove the excess of the azide-functionalized azobenzene dyes and the 2,2'-bipyridine, which are all well soluble in methanol. The pure products were filtered off and dried under vacuum for 3 days (yields: **1a** = 71 %, **1b** = 75 %, **2a** = 50 % and **2b** = 58 %)

¹H-NMR (400 MHz, DMSO, δ, ppm, **polymer-1b**): 10.55, (s, 1H), 8.70, (s, 1H), 8.17 (d, 2H, J = 8.03 Hz), 8.07 (d, 2H, J = 8.23 Hz), 7.96 (d, 2H, J = 8.30 Hz), 7.77 (d, 2H, J = 8.81 Hz), 7.64 (d, 2H, J = 8.02 Hz), 6.66 (d, 2H, J = 8.12 Hz), 6.00 (s, 2H), 4.30 (t, 2H, J = 6.5 Hz), 3.98 (t, 65H, J = 6.7 Hz), 3.28 (t, 2H, J = 6.4 Hz), 2.74 (t, 2H, J = 6.1 Hz), 2.24 (t, 65H, J = 6.7 Hz), 1.54 (m, 130H), 1.28 (m, 65H).

¹H-NMR (400 MHz, DMSO, δ, ppm, **polymer-2b**): 8.58, (s, 4H), 8.08 (m, 8H), 7.85 (m, 8H), 4.32 (t, 4H, J = 6.0 Hz),

3.94 (t, 238H, J = 5.9 Hz), 3.31 (m, 4H), 2.72 (m, 4H), 2.24 (t, 238H, J = 6.7 Hz), 1.54 (m, 476H), 1.28 (m, 238H).
IR (cm⁻¹, **2b**): 3475.6, 2945.9, 2866.1, 2439.6, 1802.6, 1727.9, 1646.4, 1451.1, 1344.6, 1315.4, 1185.5, 1108.6, 1044.1, 963.1, 812.9, 741.7.



Scheme 1. Synthetic approach for the modified azobenzenes (**2** and **3**) and the polymer incorporated azobenzenes (**polymer-1** and **polymer-2**).

Table 1. Results of the synthesis of PCL-alkynes and the PCL-functionalized azobenzenes

Samples	M_n (NMR) (g/mol)	DP ^a (NMR)	M_n (GPC) (g/mol) ^b	M_w/M_n (GPC)	Yield ^c (%)
PCL-alkyne1	1111	9	985	1.2	95
PCL-alkyne3	3306	29	2900	1.1	98
polymer-1a	1920	9	1700	1.4	71
polymer-1b	3800	29	3220	1.2	75
polymer-2a	2850	18	2500	1.4	50
polymer-2b	7200	58	7100	1.1	58

^aDegree of polymerization obtained via NMR spectroscopy, ^bCorrected molecular weight from GPC (correction factor = 0.59), ^cIsolated yields after purification

Results and Discussion

Synthesis of photoswitchable PCL-azobenzene polymers

Conceptually, we planned to address possible synthetic strategies for obtaining switchable mono-functional polymers (**polymer-1**) and bi-functional polymers (**polymer-2**) via a grafting-to approach by “click-chemistry” (see Scheme 1). For this purpose, polymerization of ϵ -caprolactone using a coordination insertion ring opening polymerization[246] method was carried out as described in the experimental section. Subsequently, the polymers were attached to azido functionalized azobenzene dyes via the azide/alkyne “click” reaction [50-51]. The developed synthetic route is presented in Scheme 1. The first step for the synthesis of the photoswitchable polymeric compounds was an

amidation reaction between a commercially available azobenzene dye (**1**) and 4-azidobenzoylchloride in the presence of a base (DIPEA) to yield a mono-substituted 4-(azidobenzamido)-4'-(amino)azobenzene (**2**) and a di-substituted 4,4'-bis(benzamido) azobenzene (**3**). Click-chemistry between the dyes (**2** and **3**) and an already synthesized PCL-alkyne (Table 1) with varying molecular weights (1000 g/mol and 3000 g/mol) were performed in THF to yield the products (**polymer-1a**, **polymer-1b**, **polymer-2a** and **polymer-2b**) respectively. After several purification techniques including column chromatography, precipitation, extraction, the final purified products were characterized using HPLC, ESI-TOF-MS, MALDI-TOF-MS, IR, ¹H-NMR, ¹H-¹H-COSY NMR and GPC techniques.

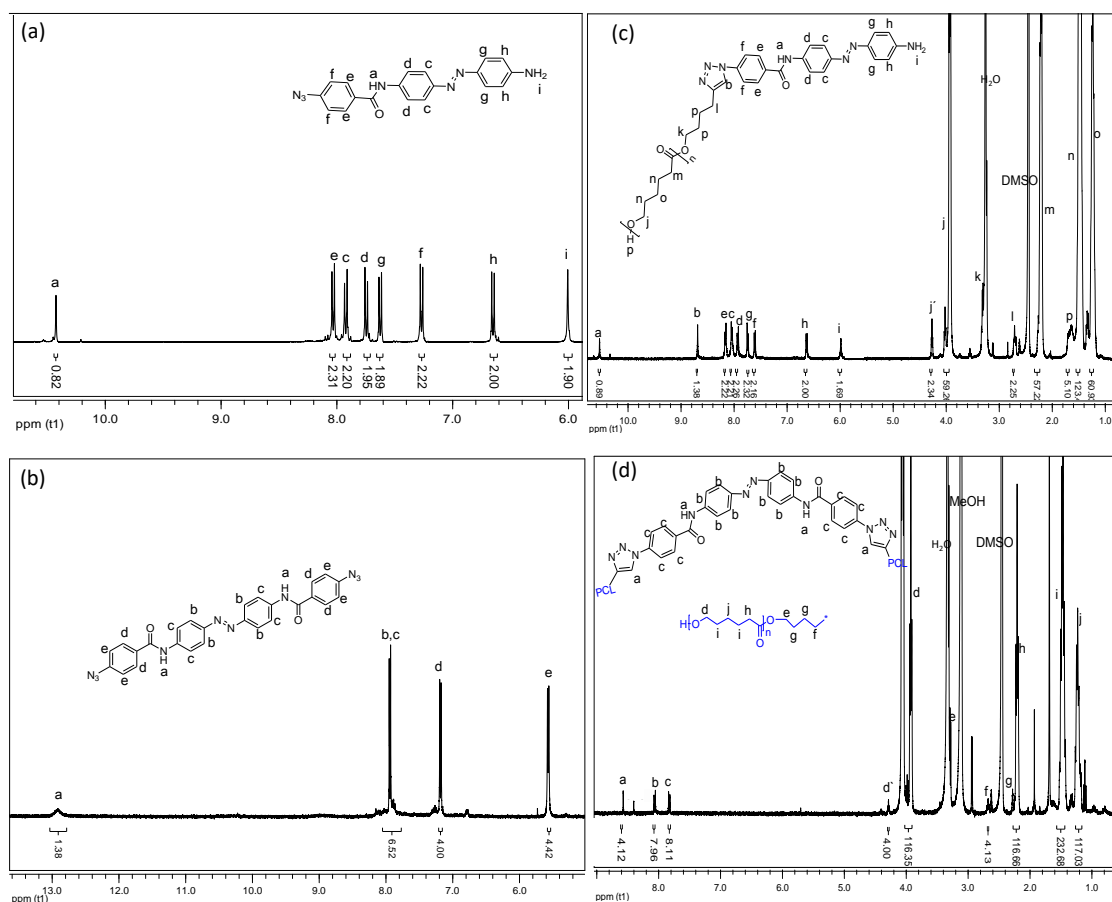


Figure 2. $^1\text{H-NMR}$ spectra of all the synthesized compounds; a) 4-(azidobenzamido)-4'-(amino) azobenzene (**2**), b) 4,4'-bis(benzamido) azobenzene (**3**), c) 4-(poly(ϵ -caprolactone)-benzamido)-4'-(amino)azobenzene (**polymer-1b**), d) 4,4'-bis(poly(ϵ -caprolactone)-benzamido)azobenzene (**polymer 2b**).

Characterization of the photoswitchable PCL-azobenzenes

The structures of all the photoswitchable PCL-azobenzenes were initially confirmed by GPC and $^1\text{H-NMR}$. The GPC curves were monomodal with molecular weight distributions of 1.2-1.4. Figure 2 shows the $^1\text{H-NMR}$ spectra of the synthesized compounds including the photoswitchable PCL-azobenzenes. All compounds showed the expected resonances in the NMR spectroscopy. Importantly the molecular weights from GPC and NMR of the photoswitchable PCL-azobenzenes matched well, proving a complete

endgroup transformation of the compounds (Table 1).

The degree of the end functionalization was obtained by comparing the intensity of the signal 'h' and signal 'j' for the case of the mono-armed photoswitchable **polymer-1** and the peaks 'd' and 'c' for the bi-armed photoswitchable **polymer-2**. The result showed the completeness of the 'click' chemistry. The structures were further confirmed by FTIR spectroscopy (supporting information), in which the vibration peaks of $-\text{OH}$ and $-\text{NH}-$ (the broad peak at around 3475 cm^{-1}) both shifted to higher wavenumbers compared to their starting precursors ($< 3300\text{ cm}^{-1}$).

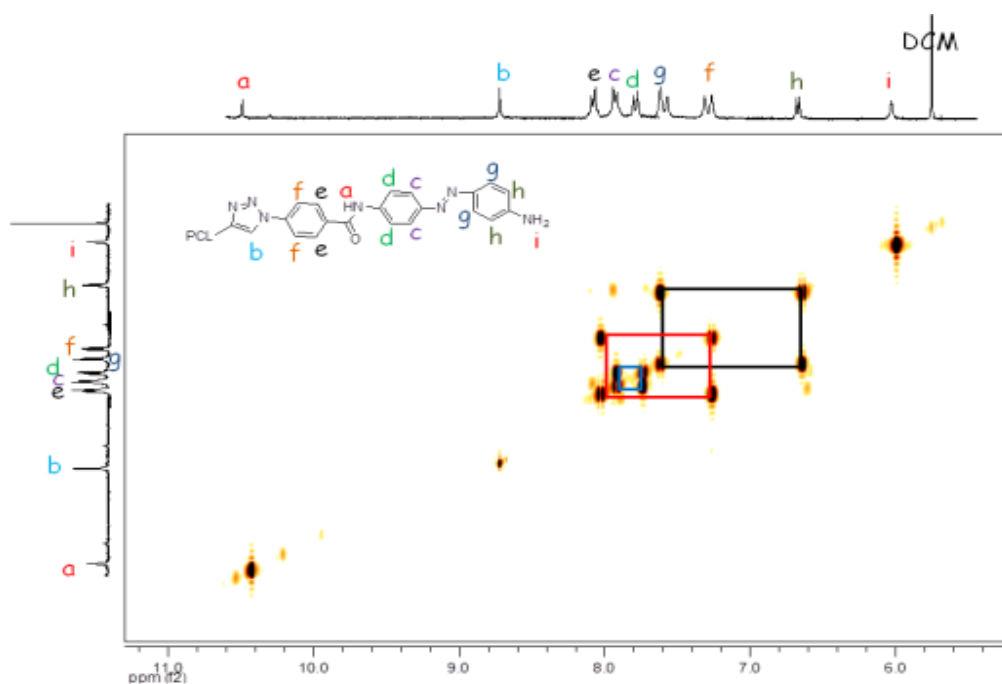


Figure 3. Expanded proton homonuclear correlated 2-dimensional ^1H - ^1H COSY NMR of polymer-1b.

Two-dimensional H/H COSY NMR analysis of the photoswitchable azobenzene polymers

Based on the complexity of the photoswitchable PCL-azobenzene polymers, we conducted 2D-NMR techniques, including ^1H - ^1H COSY NMR. Figure 3 shows the proton homonuclear correlated 2-dimensional ^1H - ^1H COSY NMR of **polymer-1b**. The backbone azobenzene moiety of this photoswitchable polymer could be traced through its J-coupling [52]. In the H,H-COSY of **polymer-1b**, a long-range coupling by arrangement of protons are observed between the doublet at 7.77 ppm (2H, $J = 8.81$ Hz) and the doublet at 6.66 ppm (2H, $J = 8.12$ Hz). The upfield shifted benzylic doublet is assigned to the protons *ortho*- to the amide functionality (i.e., 2H, signal-e) whereas the low field *doublet* is assigned to the protons *ortho*- to the amine group (i.e., 2H, signal-h).

The aromatic benzylic protons are associated to their neighboring protons via a 1,3 bond with a strong J-coupling distance of about ~ 8.03 Hz. Protons a, b and i are being separated by their neighboring protons via a weak 1,4 bonding interaction and therefore show a very weak coupling effect, thus, appearing as singlet in the spectrum. While the coupling behavior of the mono-armed **polymer-1** is well observable in the COSY spectrum, the bi-armed polymers (**polymer-2**) are significantly more difficult to resolve. The signals appear as multiplets instead of individual doublet structures (see Figure 2d and supplementary). The COSY correlations helped to precisely assign the protons of the compounds observed in the 1-dimensional ^1H -NMR especially in the mono-armed polymers and to further confirm the obtained structures (Fig. 4).

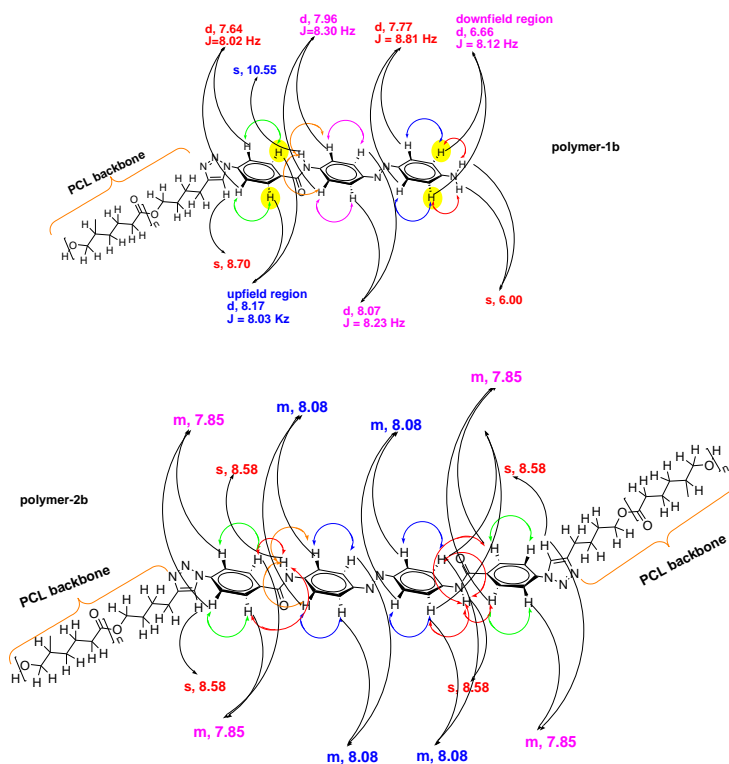


Figure 4. Main 2D-H/H-COSY correlations of polymer-1b and polymer-2b. The colored double headed arrows represent the long and short range couplings of protons from the H,H-COSY analysis, with the red ones showing the weak 1,4 coupling interactions.

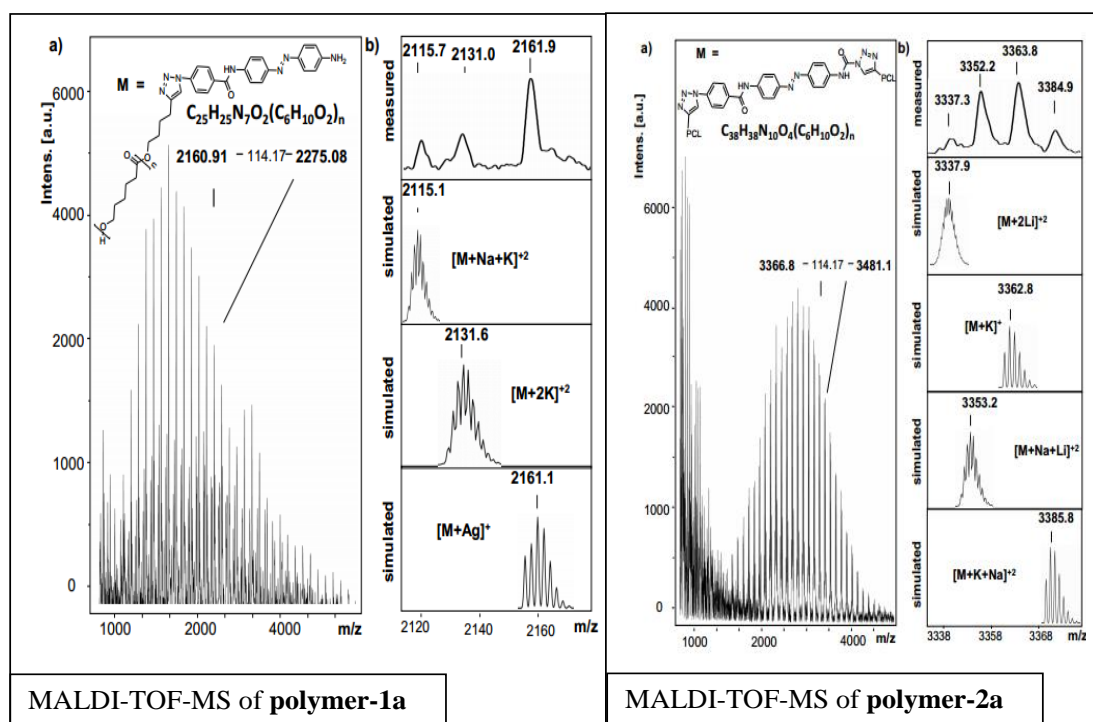


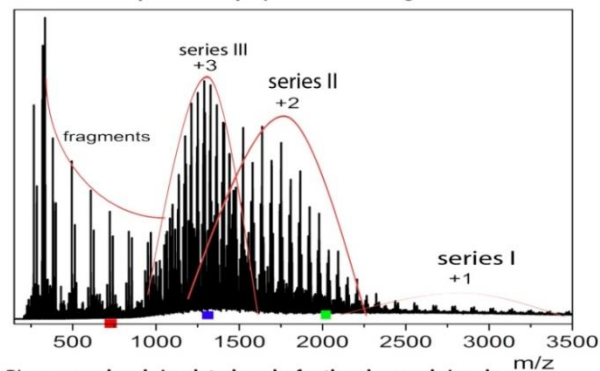
Figure 5. (a) Full MALDI-TOF-MS spectrum of polymer-1a and polymer-2a and (b) measured and simulated patterns of different series observed.

MALDI-TOF MS and ESI-TOF MS analysis of the photoswitchable azobenzene polymers.

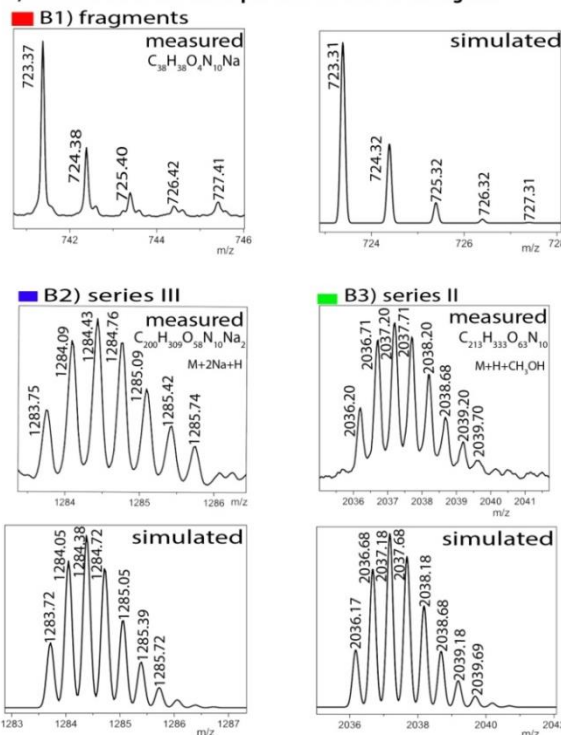
In order to prove the expected chemical composition of the photoswitchable polymers, a straight forward MALDI-TOF-MS analysis was conducted. Figure 5, depicts the MALDI-TOF spectra of the photoswitchable polymers. Three main series are observed for **polymer-1a**, while **polymer-2a** shows four series. Each series shows a difference of 114 units, corresponding to the PCL repeating unit and is observed to be PCL containing the photoswitchable azobenzene dye moiety with different ions attached. According to Figure 5 the signal appearing at 2161.9 g/mol can be simply assigned to a PCL containing the photoswitchable dye moiety with the chemical formula $[C_{109}H_{165}N_7O_{30}Ag]^+$ (with $n = 14$), while the signal at 2131.0 g/mol can be represented by $[M+2K]^{+2}$. The signal at 2115.7 g/mol is also identified by the chemical formula $[M+Na+K]^{+2}$.

However, to fully proof the structures being presented in scheme 1, we embarked on ESI-TOF MS investigations to further support the chemical composition of the two photoswitchable polymers. Figure 6 and Figure S12 (supplementary information) show detailed spectra of all the different series of **polymer-1a** and **polymer-2a**. Whereas the monofunctional **polymer-1a** shows a single charged state, the bifunctional **polymer-2a** shows multiple charged states (+1, +2 and +3 ions). All the observed peaks were successfully simulated to match to the corresponding species. Thus e.g. the isotopic peaks of **polymer-2a** at m/z value of 723.37 g/mol correspond to fragments generated during the analysis (see supplementary information for the fragmented structures).

A) full ESI-TOF spectrum of polymer-2a, showing the various series



B) measured and simulated peaks for the observed signals



*the distance between serial peaks suggested CL units
series I: similar structures as shown for series II and III

Figure 6. ESI-TOF MS spectra of the bifunctional photoswitchable polymer-2a, showing the observed and simulated signals.

The isotopic peak at $m/z = 2036.20$ g/mol with a charge state of +2 is observed to correspond to the species $[M+H+CH_3OH]^{+2}$, while the molecular ions peak at $m/z = 1283.75$ g/mol is identified as the high charge state of +3, corresponding to the species $[M+2Na+H]^{+3}$. The proof of an existence of a purely mono-armed polymer (**polymer-1**) and a bi-armed polymer (**polymer-2**) was evident from the presence of one detected 1,2,3-triazole group (C_2HN_3) and two detected 1,2,3-triazole groups

($2C_2HN_3$) for **polymer-1** and **polymer-2** respectively. From the measured and simulated pattern results, it was obvious that the ESI-TOF analysis truly confirmed the structures of the compounds being presented.

One-Dimensional Liquid Chromatography (SEC and HPLC) and UV-VIS investigations

SEC analysis

The photoswitchable polymers as well as the alkyne-functionalized PCL samples were examined using conventional size exclusion chromatography (calibrated against PS standards) and HPLC analysis at LCCC conditions [53] (methanol:DCM = 8:92). Figure 7 shows the GPC traces of the photoswitchable **polymers -1b** and **-2b** as well as the alkyne-functionalized PCL precursors (**PCL-alkyne3**). The peak maximum of the polar sample **polymer-1b** shifted slightly towards higher retention time ($R_t = 8.12$ min) compared to the retention time of **polymer-2b** ($R_t = 7.74$ min). The symmetric monomodal distribution nature of the curves with different retention times, coupled to an exact match of the M_n values from NMR and GPC allowed the conclusion that the investigated samples were highly pure and were void of contaminants from their starting precursors.

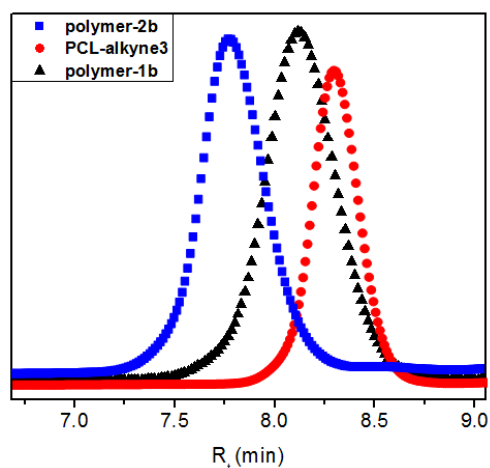


Figure 7. SEC traces of PCL-alkyne3, polymer-1b and polymer-2b.

HPLC analysis Chromatographic techniques involving HPLC analysis at critical conditions [247] [248] for the

attached PCL-chains (methanol:DCM = 8:92, using non polar reverse phase Atlantis-RP C18 column) were furthermore conducted to confirm the purity of the obtained compounds, mainly to prove whether the structures presented in Scheme 1 were truly void of contaminants from their starting precursors and also not a mixture of the respective mono- and bi-substituted products. Figure 8 shows the HPLC separation chromatogram of **polymer-1b** and **-2b**, as well as their starting precursors (**2** and **3**). The elution peaks of both **polymer-1b** and **polymer-2b** are well separated from each other. **Polymer-2b** elutes at a retention time of 10.2 min, 2.7 min higher than the retention time of **polymer-1b**. This difference is basically due to the PCL-unit being attached to the both ends of **polymer-2b**. Thus, incorporation of the PCL group onto both ends of **polymer-2b** reduces its polarity and hence leads to increased interaction within the Atlantis column, thereby resulting in higher retention times. The elution times of the polymers with similar functionalities (e.g. **polymer-2a** and **-2b**) were nearly the same, proving the LCCC conditions at these experiments.

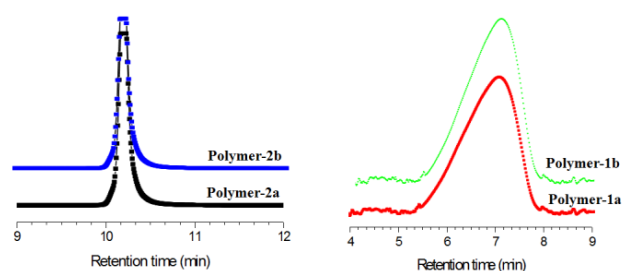


Figure 8. LC-UV traces analysis of the purified PCL-azobenzene polymers at LCCC conditions.

LC/ESI-TOF MS analysis. Gradient elution profile technique was also developed to characterize the azobenzene polymers (Figure 9). This technique involves the coupling of a liquid chromatography (LC) at LCCC conditions to an ESI-TOF MS source [53, 54]. Thus the LC method separates the polymers based on their

functionality at a specific retention time. The separated polymers subsequently enters directly into the ESI-TOF MS source for detailed structure elucidation: if mixtures with the polymers should be present (thus, e.g. possible contaminants in the case of our investigated samples or mixtures of bi-armed and mono-armed samples and azobenzene compounds **1**, **2** and **3**), then different peaks from the LC chromatogram should result, leading to a mixture of different structures in the ESI-TOF MS spectrum and thus a more complex spectrum.

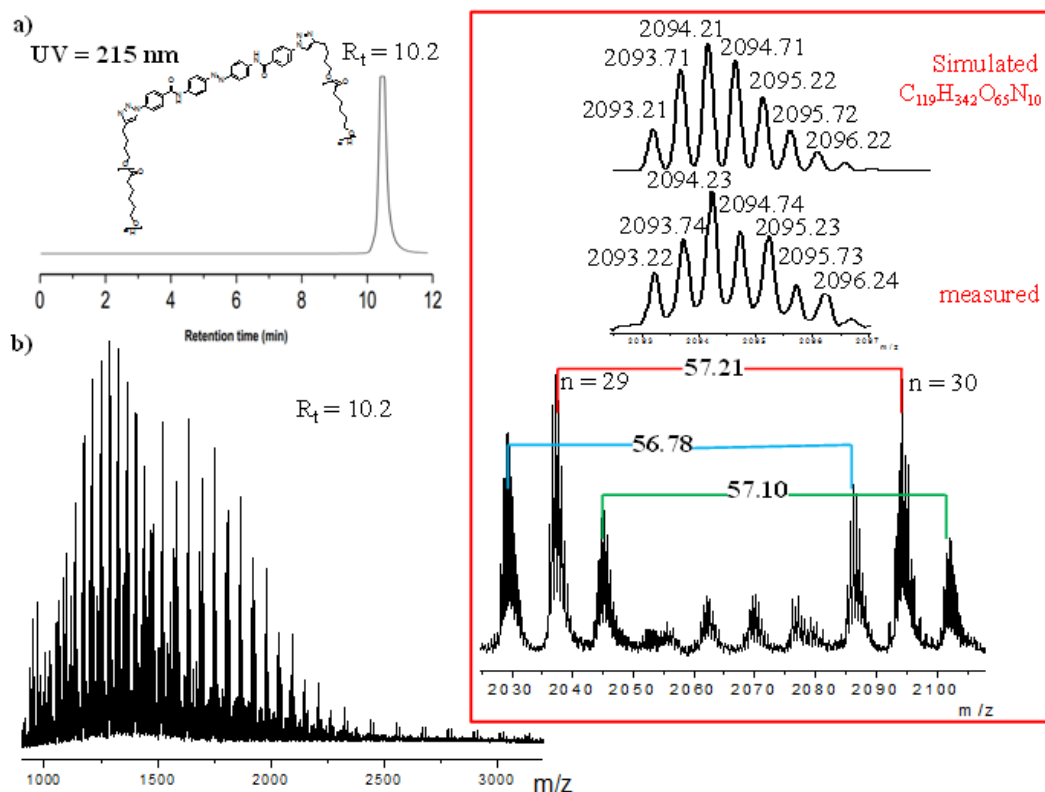


Figure 9. (a) LC-ESI-TOF-MS of polymer-2a indicating the purity of the sample. (b) Comparison between the measured and simulated isotopic pattern of a doubly charged species ($R_t = 10.2$ min) proving the final structure. However, in the case of e.g. **polymer-2a**, one observes a single LC chromatogram (Figure 9a) and the recorded ESI-TOF MS spectrum (Figure 9b), demonstrating a functionality distribution of the polymer with repeating units of 114 g/mol, 57 g/mol and 38 g/mol assigned to a singly, doubly and triply charged desorbed ion states respectively. In all peaks of the ESI-TOF only one species, indicative of the bifunctional structure of **polymer-2a** could be detected.

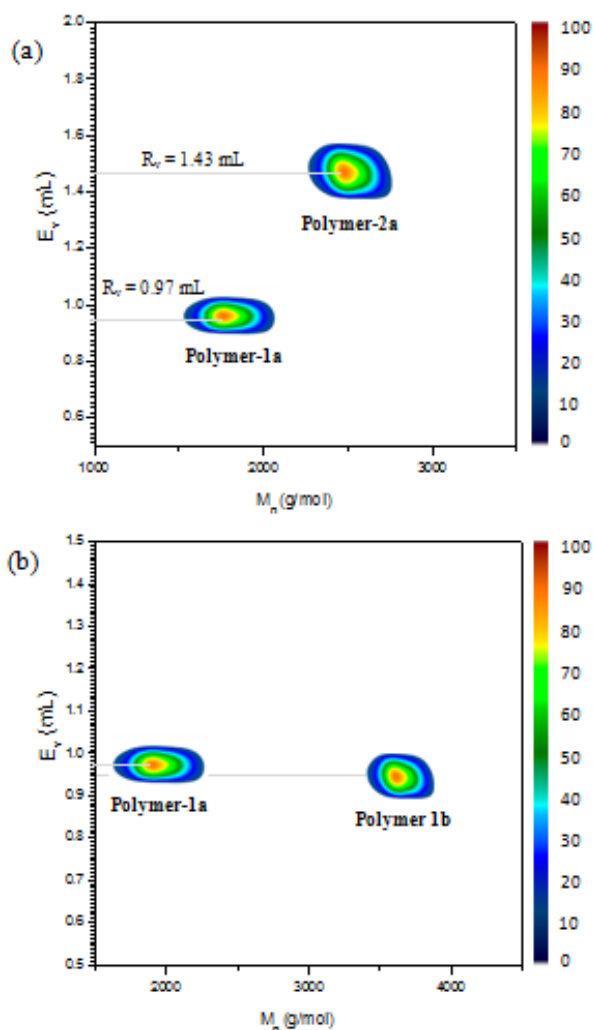


Figure 10. 2D LC/SEC plots of (a) polymer-1a and polymer-2a showing separation based on their functionalities and (b) polymer-1a and polymer-2a with similar endgroup functionalities showing no noticeable changes in their LC-retention volumes, but a significant difference in their molecular weight in SEC.

Multidimensional chromatography (2D-LC/ SEC) of the photoswitchable polymers.

2D LC/SEC experiments were also conducted on the azobenzene polymers (see Figure 10) with different molecular weights and end group functionalities. Figure 10b shows the experiments on **polymer-1a** and **-1b**, having similar end group functionalities but different molecular weights. Thus on the LC-trace one observes nearly equal elution volume for the two polymers at

~0.97 mL retention volume. This shows the experiments are under LCCC conditions and the retention times of the polymers at this point are independent on the molecular masses. Thus changes in the functionalities of the compounds should be the only means to result in a noticeable shift in the 2D contour diagram. Hence a comparison between **polymer -1** and **-2** having different endgroup functionalities should result in a significant change in the retention times. Figure 10a shows a comparison of **polymer-1a** and **-2a** having different endgroup functionalities. The experiments unveiled a complete separation of the two photoswitchable polymers based on their functionality type distributions. Thus, as **polymer-1a** elutes at retention volume of 0.97 mL, **polymer-2a** elutes at 1.43 mL retention volume, which clearly indicates that the two polymers were different in terms of their functionalities and also proves the structures presented in scheme 1 to be pure and void of contaminants from each other.

Conclusion

We here report a simple and efficient synthesis to obtain mono- and bi-armed azobenzene-containing polymers using "click" chemistry. The mono- and bi-armed PCL-azobenzene polymers were synthesized using the copper catalyzed azide-alkyne Huisgen cycloaddition reactions, attaching different molecular weights, ranging from 1000 g/mol to 7000 g/mol, onto the azobenzene-backbone. The structure of the mono- and bi-armed polymers was proven via chromatographic techniques (HPLC under LCCC-conditions, LC/ESI-TOF MS) as well as 2D H/H COSY NMR experiments, also proving the purity of all of the samples and the excellent separation of the mono-armed polymers (**polymer 1**) from the bi-armed polymers (**polymer 2**). The investigated samples showed a significant thermal stability, when compared to their starting PCL-alkyne precursors.

Acknowledgements

The authors express thanks for Grant SFB TRR 102 (CA, WHB) (Project A03) for financial support

References

- Jochum, F. D.; Theato, P. *Chem. Soc. Rev.* **2013**, *42*, 7468.
- Jochum, F. D.; zur Borg, L.; Roth, P. J.; Theato, P. *Macromolecules* **2009**, *42*, 7854.
- (a) García-Amorós, J.; Velasco, D. *Beilstein J. Org. Chem.* **2012**, *8*, 1003.
(b) Fang, L.; Zhang, H.; Li, Z.; Zhang, Y.; Zhang, Y.; Zhang, H. *Macromolecules* **2013**, *46*, 7650.
- Moller, S.; Pliquet, U.; Hoffmann, C. *RSC Adv.* **2012**, *2*, 4792.
- Yu, H. *J. Mater. Chem. C* **2014**, *2*, 3047.
- Lee, B. K. M.; Koerner, H.; Wang, D. H.; Tan, L.-S.; White, T. J.; Vaia, R. A. *Macromolecules* **2012**, *45*, 7527.
- Irie, M.; Tanaka, H. *Macromolecules* **1983**, *16*, 210.
- Agolini, F.; Gay, F. P. *Macromolecules* **1970**, *3*, 349.
- Eisenbach, C. D. *Polymer* **1980**, *21*, 1175.
- Blair, H. S.; Pague, H. I.; Riordan, J. E. *Polymer* **1980**, *21*, 1195.
- Li, X.; Wen, R.; Zhang, Y.; Zhu, L.; Zhang, B.; Zhang, H. *J. Mater. Chem.* **2009**, *19*, 236.
- Weber, C.; Liebig, T.; Gensler, M.; Pithan, L.; Bommel, S.; Bléger, D.; Rabe, J. P.; Hecht, S.; Kowarik, S. *Macromolecules* **2015**, *48*, 1531.
- Yager, K. G.; Barrett, C. J. *J. Photochem. Photobiol. A: Chem.* **2006**, *182*, 250.
- (a) Stuart, C. M.; Frontiera, R. R.; Mathies, R. A. *J. Phys. Chem. A* **2007**, *111*, 12072.
(b) Fanghänel, D.; Timpe, G.; Orthman, V. In *Organic Photochromes*; El'tsov, A. V., Ed.; Consultants Bureau: New York, **1990**; chap. 3.
- Yager, K. G.; Barrett, C. J. *RSC* **2008**, 424.
- Cembran, A.; Bernardi, F.; Garavelli, M.; Gagliardi, L.; Orlandi, G. *J. Am. Chem. Soc.* **2004**, *126*, 3234.
- Crecca, C. R.; Roitberg, A. E. *J. Phys. Chem. A* **2006**, *110*, 8188.
- Barrett, C.; Natansohn, A.; Rochon, P. *Chem. Mater.* **1995**, *7*, 899.
- Kumar, G. S.; Neckers, D. C. *Chem. Rev.* **1989**, *89*, 1915.
- Meng, X.; Natansohn, A.; Rochon, P. *J. Polym. Sci. Part B: Polym. Phys.* **1996**, *34*, 1461.
- Kim, H.-K.; Wang, X.-S.; Fujita, Y.; Sudo, A.; Nishida, H.; Fujii, M.; Endo, T. *Macromol. Rapid Comm.* **2005**, *26*, 1032.
- Lambeth, R. H.; Moore, J. S. *Macromolecules* **2007**, *40*, 1838.
- Lomadze, N.; Kopyshev, A.; Rühle, J.; Santer, S. *Macromolecules* **2011**, *44*, 7372.
- Norikane, Y.; Kitamoto, K.; Tamaoki, N. *J. Org. Chem.* **2003**, *68*, 8291.
- Lamarre, L.; Sung, C. S. P. *Macromolecules* **1983**, *16*, 1729.
- Nagamani, S. A.; Norikane, Y.; Tamaoki, N. *J. Org. Chem.* **2005**, *70*, 9304.
- Vollmer, M. S.; Clark, T. D.; Steinem, C.; Ghadiri, M. R. *Angew. Chem. Int. Ed. Engl.* **1999**, *38*, 1598.
- Ho, M. S.; Barrett, C.; Paterson, J.; Esteghamatian, M.; Natansohn, A.; Rochon, P. *Macromolecules* **1996**, *29*, 4613.
- Natansohn, A.; Rochon, P.; Pezolet, M.; Audet, P.; Brown, D.; To, S. *Macromolecules* **1994**, *27*, 2580.
- Wang, X.; Balasubramanian, S.; Kumar, J.; Tripathy, S. K.; Li, L. *Chem. Mater.* **1998**, *10*, 1546.
- Gallot, B.; Fafiotte, M.; Fissi, A.; Pieroni, O. *Macromol. Rapid Comm.* **1996**, *17*, 493.

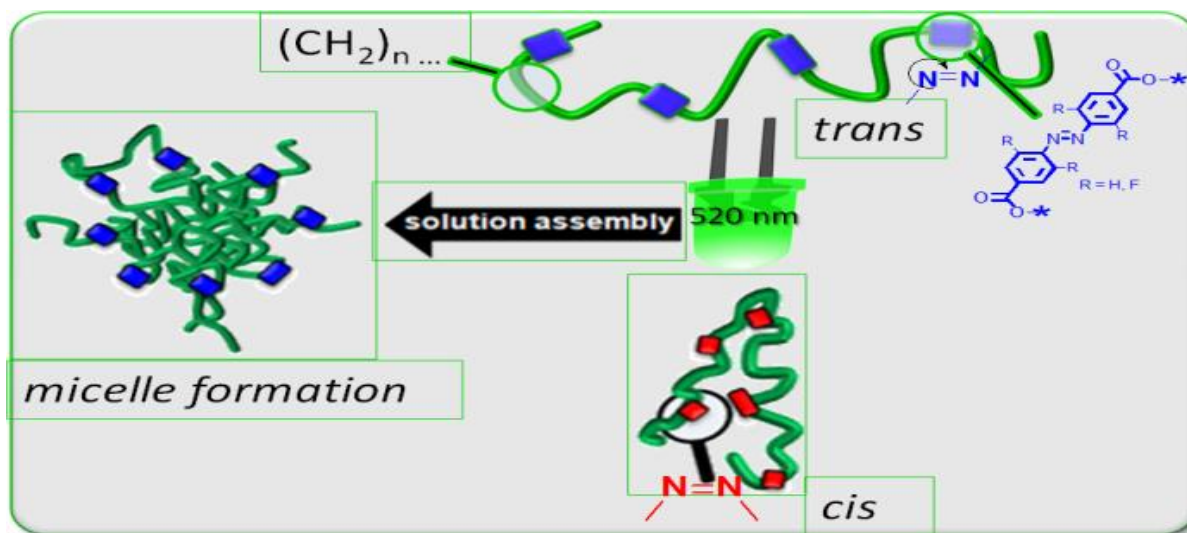
- 32 Viswanathan, N. K.; Yu Kim, D.; Bian, S.; Williams, J.; Liu, W.; Li, L.; Samuelson, L.; Kumar, J.; K. Tripathy, S. *J. Mater. Chem.* **1999**, *9*, 1941.
- 33 Meng, X.; Natansohn, A.; Barrett, C.; Rochon, P. *Macromolecules* **1996**, *29*, 946.
- 34 Sisido, M.; Ishikawa, Y.; Itoh, K.; Tazuke, S. *Macromolecules* **1991**, *24*, 3993.
- 35 Sisido, M.; Ishikawa, Y.; Harada, M.; Itoh, K. *Macromolecules* **1991**, *24*, 3999.
- 36 Campbell, V. E.; In, I.; McGee, D. J.; Woodward, N.; Caruso, A.; Gopalan, P. *Macromolecules* **2006**, *39*, 957.
- 37 Momotake, A.; Arai, T. *Polymer* **2004**, *45*, 5369.
- 38 del Barrio, J.; Oriol, L.; Alcalá, R.; Sánchez, C. *Macromolecules* **2009**, *42*, 5752.
- 39 Ma, H.; Liu, S.; Luo, J.; Suresh, S.; Liu, L.; Kang, S. H.; Haller, M.; Sassa, T.; Dalton, L. R.; Jen, A. K. Y. *Adv. Funct. Mater.* **2002**, *12*, 565.
- 40 Birabassov, R.; Landraud, N.; Galstyan, T. V.; Ritcey, A.; Bazuin, C. G.; Rahem, T. *Appl. Opt.* **1998**, *37*, 8264.
- 41 Lagugné Labarthe, F.; Buffeteau, T.; Sourisseau, C. *J. Phys. Chem. B* **1998**, *102*, 2654.
- 42 Shinkai, S.; Minami, T.; Kusano, Y.; Manabe, O. *J. Am. Chem. Soc.* **1983**, *105*, 1851.
- 43 Willner, I.; Rubin, S. *Angew. Chem. Int. Ed. Engl.* **1996**, *35*, 367.
- 44 Yu, X.; Luo, Y.; Deng, Y.; Yan, Q.; Zou, G.; Zhang, Q. *Eur. Polym. J.* **2008**, *44*, 881.
- 45 Xu, C.; Wu, B.; Becker, M. W.; Dalton, L. R.; Ranon, P. M.; Shi, Y.; Steier, W. H. *Chem. Mater.* **1993**, *5*, 1439.
- 46 Irie, M.; Schnabel, W. *Macromolecules* **1981**, *14*, 1246.
- 47 Oostas, E.; Schröter, K.; Beiner, M.; Yan, T.; Thurn-Albrecht, T.; Binder, W. H. *J. Polym. Sci. Part A: Polym. Chem.* **2011**, *49*, 3404.
- 48 Appiah, C.; Akbarzadeh, J.; Peterlik, H.; Binder, W. H. *Euro. Polym. J.* **2015**, *64*, 138.
- 49 Mespouille, L.; Vachaudéz, M.; Suriano, F.; Gerbaux, P.; Coulembier, O.; Dege'e, P.; Flammang, R.; Dubois, P. *Macromol. Rapid Commun.* **2007**, *28*, 2151.
- 50 Barqawi, H.; Binder, W. H. *J. Polym. Sci. Part A: Polym. Chem.* **2010**, *48*, 4855.
- 51 Stojanovic, A.; Appiah, C.; Dohler, D.; Akbarzadeh, J.; Zare, P.; Peterlik, H.; Binder, W. H. *J. Mater. Chem. A* **2013**, *1*, 12159.
- 52 Baptiste, B. t.; Douat-Casassus, C. I.; Laxmi-Reddy, K.; Godde, F. d. r.; Huc, I. *J. Org. Chem.* **2010**, *75*, 7175.
- 53 Barqawi, H.; Oostas, E.; Liu, B.; Carpentier, J.-F.; Binder, W. H. *Macromolecules* **2012**, *45*, 9779.
- 54 Barqawi, H.; Schulz, M.; Olubummo, A.; Saurland, V.; Binder, W. H. *Macromolecules* **2013**, *46*, 7638.

3.2 Synthesis of Photoresponsive Main-Chain Oligomers with Azobenzene Moieties via ADMET Oligomerization and their Micellization Properties.

Clement Appiah,^a Georg Woltersdorf,^b and Wolfgang H. Binder*^a

^aChair of Macromolecular Chemistry, Faculty of Natural Science II (Chemistry, Physics and Mathematics), Martin Luther University Halle-Wittenberg, von-Danckelmann-Platz 4, Halle (Saale) D-06120, Germany.

^bInstitute of Physics, Martin Luther University Halle-Wittenberg, Von-Danckelmann-Platz 3, D-06120, Halle (Saale), Germany.



Polym. Chem., 2017, 8, 2752

Abstract: We report the synthesis of a straightforward and efficient strategy to obtain azobenzene functionalized linear unsaturated/saturated oligomers. Using mild reaction conditions and different ruthenium-based catalysts, the azobenzene moieties are precisely placed in olefin chains via acyclic diene metathesis (ADMET) reaction ($M_{n,SEC} = 3.0$ kDa-8.0 kDa). Subsequent hydrogenation reactions with *p*-toluenesulfonylhydrazide, yields the fully saturated azobenzene oligomers, which are thoroughly characterized by ¹H-NMR, FTIR and liquid chromatography under critical conditions (LCCC). The obtained saturated and unsaturated azobenzene oligomers are proven to form micelles in solution, where their sizes and morphologies are characterized by DLS and TEM. As a result of photo-isomerisation from the *trans* to *cis* state, the aggregates reduce in size, which is accompanied by a visible change of the solution from turbid to clear.

Introduction

Photoswitchable moieties in oligomers/polymers such as azobenzenes [1], have become essential elements to induce solid/liquid transition [2-4],

changes in phase transition [5-7] or induce surface gratings in thin films [8-14].

One of the most interesting among the properties of such chromophores is their readily induced and reversible *trans*–*cis* photoisomerization of the azo bond [15-22] and the geometric changes that result

when the azo chromophores are incorporated into polymers and other materials [23-29].

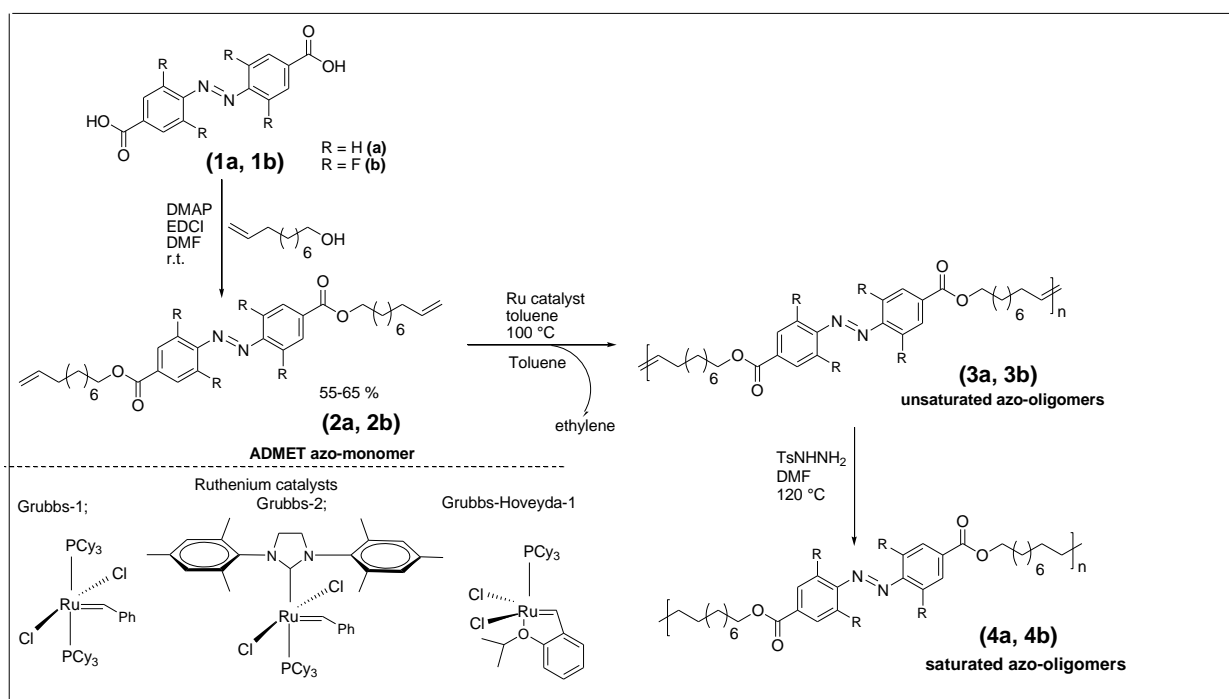
These changes in shape and aggregate size of photoresponsive azo-micelles have been demonstrated [30-34], and in most instances, the self-assembled azo-polymers is proven to reduce in size upon switching from the *trans* to the *cis* state. A large number of photo-responsive self-assembled systems based on azobenzene and macrocycles has also been shown in dual stimuli-responsive self-assembly supramolecular nanoparticles based on the ternary host-guest complexation between cucurbituril [35], a methyl viologen polymer, and mono- and multivalent azobenzene functionalized molecules [36].

This reversible isomerisation process has also been shown [37-39] to depend mainly on the chromophore type, the type of attachment of groups to the chromophore, the glass transition temperature (T_g), and the crystallinity of components attached to the azo group. Thus, based on these findings, considerable work has gone into the stabilization of these *cis* isomers. Notable among these studies is e.g. the macrocyclic strain in azobenzenophanes reported by the group of Tamaoki [40-42], who prepared photoinduced molecular hinges where the (*trans,trans*)-isomer shows a flat geometry, while the (*cis,cis*)-isomer has a bent structure with an angle of 112°. The bent (*cis,cis*)-isomer was found to have an exceptionally long lifetime of 6.4 years. The lifetime of the intermediate mixed isomer (*trans,cis*)-isomer was however found to be only 2.73 min as a result of the high distortion between mixed (*trans,cis*) conformers. The use of fluorinated (F)-azobenzenes thus has become a major breakthrough in the stabilization of the *cis*-isomer of azobenzene. A half-life of 2 years for the *cis*-isomer has been measured

at room temperature for some azobenzenes [43]. The group of Bléger [16, 20-22, 44] has utilized this chromophore in several applications to proof the stability of the *cis*-isomers in F-azobenzenes, by increasing the lifetime from hours to days depending on the attached functional groups to the chromophore and the number of F-atoms on the chromophore.

So far, a significant number of azo-molecules with various architectures have been developed through diverse methods; i.e. either through direct polymerization of a monovinyl azo monomer [45, 46], or through post-functionalization of a polymer onto an azo-chromophore [14, 47]. Based on these methodologies both side-chain [48-52] [249] and main-chain [53-60] azobenzene polymers have been prepared. However, to the best of our knowledge, the preparation of precise oligomers/ polymers containing azo-functional groups and subsequent hydrogenation to obtain semi-crystalline oligomers/polymers having azobenzene moieties within the main chain has not been exploited so far, presumably due to the tedious chemistry needed to preserve the azo-chromophore upon hydrogenation and/or the time-consuming complicated purification procedures.

We hereby describe a novel synthetic approach using ADMET technique, to introduce repetitive azobenzenes into olefins, targeted to the generation of saturated and unsaturated azo-oligomers. We also show the successful hydrogenation of the azobenzene containing olefins with a precisely defined structure, to demonstrate that the azo (-N=N-) bond survives both, the metathesis and the subsequent hydrogenation chemistry. Furthermore, we address the photoresponsive behavior of the azobenzenes and their aggregation state in solution.



Scheme 1. Synthesis of fluorinated and non-fluorinated azo-monomers and subsequent ADMET polymerization of the monomers using Grubbs or Grubbs-Hoveyda catalyst and final hydrogenation of the polymers using *p*-toluenesulfonylhydrazide.

Experimental

Materials

All chemicals used for the synthesis were purchased from Sigma-Aldrich and CHEMOS chemicals. *N,N*-dicyclohexylcarbodiimide (DCC), and *N,N*-dimethylamino-4-pyridine (DMAP) were used as such without further purification. Tetrahydrofuran (THF) was predried over sodium hydroxide (NaOH) for several days followed by heating over sodium/benzophenone and final distillation under an argon atmosphere before use. Toluene was heated over sodium/benzophenone and distilled under an argon atmosphere. Dichloromethane and dimethylformamide were distilled over calcium hydride under nitrogen atmosphere before use.

General Experimental Methods

Most of the reported syntheses were carried out under a nitrogen atmosphere. Products were purified by chromatography on silica gel (200-400 mesh). Analytical thin-layer chromatography (TLC) was performed on precoated silica gel glass plates (silica gel, 0.25 mm thickness). The compounds were visualized with a UV lamp or the treatment with an oxidizing reagent comprised of cerium (IV) sulphate tetrahydrate, sulphuric acid and water, followed by heating. The synthesis of the azo-compound (**1b**) was accomplished according to previous reports [13, 39] (see supplementary information).

Characterization

^1H -, ^{13}C - and ^{19}F -NMR spectra were recorded on a Varian spectrometer (Gemini 400) at 400 MHz at 27 °C. CDCl_3 (Armar AG, 99.8 Atom%D) was used as solvent and tetramethylsilane was used as internal standard. The coupling constants were given in Hz, the chemical shifts in ppm, and referred to the solvent residue peak [CDCl_3 7.26 ppm (^1H) and 77.0 ppm (^{13}C)]. For the interpretation of the spectra, MestReNova v. 6.0.2–5475 was used.

For Gel permeation chromatography (GPC) measurements, a Viscotek GPCmax VE 2002 with an $\text{H}_{\text{HR}}\text{H}$ Guard-17369 and a $\text{GM}_{\text{HR}}\text{N}$ -18055 column in tetrahydrofuran (THF) was used. 100 μL of 1 mg mL^{-1} samples were injected at 22 °C. Detection was carried out with a Viscotek VE3580 RI detector at 35 °C and a flow rate of 1 mL min^{-1} . Polystyrene standards with molecular weights of 1050, 2790, 6040, 13 400, and 29 600 g mol^{-1} were used for external calibration.

Matrix-assisted laser desorption/ionization time-of-flight mass spectrometry (MALDI-ToF-MS) measurements were performed on a Bruker Autoflex III system (Bruker Daltonics) operating in reflection and linear modes. Data evaluation was carried out with the aid of the DataAnalysis software package. Ions were formed by laser desorption (smart beam laser at 355, 532, 808, and 1064 ± 5 nm; up to 2500 Hz repetition rate), accelerated by a voltage of 20 kV and detected as positive ions. The matrix solution was prepared by mixing *trans*-2-[3-(4-*tert*butyl phenyl)-2-methyl-2-propenylidene]malononitrile (DCTB) in THF at a concentration of 20 mg mL^{-1} . The salt solution was prepared by dissolving lithium trifluoroacetate (LiTFA) in THF at a concentration of 20 mg mL^{-1} . The samples were dissolved in THF at a concentration of 20 mg mL^{-1} . The solutions of the matrix, the analyte, and the salt were mixed in a volume ratio of 25:5:1 and 1 μL of each mixture were spotted on the MALDI target.

HRMS (ESI) measurements were carried out on a Bruker Daltonics microgel time-of-flight LC-MS system. Spectra were recorded in a positive and negative mode with an accelerator voltage of 4.5 kV, a transfer line with 190 °C and a scan range of 50–2000 m/z at the spectral rate of 1 Hz. The spectra were processed on Bruker Daltonics ESI compass 1.3. The sample preparation was performed by dissolving 1–5 mg of the respective compound in 1 mL mixture of acetonitrile.

High performance liquid chromatography (HPLC) measurements were performed on Elite LaChrom HPLC, Hitachi VWR instrument, equipped with an autosampler, a quaternary gradient pump, a degasser, a diode array detector (UV-DAD) operating at 190–900 nm, and a column oven with temperature control (temperature = 25 °C). The temperature was maintained constant (± 0.2 °C) throughout the experiment, and the injected sample volume was 10 μL . The samples were prepared by dissolving a few mg in the solvent mixture (ACN/THF = 8/92), with annealing at 150 °C to obtain a complete dissolution. The analytes were later switched using UV-light with 300 nm wavelength to generate essentially the *trans*-form. Liquid chromatography at critical conditions (LCCC) was subsequently carried out on a non-polar reversed-phase Atlantis-RP C18 column, 100 Å , 5 μm , with dimensions of 4.6 mm \times 250 mm using ACN/THF = 8/92 as the mobile phase with a flow rate of 0.50 mL/min. The DAD signals were recorded using the EZchrom Elite software package with an operating wavelength from 190 to 900 nm at a sampling width of 200 ms to obtain sufficient density of data points to resolve the peaks.

FTIR spectra were recorded on a Bruker Vertex70MIR spectrometer using an ATR Golden Gate unit with a diamond crystal. The scan number was 32 scans per spectrum with a resolution of 2 cm^{-1} .

Differential scanning calorimetry (DSC) measurements were carried out on a NETZSCH DSC 204F1 Phoenix, which was calibrated with indium, tin, bismuth, and zinc. Samples with a mass of about 5-8 mg were placed into a standard aluminium pan and nitrogen was used as purge gas. Netzsch Proteus-Thermal Analysis (version 5.2.1.) was used for the interpretation of the obtained data. For the melting point measurements, the samples were heated with a heating rate of 10°C/min to 180 °C, at an annealing time of 10 min, and cooled down slowly to -50 °C with a cooling rate of 10 °C/min. The melting temperature was evaluated from the peak maximum of the heating run.

UV-VIS absorption spectra were measured on a Jasco V-670 UV/VIS/NIR spectrometer. The thickness of the optical cells for the measurement was 10 mm. The irradiation was performed using high power (300 mW) UV light (300 nm) and green light (520 nm) light emitting diodes (LEDs) mounted at a distance of 5 mm from the window of the optical cell in the sample chamber of the spectrometer.

Dynamic Light Scattering, DLS measurements were performed in THF solution at a concentration of 3 mg/mL on a Viscotek 802 using an OmniSIZE software.

Synthesis of symmetric non-fluorinated azobenzene diene monomer (**2a**) and fluorinated azobenzene diene monomer (**2b**)

The synthesis of compound (**2a** and **2b**) was achieved based on a modified procedure from literature [57-58]. Briefly, to an azobenzene chromophore ((**1a**: 5 g, 18.5 mmol) or (**1b**: 5 g, 14.6 mmol)) in a Schlenk flask, 10-decenoic acid (8.1 g, 51.8 mmol), and DMAP (0.54 g, 4.4 mmol) were added. Distilled DMF (50 mL) was added and the mixture was then purged under a nitrogen atmosphere for 2 h. EDCI (8.5 g, 44.4 mmol) was

subsequently added at 0 °C with rapid stirring under a counter flow of nitrogen. Afterwards, the reaction mixture was allowed to warm to room temperature and stirred for 120 h. The obtained crude mixture was poured into water and extracted with ethyl acetate. It was finally purified on a silica gel column (DCM:ethylacetate 1:4) to yield a yellowish viscous compound (**2a**, 65 % and **2b**, 55 %).

¹H-NMR (**2a**, CDCl₃): δ(ppm) 8.14-8.33 (m, 4H, o-ArH-N=N-ArH), 7.65-8.04 (m, 4H, m-ArH-N=N-ArH), 5.73-5.78 (m, 2H, CH₂=CH), 4.89-5.00 (m, 4H, CH₂=CH), 4.30 (t, J = 6.7 Hz, 4H, CH₂OCO), 1.98-2.00 (t, J = 7.4 Hz 4H, CH₂=CHCH₂), 1.70-1.74 (dd, J = 7.3 Hz, 2.2 Hz, 4H, OCOCH₂CH₂), 1.28-1.42 (m, 20H,CH₂). ¹³C-NMR (**2a**, CDCl₃): δ(ppm) 173.2, 155.1, 139.9, 132.8, 130.3, 123.9, 115.8, 67.7, 33.4, 30.8, 25.9. IR (**2a**): 2917, 2850, 1701, 1638, 1596, 1384, 1014, 832. HRMS (ESI) calcd for C₃₄H₄₇N₂O₄ ([M+H]⁺) 547.3563, found 547.3530. ¹H-NMR (**2b**, CDCl₃): δ(ppm) 7.07-7.33 (m, 4H, m-ArH-N=N-ArH), 5.75-5.85 (m, 2H, CH₂=CH), 4.90-5.00 (m, 4H, CH₂=CH), 3.64 (t, J = 6.6 Hz, 4H, CH₂OCO), 2.00-2.06 (m, 4H, CH₂=CHCH₂), 1.52-1.59 (dd, J = 7.6 Hz, 2.4 Hz, 4H, OCOCH₂CH₂), 1.29-1.37 (m, 20H,CH₂). ¹³C-NMR (**2b**, CDCl₃): δ(ppm) 173.2, 156.6 (d, J = 5.0 Hz), 153.2 (d, J = 5.1 Hz), 139.9, 135.2, 130.3, 116.5, 111.5, 67.7, 33.4, 30.8, 25.9. ¹⁹F-NMR (**2b**, CDCl₃): δ(ppm) -118 (d, J = 6.1 Hz), -119 (d, J = 8.5 Hz). IR (**2b**, cm⁻¹): 3328, 3102, 2925, 2854, 1701, 1640, 1600, 1424, 1349, 1091, 994, 839. HRMS (ESI) calcd for C₃₄H₄₃F₄N₂O₄ ([M+H]⁺) 619.3663, found 619.3654.

ADMET oligomerization of the azobenzene monomers (**2a** and **2b**)

In a nitrogen-filled Schlenk tube containing a solution of the appropriate catalyst in 0.1 mL of degassed toluene was subjected to three freeze vacuum thaw cycles. A degassed solution of the

diene monomer (**2a** or **2b**, 0.2 mol, (250:1 monomer to catalyst ratio)) in 0.4 mL of toluene was subsequently added to the schlenk flask, degassed for additional 30 min, and stirred for 120 h at 100 °C. The polymerization was finally quenched by adding ethyl vinyl ether (0.5 mL) with additional stirring for 30 min. The crude solution was precipitated in excess methanol, and the precipitate was isolated by filtration, dried in vacuo to give the unsaturated azobenzene oligomers (**3a** and **3b**).

¹H-NMR (**3a**, unsaturated H-AP3, CDCl₃): δ(ppm) 8.14-8.33 (m, 4H, m-ArH-N=N-ArH), 7.65-8.04 (m, 4H, m-ArH-N=N-ArH), 5.28-5.41 (m, 2H, CH=CH), 4.17-4.30 (m, 4H, CH₂OCO), 1.98-2.00 (m, 4H, CH₂=CHCH₂), 1.70-1.74 (m, 4H, OCOCH₂CH₂), 1.28-1.42 (m, 20H, CH₂). ¹³C-NMR (**3a**, CDCl₃): δ(ppm) 173.1, 155.2, 139.8, 132.1, 130.8, 123.8, 118.1, 66.3, 35.7, 29.8, 25.5. IR (**3a**, unsaturated H-AP3, cm⁻¹): 2917, 2850, 1701, 1638, 1596, 1384, 1014, 832. ¹H-NMR (**3b**, unsaturated F-AP3, CDCl₃): δ(ppm) 7.07-7.33 (m, 4H, m-ArH-N=N-ArH), 5.29-5.45 (m, 2H, CH=CH), 3.61-3.64 (m, 4H, CH₂OCO), 2.00-2.06 (m, 4H, CH₂=CHCH₂), 1.52-1.59 (m, 4H, OCOCH₂CH₂), 1.29-1.37 (m, 20H, CH₂). ¹³C-NMR (**3b**, CDCl₃): δ(ppm) 172.1, 156.6 (d, J = 5.1 Hz), 154.2 (d, J = 5.2 Hz), 137.8, 135.2, 132.1, 131.3, 125.2, 117.6, 63.4, 33.1, 29.4, 25.6. -117 (d, J = 5.1 Hz), -119 (d, J = 7.5 Hz). ¹⁹F-NMR (**3b**, unsaturated F-AP3, CDCl₃): δ(ppm): -117 (d, J = 5.1 Hz), -119 (d, J = 7.5 Hz). IR (**3b**, unsaturated F-AP3): 3328, 3102, 2925, 2854, 1701, 1640, 1600, 1424, 1349, 1091, 994, 839.

Hydrogenation reaction of the fluorinated and non-fluorinated azobenzene oligomers (**4a** and **4b**).

Based on the literature [62, 63], a dried and nitrogen filled one-necked flask equipped with a magnetic stir bar and a reflux condenser was filled with a highly degassed solution of the unsaturated ADMET oligomer (**3a** or **3b**, 100 mg), p-toluenesulfonylhydrazide (3 mol eqv.) N,N-diisopropylethylamine (3 mol eqv.) and N,N-dimethylformamide (DMF) (6 mL). The reaction mixture was heated to 120 °C under vigorous stirring for 6 h. It was then allowed to cool down to room temperature. The solvent was removed in vacuo, and the obtained saturated oligomers were precipitated in methanol (yield ~ 75 %, **4a**: melting point (DSC) = 145 °C and **4b**: melting point (DSC) = 157 °C).

¹H-NMR (**4a**, saturated H-AP3, CDCl₃): δ(ppm) 8.14-8.33 (m, 4H, m-ArH-N=N-ArH), 7.65-8.04 (m, 4H, m-ArH-N=N-ArH), 4.17-4.30 (m, 4H, CH₂OCO), 1.98-2.00 (m, 4H, CH₂=CHCH₂), 1.70-1.74 (m, 4H, OCOCH₂CH₂), 1.28-1.42 (m, 20H, CH₂). ¹³C-NMR (**4a**, CDCl₃): δ(ppm) 173.1, 155.2, 132.1, 130.8, 123.8, 66.3, 35.7, 29.8, 25.5, 21.6, 17.7. IR (**4a**, saturated H-AP3, cm⁻¹): 2917, 2850, 1638, 1596, 1384, 1014, 832. ¹H-NMR (**4b**, saturated F-AP, CDCl₃): δ(ppm) 7.07-7.33 (m, 4H, m-ArH-N=N-ArH), 3.61-3.64 (m, 4H, CH₂OCO), 2.00-2.06 (m, 4H, CH₂=CHCH₂), 1.52-1.59 (m, 4H, OCOCH₂CH₂), 1.29-1.37 (m, 20H, CH₂). ¹³C-NMR (**4b**, CDCl₃): δ(ppm) 171.8, 157.4 (d, J = 5.1 Hz), 154.5 (d, J = 5.3 Hz), 132.1, 131.3, 127.8, 63.6, 33.4, 29.4, 25.8, 21.7, 17.8. ¹⁹F-NMR (**4b**, saturated F-AP3, CDCl₃): δ(ppm): -117 (d, J = 5.1 Hz), -119 (d, J = 7.5 Hz). IR (**4b**, saturated F-AP3): 3328, 3102, 2925, 2854, 1640, 1600, 1424, 1349, 1091, 994, 839.

Table 1. Experimental conditions for the azo-oligomers using Grubbs first generation (G1), second generation (G2), third generation (G3) and Hoveyda-Grubbs first generation (GH1) catalysts.

Run nr.	Monomer	Oligomer ^{a,b}	Catalyst	[monomer] ₀ /[cat.] ₀ ^d	Time /h	Temp. /°C	M _{n,SEC} ^c /g/mol	M _w /M _n ^c	Yield ^e /%
1	2a	-	G1 G3	250/1	120	100	no polymer	-	-
2	2a	H-AP3	G2	250/1	120	100	2,850	1.5	35
3	2a	H-AP3	GH1	250/1	120	100	3200	1.3	67
4	2a	H-AP7	GH1	250/1	120	100	7200	1.7	52
5	2b	-	G1 G3	250/1	120	100	no polymer	-	-
6	2b	F-AP3	G2	250/1	120	100	2,850	1.9	15
7	2b	F-AP3	GH1	250/1	120	100	3,160	1.6	42
8	2b	F-AP8	GH1	250/1	120	100	7830	1.4	58

^a N₂ atmosphere; solvent, toluene; temperature, 100 °C.; monomer: azobenzenes; e.g. M.W._{[monomer, 2b]} = 618 g/mol, [monomer]₀/[cat.] = 4.0x10⁻⁴ mol L⁻¹/ 1.6x10⁻⁶ mol L⁻¹. ^b No defined endgroup for M_n determination from ¹H-NMR, ^cDetermined by SEC in THF using polystyrene standards. ^dmonomer-to-catalyst ratio. ^eIsolated yields after purification.}

Results and discussion

Monomer and ADMET oligomerization synthesis.

Conceptually, *cis-trans* back isomerisation in azobenzenes mainly depends on the chromophore type; thus, different groups on the aromatic benzene ring affect the photochemical back conversion of the *cis* isomer in the dark. Based on this influence and our desire to obtain azobenzene systems having a more stable *cis*-form after switching, we strategically designed two different azo-monomers (**2a** and **2b** see Scheme 1) containing hydrogen and fluorine atoms on the azobenzene chromophore. These different atoms on the aromatic benzene ring are expected to display a variable influence on the physicochemical properties of the azo-monomers (**2a** and **2b**) and the final

oligomer [20]. We subsequently accomplished the synthesis of the azo-monomers and the oligomerizations of the monomers based on modified procedures from literature [20, 57-58]. Figure 1 shows the ¹H-NMR spectrum of the azo-monomers and -oligomers. Starting from the azo-monomers, we could explicitly assign all the observed resonances to the aromatic group (**2a**: 8.14-8.33 and 7.65-8.04 ppm; **2b**: 7.33 ppm), the terminal vinyl protons (~5.77 and ~4.93 ppm), and the methylene groups at (1.56-2.06 ppm). Furthermore, by using HRMS (ESI), we could proof the purity of the synthesized monomers (**2a** and **2b**, see Figure S13-S15, Supporting Information), eliminating any presence of residual compounds of 1 and the 10-decenoic acid.

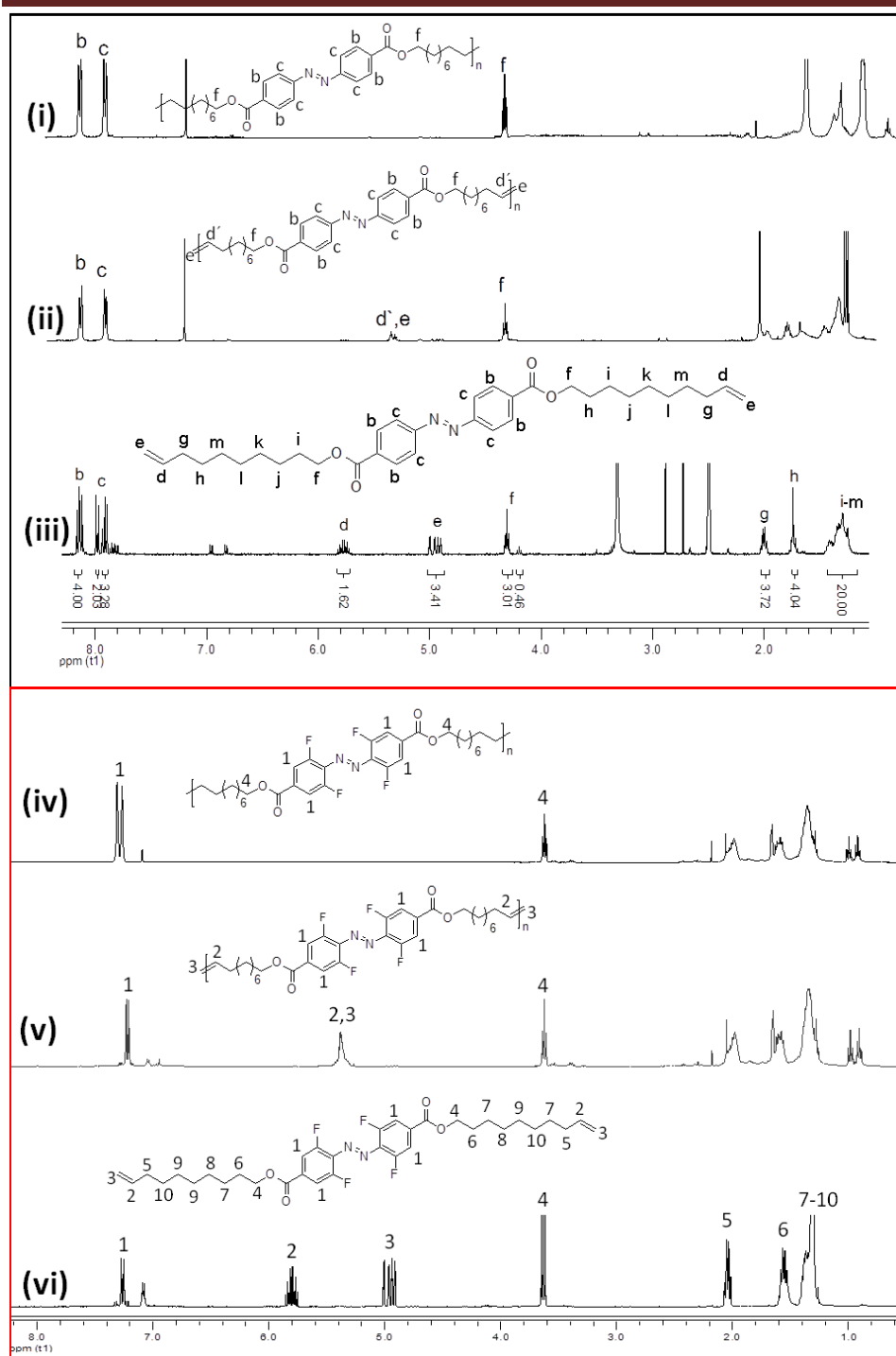


Figure 1: $^1\text{H-NMR}$ of the fluorinated azobenzenes (bottom three) and non-fluorinated azobenzenes (upper three). The numbers (iii and vi) show the azo-monomers (**2a** and **2b**) (ii and v) show the unsaturated azo-oligomers (**3a** and **3b**) (i and iv) show the saturated azo-oligomers (**4a** and **4b**).

The obtained azo-dienes (**2a** and **2b**) were further subjected to ADMET oligomerizations in solution, using toluene as solvent and stirring at $100\text{ }^\circ\text{C}$ for 120 h. Different ruthenium catalyst (Grubbs first generation (G1), second generation (G2), third generation (G3), and Hoveyda-Grubbs first

generation (GH1)) were investigated with respect to the yield and polydispersity of the azo-oligomers (**3a** and **3b**). After several reactions with these catalysts, Grubbs second generation, and Hoveyda-Grubbs first generation catalyst were found to be the most efficient catalyst for the aforementioned reaction conditions.

Yields in the range of 15-67 % were obtained. As already reported in the literature [64-67], ruthenium-based catalysts also catalyze non-metathetic reactions, such as the isomerization of alkenes [68-70]. Table 1 summarizes the results obtained for the various oligomers. The molecular weights of the isolated oligomeric materials were in the range of 3,000-8,000 g/mol, and the substances were readily soluble in THF. The GPC-traces for the oligomers showed the expected monomodal peak with a surprisingly narrow molecular weight distribution of 1.4-1.9.

The $^1\text{H-NMR}$ spectra of the azo-oligomers (Figure 1), demonstrated the almost complete disappearance of the terminal double bonds (5.77 and 4.93 ppm) and a formation of the internal double bonds (5.39 ppm) after an oligomerization time of 120 h. FTIR spectra for the azo-monomers and -oligomers (**3a** and **4a**) are shown in Figure S1, displaying the absorption bands at 2917-2850, 1550, 1638, 1596 and 1384, 1014-832 cm^{-1} , attributed to the stretching vibration of unsaturated/saturated C-H, -N=N-, carboxyl, azobenzene, -C-O and out-of-plane bending vibrations of the aliphatic hydrocarbons respectively. The absorption bands of the oligomers proved that the oligomers have a similar backbone structure compared to the monomers, most importantly the presence of the N=N azo-bond.

MALDI-ToF MS measurements were recorded to further elucidate the structures of the synthesized azo-oligomers (Figure 2 and S6). One main peak

series was observed for the azo-oligomers, showing a mass difference of 590.65 g/mol and 518.70 g/mol. This corresponded to the repeat unit of the azo-monomers 2b and 2a in the oligomeric chain, with a loss of ethylene unit ($\text{CH}_2=\text{CH}_2$). From Figure 2, the signal at 3573.15 g mol^{-1} could be assigned to our linear oligomer. This also agreed with the calculated value of 3572.9 g mol^{-1} as an H adduct. In the MALDI spectra of compound 3a (Figure S6), one also observes some additional small peaks close to the linear oligomeric peaks. These signals were assigned to cyclic oligomers within our linear azo-oligomers. For e.g. the signal at 2566.36 g/mol was assigned to a cyclic oligomer with a displaced ethylene unit ($\text{CH}_2=\text{CH}_2$) as a hydrogen adduct. The presence of these cyclic oligomers was highly probable from the mechanistic standpoint of ADMET reactions.

Hydrogenation of the azo-oligomers

Azo bonds (-N=N-) can easily be hydrogenated to hydrazobenzene, often even in the presence of oxygen. However, reformation of the azo bond can be accomplished by subjecting the hydrazobenzene to an oxidizing agent (e.g. tert-butylhypochlorite, t-BuOCl) in an N_2 atmosphere [63a]. Never the less, the complete removal of oxygen from the reaction mixture was reported to retain the azo-bond, even under reaction with hydrazides [63] at elevated temperatures. Thus, hydrogenation of the olefinic double bonds of all our ADMET oligomers (**3a** and **3b**) was conducted using *p*-toluenesulfonylhydrazide (TsNHNH_2) and *N,N*-diisopropylethylamine in DMF at 120 °C under a highly inert nitrogen atmosphere and a complete removal of oxygen from the reaction mixture. The NMR spectra (Figure 1i and iv) show the comparison of the oligomers before and after hydrogenation. We observed the

disappearance of the resonance peak at 5.39 ppm, assigned to the internal olefinic protons of the unsaturated oligomers after the hydrogenation reaction. This showed that saturated ethylene-based oligomers (4a and 4b) were produced after the exhaustive hydrogenation reaction. Also, the FTIR measurements of the saturated azo-oligomers, Figure S1, showed the disappearance of the characteristic band at 967 cm⁻¹

(out of plane olefin C-H wagging vibrational mode) for the olefinic internal double bonds, which also proved the conversion of the unsaturated to the saturated azo-oligomers. The presence of the -N=N- bond could also be traced from the vibration band at ~1550 cm⁻¹ in the FTIR spectrum to confirm the success of the hydrogenation reaction

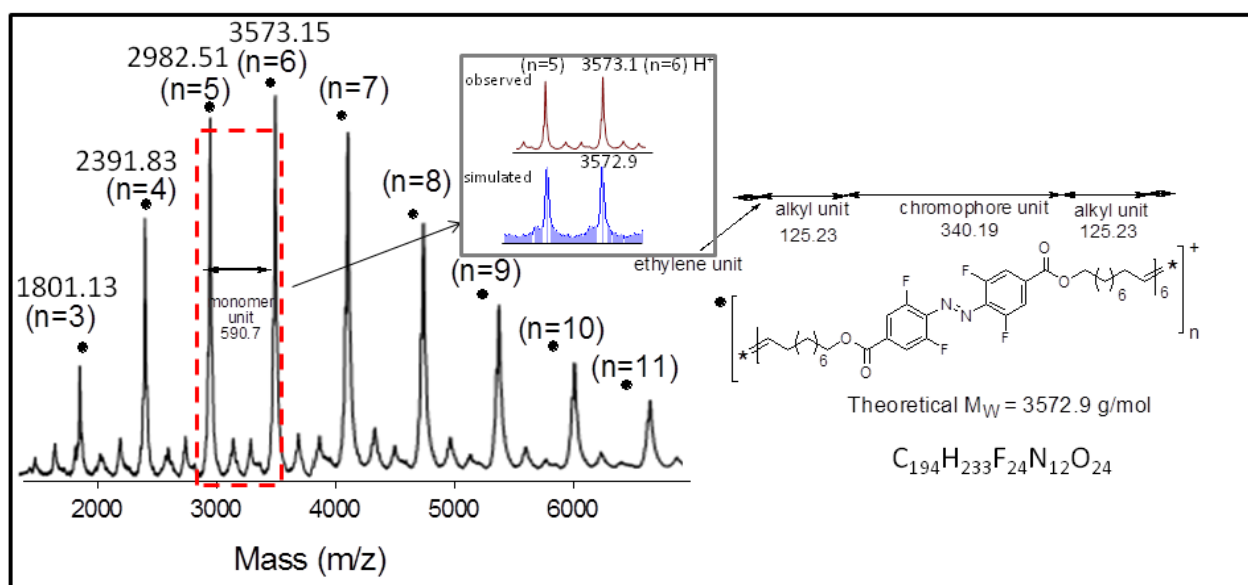


Figure 2. MALDI-ToF MS spectra of the unsaturated azo-oligomer (3b, run 7)

Liquid chromatography at critical conditions (LCCC) [19] was conducted to further support the proof of the successful exhaustive hydrogenation transformation from the unsaturated **3a** and **3b** to the saturated azo-oligomers **4a** and **4b**. To this end, the azo-monomers (**2a** and **2b**), the unsaturated oligomers (**3a** and **3b**) and the saturated azo-oligomers (**4a** and **4b**) were subsequently characterized by LC at near-critical conditions (THF/ACN, 92/8, v/v at 25 °C). The results from the LC (Figure 3) showed different retention times for the two different azo-monomers and oligomers. Thus, while the non-fluorinated compounds (**2a**, **3a**, and **4a**) eluted at low retention times (in a range of

8.8-9.6 min), the fluorinated compounds (**2b**, **3b**, and **4b**) on the other hand eluted at higher retention times (between 10.0-11.2 min). The difference in the retention times was due to the different azo-chromophores for these two molecules. Most importantly, the retention times of the unsaturated azo-oligomers and the saturated azo-oligomers were different with a retention time difference of 0.63 min (Figure 3; middle red and bottom blue). The elution peak of the unsaturated azo-oligomers was not present in the spectrum of the saturated azo-oligomers, which further supports the successful transformation of the double bonds to single bonds within the oligomeric chains.

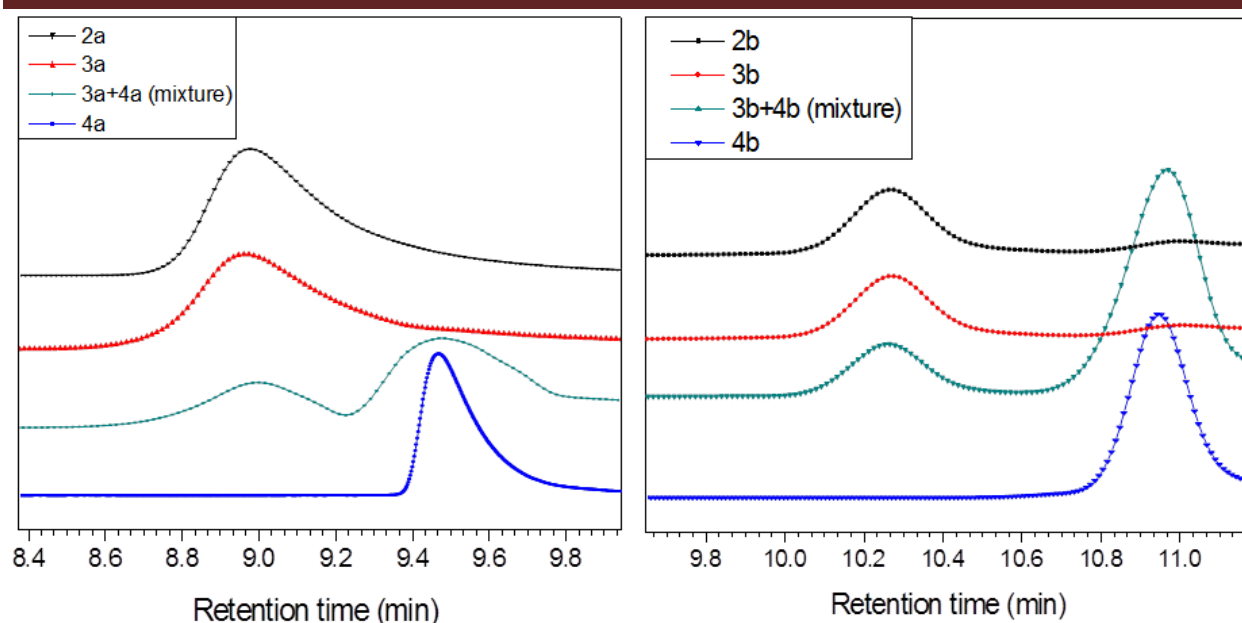


Figure 3. LC chromatograms at LCCC conditions for non-fluorinated azobenzenes (**2a**, **3a** and **4a**, left) and fluorinated azobenzenes (**2b**, **3b** and **4b**, right). Beginning from the top is the azo-monomer (**2a** and **2b** black), unsaturated azo-oligomer (**3a** and **3b**, middle red, $M_n = 3000$ g/mol.), 1/1-mixture of unsaturated and saturated azo-oligomer (middle, green), and saturated azo-oligomer (**4a** and **4b**, bottom, $M_n = 3000$ g/mol.) showing excellent separation based on their functionality. Runs 4 and 8 in Table 1 were used for this investigation.

Azobenzene switchability in solution and the solid state.

UV-VIS spectra of the bis-*o*-fluorinated-azo-monomer (**2b**, Figure 4i) showed a π - π^* absorption band at ~ 320 nm and an n - π^* absorption band at ~ 428 nm. Irradiation of the monomer in solution with green light ($\lambda \sim 520$ nm) decreased the intensity of the π - π^* absorption band while the n - π^* absorption band intensity increased slightly with a concomitant blue-shift of 13 nm. Contrary to our expectations, excitation by UV light ($\lambda \sim 300$ nm) shifted the two bands to their original position,

implying that the *cis* azobenzene monomer was reversibly changed to the *trans* state. However, the intensity of the strongest absorption band recovered only partially to its initial value, suggesting that a portion of the *cis* form remained unchanged upon UV light excitation. Remarkably, the *cis* form of the fluorinated azo-monomer (**2b**) was stable over a period of ~ 14 h before a full recovery to the *trans* state was observed, whereas the *cis* form of the non-fluorinated azo-monomer (**2a**) recovered much faster within a period of 1 h (Figure 5).

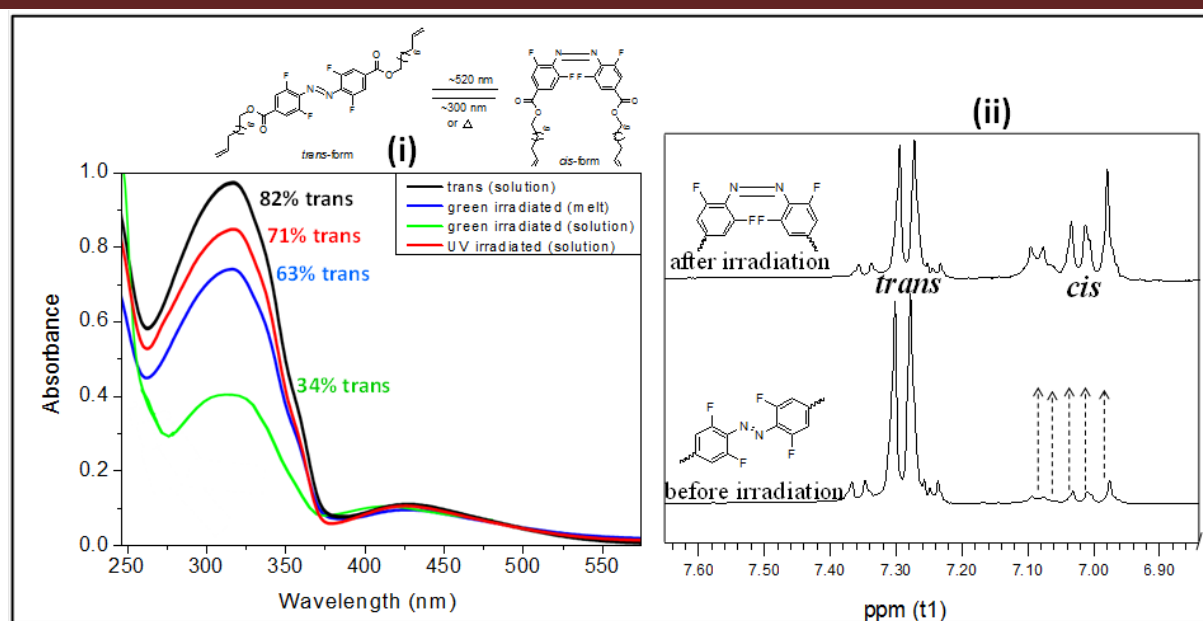


Figure 4. (i) UV-vis spectra of the green irradiated fluorinated azobenzene monomer (**2b**, 1.94×10^{-4} mol/L) in THF solution and melt state for 1 h. *trans* (solution) peak is recorded at 0 min before switching, green irradiated (melt) and (solution) are the peaks for ~ 520 nm irradiation in the melt state and solution state, and UV irradiated (solution) is the peak for 300 nm irradiation for the recovery of the *trans* isomer after the switching process. (ii) $^1\text{H-NMR}$ spectra of the azo-monomer before irradiation and after irradiation. The broken arrows show the changes of the resonance of the *cis* peak after the irradiation process.

The time profile of the azo-monomers **2a** and **2b** showed an exponential behavior and a fit by the function $\Delta A_t = \Delta A_\infty + \Delta A_0 \cdot e^{-t/\tau}$ yielded a time constant of $\tau = 30$ min ($k = 1/\tau = 5.56 \times 10^{-4} \text{ s}^{-1}$) for monomer **2a** and 164 min ($k = 1/\tau = 1.02 \times 10^{-4} \text{ s}^{-1}$) for monomer **2b**. The estimated energy of activation, ΔG^\ddagger at 298 K for monomer **2b** (Figure S17) was approximately 96 kJ/mol. The high stability of the *cis* state in the azo-monomer **2b** has been demonstrated previously [20, 22] to result from the electron-withdrawing substitution ability of the two *o*-fluorine atoms. The change in the structural morphology of the chromophore after irradiation was additionally confirmed by $^1\text{H-NMR}$ spectroscopy (see Figure 4ii). As shown in the Figure, the intensity of the resonance signal of the *cis* isomer increased with a slight decrease in the resonance signal of the

trans isomer, suggesting that a transformation from *trans* to *cis* due to UV-VIS photo-switching had occurred.

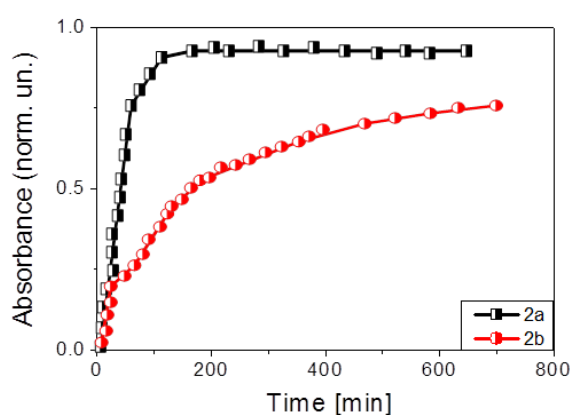


Figure 5. Cis-trans thermal isomerisation of the azobenzenes in the dark. The isomerisation process in the dark obeys the equation $\Delta A_t = \Delta A_\infty + \Delta A_0 \cdot e^{-t/\tau}$

Trans to *cis* switching of the azo-monomer (**2b**) in the melt was also conducted (Figure 4i) by dissolving *trans* (**2b**) in THF and subsequently freeze-drying to remove the solvent, generating a thin film around the walls of the cuvette. This film was then subjected to UV irradiation using green light (520 nm) for 1 h. As seen in Figure 4i, only 19 % of the *cis*-form was obtained. Compared to the solution state switching, a difference of about 47% was observed to exist between the two switching modes. The low conversion yield to the *cis*-form in the melt state switching has been observed in other experiments [71-74] to result from the hindrance of the UV irradiation of the azo bond by the chromophore backbone, which in consequence leads to a reduction in their rate of *trans* to *cis* photoisomerisation.

Finally, the azo-monomers (**2a** and **2b**, before switching) were subjected to temperature heating kinetics to study the influence of heat on the *cis-trans* conversion of the monomers. Figure 6 shows the results of this heating experiment. The samples were thermally annealed using differential scanning calorimeter (DSC) at 10 K/min for 1 h at temperatures starting from 50 °C to 150 °C. As can be seen from Figure 6, the heating experiment of samples **2a** and **2b** had a strong influence on the *trans-cis* ratio of the azo-monomers only at temperatures of 100 °C and above, where most of the *cis*-isomers were converted to the *trans* form. Also, no additional resonances were seen in the ¹H-NMR spectra during the heating process, proving the stability of the compound even at elevated temperatures up to 150 °C (*T_d* for 5% weight loss ~200 °C, see supporting information Figure S3).

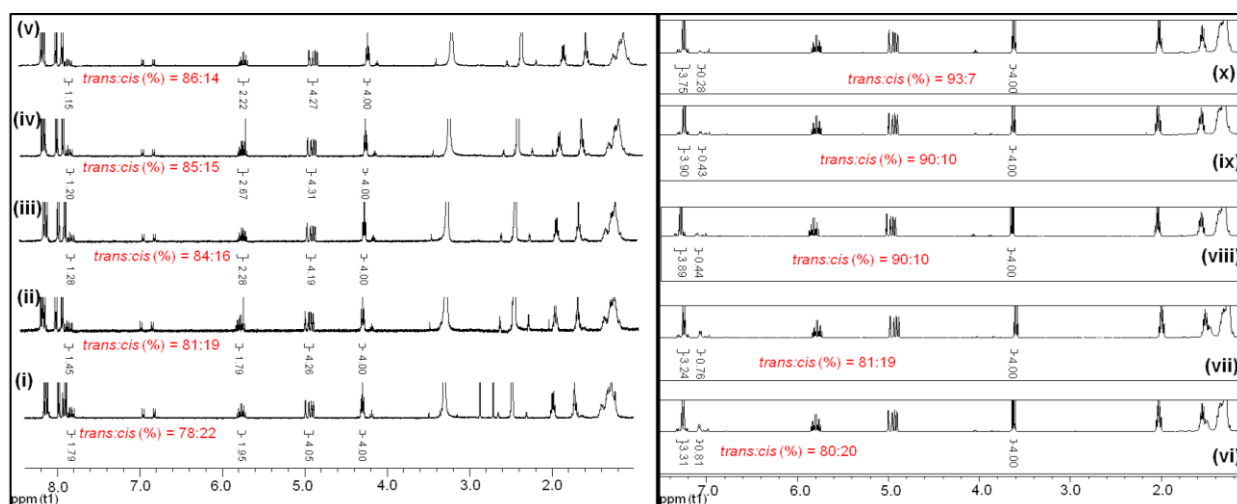


Figure 6. ¹H-NMR investigations on the temperature dependent kinetics measurements of the non-fluorinated azo-monomer (**2a**, i-v, left) and the fluorinated azo-monomer (**2b**, vi-x, right), showing the *trans* : *cis* ratio of the monomers after thermally annealing the samples in DSC at different temperatures for 1h (rate of heating is 10 K/min, *trans* : *cis* ration before start of experiment is ~80:20 respectively). Experiment (i and vi) was conducted at 50 °C, (ii and vii) was conducted at 75 °C, (iii and viii) was conducted at 100 °C, (iv and ix) was conducted at 125 °C and (v and x) was conducted at 150 °C.

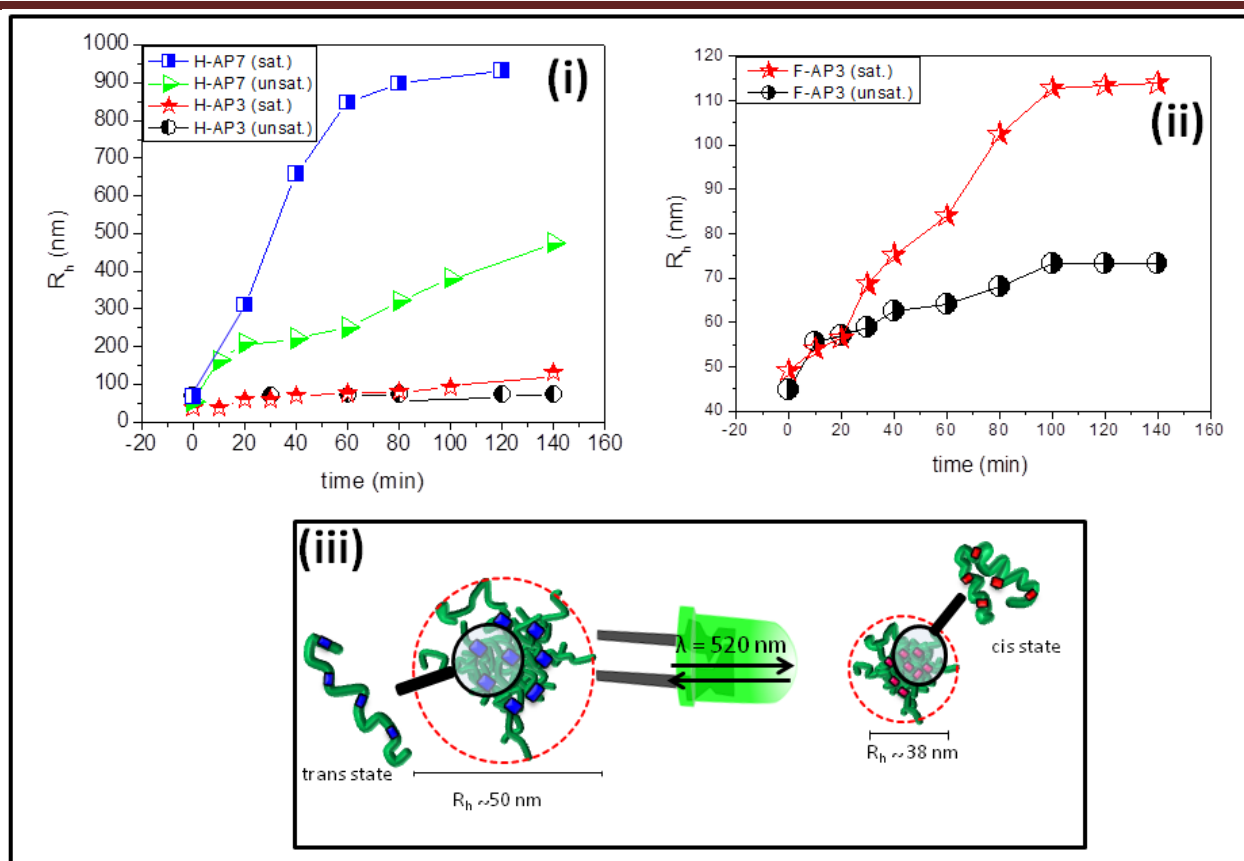


Figure 7. Aggregation behavior of the azo-oligomers in THF solution (3 mg/ml); (i) Shows the time dependent micellar aggregation of the non-fluorinated azo-oligomers, (ii) shows the time dependent micellar aggregation of the fluorinated azo-oligomers (iii) shows the hydrodynamic radius of the aggregates before (trans state) and after switch (cis state) of the azo-oligomers.

Micellization of the azo-oligomers

It is well known that azo-oligomers and -polymers easily aggregate in solutions and upon UV light irradiation or thermal conditions reduce in size from trans to cis state [31-32, 34, 75]. The isomerisation of azo-oligomers via photo/thermal stimulation therefore can have a significant influence on the size and morphology of the self-assembled micelles. Thus, aiming to obtain an insight into the morphology and size of our azo-compounds before and after switching, we subjected our samples to DLS and TEM measurements. Figure 6 shows the examined size distribution of the aggregates of the azo-oligomers using DLS. The results indicated

that the azo-oligomers formed well-defined aggregates with an average hydrodynamic radius (R_h) in the range of 40-60 nm in THF. Time-dependent growth of the aggregates over a period of 140 min (Figure 7), showed that the aggregates grew linearly in size over an 80-100 min period at room temperature; subsequently, the growth saturated, and no larger aggregates resulted. The aggregates growth with time was observed to depend on the molecular weight of the oligomers. Larger molecular weight oligomers led to higher aggregation sized micelles. The saturated azo-oligomers (Figure 7i and ii) were also observed to show bigger aggregate-sizes when compared to their unsaturated

counterparts, and they also grew more rapidly with time.

Subjecting the micellar samples to UV-VIS irradiation resulted in a significant change in the size of the aggregates as a consequence of the switched morphology. Figure 7iii shows the azo-oligomers before and after photo-irradiation. As seen from the figure, the obtained results revealed a decrease in the hydrodynamic radius of the micelles by approximately 13.6 percent, which was consistent with literature for similar azo-chromophores previously reported [76]. The size reduction of the aggregates after UV irradiation was attributed by many experimentalists [30, 33-34, 75] to the increased polarity induced by isomerisation of the azobenzene from its planar rod-shaped trans-form to the non-planar bent-shaped cis-form, which in consequence solubilizes them in polar solvents, such as THF. TEM measurements (Figure S4) were additionally conducted to confirm the size reduction of the micelles after the switching process. Most of the well-dispersed aggregates had an average diameter of 62 nm (before switching, trans-form) and 46 nm (after switching, cis-form). The sizes detected were however smaller than those obtained by DLS presumably due to solvation effects [77].

Conclusion

A synthetic approach to obtain saturated and unsaturated azo-oligomers, bearing hydrogenated and fluorinated moieties is reported. Benefiting from the ADMET oligomerization reaction, azobenzene chromophores **2a**, **2b** were precisely placed in olefin chains using Grubbs ruthenium catalyst. Subsequent hydrogenation of the obtained unsaturated azo-oligomers **3a**, **3b** resulted in saturated azo-oligomers **4a**, **4b**. ¹H-NMR, FTIR and LCCC of the oligomers revealed the successful generation of the hydrogenated azobenzene containing olefins, demonstrating that the

azo (-N=N-) bond survived both, the metathesis and the hydrogenation chemistry. Subsequently, the photoisomerization processes of the azo-monomers were monitored using UV-VIS spectroscopy, revealing the possibility to induce trans-cis isomerisation reaction in both, the monomer and the oligomers, yielding stable cis-configurations in the case of the o-difluorinated azo-compounds. The self-assembly behavior of the azo-oligomers before and after irradiation was studied. The sizes and morphologies of the aggregates were investigated using DLS and TEM measurements, revealing marked changes before and after switching of the azo group. This current work is an expansion of the scope of precision ADMET oligomers and polymers with azobenzene defects, aiding further to the generation of their saturated forms for further studies in the crystallization state.

Acknowledgements

CA and WHB are grateful for the financial support from the German research foundation (DFG) via collaborative research centre SFB/-TRR 102 (Project A3). We thank Ingrid Stössel from the Institute of Physics, Martin Luther University Halle-Wittenberg for the help with the UV-VIS measurements. We also thank Annette Meister from the Physical Chemistry, Martin Luther University Halle-Wittenberg for the TEM measurements.

Notes and references

- 1 García-Amorós, J.; Velasco, D. *Beilstein J. Org. Chem.* 2012, 8, 1003.
- 2 Zhou, H.; Xue, C.; Weis, P.; Suzuki, Y.; Huang, S.; Koynov, K.; Auernhammer, G. K.; Berger, R.; Butt, H.-J.; Wu, S. *Nat. Chem.* 2016, 1.
- 3 Baroncini, M.; d'Agostino, S.; Bergamini, G.; Ceroni, P.; Comotti, A.; Sozzani, P.; Bassanetti, I.;

- Grepioni, F.; Hernandez, T. M.; Silvi, S.; Venturi, M.; Credi, A. *Nat. Chem.* 2015, 7, 634.
- 4 Lee, S.; Kang, H. S.; Park, J.-K. *Adv. Mater.* 2012, 24, 2069.
- 5 Vapaavuori, J.; Laventure, A.; Bazuin, C. G.; Lebel, O.; Pellerin, C. J. *Am. Chem. Soc.* 2015, 137, 13510.
- 6 Hoshino, M.; Uchida, E.; Norikane, Y.; Azumi, R.; Nozawa, S.; Tomita, A.; Sato, T.; Adachi, S.-i.; Koshihara, S.-y. *J. Am. Chem. Soc.* 2014, 136, 9158.
- 7 Yager, K. G.; Barrett, C. J., ch. 8: Light-Induced Nanostructure Formation using Azobenzene Polymers. *Am. Sci. Pub.* 2006, 0, p: 1-38.
- 8 Kim, D. Y.; Tripathy, S. K.; Li, L.; Kumar, J. *Appl. Phys. Lett.* 1995, 66, 1166.
- 9 Rochon, P.; Batalla, E.; Natansohn, A. *Appl. Phys. Lett.* 1995, 66, 136
- 10 Rau, H.; Rötger, D. *Mol. Cryst. Liq. Cryst. Sci. Technol., sect. A* 1994, 246, 143.
- 11 Hamon, F.; Djedaini-Pillard, F.; Barbot, F.; Len, C. *Tetrahedron* 2009, 65, 10105.
- 12 Jochum, F. D.; Theato, P. *Chem. Soc. Rev.* 2013, 42, 7468.
- 13 Jochum, F. D.; zur Borg, L.; Roth, P. J.; Theato, P. *Macromolecules* 2009, 42, 7854.
- 14 Fang, L.; Zhang, H.; Li, Z.; Zhang, Y.; Zhang, Y.; Zhang, H. *Macromolecules* 2013, 46, 7650.
- 15 Yu, H. J. *Mater. Chem. C* 2014, 2, 3047.
- 16 Moreno, J.; Gerecke, M.; Dobryakov, A. L.; Ioffe, I. N.; Granovsky, A. A.; Bléger, D.; Hecht, S.; Kovalenko, S. A. *J. Phy. Chem. B* 2015, 119, 12281.
- 17 Delaire, J. A.; Nakatani, K. *Chem. Rev.* 2000, 100, 1817.
- 18 Yesodha, S. K.; Sadashiva Pillai, C. K.; Tsutsumi, N. *Prog. Polym. Sci.* 2004, 29, 45.
- 19 Appiah, C.; Siefertmann, K. R.; Jorewitz, M.; Barqawi, H.; Binder, W. H. *RSC Adv.* 2016, 6, 6358.
- 20 Bléger, D.; Schwarz, J.; Brouwer, A. M.; Hecht, S. *J. Am. Chem. Soc.* 2012, 134, 20597.
- 21 Bléger, D. *Macromol. Chem. Phys.* 2016, 217, 189.
- 22 Bléger, D.; Liebig, T.; Thiermann, R.; Maskos, M.; Rabe, J. P.; Hecht, S. *Angew. Chem. Int. Ed.* 2011, 50, 12559.
- 23 Yamamoto, H.; Nishida, A.; Takimoto, T.; Nagai, A. *J. Polym. Sci. Part A: Polym. Chem.* 1990, 28, 67.
- 24 Arai, K.; Kawabata, Y. *Macromol. Rapid Commun.* 1995, 16, 875.
- 25 Mahimwalla, Z.; Yager, K. G.; Mamiya, J.-i.; Shishido, A.; Priimagi, A.; Barrett, C. J. *Polym. Bull.* 2012, 69, 967.
- 26 Ebralidze, T. D.; Mumladze, A. N. *Appl. Opt.* 1990, 29, 446.
- 27 Aoki, K. i.; Nakagawa, M.; Ichimura, K. *J. Am. Chem. Soc.* 2000, 122, 10997.
- 28 Kadota, S.; Aoki, K.; Nagano, S.; Seki, T. *J. Am. Chem. Soc.* 2005, 127, 8266.
- 29 Grebel-Koehler, D.; Liu, D.; De Feyter, S.; Enkelmann, V.; Weil, T.; Engels, C.; Samyn, C.; Müllen, K.; De Schryver, F. C. *Macromolecules* 2003, 36, 578.
- 30 Xiang, Y.; Xue, X.; Zhu, J.; Zhang, Z.; Zhang, W.; Zhou, N.; Zhu, X. *Polym. Chem.* 2010, 1, 1453.

- 31 Cai-Cai Zhang; Li, S.-H.; Cui-FangZhang; Liu, Y. *Sci. Rep.* 2016, 1.
- 32 Concellón, A.; Blasco, E.; Martínez-Felipe, A.; Martínez, J. C.; Šics, I.; Ezquerra, T. A.; Nogales, A.; Piñol, M.; Oriol, L. *Macromolecules* 2016, 49, 7825.
- 33 Sun, Y.; Zhou, N.; Zhang, W.; Li, Y.; Cheng, Z.; Zhu, J.; Zhang, Z.; Zhu, X. *Polym. Chem.* 2012, 50, 3788.
- 34 Wang, S.; Zhang, N.; Ge, X.; Wan, Y.; Li, X.; Yan, L.; Xia, Y.; Song, B. *Soft Matter* 2014, 10, 4833.
- 35 Turansky, R.; Konopka, M.; Doltsinis, N. L.; Stich, I.; Marx, D. *Phys. Chem. chem. phys.* 2010, 12, 13922.
- 36 Stoffelen, C.; Voskuhl, J.; Jonkheijm, P.; Huskens, J. *Angew. Chem. Int. Ed.* 2014, 53, 3400.
- 37 Kumar, G. S.; Neckers, D. C. *Chem. Rev.* 1989, 89, 1915.
- 38 Barrett, C.; Natansohn, A.; Rochon, P. *Macromolecules* 1994, 27, 4781.
- 39 Barrett, C.; Natansohn, A.; Rochon, P. *Chem. Mater.* 1995, 7, 899.
- 40 Nagamani, S. A.; Norikane, Y.; Tamaoki, N. J. *Org. Chem.* 2005, 70, 9304.
- 41 Norikane, Y.; Katoh, R.; Tamaoki, N. *Chem. Commun.* 2008, 1898.
- 42 Norikane, Y.; Tamaoki, N. *Org. Lett.* 2004, 6, 2595.
- 43 Siewertsen, R.; Neumann, H.; Buchheim-Stehn, B.; Herges, R.; Näther, C.; Renth, F.; Temps, F. J. *Am. Chem. Soc.* 2009, 131, 15594.
- 44 Knie, C.; Utecht, M.; Zhao, F.; Kulla, H.; Kovalenko, S.; Brouwer, A. M.; Saalfrank, P.; Hecht, S.; Bléger, D. *Chem. Eur. J.* 2014, 20, 16492.
- 45 Ho, M. S.; Barrett, C.; Paterson, J.; Esteghamatian, M.; Natansohn, A.; Rochon, P. *Macromolecules* 1996, 29, 4613.
- 46 Natansohn, A.; Rochon, P.; Pezolet, M.; Audet, P.; Brown, D.; To, S. *Macromolecules* 1994, 27, 2580.
- 47 Wang, X.; Balasubramanian, S.; Kumar, J.; Tripathy, S. K.; Li, L. *Chem. Mater.* 1998, 10, 1546.
- 48 Gallot, B.; Fafiotte, M.; Fissi, A.; Pieroni, O. *Macromol. Rapid Commun.* 1996, 17, 493.
- 49 Viswanathan, N. K.; Yu Kim, D.; Bian, S.; Williams, J.; Liu, W.; Li, L.; Samuelson, L.; Kumar, J.; K. Tripathy, S. J. *Mater. Chem.* 1999, 9, 1941.
- 50 Meng, X.; Natansohn, A.; Barrett, C.; Rochon, P. *Macromolecules* 1996, 29, 946.
- 51 Sisido, M.; Ishikawa, Y.; Itoh, K.; Tazuke, S. *Macromolecules* 1991, 24, 3993.
- 52 Sisido, M.; Ishikawa, Y.; Harada, M.; Itoh, K. *Macromolecules* 1991, 24, 3999.
- 53 Campbell, V. E.; In, I.; McGee, D. J.; Woodward, N.; Caruso, A.; Gopalan, P. *Macromolecules* 2006, 39, 957.
- 54 Momotake, A.; Arai, T. *Polymer* 2004, 45, 5369.
- 55 del Barrio, J.; Oriol, L.; Alcalá, R.; Sánchez, C. *Macromolecules* 2009, 42, 5752.
- 56 Ma, H.; Liu, S.; Luo, J.; Suresh, S.; Liu, L.; Kang, S. H.; Haller, M.; Sassa, T.; Dalton, L. R.; Jen, A. K. Y. *Adv. Funct. Mater.* 2002, 12, 565.
- 57 Ding, L.; Xu, M.; Wang, J.; Liao, Y.; Qiu, J. *Polymer* 2014, 55, 1681.
- 58 Ding, L.; Zhang, L.; Han, H.; Huang, W.; Song, C.; Xie, M.; Zhang, Y. *Macromolecules* 2009, 42, 5036.

- 59 Matloka, P. P.; Sworen, J. C.; Zuluaga, F.; Wagener, K. B. *Macromol. Chem. Phys.* 2005, 206, 218.
- 60 Winkler, M.; Mueller, J. O.; Oehlenschlaeger, K. K.; Montero de Espinosa, L.; Meier, M. A. R.; Barner-Kowollik, C. *Macromolecules* 2012, 45, 5012.
- 61 Zhang, L.; Zhang, H.; Gao, F.; Peng, H.; Ruan, Y.; Xu, Y.; Weng, W. *RSC Adv.* 2015, 5, 12007.
- 62 Reimann, S.; Baumeister, U.; Binder, W. H. *Macromol. Chem. Phys.* 2014, 215, 1963.
- 63 (a) Okumura, S.; Lin, C.-H.; Takeda, Y.; Minakata, S. *J. Org. Chem.* 2013, 78, 12090. (b) Rollas, S. *Marmara Pharm. J.* 2010, 14, 41. (c) Koppes, W. M.; Moran, J. S.; Oxley, J. C.; Smith, J. L. *Tetrahedron Lett.* 2008, 49, 3234.
- 64 Schmidt, B. *Chem Commun.* 2004, 742.
- 65 Schmidt, B. *Angew. Chem. Int. Ed.* 2003, 42, 4996.
- 66 Arisawa, M.; Terada, Y.; Nakagawa, M.; Nishida, A. *Angew. Chem. Int. Ed.* 2002, 41, 4732.
- 67 Alcaide, B.; Almendros, P. *Chem. Eur. J.* 2003, 9, 1258.
- 68 Finnegan, D. F.; Snapper, M. L. *The J. Org. Chem.* 2011, 76, 3644.
- 69 Finnegan, D.; Seigal, B. A.; Snapper, M. L. *Org. Lett.* 2006, 8, 2603.
- 70 Gimeno, N.; Formentín, P.; Steinke, J. H. G.; Vilar, R. *Eur. J. Org. Chem.* 2007, 2007, 918.
- 71 Kumar, G. S.; Neckers, D. C. *Chem. Rev.* 1989, 89, 1915.
- 72 Lamarre, L.; Sung, C. S. P. *Macromolecules* 1983, 16, 1729.
- 73 Irie, M.; Schnabel, W. *Macromolecules* 1981, 14, 1246.
- 74 Chen, D. T.-L.; Morawetz, H. *Macromolecules* 1976, 9, 463.
- 75 Blasco, E.; Serrano, J. L.; Piñol, M.; Oriol, L. *Macromolecules* 2013, 46, 5951.
- 76 Ding, L.; Li, J.; Jiang, R.; Song, W. *Materials* 2016, 9, 1.
- 77 Xie, M.; Han, H.; Wang, W.; He, X.; Zhang, Y. *Macromol. Chem. Phys.* 2008, 209, 544.

3.3 Crystallization behavior of ADMET Polyethylene Containing Azobenzene Defects

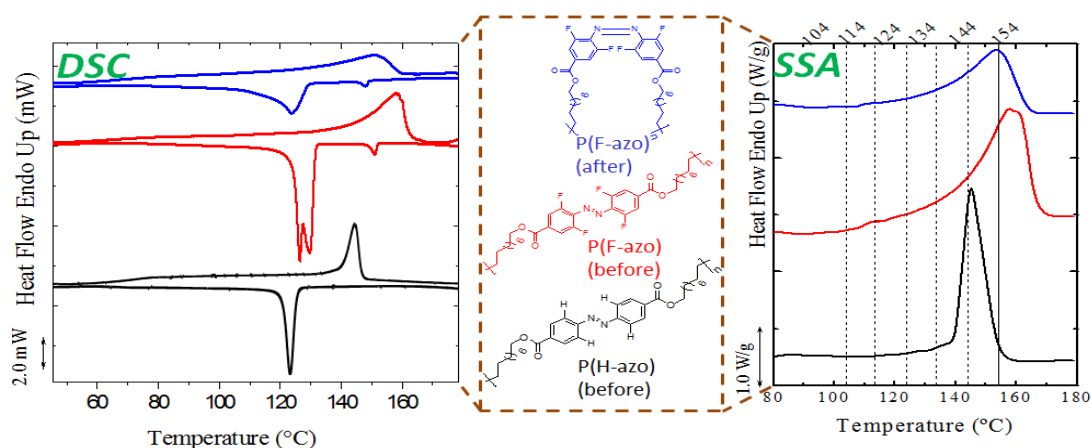
Clement Appiah,[†] Georg Woltersdorf,^{‡‡} Ricardo A. Pérez-Camargo,[§] Alejandro J. Müller,^{§,‡} and Wolfgang H. Binder^{*,†}

[†]Institute of Chemistry, Chair of Macromolecular Chemistry, Faculty of Natural Science II (Chemistry, Physics and Mathematics), Martin Luther University Halle-Wittenberg, von-Danckelmann-Platz 4, D-06120, Halle (Saale), Germany.

^{‡‡}Institute of Physics, Faculty of Natural Science II (Chemistry, Physics and Mathematics), Martin Luther University Halle-Wittenberg, von-Danckelmann-Platz 3, D-06120, Halle (Saale), Germany.

[§]POLYMAT and Polymer Science and Technology Department, Faculty of Chemistry, University of the Basque Country UPV/EHU, Paseo Manuel Lardizabal 3, 20018, San Sebastián, Spain.

[‡]IKESBASQUE, Basque Foundation for Science, Bilbao, Spain.



Eur. Polym. J. 2017, submitted

Abstract: The crystallization of precision oligomers/polymers containing (cis/trans)-azo-benzenes as defects within a polyalkylene-chain, prepared via ADMET and subsequent hydrogenation, is reported. The oligomers/polymers are designed such that after exactly 18 $-\text{CH}_2-$ units an azobenzene-moiety (bearing either a o,o-dihydrogen (H-azo) or an o,o-difluorinated azo-moiety (F-azo) is placed, able to photochemically switch a cis/trans configuration, thus changing the geometrical constraint exerted on the alkyl-moiety during crystallization and its crystal packing. The morphology of these oligomers/polymers ($M_n = 3100$ to $17\,000$ g/mol) is investigated using differential scanning calorimetry (DSC), wide-angle X-ray diffraction (WAXD) and successive self-nucleation and annealing (SSA) experiments, putting a special emphasis on the crystallization of the alkyl moieties. H/F-azo defects within the poly(alkyl)-chains significantly increase the melting point of the polymers compared to ADMET polymers without defect. Successive self-nucleation and annealing (SSA) and WAXS analysis show inclusion of the azo-moieties into the PE crystal. Changing the aromatic azo units from hydrogen (H-azo) to fluorine (F-azo) atoms also increases the enthalpy of melting and the melting point of the azo-oligomers/polymers. Photochemical trans-to-cis isomerization of the (F-azo)-polymers increases lattice disorder throughout the entire sample to an extent sufficient to disrupt the long-range structuring of the sample, thus causing the reduction in their crystallinities.

Introduction

Structural defects in synthetic polymers, such as branching, chemical irregularities in monomer-composition or in stereochemistry are well known, as they significantly influence the chemical microstructure of polymers [1-4]. Defects can be either excluded or included into a polymer crystal, depending on their size and nature, finally strongly influencing the thermal and mechanical properties [5-10]. Thus in the case of side group defects, the exclusion of larger-sized defects from the crystalline lamellar structure is often reported [11-16]. For example propyl-, styrene and vinyl acetate- side groups within a polyethylene (PE) chain are typically excluded from the PE crystal lattice [11-17]. Alamo and Mandelkern [12] reported that only small groups, such as methyl, chlorine, oxygen, and hydroxyl-moieties are partially incorporated into the crystal lattice, whereas bigger defects are expelled from the crystal. Hosoda et al. [18] prepared various ethylene/ α -olefin copolymers showing that the probability of branch inclusion into the crystal is strongly dependent on branch identity and is in the order of methyl > ethyl > butyl = hexyl = decyl > isobutyl. While the side group defects are mostly excluded from the crystal lattice, the reverse is mostly seen in defects situated within the main chain [19-25]. Notwithstanding, some reported cases of exclusion of larger size defects in the main chain of polymers have also been demonstrated [12,26], leading to a decrease in the equilibrium melting temperature T_m^0 [27,19]. Thus e.g. larger-sized defects such as meta- and para-substituted arylene- or naphthylene ether units on every 21st carbon can be included in the crystal lamella, leading to expansion of interchain distances and increase of lamellar thickness [23].

Acyclic diene metathesis (ADMET) polymerization enables to synthetically introduce a sequence of exact chemical repeat unit structures, obtaining polymers with precisely placed defect units [28,29]. We recently have

effected the placement of photoresponsive azo-moieties repetitively within a poly(alkyl)-chain, interrupting the alkyl-chain after every 18 $-(CH_2)$ -units [30]. Such azo-moieties can reversibly change from a trans- to a cis-conformation upon photo-isomerisation, known to induce significant structural changes in polymers [31-36] such as crystallization [37,38], phase changes [39], phase separation (or reversal of phase separation) [40] in e.g., surface gratings in thin films [41,42] Also significant changes in thermal properties, such as the glass-transition temperature can be photochemically achieved, inducing photoinduced solid-to-liquid transitions [43] or changes in porosity by photoisomerization [44].

We hereby describe a new series of hydrogenated/fluorinated azobenzene (H-azo and F-azo)-oligomers/polymers, wherein the defects are precisely and periodically distributed along the main polyalkyl chain via ADMET polymerization. The (H-azo and F-azo)-azobenzenes not only differ in their polarity (the F-azo-oligomer/polymer being significantly more polar due to the presence of the fluorine moieties) but also in their stability after photoswitching. The crystallization; melting/cooling enthalpies, the photoswitchable glass transition temperature, T_g and reversible photo-isomerisation of these materials are described, encompassing the influence of the H-azo and F-azo defects on the crystal structure of the obtained oligomers/polymers.

Experimental

Materials. Two series of precision oligomers/polymers containing (cis/trans)-azo-benzenes (H-azo and F-azo) have been studied. The synthesis of these materials has been accomplished according to a previous publication (see citation [30]) via ADMET of H-azo-monomer and F-azo-monomer, furnishing the H-azo and F-azo-oligomers/polymers with a molecular weight as shown

in Table 1. Data relevant to the molecular and thermal characterization of these materials are as well shown in Table 1.

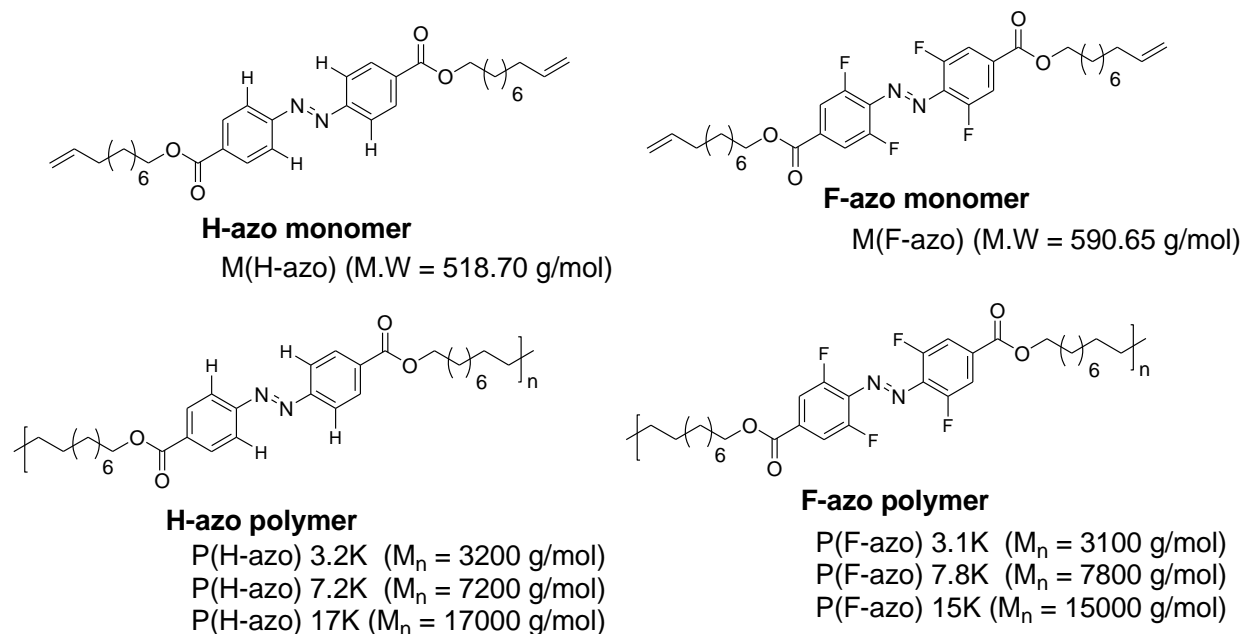


Figure 1. Representative chemical structures of the H-azo and F-azo monomers, and the saturated oligomers and polymers (after catalytic hydrogenation) used for the investigations [30].

Characterization. ^1H -, ^{13}C - and ^{19}F -NMR spectra were recorded on a Varian spectrometer (Gemini 400) at 400 MHz at 27 °C. CDCl_3 (Armar AG, 99.8 Atom%D) was used as solvent and tetramethylsilane was used as internal standard. The coupling constants were given in Hz, the chemical shifts in ppm, and referred to the solvent residue peak [CDCl_3 7.26 ppm (^1H) and 77.0 ppm (^{13}C)]. For the interpretation of the spectra, MestReNova v. 6.0.2–5475 was used.

For Gel permeation chromatography (GPC) measurements, a Viscotek GPCmax VE 2002 with an $\text{H}_{\text{HR}}\text{H}$ Guard-17369 and a $\text{GMH}_{\text{HR}}\text{N}$ -18055 column in tetrahydrofuran (THF) was used. 100 μL of 1 mg mL^{-1} samples were injected at 22 °C. Detection was carried out with a Viscotek VE3580 RI detector at 35 °C and a flow rate of 1 mL min^{-1} . Poly(styrene) standards with molecular weights of 1050, 2790, 6040, 13 400, and 29 600 g mol^{-1} were used for external calibration.

FTIR spectra were recorded on a Bruker Vertex70MIR spectrometer using an ATR Golden Gate unit with a diamond crystal. The scan number was 32 scans per spectrum with a resolution of 2 cm^{-1} .

UV-VIS absorption spectra were measured using a Jasco V-670 UV/VIS/NIR spectrometer. The thickness of the optical cells for the measurement was 10 mm. The light exposure (for photoswitching) was performed using high power (300 mW) ultraviolet (300 nm) and green (520 nm) light emitting diodes (LEDs) mounted at a distance of 5 mm from the window of the optical cell in the sample chamber of the spectrometer.

Differential scanning calorimetry (DSC) measurements were carried out on a NETZSCH DSC 204F1 Phoenix, which was calibrated with indium, tin, bismuth, and zinc. Samples with a mass of about 5-8 mg were placed into a standard aluminium pan and nitrogen was used as purge gas. Netzsch Proteus-Thermal Analysis (version 5.2.1.) was used for the interpretation of the obtained data. For

the non-isothermal measurements, the samples were heated with a heating rate of 10 °C/min to 180 °C, at an annealing time of 10 min, and cooled down to -50 °C with a cooling rate of 10 °C/min. The melting/cooling temperatures were evaluated from the peak maximum of the heating/cooling runs respectively.

X-ray scattering experiments were performed in transmission mode using a SAXSLAB laboratory setup (Retro-F) equipped with an AXO microfocus X-ray source with an AXO multilayer X-ray optic (ASTIX) as monochromator for Cu K α radiation ($\lambda = 0.154$ nm). A DECTRIS PILATUS3 R 300 K detector was used to record the 2D scattering patterns. As sample holders, two-millimeter thick aluminum discs with a central hole were used. The measurements were performed in vacuum at three sample to detector distances to cover a wider q -range ($q = 0.05$ - 3 nm $^{-1}$; 0.25 - 7 nm $^{-1}$ and $q = 1$ - 29 nm $^{-1}$).

ADMET oligomerization/polymerization of the azobenzene monomers (M(H-azo) and M(F-azo)) [30]

In a nitrogen-filled Schlenk tube containing a solution of the appropriate catalyst in 0.1 mL of degassed toluene was subjected to three freeze vacuum thaw cycles. A degassed solution of the diene monomer M(H-azo) and M(F-azo), 0.2 mol, (250:1 monomer to catalyst ratio) in 0.4 mL of toluene was subsequently added to the Schlenk flask, degassed for additional 30 min, and stirred for 120 h at 100 °C. The polymerization was finally quenched by adding ethyl vinyl ether (0.5 mL) with additional stirring for 30 min. The crude solution was precipitated in excess methanol, and the precipitate was isolated by filtration, dried in vacuo to give the unsaturated azobenzene oligomers and polymers (Table 1).

$^1\text{H-NMR}$ (unsaturated P(H-azo) 17K, CDCl_3): δ (ppm) 8.14-8.33 (m, 4H, m-ArH-N=N-ArH), 7.65-8.04 (m, 4H, m-ArH-N=N-ArH), 5.28-5.41 (m, 2H, CH=CH), 4.17-4.30 (m, 4H, CH_2OCO), 1.98-2.00 (m, 4H,

$\text{CH}_2=\text{CHCH}_2$), 1.70-1.74 (m, 4H, $\text{OCOCH}_2\text{CH}_2$), 1.28-1.42 (m, 20H, CH_2). $^{13}\text{C-NMR}$ (unsaturated P(H-azo) 17K, CDCl_3): δ (ppm) 173.1, 155.2, 139.8, 132.1, 130.8, 123.8, 118.1, 66.3, 35.7, 29.8, 25.5. IR (unsaturated P(H-azo) 17K, cm^{-1}): 2917, 2850, 1701, 1638, 1596, 1384, 1014, 832. $^1\text{H-NMR}$ (unsaturated P(F-azo) 15K, CDCl_3): δ (ppm) 7.07-7.33 (m, 4H, m-ArH-N=N-ArH), 5.29-5.45 (m, 2H, CH=CH), 3.61-3.64 (m, 4H, CH_2OCO), 2.00-2.06 (m, 4H, $\text{CH}_2=\text{CHCH}_2$), 1.52-1.59 (m, 4H, $\text{OCOCH}_2\text{CH}_2$), 1.29-1.37 (m, 20H, CH_2). $^{13}\text{C-NMR}$ (unsaturated P(F-azo) 15.0K, CDCl_3): δ (ppm) 172.1, 156.6 (d, $J = 5.1$ Hz), 154.2 (d, $J = 5.2$ Hz), 137.8, 135.2, 132.1, 131.3, 125.2, 117.6, 63.4, 33.1, 29.4, 25.6. -117 (d, $J = 5.1$ Hz), -119 (d, $J = 7.5$ Hz). $^{19}\text{F-NMR}$ (unsaturated P(F-azo) 15K, CDCl_3): δ (ppm): -117 (d, $J = 5.1$ Hz), -119 (d, $J = 7.5$ Hz). IR (unsaturated P(F-azo) 15K, cm^{-1}): 3328, 3102, 2925, 2854, 1701, 1640, 1600, 1424, 1349, 1091, 994, 839.

Hydrogenation reaction of the fluorinated and non-fluorinated unsaturated azobenzene polymers (P(H-azo) 17K and P(F-azo) 15K).

A dried and nitrogen filled one-necked flask equipped with a magnetic stir bar and a reflux condenser was filled with a highly degassed solution of the unsaturated ADMET polymer (P(H-azo) 17K or P(F-azo) 15K, 100 mg), *p*-toluenesulfonylhydrazide (3 mol eqv.) *N,N*-diisopropylethylamine (3 mol eqv.) and *N,N*-dimethylformamide (DMF) (6 mL). The reaction mixture was heated to 120 °C under vigorous stirring for 6 h. It was then allowed to cool down to room temperature. The solvent was removed in vacuo, and the obtained saturated polymers were precipitated in methanol (yield ~ 75 %).

$^1\text{H-NMR}$ (saturated P(H-azo) 17K, CDCl_3): δ (ppm) 8.14-8.33 (m, 4H, m-ArH-N=N-ArH), 7.65-8.04 (m, 4H, m-ArH-N=N-ArH), 4.17-4.30 (m, 4H, CH_2OCO), 1.98-2.00 (m, 4H, $\text{CH}_2=\text{CHCH}_2$), 1.70-1.74 (m, 4H,

OCOCH₂CH₂), 1.28-1.42 (m, 20H,CH₂). ¹³C-NMR (saturated P(H-azo) 17K, CDCl₃): δ(ppm) 173.1, 155.2, 132.1, 130.8, 123.8, 66.3, 35.7, 29.8, 25.5, 21.6, 17.7. IR (saturated P(H-azo) 17K, cm⁻¹): 2917, 2850, 1638, 1596, 1384, 1014, 832. ¹H-NMR (saturated P(F-azo) 15K, CDCl₃): δ(ppm) 7.07-7.33 (m, 4H, m-ArH-N=N-ArH), 3.61-3.64 (m, 4H, CH₂OCO), 2.00-2.06 (m, 4H, CH₂=CHCH₂), 1.52-1.59 (m, 4H, OCOCH₂CH₂), 1.29-1.37 (m, 20H,CH₂). ¹³C-NMR (saturated P(F-azo) 15K, CDCl₃): δ(ppm) 171.8, 157.4 (d, J = 5.1 Hz), 154.5 (d, J = 5.3 Hz), 132.1, 131.3, 127.8, 63.6, 33.4, 29.4, 25.8, 21.7, 17.8. ¹⁹F-NMR (saturated P(F-azo) 15K, CDCl₃): δ(ppm): -117 (d, J = 5.1 Hz), -119 (d, J = 7.5 Hz). IR (saturated P(F-azo) 15K, cm⁻¹): 3328, 3102, 2925, 2854, 1640, 1600, 1424, 1349, 1091, 994, 839.

Table 1. Molecular and thermal characterization of the saturated azo oligomers and polymers

Polymer	trans:cis (NMR)	trans:cis (UV-VIS)	Mn,SEC ^a /(g/mol)	Mw/Mn ^a	T _c ,DSC ^b /(°C)	T _m ,DSC ^b /(°C)	ΔH _m ,DSC ^b /(J/g)
Oligomers							
P(H-azo) 3.2K	84:16	87:13	3200	1.3	122	145	61
P(H-azo) 7.2K	84:16	89:11	7200	1.7	125	147	69
P(F-azo) 3.1K	88:12	86:18	3100	1.6	127, 130	159	112
P(F-azo) 3.1K (after switch)	32:68	36:64	3100	1.6	124	151	81
P(F-azo) 7.8K	90:10	87:17	7800	1.4	126, 131	158	114
P(F-azo) 7.8K (after switch)	35:65	33:67	7800	1.4	125	151	87
Polymers							
P(H-azo) 17K	82:18	85:15	17000	2.0	124	138, 141	72
P(F-azo) 15K	90:10	88:18	15000	1.8	124,130	159	117
P(F-azo) 15K (after switch)	36:64	31:69	15000	1.9	130	153	90

^aDetermined by SEC in THF using polystyrene standards. ^bDetermined by DSC from 1st heating/cooling cycle

Results and Discussion

We prepared two types of oligomers and polymers by ADMET (see Figure 1), both containing an azo-moiety within the main chain after exactly 18 -CH₂-units: whereas the H-azo-oligomers/polymers contain hydrogen on both o-positions within the aromatic rings, the F-azo-oligomers/polymers contain o,o-difluoro-aromatic moieties, known to display an increased stability of the cis-form of the azobenzene-moiety [31]. Hydrogenation of all olefinic double bonds of the H-azo and F-azo oligomers/polymers is conducted using p-toluenesulfonylhydrazide (TsNHNH₂) and N,N-diisopropylethylamine in DMF at 120 °C under a highly inert nitrogen atmosphere and a complete removal of

oxygen from the reaction mixture. The investigated oligomers/polymers are obtained with molecular weights in the range of 3100 - 17000 gmol⁻¹ (see Table 1)- ¹H-NMR measurements show the disappearance of the resonance peak at 5.39 ppm, assigned to the internal olefinic protons of the unsaturated oligomers after the hydrogenation reaction [30], thus proving the complete transformation after the exhaustive hydrogenation reaction. FTIR and HPLC measurements are also conducted to support the proof of the exhaustive hydrogenation reaction (see citation [30]).

The azobenzene groups in the as-prepared saturated oligomers/polymers bearing the bis-o-fluorinated-azo-oligomers/polymer P(F-azo) are in a primarily stable

trans state and exhibit a strong π - π^* absorption band at 320 nm (see Figure 2). Irradiation of the solution with green light ($\lambda \sim 520$ nm) decreases the intensity of the π - π^* absorption band while the n - π^* absorption band intensity at 426 nm slightly increases. Subsequent UV light irradiation (~ 300 nm) on the cis-compounds (P(F-azo) (switch)) switches the molecules back to the trans state [30]. The switched cis form has a lifetime of approximately 14 h before it relaxes by thermal recovery

to the trans-state, indicating an increased thermal stability of the bis-o-fluorinated-azo-oligomer/polymer in solution [30]. Comparison of the two different molecular weights, P(F-azo) 3.1K, Figure 2i and P(F-azo) 15K, Figure 2ii reveals no significant differences in their UV switching. The photostationary state for the two materials is however reached at the same time at approximately 60 min of irradiation.

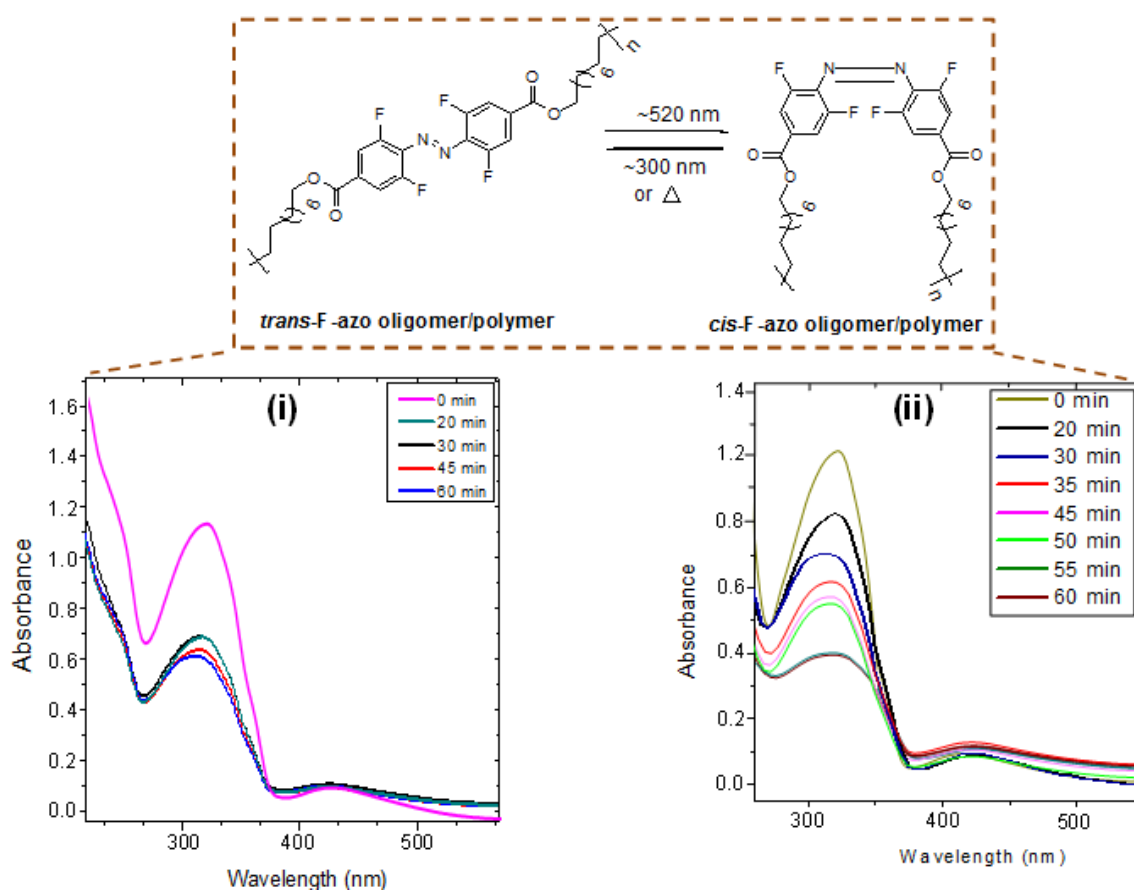


Figure 2. UV-VIS spectra of the saturated F-azo oligomers (left, P(F-azo) 3.1K, 2.34×10^{-4} mol/L) polymer (right, P(F-azo) 15K, 2.72×10^{-4} mol/L) in THF solution before irradiation at 0 min, and after complete irradiation (520 nm) for 1 h.

Figure 2i shows the change of the absorption spectrum for the F-azo oligomer upon illumination of the sample with 520 nm light. Already within the first 20 min the spectrum changes significantly due to light-induced switching of trans isomers into cis isomers. A photostationary state is reached after ~ 60 min of

irradiation. In the photostationary state, the vast majority of the F-azo oligomer molecules exist in the *cis* configuration. The two isosbestic points at 320 nm and 426 nm indicate that only two species are present (*trans*- and *cis*-) and no additional photochemical reactions occur. Light-induced switching from *trans* to

cis isomer is also observed for the F-azo polymer (Figure 2ii). The photostationary state is also reached after ~60 min of irradiation. The length of the PE chain does not seem to influence the properties of the photostationary state, as the spectral and temporal behaviors of the different molecular weight materials are identical within experimental uncertainties.

The photo-induced trans/cis-isomerisation in the saturated oligomer/polymer can also be followed via ^1H -NMR-spectroscopy, as visible in Figure 3. The NMR data of the polymer (P(F-azo) 15K) show a final cis : trans ratio of 69 : 31 % after the UV-VIS irradiation, accompanied by an increase in the cis resonance peak at around 7.10 ppm and a decrease in the trans resonance

peak at 7.20 ppm, proving a transformation from the trans to the cis structures due to the UV-VIS photo-switching.

Due to their reasonable thermal stability, coupled to the efficient cis/trans switching, the so obtained bis-o-fluorinated-azo-oligomers/polymers (P(F-azo) 3.1K, P(F-azo) 7.8K and P(F-azo) 15K) are thus ideal candidates for studying the crystallization in the trans- and cis-forms, respectively, most of all in terms of their impact on thermal transitions and crystal-structure. The corresponding H-azo-oligomers/polymers P(H-azo) 3.2K, P(H-azo) 7.2K and P(H-azo) 17K are discussed in comparison, although their cis-forms here are thermally too labile for a crystallization study.

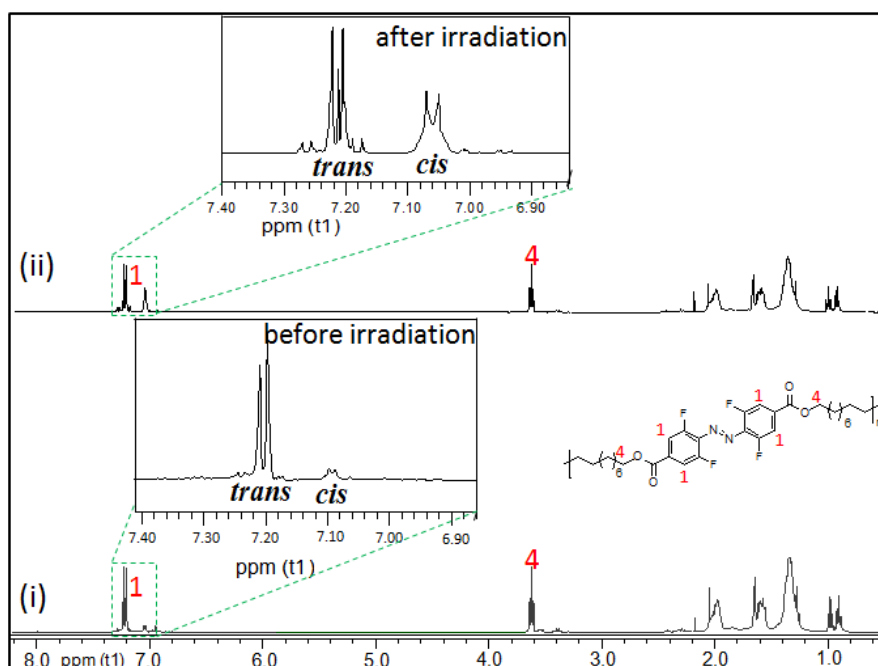


Figure 3. ^1H - NMR spectrum of the F-azo-polymer P(F-azo) 15K before (i) and after (ii) green light irradiation ($\lambda \sim 520$ nm), showing the changes in the cis/trans resonance peaks.

Differential scanning calorimetry (DSC) measurements.

The thermal behavior of the monomers, oligomers and polymers is determined via DSC measurements. Non-isothermal heating curves for the F-azo- (M(F-azo)) and H-azo- (M(H-azo)) monomers are shown in Figures S2-3 (see SI). Comparing the crystallization and melting

curves of the two azo monomers M(F-azo) and M(H-azo), a clear difference between the two monomers is observed. Whereas M(H-azo) is 100 % amorphous and shows no melting transition but only a glass transition, T_g at 68 °C (Figure S3), M(F-azo) shows a crystalline structure (Figure S2) with melting (T_m) and crystallization

(T_c)-values at temperatures of $T_{m1} = -19.3$ °C, $T_{m2} = -13.4$ °C and $T_c = -36.4$ °C. In the DSC curves (see Figure S2 - Supporting information) of the F-azo monomer M(F-azo) before irradiation, fractionation of the melting peak is noticeable upon heating of the monomer from 50 °C to 130 °C, explainable by the occurrence of both cis- and trans-form crystals. At elevated temperatures of 150 °C and above, a single sharp endotherm is observed due to the increased trans content at this temperature (note: $^1\text{H-NMR}$ studies of the cis : trans ratio of the F-azo monomer before irradiation at room temperature and at 150 °C were reported to be 20 : 80 and 7 : 93 respectively, see supporting information, Figure S5) [30]. Upon photochemical switching of the monomer (Figure 4) a transformation from the trans- to the cis- form occurs, clearly changing the DSC curve of the F-azo monomer, as visible in the heating/cooling scans of the F-azo monomer M(F-azo) after UV-VIS photoswitching.

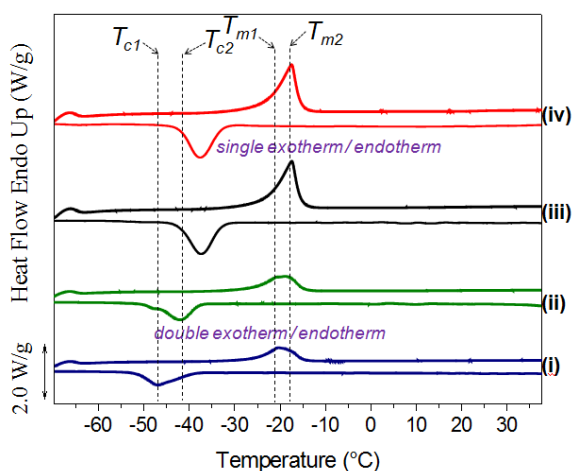


Figure 4. DSC heating/cooling scans of the F-azo monomer M(F-azo) after green light irradiation ($\lambda \sim 520$ nm). Measurements were conducted by annealing the samples at 10 K/min for 1h at temperatures of; (i) 75 °C (ii) 125 °C (iii) 150 °C and (iv) 175 °C. Data are rescaled and shifted vertically for clarity.

Double broad endothermic ($T_{m1} = -20.9$ °C, $T_{m2} = -17.9$ °C) /exothermic ($T_{c1} = -47.5$ °C, $T_{c2} = -41.6$ °C) peaks are noticeable upon heating the monomer from 75 °C to 125 °C, with a slight shift of the exothermic peaks to lower temperatures when compared to the exothermic peak of the monomer before irradiation ($T_c = -36.4$ °C). At a temperature at 150 °C and above, the double broad exothermic/endothermic peaks merge to form a single sharp peak with an accompanied shift of the exothermic peak ($T_c = -37.1$ °C) back to nearly the same position to the peak before the switching process. This behavior shows that, at elevated temperatures (≥ 150 °C), the thermally generated trans azo-isomer within our monomer is regenerated above this temperature.

Crystallization studies of the oligomers/polymers before and after the photo-irradiation at 520 nm are subsequently conducted at a heating/cooling rate of 10 °C/min. P(F-azo) 15K (before switching) shows a T_g of 91.8 °C in the first and second heating curves, with a slight shift of the T_g to higher temperature (95.8 °C) in the third heating. In contrast to P(F-azo) 15K (before switching), P(F-azo) 15K (after switching) shows a significantly lower T_g at 70.6 °C in the first heating curve (Figure 5). The second heating DSC T_g curve of this sample is nearly the same as that of the initial P(F-azo) 15K (before switching), indicating that cis P(F-azo) 15K (after switching) is thermally converted to trans P(F-azo) 15K (before switching) in the second heating process as a result of a first photo-induced trans-to-cis isomerization, followed subsequently by a thermally-induced cis-to-trans isomerisation process.

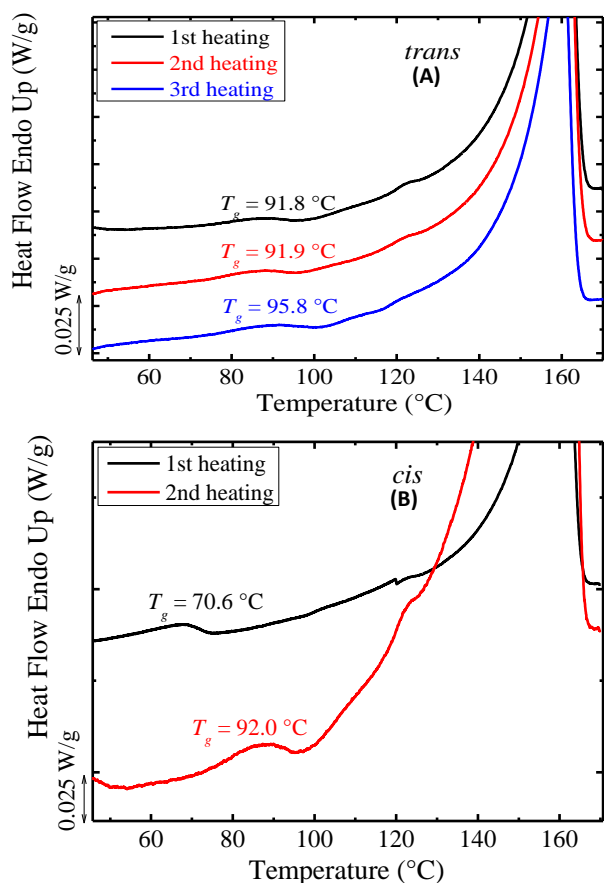


Figure 5. DSC heating scans of the saturated trans-F-azo polymer (A, P(F-azo) 15K (before switching)) and the saturated cis-F-azo polymer (B, P(F-azo) 15K (after switching)). The T_g value of cis-F-azo polymer is lower than that of trans-F-azo polymer. Data are rescaled and shifted vertically for clarity.

The heating and cooling curves for the oligomers/polymers are shown in Figure 6 for both, the crystallization and the melting, and the results are summarized in Table 1. When we compare our results to PE (prepared by ADMET) without defects ($T_m = 134$ °C, $\Delta H_m = 211$ J/g) (data from literature for same heating rate to our measurements) [45], a decrease in the melting enthalpy and a shift of the T_m values to high temperatures is observed. The decrease in melting

enthalpy can be attributed to a reduction in the degree of crystallinity, as the azobenzene defects within our poly(alkyl) chains hinder the crystallization. However, the increase in T_m may be due to the inclusion of the defects within the crystalline lamellae. The exclusion of the defect would interrupt the linear aliphatic chain sequences and therefore reduce lamellar size and melting point. A high extent of supercooling ($\Delta T = T_m - T_c$) additionally exist between our investigated oligomers/polymers; e.g. P(H-azo) 3.2K ($\Delta T = 23$ °C) and P(F-azo) 3.1K ($\Delta T = 27-31$ °C). The high supercooling of the azo-polymers implies a slower overall non-isothermal crystallization rate from the melt [2,23]. Increasing the molecular weight of the azo-polymers (Table 1) does not lead to significant changes in the crystallization/melting temperatures, but a slightly increased enthalpy as compared to the low molecular weight oligomers.

Furthermore, upon changing the molecular structure of the defect from hydrogenated to fluorinated azobenzenes, leads to an increase in the melting temperatures of about 14 °C and an increased enthalpy of about 51 J/g. This is due to the strong dipolar interactions of the F atoms in the fluorinated azobenzenes that stabilize the chain conformations in the crystalline state, thus enhancing the thermal stability of these oligomers and polymers. In the cooling curve of the F-azo oligomer/polymer (P(F-azo)) fractionated exotherms are visible at (P(F-azo) 3.1K = 127 °C, 130 °C and P(F-azo) 15K = 124 °C, 130 °C), suggestive of the occurrence of both, trans- and cis-isomers during crystallization. In contrast to the P(F-azo) 3.1K (before switching), P(F-azo) 3.1K (after switching) shows a single broad exothermic peak at 124 °C due to the thermal cis-to-trans isomerisation as demonstrated in literature [43].

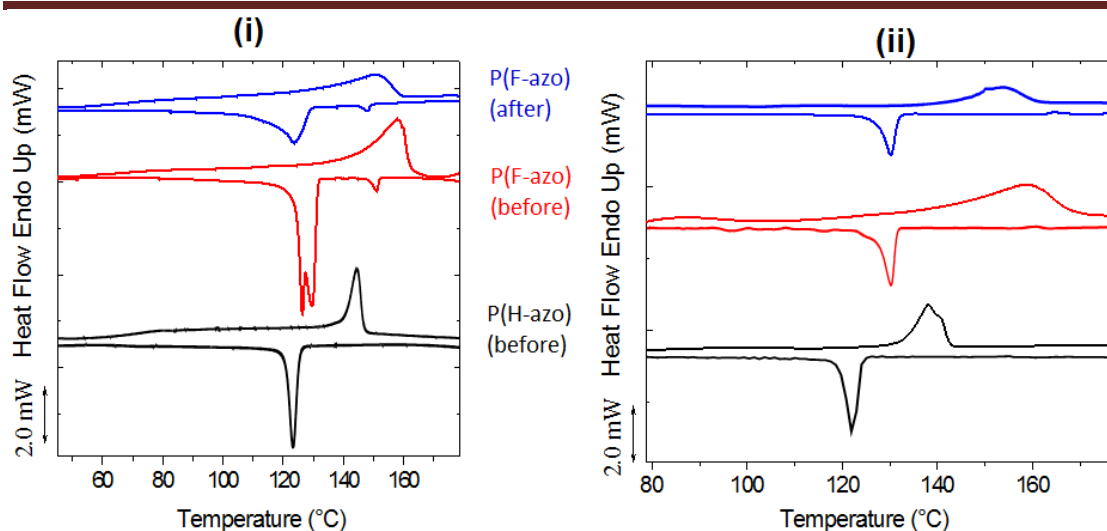


Figure 6. DSC cooling and heating curves for the saturated H-azo oligomers (left) and saturated polymers (right): (P(H-azo) 3.2K, and P(H-azo) 17K, black), F-azo polymer (P(F-azo) 3.1K, and P(F-azo) 15K red) before irradiation and F-azo polymer (P(F-azo) 3.1K, and P(F-azo) 15K blue) after irradiation. Data are rescaled and shifted vertically for clarity.

Self-Nucleation (SN) and Successive Self-Nucleation and Annealing (SSA) results. SSA is a thermal fractionation protocol designed to deconvolute DSC melting endotherms into elementary components. It is particularly useful to fractionate polymers that incorporate defects in their linear crystallizable chains (e.g., branches, comonomers, crosslinks, stereo-defects or any other molecular defects) [46]. In this work, SSA is used to study whether the known defects are included or excluded from the polymer crystals. Exclusion of defects will provoke large fractionation effects [46]. Thus, to this end, we performed SN tests on the saturated F-azo oligomers/polymer before switch to determine the ideal self-nucleation temperature, T_s . This temperature is needed to adequately perform SSA tests [46]. The F-azo oligomer/polymer is selected for the SN test, since it has the highest melting temperature from all the samples used. The experiment is carried as follows to obtain the ideal self-nucleated state;

- Erase of previous thermal history and crystalline memory by heating the sample to 185 °C for 3 min.
- Creation of the initial “standard” semi-crystalline state by cooling the molten sample at 20 °C/min down to -20 °C.
- Heating at 20 °C/min from -20 °C up to a selected self-nucleation temperature (denoted T_s), and then holding the sample at this T_s temperature for 3 min. During this thermal conditioning stage at T_s , the sample could melt, self-nucleate or self-nucleate and anneal depending on the temperature value.
- Subsequent cooling at 20 °C/min from T_s down to -20 °C.
- Final heating. The sample is heated at 20 °C/min from -20 to 185 °C.

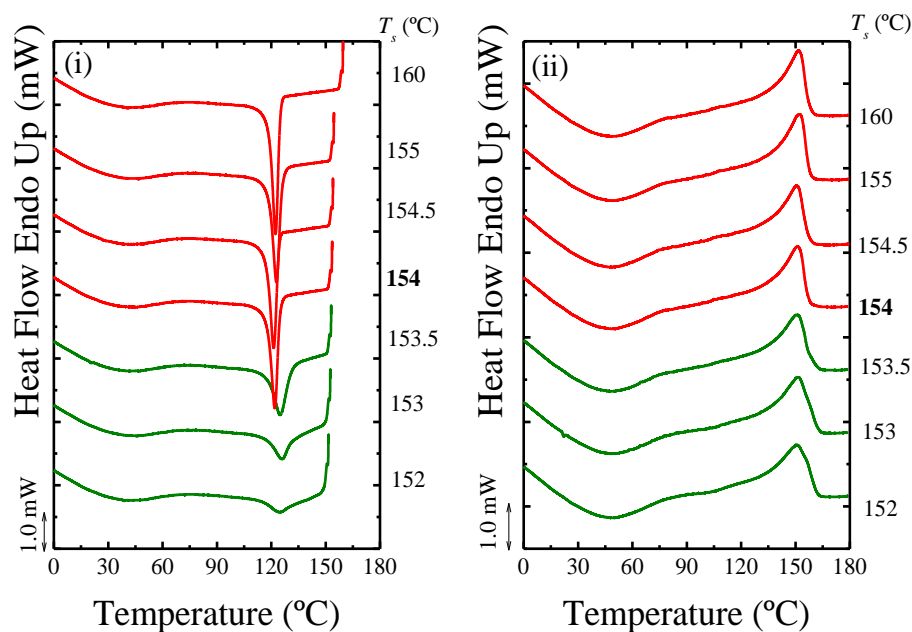


Figure 7. (i) Cooling and (ii) heating of the saturated P(F-azo) 15K (before irradiation) after 5 min at the indicated self-nucleation temperature (154 °C).

Figures 7i and ii depict the DSC cooling and heating scans obtained from the above protocol for the F-azo sample (P(F-azo) 15K, before switch) after holding the sample for 3 minutes at the indicated T_s . In Figure 7i sharp crystallization peaks at temperatures higher than 154 °C, are observed while the peak crystallization temperature does not change. Below this temperature the peaks become broader and shift to higher T_c values. However, close examination of Figure 7ii reveals that at T_c values lower than 154 °C, the melting traces change and exhibit a shoulder or small peak at higher temperatures indicative of annealing of a small crystal population. These results correspond to a change from Domain I (at T_s temperatures equal or higher than 154 °C) to Domain III (at T_s values lower than 154 °C). In other words the polymer does not exhibit Domain II or exclusive self-nucleation domain. This situation has been already reported for materials that have a very high density of heterogeneities that can act as nuclei [47,48]. In these cases, the only way to significantly increase the already saturated nucleation is to enter Domain III, where a

significant increase in nucleation will inevitably occur as partial melting will leave many crystal fragments available as self-nuclei. From the self-nucleation experiments shown in Figure 7, a $T_s = 154$ °C was selected as the initial temperature of the SSA protocol, as this is the lowest temperature in Domain I before the sample changes to Domain III. The idea is to select a temperature where no annealing occurs. This is a typical case, as normally the lowest temperature in Domain II would be selected.

Figure 8 shows the final heating DSC scan after the samples were subjected to the SSA experiments. In this work, the fractionation window was set at 10 °C, which mean that in every cycle, the following temperature is employed: $T_{s,n} = T_{s,n-1} - 10$ °C, where n is the number of cycles ($n=0$ correspond to the $T_{s, ideal}$). The selected number of cycles is 6 cycles (including the $T_{s, ideal}$) [48-50]. According to Figure 8, SSA did not cause a significant fractionation, indicating that defects are included within the lamellar regions of the sample. These results are strong evidence supporting the inclusion of the azo

groups in the polyethylene-like crystalline cell. Further confirmation of such inclusion is provided below by WAXS results. It must be noted that the melting temperature after SSA of the sample before the switch is higher than that after the switch. This indicates a possible rearrangement of the polymeric lamellar crystals (i.e., higher T_m values indicate increasing crystal stability and thicker lamellar crystals). It is worth pointing out that the equilibrium melting point for high molar mass linear polyethylene crystals has been estimated to be close to 145 °C [14]. This is an extrapolated value that cannot be obtained experimentally, as it correspond to an infinite crystal with no surfaces. It is obvious from Figure 8 that the samples employed here are melting at 145 °C (in the case of P(H-azo) 3.2K before switching) or even up to 10 °C higher than that value. The only way to explain this result is by an inclusion of the azo groups inside the lamellar crystals.

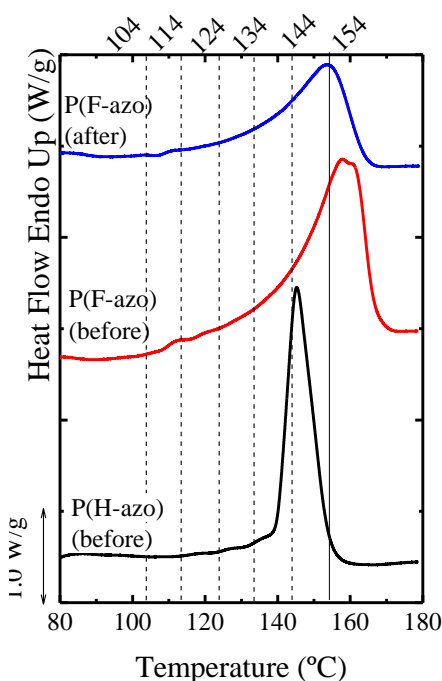


Figure 8. Final heating scans after applying SSA protocol on the saturated H-azo polymer (P(H-azo) 17K, black),

saturated F-azo polymer (P(F-azo) 15K, red) before irradiation and saturated F-azo polymer (P(F-azo) 15K, blue) after irradiation.

WAXS results. The WAXS patterns of the ADMET polymers containing H-/F-azo defects are shown in Figure 9. It is evident from the Figure that all the investigated samples display sharp scattering peaks, and in addition to them some broad and overlapped peaks can be seen. Many crystallographic peaks are observed in the F-azo compounds, especially in the trans state as compared to the WAXS pattern of the H-azo compounds. This behavior can be due to the higher crystallinity of the F-azo compounds (as indicated by their melting enthalpies: P(F-azo) 15K (before switching) = 117 J/g, P(F-azo) 15K (after switching) = 90 J/g) as compared to the H-azo compound (P(H-azo) 17K = 72 J/g).

Different mixed crystal structures are formed in all the investigated polymers. Figure 9 shows the collected WAXS patterns. The reflections reported in the literature for both orthorhombic and monoclinic polyethylene unit cells are indicated as vertical lines. It is observed from Figure 9 that the P(H-azo) 17K, having H-azo as intra crystalline defect exhibits two sharp scattering peaks at q of 15.01 nm and 16.27 nm which may correspond to the (110) and (200) crystal planes of orthorhombic PE crystal [51]. The calculated lattice parameters ($a = 7.72 \text{ \AA}$ and $b = 4.94 \text{ \AA}$), when compared to orthorhombic ADMET PE without defects ($a = 7.40 \text{ \AA}$ and $b = 4.93 \text{ \AA}$) [45] shows that the b -axis of the P(H-azo) 17K is almost the same, but the a -axis is evidently larger. The larger value of “ a ” implies dilation of the unit cell (i.e., by 4% approximately), which is consistent with the expansion of the orthorhombic unit cell needed to accommodate the azo defect. The shift of the WAXS pattern to lower q values when compared to polyethylenes and paraffins

are evidence of the inclusion of the azo-groups in the unit cell of the polyethylene.

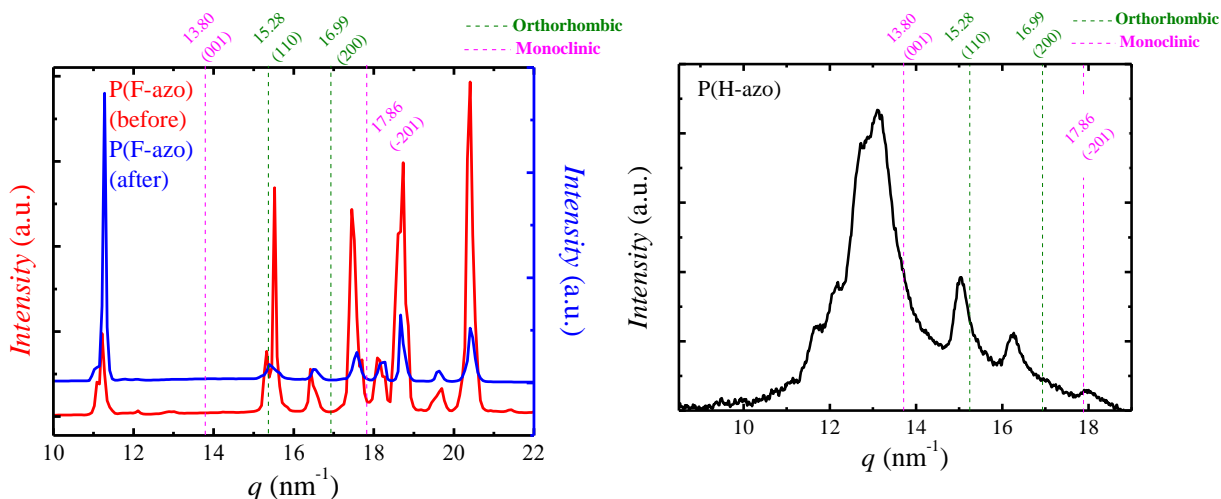


Figure 9. Wide angle X-ray scattering patterns for the saturated F-azo defect polymers (P(F-azo) 15K, left) and saturated H-azo defect polymers (P(H-azo) 17K, right). The inlet dotted lines show the indexing of PE without defect for comparison.

The F-azo polymers on the other hand exhibit an entirely different scattering pattern with a series of new reflections which are not normally found in neat PE WAXS diffractograms. The scattering peaks are much sharper with less pronounced amorphous halo. Many scattering peaks are observed for this polymer and their detailed indexing is outside the scope of the present work (Figure 9, left). The scattering peaks at $q = 15.33$ nm and 16.42 nm may be assigned to orthorhombic crystal structure of PE, whereas the one at $q = 17.52$ nm correspond to the monoclinic crystal structure of PE. A shift of the observed peaks to low q values when compared to crystallographic planes of PE [23,51] without defect signifies a larger unit cell, which is also a result of the incorporation of the F-azo defects within the crystal unit cells. A similar effect has been seen for different defect PE structures [2,7,23,45]. Also, the WAXS pattern in Figure 9 for the cis P(F-azo) 15K (after switching) displays a decreased intensity (with samples of the same mass, volume and shape) of all the peaks noticeable in the trans compound. As observed in literature,⁴⁴ this behavior indicates that the P(F-azo) 15K

(after switching) loses some amount of its crystalline properties upon switching; which can be further verified by the reduction of the ΔH_m value in the non-isothermal DSC measurements. Thus, we can hypothesize similarly to previous findings [44,52,53] that the trans-to-cis isomerization of the polymers increases lattice disorder throughout the entire sample to an extent sufficient to disrupt the long-range structuring of the sample, thus causing the reduction in their crystallinities

Conclusion

The influence of different (trans- and cis-)azobenzene defects on the crystallization and melting behavior, as well as on the crystal morphology of the PE structure has been investigated using DSC, SSA and X-ray scattering experiments. The following results clearly support the inclusion of the azobenzene defects within the crystal lattice: 1. Increases in melting points, 2. Lack of fractionation after SSA experiments and 3. Changes in crystal structure. Changing the aromatic azo units from hydrogen to fluorine atoms shows pronounced effect on the enthalpy of melting and peak melting transition of

the oligomers/polymers. Accordingly, P(F-azo) 15K (before switching) has the highest T_m , but the T_m of P(H-azo) 3.2K is the lowest. Upon conducting SSA experiments, the temperature after SSA of the sample before the switch was higher than that after the switch, which is due to a possible rearrangement of the polymeric lamellar crystals (i.e., higher T_m values indicate increasing crystal stability and thicker lamellar crystals). The obtained results will help in advancing the highly intense research on ADMET polymers, by taken into consideration switchable defects that can tune the properties of the obtained polymer upon changing from the trans to the cis state.

Associated content

Supporting Information

NMR spectra and DSC thermographs of the azo-polymers.

Author information

Corresponding Author

*E-mail: wolfgang.binder@chemie.uni-halle.de (W.H.B)

Notes

The authors declare no competing financial interest.

Acknowledgements

We are grateful for the financial support from the German research foundation (DFG) via collaborative research centre SFB/-TRR 102 (Project A3). We thank Georg Woltersdorf and Ingrid Stössel from the Institute of Physics, Martin Luther University Halle-Wittenberg for the help with the UV-VIS measurements. R.A.P.-C. also gratefully acknowledges the award of a PhD fellowship by POLYMAT Basque Centre for Macromolecular Design and Engineering.

References

- (1) Inci, B.; Wagener, K. B. *J. Am. Chem. Soc.* **2011**, *133*, 11872-11875.
- (2) Qiu, W.; Sworen, J.; Pyda, M.; Nowak-Pyda, E.; Habenschuss, A.; Wagener, K. B.; Wunderlich, B. *Macromolecules* **2006**, *39*, 204-217.
- (3) Rojas, G.; Inci, B.; Wei, Y.; Wagener, K. B. *J. Am. Chem. Soc.* **2009**, *131*, 17376-17386.
- (4) Rojas, G.; Wagener, K. B. *Macromolecules* **2009**, *42*, 1934-1947.
- (5) Androsch, R.; Blackwell, J.; Chvalun, S. N.; Wunderlich, B. *Macromolecules* **1999**, *32*, 3735-3740.
- (6) Bassett, D. C.; Block, S.; Piermarini, G. J. *J. Appl. Phy.* **1974**, *45*, 4146-4150.
- (7) Baughman, T. W.; Sworen, J. C.; Wagener, K. B. *Macromolecules* **2006**, *39*, 5028-5036.
- (8) Boz, E.; Wagener, K. B.; Ghosal, A.; Fu, R.; Alamo, R. G. *Macromolecules* **2006**, *39*, 4437-4447.
- (9) Dong, X.-H.; Van Horn, R.; Chen, Z.; Ni, B.; Yu, X.; Wurm, A.; Schick, C.; Lotz, B.; Zhang, W.-B.; Cheng, S. Z. D. *J. Phy. Chem. Lett.* **2013**, *4*, 2356-2360.
- (10) Du, Z. X.; Xu, J. T.; Dong, Q.; Fan, Z. Q. *Polymer* **2009**, *50*, 2510-2515.
- (11) Alamo, R.; Domszy, R.; Mandelkern, L. *J. Phy. Chem.* **1984**, *88*, 6587-6595.
- (12) Alamo, R. G.; Mandelkern, L. *Thermochim. Acta* **1994**, *238*, 155-201.
- (13) Isasi, J. R.; Haigh, J. A.; Graham, J. T.; Mandelkern, L.; Alamo, R. G. *Polymer* **2000**, *41*, 8813-8823.
- (14) Mandelkern, L., *Crystallization of Polymers*, 2nd ed.; Cambridge University Press, 2004; Vol. 2, p. 1-455.

- (15) Ortmann, P.; Trzaskowski, J.; Krumova, M.; Mecking, S. *ACS Macro Lett.* **2013**, *2*, 125-127.
- (16) Russell, K. E.; Hunter, B. K.; Heyding, R. D. *Eur. Polym. J.* **1993**, *29*, 211-217.
- (17) Flory, P. J. *Trans. Faraday Soc.* **1955**, *51*, 848-857.
- (18) Hosoda, S.; Nomura, H.; Gotoh, Y.; Kihara, H. *Polymer* **1990**, *31*, 1999-2005.
- (19) Sworen, J. C.; Smith, J. A.; Wagener, K. B.; Baugh, L. S.; Rucker, S. P. *J. Am. Chem. Soc.* **2003**, *125*, 2228-2240.
- (20) Richardson, M. J.; Flory, P. J.; Jackson, J. B. *Polymer* **1963**, *4*, 221-236.
- (21) Tasaki, M.; Yamamoto, H.; Hanesaka, M.; Tashiro, K.; Boz, E.; Wagener, K. B.; Ruiz-Orta, C.; Alamo, R. G.. *Macromolecules* **2014**, *47*, 4738-4749.
- (22) Zheng, Y.-R.; Tee, H. T.; Wei, Y.; Wu, X.-L.; Mezger, M.; Yan, S.; Landfester, K.; Wagener, K.; Wurm, F. R.; Lieberwirth, I. *Macromolecules* **2016**, *49*, 1321-1330.
- (23) Song, S.-F.; Guo, Y.-T.; Wang, R.-Y.; Fu, Z.-S.; Xu, J.-T.; Fan, Z.-Q. *Macromolecules* **2016**, *49*, 6001-6011.
- (24) Lieser, G.; Wegner, G.; Smith, J. A.; Wagener, K. B. *Colloid Polym Sci.* **2004**, *282*, 773-781.
- (25) Kaner, P.; Ruiz-Orta, C.; Boz, E.; Wagener, K. B.; Tasaki, M.; Tashiro, K.; Alamo, R. G. *Macromolecules* **2014**, *47*, 236-245.
- (26) Turner-Jones, A. T. *J. Polym. Sci.* **1962**, *62*, S53-S56.
- (27) Martuscelli, E.; Pracella, M. *Polymer* **1974**, *15*, 306-314.
- (28) Schulz, M. D.; Wagener, K. B. *Macromol. Chem. Phys.* **2014**, *215*, 1936-1945.
- (29) Atallah, P.; Wagener, K. B.; Schulz, M. D. *Macromolecules* **2013**, *46*, 4735-4741.
- (30) Appiah, C.; Woltersdorf, G.; Binder, W. H. *Polym. Chem.* **2017**, *8*, 2752-2763.
- (31) Bléger, D.; Schwarz, J.; Brouwer, A. M.; Hecht, S. *J. Am. Chem. Soc.* **2012**, *134*, 20597-20600.
- (32) Bléger, D. *Macromol. Chem. Phys.* **2016**, *217*, 189-198.
- (33) Bléger, D.; Liebig, T.; Thiermann, R.; Maskos, M.; Rabe, J. P.; Hecht, S. *Angew. Chem. Int. Ed.* **2011**, *50*, 12559-12563.
- (34) Yamamoto, H.; Nishida, A.; Takimoto, T.; Nagai, A. *J. Polym. Sci. Part A: Polym. Chem.* **1990**, *28*, 67-74.
- (35) Arai, K.; Kawabata, Y. C. *Macromol. Rapid Commun.* **1995**, *16*, 875-880.
- (36) Mahimwalla, Z.; Yager, K. G.; Mamiya, J.-i.; Shishido, A.; Priimagi, A.; Barrett, C. J. *Polym. Bull.* **2012**, *69*, 967-1006.
- (37) Ebralidze, T. D.; Mumladze, A. N. *App. Opt.* **1990**, *29*, 446-447.
- (38) Appiah, C.; Siefertmann, K. R.; Jorewitz, M.; Barqawi, H. J.; Binder, W. H. *RSC Adv.* **2016**, *6*, 6358-6367.
- (39) Aoki, K. I.; Nakagawa, M.; Ichimura, K., *J. Am. Chem. Soc.* **2000**, *122*, 10997-11004.
- (40) Kadota, S.; Aoki, K.; Nagano, S.; Seki, T. *J. Am. Chem. Soc.* **2005**, *127*, 8266-8267.
- (41) Kim, D. Y.; Tripathy, S. K.; Li, L.; Kumar, J. *App. Phys. Lett.* **1995**, *66*, 1166-1168.

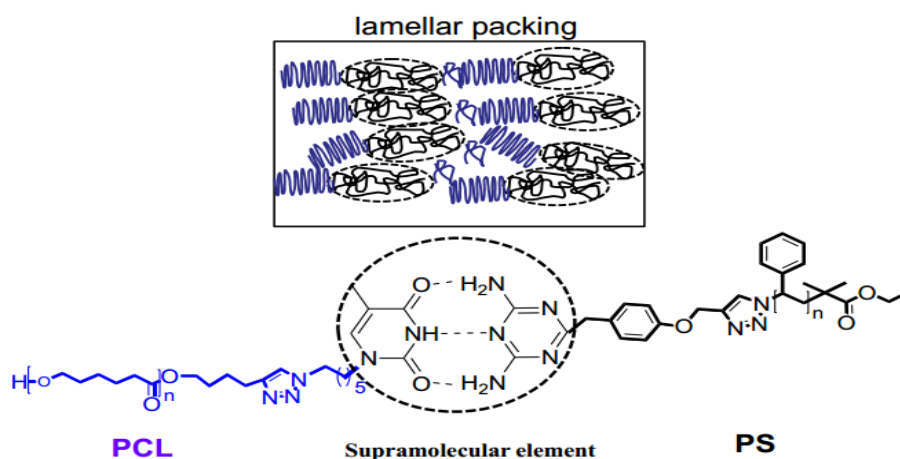
-
- (42) Rochon, P.; Batalla, E.; Natansohn, A. *App. Phys. Lett.*, **1995**, 66, 136-138.
- (43) Zhou, H.; Xue, C.; Weis, P.; Suzuki, Y.; Huang, S.; Koynov, K.; Auernhammer, G. K.; Berger, R.; Butt, H.-J.; Wu, S. *Nat. Chem.* **2016**, 1-7.
- (44) Baroncini, M.; d'Agostino, S.; Bergamini, G.; Ceroni, P.; Comotti, A.; Sozzani, P.; Bassanetti, I.; Grepioni, F.; Hernandez, T. M.; Silvi, S.; Venturi, M.; Credi, A. *Nat. Chem.* **2015**, 7, 634-640.
- (45) Inci, B.; Lieberwirth, I.; Steffen, W.; Mezger, M.; Graf, R.; Landfester, K.; Wagener, K. B. *Macromolecules* **2012**, 45, 3367-3376.
- (46) Müller, A. J.; Michell, R. M.; Pérez, R. A.; Lorenzo, A. T. *Eur. Polym. J.* **2015**, 65, 132-154.
- (47) Müller, A. J.; Arnal, M. L.; Trujillo, M.; Lorenzo, A. T. *Eur. Polym. J.* **2011**, 47, 614-629.
- (48) Michell, R. M.; Mugica, A.; Zubitur, M.; Müller, A. J. *Adv. Polym. Sci.* **2017**, 276, 215-256.
- (49) Müller, A. J.; Arnal, M. L., *Prog. Polym. Sci.* **2005**, 30, 559-603.
- (50) Müller, A. J.; Hernández, Z. H.; Arnal, M. L.; Sánchez, J. J. *Polym. Bull.* 1997, 39, 465-472.
- (51) Alamo, R. G.; Jeon, K.; Smith, R. L.; Boz, E.; Wagener, K. B.; Bockstaller, M. R. *Macromolecules* **2008**, 41, 7141-7151.
- (52) Hoshino, M.; Uchida, E.; Norikane, Y.; Azumi, R.; Nozawa, S.; Tomita, A.; Sato, T.; Adachi, S.-i.; Koshihara, S.-y. *J. Am. Chem. Soc.* **2014**, 136, 9158-9164.
- (53) Vapaavuori, J.; Laventure, A.; Bazuin, C. G.; Lebel, O.; Pellerin, C. *J. Am. Chem. Soc.* **2015**, 137, 13510-13517.

3.4 Crystallization in Segregated Supramolecular Pseudoblock Copolymers

Clement Appiah[†], Johanna Akbarzadeh[‡], Herwig Peterlik[‡], Wolfgang H. Binder^{*,†}.

[†]Institute of Chemistry, Chair of Macromolecular Chemistry, Faculty of Natural Science II (Chemistry, Physics and Mathematics), Martin-Luther University Halle-Wittenberg, Halle (Saale) D-06120, Germany.

[‡]Faculty of Physics, Dynamics of Condensed Systems, University of Vienna, Strudlhofgasse 4, 1090 Vienna, Austria.



Eur. Polym. J., 2015, 64, 138

Abstract: Crystallization in polymers under confinement can lead to strong effects, depending on the physical nature of the confining blocks. The present publication addresses crystallization in segregated supramolecular pseudoblock copolymers (SPBCPs, **(PCL-Thy)-s-(PS-Tr)**) where two constraints are present: one constraint is formed by a hydrogen bonding system connecting two microphase-segregating polymers, the second constraint is formed by the phase boundary of the segregating (PS)-polymer block. Thus mono-functionalized polymers bearing either a thymine end group or 2,4-diaminotriazine end group are prepared and blend together via the association of H-bonding interactions. Thymine functionalized crystallizable poly(ε-caprolactone) (**PCL-Thy**) and 2,4-diaminotriazine functionalized poly(styrene) (**PS-Tr**) with molecular weights ranging from 3000 g/mol to 6000 g/mol and 3000 g/mol to 11000 g/mol respectively exhibit complete end group transformation as proven by NMR and MALDI methods. Crystallization studies via DSC experiments show a strong influence on the melting behavior of the PCL crystals upon attaching the PS block. Two distinct T_g s (DSC studies) corresponding to the respective polymers (PCL and PS) is shown for SPBCPs with higher PS block ratio, while 'cold crystallization' behavior is shown for samples with nearly equal volume fraction of PCL and PS blocks. In-situ temperature dependent SAXS studies of the SPBCPs indicates a confinement effect of the PS-blocks on the crystallization of PCL, leading to an ordered arrangement of the PCL crystals.

Introduction

Confinement effects in crystalline polymers lead to peculiar dynamic effects [1] as a result of a constraining 'hard' amorphous block or barrier, thus representing an important model-system of nanostructural control in polymer science. 'Hard' confining barriers, such as nanosized porous alumina-walls [2,3], nanostructured surfaces [4,5] or microphase-separated block copolymers [6] have been used to influence the crystallization behavior of polymers depending on their geometry and dimension of the isolated nanodomains (e.g. nanocylinders or nanospheres) in relation to their size.

Vast knowledge on confining systems on covalently linked block copolymers to generate a hard interface for directed crystallization has been collected [7]. Thus crystallization effects and crystal orientation of poly(ϵ -caprolactone) (PCL) confined within a 'hard' amorphous poly(styrene) (PS)-block or isolated aluminum oxide (AAO) nanopores have been extensively studied [1,8] pointing at a strong dependency on the confining diameter, the crystallization temperature and the molecular weight of the polymers. Depending on the size of the confining nanocylinders D (when $D \leq 14.9$ nm), PCL crystals have been found to show a decreasing trend in their melting temperature and crystallinity values as a result of the higher restrictions imposed on the PCL blocks [1]. Crystal orientations in nanopores have also been shown to depend on the extent of supercooling employed during crystallization [9,10]: at moderate supercoolings, the chain orientation within the cylinders is usually perpendicular to the cylinder axis [11,12].

Whereas the crystallization in hard-barrier systems of covalently linked block copolymers is well understood, the crystallization of supramolecular pseudoblock copolymers (SPBCPs) (where the chains are linked via thermally reversible non-covalent bonds like charge-

charge interactions [13-15] or hydrogen bonding interactions [16-18]) are expected to display a different behavior in their crystallization process. As now the bonds connecting the different polymeric systems are subjected to breaking and reformation on a defined timescale, a more complex crystallization-behavior in such systems results [19]. Thus crystallization within SPBCPs should not only depend on the microphase-segregation strength of the crystalline-amorphous components, but also on the (supramolecular) association strength between the blocks and the extent of temperature applied to the system [19]. Furthermore, the supramolecular moiety can affect the crystallization process either by acting as nucleus for crystal-growth or partially restricting the crystallization due to their inability to embed into the growing crystal lamellae [20]. In a previous investigation on SPBCPs **(PCL)-s-(PIB)** [19,20] a soft amorphous PIB block ($T_g \sim (-78 \text{ }^\circ\text{C})$) acted as an only weakly confining barrier, leading to a partial mixing of the PIB- and PCL-polymers and in turn to fractionated crystallization for smaller PCL block lengths, with a partial association of the hydrogen bonds between the PCL and the PIB blocks. We here investigate the crystallization of SPBCPs **(PCL-Thy)-s-(PS-Tr)**, where (PS) serves as a hard amorphous barrier (high T_g) for the PCL crystallization. For this purpose a poly(styrene) block ($T_g \sim 100 \text{ }^\circ\text{C}$) is used in place of the previously used soft amorphous PIB block. Based on the different possibilities which PS and PCL-polymers can exert (see Figure 1) a variety of different effects on crystallization can be expected, starting from an expected disordered PS-phase within the PCL-melt: thus a segregated structure may exist, where PS-phase could confine PCL-crystallization similar to hard spheres in nanocomposites [21]. The current publication investigates the structural aspects of these possibilities via synthetic methods and structural investigations.

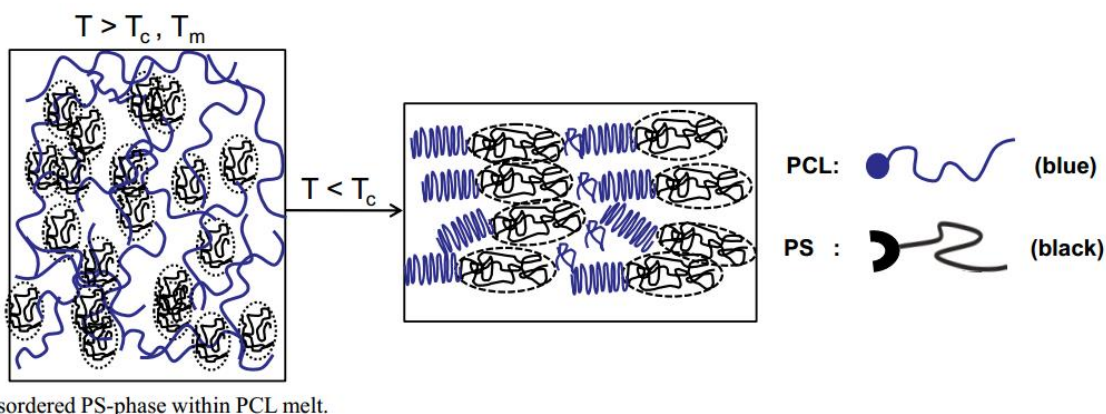


Figure 1. Concept for the crystallization of a PCL-block within the pseudoblock copolymer **(PCL-Thy)-s-(PS-Tr)**.

Experimental

Materials

All chemicals used for the synthesis were purchased from Sigma-Aldrich. ϵ -Caprolactone was stirred and distilled over calcium hydride (100 °C, 10 mbar). Tin(II)-2-ethylhexanoate and 5-hexyn-1-ol were also distilled before use, using distillation procedures as described in literature [19]. Cu(I)Br was stirred for 2 days in acetic acid/anhydride, washed with dry diethyl ether several times, and dried *in vacuo* under an argon atmosphere. *N,N*-Diisopropylethylamine (DIPEA), *N,N,N',N'',N''*-pentamethyldiethylenetriamine (PMDETA) and 2,2'-bipyridine were used without further purification. Toluene and tetrahydrofuran (THF) were predried over NaOH for several days followed by heating over sodium/benzophenone and final distillation under an argon atmosphere before use.

Measurements

NMR spectroscopy was recorded on a Varian Gemini 2000 FT-NMR spectrometer (400 MHz). Chloroform (99.8 atom % D) and dimethyl sulfoxide- d_6 (99.9 atom % D) were used as solvents, using Mestrec software version 4.7.0.0 for the FIDs analysis. Chemical shifts (δ) were recorded in parts per million (ppm) and referenced to residual protonated solvent ($CDCl_3$: 7.26 ppm (1H),

77.0 ppm (^{13}C), $(CD_3)_2SO$: 2.54 ppm (1H), 39.52 ppm (^{13}C); coupling constants (J) are given in Hertz (Hz) using standard abbreviations (s = singlet, d = doublet, t = triple, m = multiplet).

GPC measurements were conducted on a Viscotek GPCmax VE 2001 with a Styragel linear column GMHHR. THF was used as a carrier solvent at 1 mL/min at room temperature. The sample concentration was approximately 3 mg/mL. Poly(styrene) standards (in the range of 1050-1,870,000 g/mol) were used for conventional external calibration, using a Waters RI 3580 refractive index detector (detector temperature 35 °C). FTIR spectra were recorded with a Bruker Vertex70MIR spectrometer using an ATR Golden Gate unit with a diamond crystal. The scan number was 32 scans per spectra with a resolution of 2 cm^{-1} . The heating program was conducted by initial heating of the samples from room temperature to 140 °C at 20 °C intervals with an annealing time of 5 min. The samples were subsequently cooled down to room temperature with a second heating kinetics performed and used for analysis.

MALDI-TOF-MS was done on a Bruker Autoflex III Smartbeam using a nitrogen laser source ($\lambda = 337$ nm) in reflection and linear modes. The polymer samples were dissolved in THF at a concentration of 20 mg/mL; 1,8,9-anthracenetriol in THF (20 mg/mL) was used as matrix

material; sodium trifluoroacetate (NaTFA) in THF (20 mg/mL) was used as salt for both PCL and PS samples. The solutions of the polymer, the matrix, and the salt were mixed in a volume ratio of 100:20:2 and 2 μ L of this mixture were spotted on the MALDI target plate. The instrument was calibrated with a poly(ethylene glycol) standard ($M_p = 2000$ g/mol) using a quadratic calibration method.

DSC measurements were performed on a NETZSCH DSC 204F1 Phoenix instrument, calibrated with indium, tin, bismuth and zinc. Samples with a mass of 5-8 mg were placed in standard aluminum pans using nitrogen as purge gas. The evaluation of the data was conducted using Proteus Software (version 5.2.1). For non-isothermal measurements the samples were pre-heated with a heating rate of 10°C/min to 150 °C, at an annealing time of 10 min, and cooled down slowly to -120 °C with a cooling rate of 10 °C/min. A second heating run was performed at a rate of 10 °C/min to 150 °C, annealed for 10 min and cooled again to -120 °C at a rate of 10 °C/min, with an annealing time of 10 min. The melting temperature was evaluated from the peak maximum of the second heating run and the crystallization temperature was evaluated from the peak maximum of the first cooling run.

Small angle X-ray scattering experiments were carried out at the Slovak Academy of Science (Bratislava, Slovakia) on a BRUKER NanoStar with a Gallium based Metal Jet X-ray source (Excillum, Stockholm) operating at 70 kV and 1 mA with a focal size of 80x20 microns. The scattered intensity was collected via a 2D position sensitive detector (VÅNTEC 2000) with microgap technology. The scattering patterns were radially averaged and corrected for background scattering in order to obtain the scattering intensity in dependence on the scattering vector $q = 4\pi/\lambda \sin(\theta)$ where $\lambda=0.13414$ nm is the X-ray wavelength and 2θ is the scattering angle. The samples were placed between

commercially available aluminum foils and measured for 100 s. For the in-situ SAXS measurements a heating/cooling stage (BRUKER, Karlsruhe) was used, which allowed stepwise heating between 10-300 °C.

Synthesis of alkyne-functionalized PCL (PCL-alkyne) and thymine-functionalized PCL homopolymers (PCL-Thy).

The synthesis of alkyne-functionalized PCL and thymine-functionalized PCL homopolymers was accomplished based on the procedure already described by Ostas *et al.* [19,20].

Synthesis of bromo PS (PS-Br) via ATRP ($M_n = 3000$, $M_w/M_n = 1.2$)

The synthesis of PS-Br was accomplished according to an already published procedure in the literature [22]. Neat styrene (2.2 ml, 0.713 mmol) was added into a schlenk flask and deoxygenated six times via a freeze-pump-thaw method. CuBr (52 mg, 0.357 mmol) was then added and the flask was evacuated and backfilled with nitrogen 3 times. PMDETA (0.074 ml, 0.357 mmol) was injected via a syringe into the flask and purged for three times. The flask was placed in an 80 °C oil bath, with the initiator (ethyl-2-bromoisobutyrate, 139.1 mg, 0.713 mmol) injected via a nitrogen-purged syringe to the reaction mixture. After 5 h of reaction time, the flask was opened and diluted with THF. The mixture was passed through an alumina filled column to remove the CuBr. It was concentrated on a rotary evaporator and precipitated three times in methanol. The obtained product was filtered and dried under vacuum. $^1\text{H-NMR}$ (400 MHz, CDCl_3) δ ppm: 7.13 (m, n \cdot 3H), 6.64 (d, n \cdot 2H), 4.04 (3, 1H), 3.72 (m, 2H), 1.93 (m, n \cdot 1H), 1.54 (m, n \cdot 2H), 1.04 (m, 9H).

Synthesis of azide functionalized PS (PS-N₃)

To a solution of PS-Br (1 g, 0.333 mmol) in DMF was added NaN₃ (86.5 mg, 1.332 mmol) and the mixture was allowed to stir at room temperature for 24 h.

Subsequently the polymer was precipitated in methanol (3 times), filtered and dried under vacuum.

$^1\text{H-NMR}$ (400 MHz, CDCl_3) δ ppm: 7.13 (m, n \cdot 3H), 6.64 (d, n \cdot 2H), 3.98 (3, 1H), 3.72 (m, 2H), 1.93 (m, n \cdot 1H), 1.54 (m, n \cdot 2H), 1.04 (m, 9H).

Synthesis of 2,4-diaminotriazine-terminated PS (PS-Tr) via azide/alkyne "Click"-chemistry.

2,4-Diaminotriazine-terminated poly(styrene) (**PS-Tr**) was obtained via click-reaction between azido telechelic poly(styrene) (**PS-N₃**) and 6-(4-(prop-2-yn-1-yloxy)benzyl)-1,3,5-triazine-2,4-diamine (**Tr**). **PS-N₃** (0.05 mmol) and Cu(I)Br (1 equiv) were added into a Schlenk flask, evacuated and backfilled with nitrogen five times. The ligand, PMDETA (4 equiv.), 6-(4-(prop-2-yn-1-yloxy)benzyl)-1,3,5-triazine-2,4-diamine (2 equiv.) and DMF as solvent (4 mL) were then added to the flask and further degassed with nitrogen. The reaction was allowed to proceed at room temperature for 24 hours, subsequently, the crude product was concentrated under vacuum, dissolved in a small amount of DCM and injected onto a silica gel packed column. The column was flushed with DCM to completely remove the unreacted **PS-N₃**. The product was obtained in a solvent mixture of DCM: ethyl acetate in a ratio 1:1, $R_f = 0.61$. Finally, the isolated product was precipitated in methanol (3 times) to ensure complete removal excess of 6-(4-(prop-2-yn-1-yloxy)benzyl)-1,3,5-triazine-2,4-diamine. $^1\text{H-NMR}$ (400 MHz, CDCl_3 , 3kDa) δ ppm: 7.28 (s, 1H), 7.09 (m, 109H), 6.60 (m, 72H), 5.04 (m, 6H), 4.08 (dd, $J = 2.8$ Hz, 1H), 3.76 (m, 2H), 3.63 (m, 2H), 0.84-2.12 (m, 162H).

Preparation of supramolecular pseudo-block copolymers (PCL-Thy)-s-(PS-Tr).

The supramolecular pseudoblock copolymers (**PCL3-Thy)-s-(PS3-Tr)**, (**PCL3-Thy)-s-(PS7-Tr)**, (**PCL3-Thy)-s-(PS11-Tr)**, (**PCL6-Thy)-s-(PS3-Tr)**, (**PCL6-Thy)-s-(PS7-Tr)** and (**PCL6-Thy)-s-(PS11-Tr)** were prepared via solvent

blending of equimolar amounts of thymine functionalized PCL and 2,4-diaminotriazine functionalized PS. Thymine-functionalized PCL and 2,4-diaminotriazine functionalized poly(styrene) were dissolved separately in dry CHCl_3 . The two solutions were then mixed together, filtered, and the solvent was finally removed by evaporation. The mixture was dried under high vacuum for 2 days, then purged with argon, and annealed at 110-120 °C for 5 days to promote the formation of the equilibrium structures.

Results and Discussion

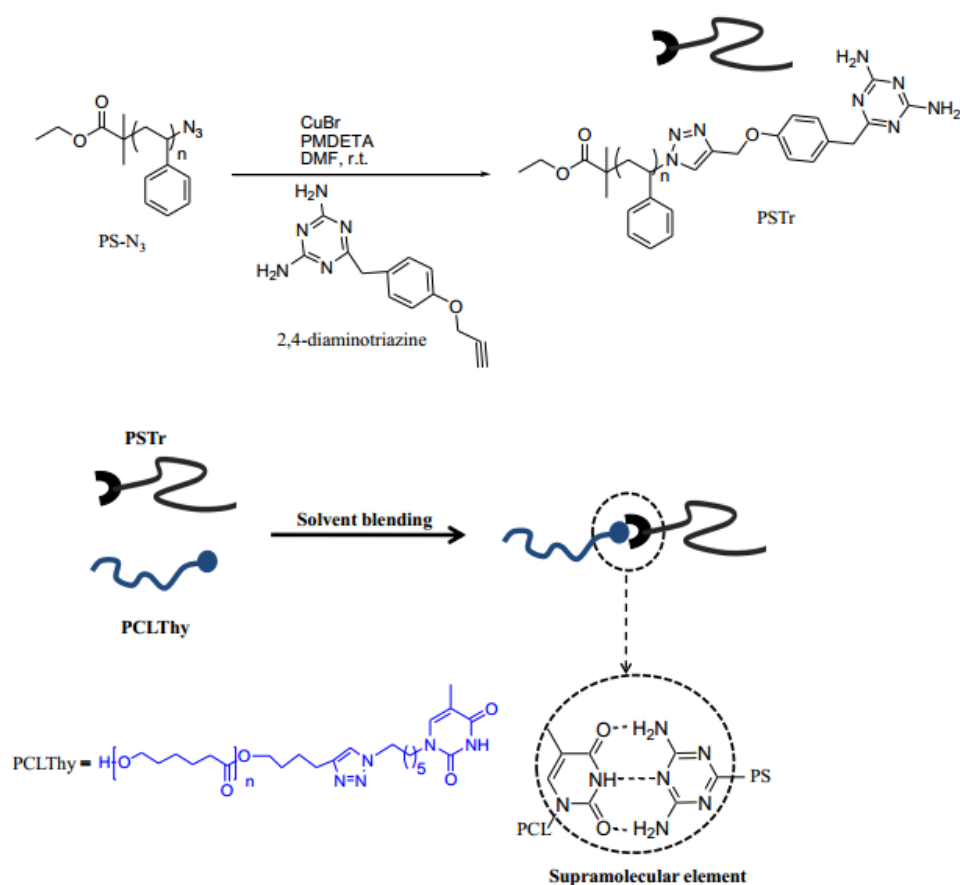
Conceptually we planned to address various microphased structures of the supramolecular poly(ϵ -caprolactone)-s-poly(styrene) (**PCL-Thy)-s-(PS-Tr)** pseudoblock copolymers (SPBCPs) connected via thymine (**Thy**) and 2,4-diaminotriazine (**Tr**) bonds. Therefore various molecular weights of the PCL-block (**PCL-Thy**) ranging from 3000 (3 kDa) to 6000 (6 kDa) and the PS-Tr-block 3000 (3kDa), 7000 (7kDa) and 11000 (11kDa) were synthetically addressed and the final supramolecular polymers were then investigated via thermal (DSC) and scattering (SAXS)-methods. The main aim was to address the morphological confinement effects of the SPBCPs to enable systematic studies of their crystallization behavior.

Synthesis and characterization of (PCL-Thy) and (PS-Tr).

Thymine-functionalized PCL's of different molecular weights (3 kDa and 6 kDa) were synthesized on the basis of a previous publication [20]. No further modification of the synthetic procedure was done, as the investigated structures showed a full optimization of the reaction conditions. The obtained compounds were fully characterized via MALDI-TOF-MS, ^1H and $^{13}\text{C-NMR}$ spectroscopy (see Supporting Information). GPC and NMR data presented in Table 1 revealed a good agreement between the various molecular weights, hence indicating a complete end group transformation.

The synthesis of the **(PS-Tr)'s** were based on a polymerization of styrene using ATRP techniques to produce polymers with a bromine end group [22], which were subsequently transformed into the azido end group for further click- functionalization [23,24] with 2,4-diaminotriazine (**Tr**). Different polymers ranging from 3 kDa to 11 kDa were prepared for this purpose, confirming the structures of all prepared **(PS-Tr)** via NMR

spectroscopy, GPC and MALDI-TOF-MS (see Table 1 and supporting information). The important resonances indicating the success of the click reaction were revealed via NMR analysis, proving the appearance of the triazole ring at 7.28 ppm. Furthermore, no resonances originating from the unreacted azido telechelic PS and 6-(4-(prop-2-yn-1-yloxy)benzyl)-1,3,5-triazine-2,4-diamine (**Tr**) could be observed in the ¹H-NMR.



Scheme 1: Synthetic approach towards the preparation of the **PS-Tr** homopolymers and subsequent formation of **(PCL-Thy)-s-(PS-Tr)** supramolecular pseudoblock copolymers (SPBCPs) by blending with **PCL-Thy** homopolymers.

Table 1. Experimental results for the synthesized PCL- and PS-homopolymers. (see scheme 1 for structural details)

Entry	Polymer	Yield (%)	M_n (NMR) (g/mol)	M_n (GPC) (g/mol)	M_n (MALDI) (g/mol)	M_w/M_n (GPC)
1	PCL3-alkyne	73	3510	3200	2900	1.2
2	PCL6-alkyne	75	6410	5900	6250	1.1
3	PCL3-Thy	68	3820	3400	3800	1.4
4	PCL6-Thy	76	7180	6300	6800	1.3
5	PS3-Br	88	3080	3000	3300	1.2
6	PS7-Br	90	7420	6800	6950	1.1
7	PS11-Br	85	11880	11200	10900	1.2
8	PS7-N ₃	95	3780	3100	3430	1.2
9	PS7-N ₃	97	7330	6900	6750	1.2
10	PS11-N ₃	94	12110	11800	11180	1.3
11	PS3-Tr	78	3330	- ^b	3700	- ^b
12	PS7-Tr	62	7560	- ^b	6880	- ^b
13	PS11-Tr	56	11340	10800	10790	1.3

^aisolated yields after purification. ^bThe molecular weight could not be determined because of adsorptive interactions with the GPC column.

Non-isothermal DSC investigations of the SPBCPs.

Prior to the crystallization studies of the SPBCPs, thermal degradation analysis of the homopolymers and the individual blocks was probed. Two decomposition steps for the SPBCPs (**PCL-Thy**)-s-(**PS-Tr**) (~200 °C and ~375 °C) were observed, specifying the decomposition temperatures of the **PS-Tr** and **PCL-Thy** blocks respectively (supporting information, Figure S7). Incorporation of the supramolecular elements was found to increase the decomposition temperatures of all the investigated polymers. Increase in molecular weights for both the crystalline and the amorphous block did not have any significant influence on the decomposition temperatures. As the two decomposition steps were all above the T_g 's of the blocks, crystallization studies of the SPBCPs (**PCL-Thy**)-s-(**PS-Tr**) at elevated temperatures, high above their glass transition temperatures but below their decomposition temperatures (50 °C below) cannot lead to thermal degradation and thus should not influence the thermal investigations.

With this idea in mind, our crystallization studies were conducted (see Figure 2a and Table 2): essentially, all

PCL homopolymers displayed single melting peaks with melting temperatures between 55-57 °C.

Figure 2b and Figure 3 shows DSC thermograms of the SPBCPs with a high molecular weight PS-block and the (**PS7-Tr**) homopolymer for comparison. Two transitions (T_g 's) of the two constituent polymers are observed for the SPBCPs. The T_g s of the PS-block shift to lower temperatures while the PCL-block T_g s shift to higher temperatures, indicating a partially miscible blend behavior [25], where part of the PS/PCL phases are not mixed. For these blends, the T_g 's of the hard PS-phase increase for samples with larger PS volume fraction. Increasing the PCL block results in an increase of the hard phase T_g , but with minimal influence on the T_m and T_c values. As T_g 's in general are difficult in interpretation [26], the appearance of two distinct T_g s, corresponding to the respective polymer blocks, have been accepted in literature [25,27] to occur as a result of microphase separation between the blocks.

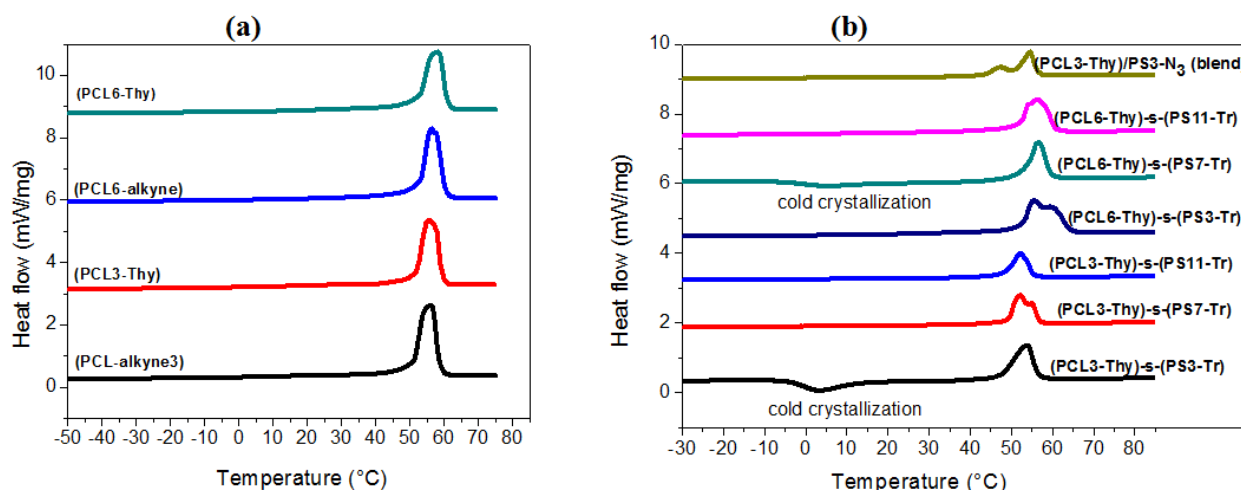


Figure 2. Heating DSC thermograms (10 K/min) for (a) PCL homopolymers and (b) SPBCPs (PCL-Thy)-s-(PS-Tr), with different molecular weights and a control sample ((PCL3-Thy)/PS-N₃ blend).

Table 2. Non-isothermal DSC measurement data obtained for PCL-alkyne, PCL-Thy, SPBCPs (PCL-Thy)-s-(PS-Tr) and sample blend (PCL3-Thy/PS3-N₃ blend).

Polymer	^a PCL:PS (vol %)	^b T _m (°C)	^c T _c (°C)	^e ΔH _m (J/g)	^f ΔH _c (J/g)	^g T _g (°C)	^h f _c (%)
PCL3-alkyne	-	56.1	32.0	86.9	82.7	-65.2	57.9
PCL6-alkyne	-	56.3	32.5	89.1	85.2	-63.7	60.1
PCL3-Thy	-	55.5	30.5	77.3	74.6	-62.3	48.1
PCL6-Thy	-	57.0	31.4	82.6	81.9	-58.5	53.8
(PCL3-Thy)-s-(PS3-Tr)	49:51	53.8	18.1, 3.5 ^d	38.3	30.4, 17.2 ^d	-50.2	13.8
(PCL3-Thy)-s-(PS7-Tr)	30:70	52.0	25.6	25.1	23.9	-51.0, 84.0*	5.2
(PCL3-Thy)-s-(PS11-Tr)	22:78	52.1	24.1	22.9	11.4	-52.4, 97.6*	3.2
(PCL6-Thy)-s-(PS3-Tr)	64:36	55.4	30.9	55.1	48.9	-55.3	24.5
(PCL6-Thy)-s-(PS7-Tr)	44:56	54.3	25.0, 5.4 ^d	53.6	45.3, 9.5 ^d	-49.6, 87.8*	17.0
(PCL6-Thy)-s-(PS11-Tr)	35:65	56.4	32.1	44.0	39.1	-56.5, 89.5*	11.1
PCL3-Thy/PS3-N ₃ (blend)	-	47.3	13.7	25.2	24.8	57.2	-

*: T_g values from the PS block, obtained in high molecular PS-blocks. ^aCalculated [38] from $\text{vol}\%_{(\text{PS})} = N^*_{\text{PS}} / (N^*_{\text{PS}} + N^*_{\text{PCL}})$, with $N^*_{\text{PS}} + N^*_{\text{PCL}} = N_{\text{PS}}(r_{\text{PCL}}/r_{\text{PS}}) + N_{\text{PCL}}(r_{\text{PS}}/r_{\text{PCL}})$. *r* are the densities, for which *N* = molecular weight of the individual blocks, $r_{\text{PCL}} = 1.146 \text{ g/cm}^3$ and $r_{\text{PS}} = 1.047 \text{ g/cm}^3$. ^bMelting temperature (peak maximum) taken from second heating scans conducted at 10°C/min, ^ccrystallization temperature (peak maximum) taken from cooling scans conducted at 10°C/min, ^dcold crystallization values, ^etotal melting enthalpy taken from heating scans(i.e. for both

T_{m1} and T_{m2} peaks), f_c total crystallization enthalpy taken from the cooling scans, T_g glass transition temperatures of the constituent blocks and h degree of crystallinity of the PCL components calculated from $f_c = (\Delta H_m \cdot M_{PCL}) / (\Delta H_m^{100\%} \cdot M_n)$, where ΔH_m is the measured melting enthalpy, $\Delta H_m^{100\%} = 146$ J/g is the melting enthalpy for 100% crystalline PCL, M_{PCL} is the molecular weight of pure PCL component (without end group and additives) and M_n is the virtual molecular weight calculated by adding up the molecular weight of all constituent blocks including end groups.

The lower molecular weight PS block samples ((PCL3-Thy)-s-(PS3-Tr) and (PCL6-Thy)-s-(PS3-Tr)) however show a single T_g (T_g of PCL-block), with a large shift towards higher temperatures in comparison to the PCL homopolymer and thus can also be viewed as a partially miscible blend with PCL. As emphasized by other recent work [25, 28-29], the presence of a single broad glass transition is not a universal feature of a fully miscible polymer blends. Our observed single T_g in some of the SPBCPs has also been found in literature [30] for PCL/PS partially miscible blends, where a single T_g (T_g of PCL) is detected for samples with lower molecular weight PS-block with the second T_g (T_g of PS) appearing near the T_m of the PCL, thus making it difficult to be detected. A closer look at our obtained results (Figure 3), shows a similar behavior where the T_g of the (PS3-Tr) homopolymer is found to be near the T_m of the PCL, hence upon attaching the (PCL-Thy)-block, a resultant downward shift in the T_g of the PS will make it overlap with the melting peak of the PCL, thereby preventing it from being resolved. Supramolecular blending of the PCL with the PS block strongly influenced the melting behavior of the PCL (Table 2 and Figure 2). A single endotherm at $\sim 55-57$ °C is observed for the neat PCL, but two melting endotherms are observed for most of the investigated SPBCPs ((PCL3-Thy)-s-(PS7-Tr), (PCL3-Thy)-s-(PS11-Tr), (PCL6-Thy)-s-(PS3-Tr) and (PCL6-Thy)-s-(PS11-Tr)). Samples with nearly equal volume fraction

of the constituent polymers however displayed only one endothermic peak, but in effect showed a crystallization peak upon heating from the T_g towards T_m of the PCL (cold crystallization), thus indicating the presence of two separate phases within a polymer blend [31] or a microphase segregated block copolymer.

The effect of the H-bonding interactions effect on our SPBCPs samples was also investigated using a controlled blend sample ((PCL3-Thy)/(PS3-N₃)) devoid of supramolecular interactions (Figure 2b). Comparison of this blend with an SPBCP sample having the same constituent block ratios (PCL3-Thy)-s-(PS3-Tr) showed a completely different behavior in their crystallization parameters. While the blend sample displayed two endothermic peaks, the SPBCP sample showed a single endothermic peak with an emergence of a cold crystallization peak.

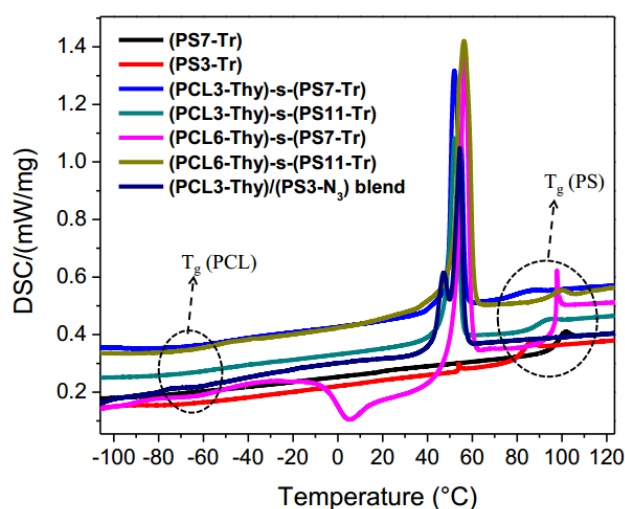


Figure 3. Heating DSC thermograms (10 K/min) for the SPBCPs **(PCL-Thy)-s-(PS-Tr)** with higher molecular weight PS-blocks, showing T_g 's of both PCL- and PS-blocks.

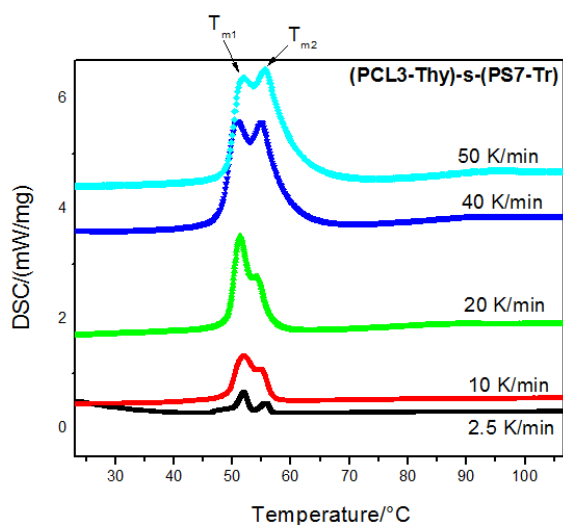


Figure 4. Heating rate effect on the melting behavior of **(PCL3-Thy)-s-(PS7-Tr)**.

Influence of heating rate kinetics on the melting behavior of the SPBCPs was additionally studied (Figure 4). As can be seen in this figure, the two endotherms persist in our investigated SPBCP upon increasing the heating rate, indicating two separate thermal events occurring within the blend. It is known that upon addition of an amorphous component to a crystallizable block the T_m value is expected to decrease as a result of morphological and thermodynamic effects [32]. As shown in Figure 2 for the SPBCPs **(PCL-Thy)-s-(PS-Tr)**, the first endothermic peak (T_{m1}) is nearly the same as in the

neat PCL, suggesting that the T_{m1} peak clearly represents a pure PCL phase outside the PS microdomains, while the T_{m2} can be attributed to phase separation of the PCL phase within the PS microdomains.

Isothermal crystallization kinetics of the SPBCPs

In order to get a detailed insight into the crystallization kinetics of the SPBCPs, isothermal DSC scans were conducted, after melting the sample for 20 min at 120 °C and quenching at 20 K/min to a specific crystallization temperature (35 °C) (Figure S10). As a generally accepted fact [33,34] the kinetics of crystallization in polymers (block copolymers, polymer blends) can be explained by Avrami exponents ranging from 1 to 3, which indicates an often constrained growth of the crystals limited by the glassy amorphous segments of the microphase-separated blocks.

Avrami exponents of about ~ 2 (second-order kinetics) were obtained for all our investigated SPBCPs, as compared to our previous (PCL)-s-(PIB) samples [19] with Avrami exponents approximately ~ 3 . This could be an indication of an at least partially confined crystallization process as a result of the embedded PS-phase. The Avrami index obtained exhibited a slightly decreasing trend upon decreasing the PCL content within the blocks (see supplementary data). The decreasing trend results obtained were in agreement with the results of Lorenzo et. al. [35] for covalently bound linear PCL-b-PS block copolymers.

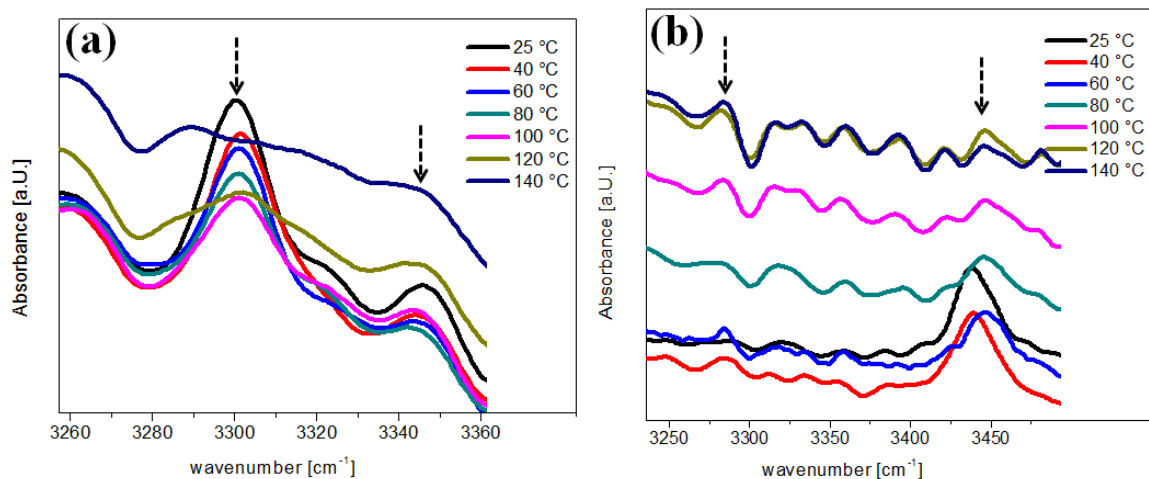


Figure 5. Temperature-dependent FTIR spectra of (a) SPBCP (**PCL3-Thy**)-s-(**PS3-Tr**) and (b) blend sample (**PCL3-Thy**)/**PS3-N₃**

FTIR Studies

The aggregation-state of the supramolecular bond of the SPBCPs was investigated using FTIR spectroscopy in the crystalline and molten state at various temperatures between 25 °C to 140 °C. Figure 5 shows a comparison between an SPBCP (**(PCL3-Thy)-s-(PS3-Tr)**) and a blend sample (**(PCL3-Thy)/(PS3-N₃ blend)**), having similar molecular weights of the respective polymers. In the case of the SPBCP, the broad absorption bands between 3280 and 3360 cm^{-1} , indicating a bound (associated) N-H stretching vibrations (hydrogen bonds between thymine and 2,4-diaminotriazine) was stable up to 100 °C. The peak shape begins to shift and flatten off at temperatures above 100 °C, indicating the opening of the hydrogen bonds. For the case of the blend sample however, significant changes (above 60 °C) in the N-H stretching vibrational peak region similar to the PCL homopolymer (**PCL3-Thy**) [19] were observed. It can be

concluded that the investigated SPBCPs thus were truly connected via an H-bonding interaction of the supramolecular elements (thymine and 2,4-diaminotriazine) during the crystallization studies.

SAXS investigations on the supramolecular pseudoblock copolymers (SPBCPs).

In order to investigate the phase behavior (ordered or disordered states), in-situ SAXS measurements of the supramolecular pseudoblock copolymers (SPBCPs, (**PCL-Thy**)-s-(**PS-Tr**)) were performed by varying the temperatures (Figure 6 and supporting information, Figure S9). The temperature program during the SAXS measurement was conducted by initial heating of the samples to a temperature of 50 °C below the T_g of the PS and then to 100 °C above the T_g of the PS, with a waiting time of 30 min.

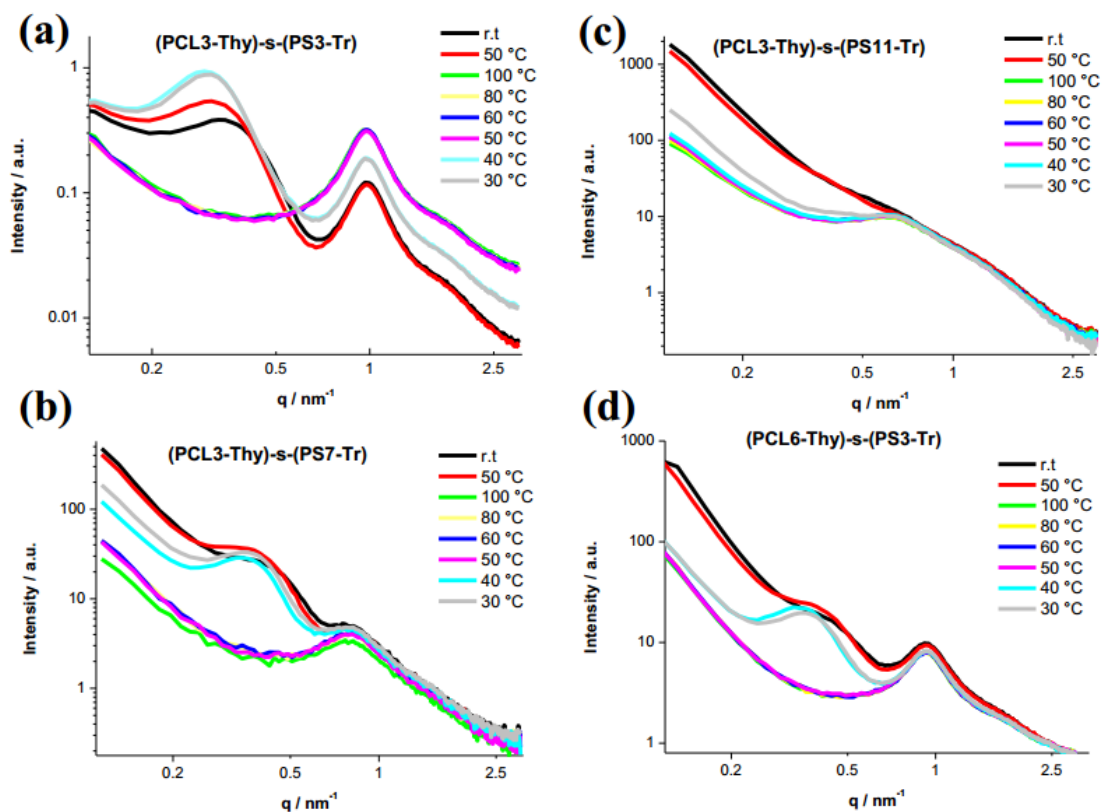


Figure 6. In-situ temperature dependent SAXS measurements for the supramolecular pseudoblock copolymers **(PCL-Thy)-s-(PS-Tr)** (a) **(PCL3-Thy)-s-(PS3-Tr)**, (b) **(PCL3-Thy)-s-(PS7-Tr)**, (c) **(PCL3-Thy)-s-(PS11-Tr)** and (d) **(PCL6-Thy)-s-(PS3-Tr)**.

Subsequently the samples were then slowly cooled down to 80 °C, 60 °C, 50 °C and 30 °C with a 30 min waiting time. SAXS curves of the supramolecular pseudoblock copolymers are shown in Fig. 6 and Fig. S9. Two prominent peaks are visible in Figs. 6a, 6b and 6d: The peak at higher q -values remains unchanged up to 100 °C and shifts to smaller q -values (larger distance in real space) for the higher molecular weight pseudoblock copolymers. In addition to these two peaks, a shoulder is visible (e.g. for **(PCL3-Thy)-s-(PS3-Tr)** with peaks at about $q=0.3$ and 1.0 nm^{-1} and a shoulder at $q=1.7 \text{ nm}^{-1}$). Due to the size of these units, this peak shifts from the material with the lowest molecular weight **(PCL3-Thy)-s-(PS3-Tr)** from $d=6.3 \text{ nm}$ to $d=7.4 \text{ nm}$ for **(PCL6-Thy)-s-(PS7-Tr)** and $d=7.6 \text{ nm}$ or the one with the highest molecular weight, **(PCL6-Thy)-s-(PS11-Tr)** (SAXS pattern

in the supporting information, evaluation by $d=2\pi/q_{\text{max}2}$ with $q_{\text{max}2}$ being the SAXS intensity peak maximum of the peak at high q -values from a fit with a Lorentzian function).

The broad peak located at low q -values (around $q = 0.3$ to 0.4 nm^{-1}) disappears above 50 °C and re-appears after being cooled to 40 °C, indicating a melt-recrystallization process in the SPBCPs. Analogously as described above, a Lorentzian function was used to describe the shift of the peak maximum $q_{\text{max}1}$, and the distance in real space is obtained from the maximum in q -space by $d=2\pi/q_{\text{max}1}$. This peak at low q -values is more pronounced after performing the temperature treatment (heating and subsequent cooling), which indicates the melt-recrystallization mechanism towards more stable and less imperfect structures as also observed for a PLLA-PCL

diblock copolymer [36]. Crystallization of the PCL core within an amorphous poly(n-butyl acrylate) (PBA) shell has also been shown in literature [37], pointing at an observation similar to our observed SAXS patterns.

For **(PCL3-Thy)-s-(PS11-Tr)** (Fig. 6c), no clear and distinct peak at around $q = 0.4 \text{ nm}^{-1}$ was observed during cooling, probably, because PS is dominating the SAXS signal due to the very low volume fraction of the crystalline PCL block in this SPBCP. Surprisingly, the distance of the units derived from this peak does not increase with increasing molecular weight. A slight decrease from $d=21.3 \text{ nm}$ **(PCL3-Thy)-s-(PS3-Tr)** to about $d=18.2 \text{ nm}$ **(PCL3-Thy)-s-(PS7-Tr)** was found. For these polymers, two melting peaks were observed indicating fractionized crystallization in confined space (data for all the SPBCPs are shown in Fig. S11 in the supporting information). SAXS and DSC thus support the view that the PS-blocks act as confined space (Figure 1) for the crystallization of the PCL, but the confinement is considerably stronger in the case of SPBCPs with strongly differing molecular weight than for equal ones.

Conclusions

Polymers bearing either thymine end group **(PCL-Thy)** or 2,4-diaminotriazine **(PS-Tr)** end groups were prepared and associated via the specific supramolecular interactions. Their crystallization behaviors were investigated by DSC studies and in-situ SAXS experiments. DSC studies revealed a partially blended microphase segregation of the SPBCP samples, especially with higher molecular weight PS block (i.e., **PS7-Tr** and **PS11-Tr**). Samples with nearly equal volume fraction of PCL/PS blocks showed a cold crystallization behavior with a single endotherm, while samples with different block ratios showed a double endotherm (fractionated crystallization). In-situ temperature dependent SAXS studies of the pseudoblocks, based on fits using Lorentzian functions for the temperature dependent and temperature independent peaks, showed that the PS-

blocks acted as confined space for the crystallization of PCL. The investigations complete the picture of crystallization in supramolecular block copolymers, indicating that miscibility effects exerted by the hydrogen bonds are dominant especially at lower molecular weights of the two immiscible blocks. Only at higher molecular weights the expected phase segregation between the PS and the PCL-blocks takes place, now leading to the formation of confined crystallization within these SPBCPs.

Acknowledgments

The authors express thanks for Grant SFB TRR 102 (CA, WHB) (Project A03) for financial support. We thank P. Siffalovic from the Slovak Academy of Sciences for the help with the measurements at the Excillum X-ray source and Prof. Thomas Thurn-Albrecht (MLU, Halle Wittenberg) for many helpful discussions.

References

- (1) Nakagawa, S.; Kadena, K.-i.; Ishizone, T.; Nojima, S.; Shimizu, T.; Yamaguchi, K.; Nakahama, S., *Macromolecules* **2012**, 45 (4), 1892-1900.
- (2) Suzuki, Y.; Duran, H.; Steinhart, M.; Butt, H.-J.; Floudas, G., *Macromolecules* **2014**, 47, 1793-1800.
- (3) Duran, H.; Steinhart, M.; Butt, H.-J.; Floudas, G., *Nano Lett.* **2011**, 11, 1671-1675.
- (4) Kim, Y. Y.; Ahn, B.; Sa, S.; Jeon, M.; Roth, S. V.; Kim, S. Y.; Ree, M., *Macromolecules* **2013**, 46, 8235-8244.
- (5) Nojima, S.; Ohguma, Y.; Namiki, S.; Ishizone, T.; Yamaguchi, K., *Macromolecules* **2008**, 41 (6), 1915-1918.
- (6) Sun, J.; Teran, A. A.; Liao, X.; Balsara, N. P.; Zuckermann, R. N., *J. Am. Chem. Soc.* **2014**, 136, 2070-2077.
- (7) He, W.-N.; Xu, J.-T., *Prog. Polym. Sci.* **2012**, 37 (10), 1350-1400.

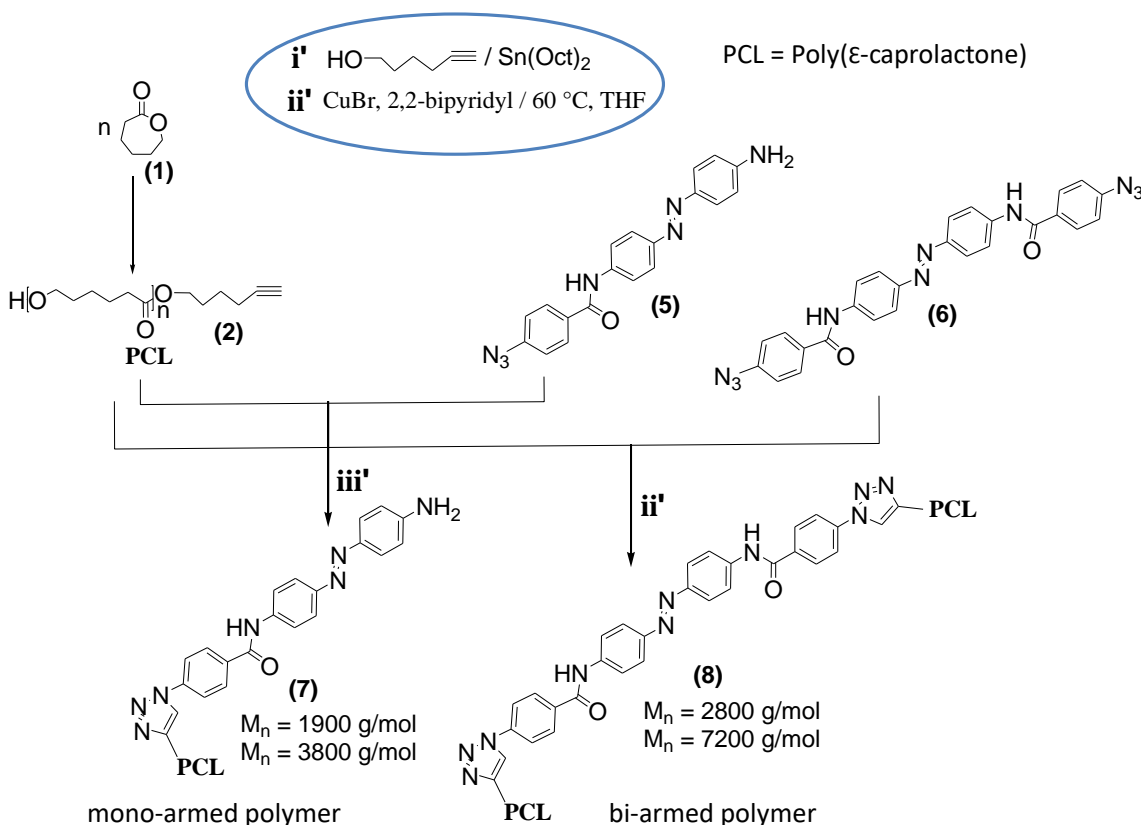
- (8) Nakagawa, S.; Tanaka, T.; Ishizone, T.; Nojima, S.; Kakiuchi, Y.; Yamaguchi, K.; Nakahama, S., *Macromolecules* **2013**, 46 (6), 2199-2205.
- (9) Quiram, D. J.; Register, R. A.; Marchand G. R., *Macromolecules*, **1997**, 30 (16), 4551-4558.
- (10) Quiram, D. J.; Register, R. A.; Marchand, G. R.; Adamson, D. H., *Macromolecules* **1998**, 31 (15), 4891-4898.
- (11) Michell, R. M.; Lorenzo, A. T.; Müller, A. J.; Lin, M.-C.; Chen, H.-L.; Blaszczyk-Lezak, I.; Martín, J.; Mijangos, C., *Macromolecules* **2012**, 45, 1517-1528.
- (12) Sun, Y.; Steinhart, M.; Zschech, D.; Adhikari, R.; Michler, G. H.; Gösele, U., *Macromol. Rapid Commun.* **2005**, 26 (5), 369-375.
- (13) Huh, J.; Jung, J. Y.; Lee, J. U.; Cho, H.; Park, S.; Park, C.; Jo, W. H., *ACS Nano* **2011**, 5 (1), 115-122.
- (14) Zare, P.; Stojanovic, A.; Herbst, F.; Akbarzadeh, J.; Peterlik, H.; Binder, W. H., *Macromolecules* **2012**, 45 (4), 2074-2084.
- (15) Stojanovic, A.; Appiah, C.; Dohler, D.; Akbarzadeh, J.; Zare, P.; Peterlik, H.; Binder, W. H., *J. Mater. Chem. A* **2013**, 1, 12159-12169.
- (16) Binder, W.; Zirbs, R., *Adv. Polym. Sci.* **2007**, 207, 1-78.
- (17) Kunz, M. J.; Hayn, G.; Saf, R.; Binder, W. H., *J. Polym. Sci. Part A: Polym. Chem.* **2004**, 42 (3), 661-674.
- (18) Hackethal, K.; Binder, W. H., *Macromol. Symp.* **2013**, 323 (1), 58-63.
- (19) Ostas, E.; Schröter, K.; Beiner, M.; Yan, T.; Thurn-Albrecht, T.; Binder, W. H., *J. Polym. Sci. Part A: Polym. Chem.* **2011**, 49 (15), 3404-3416.
- (20) Ostas, E.; Yan, T.; Thurn-Albrecht, T.; Binder, W. H., *Macromolecules* **2013**, 46 (11), 4481-4490.
- (21) Khan, J.; Harton, S. E.; Akcora, P.; Benicewicz, B. C.; Kumar, S. K., *Macromolecules* **2009**, 42 (15), 5741-5744.
- (22) Golas, P. L.; Tsarevsky, N. V.; Sumerlin, B. S.; Matyjaszewski, K., *Macromolecules* **2006**, 39 (19), 6451-6457.
- (23) Binder, W. H.; Petraru, L.; Roth, T.; Groh, P. W.; Pálfi, V.; Keki, S.; Ivan, B., *Adv. Funct. Mater.* **2007**, 17 (8), 1317-1326.
- (24) Binder, W. H.; Kunz, M. J.; Kluger, C.; Hayn, G.; Saf, R., *Macromolecules* **2004**, 37 (5), 1749-1759.
- (25) Zhao, J.; Ediger, M. D.; Sun, Y.; Yu, L., *Macromolecules* **2009**, 42 (17), 6777-6783.
- (26) Lodge, T. P.; McLeish, T. C. B. *Macromolecules* **2000**, 33 (14), 5278-5284.
- (27) Fodor, C.; Domjan, A.; Ivan, B., *Polym. Chem.* **2013**, 4 (13), 3714-3724.
- (28) Gaikwad, A. N.; Wood, E. R.; Ngai, T.; Lodge, T. P. *Macromolecules* **2008**, 41 (7), 2502-2508.
- (29) Lodge, T. P.; Wood, E. R.; Haley, J. C. *J. Polym. Sci. Part B: Polym. Phys.* **2006**, 44 (4), 756-763.
- (30) Chun, Y. S.; Kyung, Y. J.; Jung, H. C.; Kim, W. N. *Polymer* **2000**, 41 (24), 8729-8733.
- (31) Herrera, D.; Zamora, J.-C.; Bello, A.; Grimau, M.; Laredo, E.; Müller, A. J.; Lodge, T. P., *Macromolecules* **2005**, 38 (12), 5109-5117.
- (32) Nishi, T.; Wang, T. T., *Macromolecules* **1975**, 8 (6), 909-915.
- (33) Röttele, A.; Thurn-Albrecht, T.; Sommer, J.-U.; Reiter, G., *Macromolecules* **2003**, 36 (4), 1257-1260.
- (34) Lorenzo, A. T.; Arnal, M. L.; Albuern, J.; Müller, A. J., *Polym. Test.* **2007**, 26 (2), 222-231.
- (35) Lorenzo, A. T.; Müller, A. J.; Lin, M.-C.; Chen, H.-L.; Jeng, U. S.; Priftis, D.; Pitsikalis, M.; Hadjichristidis, N., *Macromolecules* **2009**, 42 (21), 8353-8364.
- (36) Castillo, R. V.; Müller, A. J.; Raquez, J.-M.; Dubois, P., *Macromolecules* **2010**, 43 (9), 4149-4160.
- (37) Fredrickson, G. H.; Bates, F. S., *Annu. Rev. Mater. Sci.* **1996**, 26 (1), 501-550.
- (38) Zhang, F.; Huang, H.; Hu, Z.; Chen, Y.; He, T. *Langmuir* **2003**, 19 (24), 10100-10108.

4.0 SUMMARY

In this thesis, the crystallization and switching dynamic studies of azobenzene copolymers and supramolecular block copolymers was investigated by synthesis of designed polymers and by physico-chemical methods. The design and synthesis of the azobenzene copolymers poly(ϵ -caprolactone)-based azobenzenes, precision ADMET poly(ethylene)-based azobenzenes) and supramolecular block copolymers (poly(ϵ -caprolactone)-*b*-poly(styrene)) served to obtain three different polymers: modified reminiscent poly(ethylene) obtained from ADMET polymerization having azobenzene units in the main chain, poly(ϵ -caprolactone) (from ROP), as well as poly(styrene) (from ATRP) bearing H-bonds with different molecular weights for the crystallization studies.

Poly(ϵ -caprolactone)-based azobenzenes

[Appiah, C.; Siefermann, K. R.; Jorewitz, M.; Barqawi, H.; Binder, W. H., Synthesis and characterization of new photoswitchable azobenzene-containing poly(ϵ -caprolactones). RSC Advances 2016, 6 (8), 6358-6367].



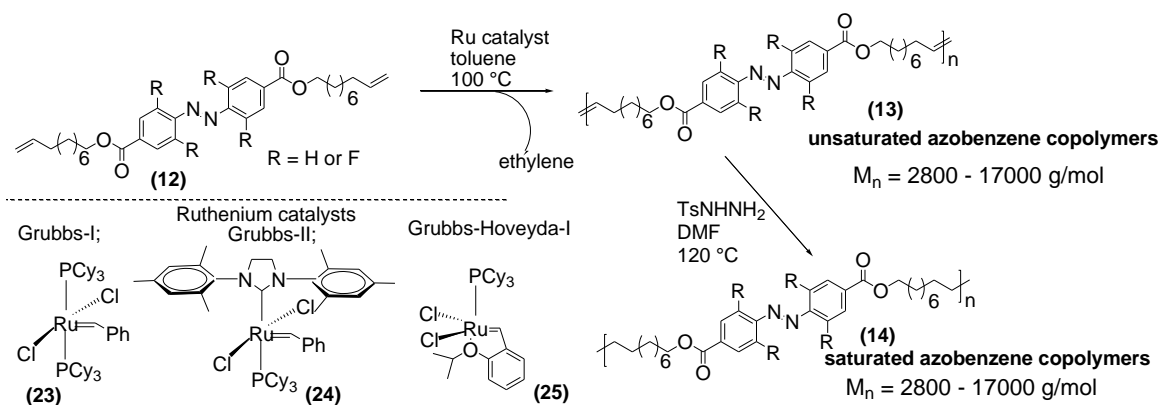
Scheme 4.1. General synthetic pathway toward the designed poly(ϵ -caprolactone)-based azobenzenes

Poly(ϵ -caprolactone)-based azobenzenes (**7** and **8**) were synthesized via ROP of PCL and post-functionalized by attaching a mono- and bi-armed azobenzene-chromophores via the copper-catalyzed azide-alkyne Huisgen cycloaddition reaction (**Scheme 4.1**). Different molecular weights of PCL, ranging from 1000 g/mol to 7000 g/mol were used for this purpose. Precise chemical structures of the mono- and

bi-armed polymers were proven via chromatographic techniques (HPLC under LCCC-conditions, LC/ESI-TOF MS, 2D LC/SEC) as well as 2D H/H COSY NMR experiments. The used techniques were able to prove the purity of all of the samples and the excellent separation of the mono-armed polymers (**7**) from the bi-armed polymers (**8**).

Poly(ethylene)-based azobenzenes

[(1) Appiah, C.; Woltersdorf, G.; Binder, W. H., Synthesis of photoresponsive main-chain oligomers with azobenzene moieties via ADMET oligomerization and their micellization properties. *Polym. Chem.* 2017, 8, 2752-2763. (2) Appiah, C.; Woltersdorf, G.; Pérez-Camargo R. A.; Müller A. J.; Binder, W. H., Crystallization behavior of ADMET Polyethylene Containing Azobenzene Defects. *Eur. Polym. J.* 2017. *accepted*].



Scheme 4.2: General synthetic pathway toward the designed precision ADMET poly(ethylene)-based azobenzenes

Poly(ethylene)-based azobenzenes, on the other hand, were synthesized via acyclic diene metathesis (ADMET) reactions, using mild reaction conditions and different ruthenium-based catalysts (Grubbs-I, Grubbs-II, and Grubbs-Hoveyda-I), in which azobenzene moieties were precisely placed within the olefin chains. Two different azobenzene polymers were synthesized: o,o H/H-azobenzene polymers and o,o F/F-azobenzene polymers (**Scheme 4.2**). The reason for the two different synthesized chemical architectures was to study the influence of electronic effects on the *cis-trans* switching dynamics of the azobenzene polymers and on their subsequent crystallization studies. Different molecular weight oligomers and polymers (**13**) were synthesized ($M_{n,SEC} = 3.0$ kDa-17.0 kDa). Subsequent hydrogenation reactions with p-toluenesulfonylhydrazide yielded the fully saturated azobenzene oligomers/polymers (**14**) (**Scheme 4.2**), which was thoroughly characterized by ¹H-NMR, FTIR and liquid chromatography under critical conditions (LCCC). The obtained saturated and unsaturated azobenzene oligomers/polymers were proven to form micelles in solution, where their size and morphologies were characterized by DLS and TEM (**Figure 9**). As a result of photo-isomerisation from the *trans*- to *cis*-state, the aggregates reduced in size, which was accompanied by a visible change of the solution from turbid to clear. The azobenzene groups in the as-prepared o,o F/F-oligomers/polymers were in a primarily stable *trans*-state and exhibited a strong π - π^*

absorption band at 320 nm. Irradiation of the solution with green light ($\lambda \sim 520$ nm) decreased the intensity of the π - π^* absorption band while the n - π^* absorption band intensity at 426 nm slightly increased. The switched *cis* form had a lifetime of approximately 14 h before it relaxed by thermal recovery to the *trans*-state. *Trans* to *cis* switching in the melt, however, yielded only 19 % of the *cis*-form. Compared to the solution state switching, a difference of about 47 % was observed to exist between the two switching modes. The low conversion yield to the *cis*-form in the melt state switching was due to the hindrance of the UV irradiation of the azo bond by the chromophore backbone. The *cis* form of the o,o H/H-oligomers/polymers on the other side was observed to relaxed much faster to its *trans*-form within 1 h time, showing that the o,o F/F-azobenzene polymers having the higher electronic stabilization effect, displayed an increased stability on the *cis*-isomer in comparison to the o,o H/H-azobenzene polymers.

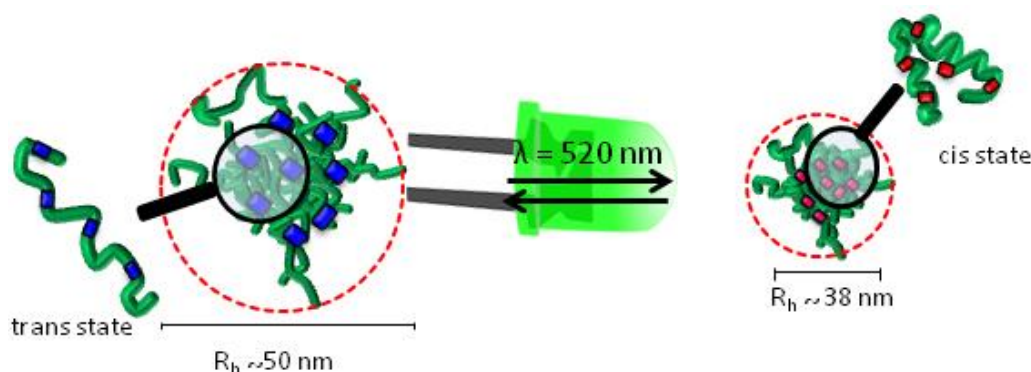
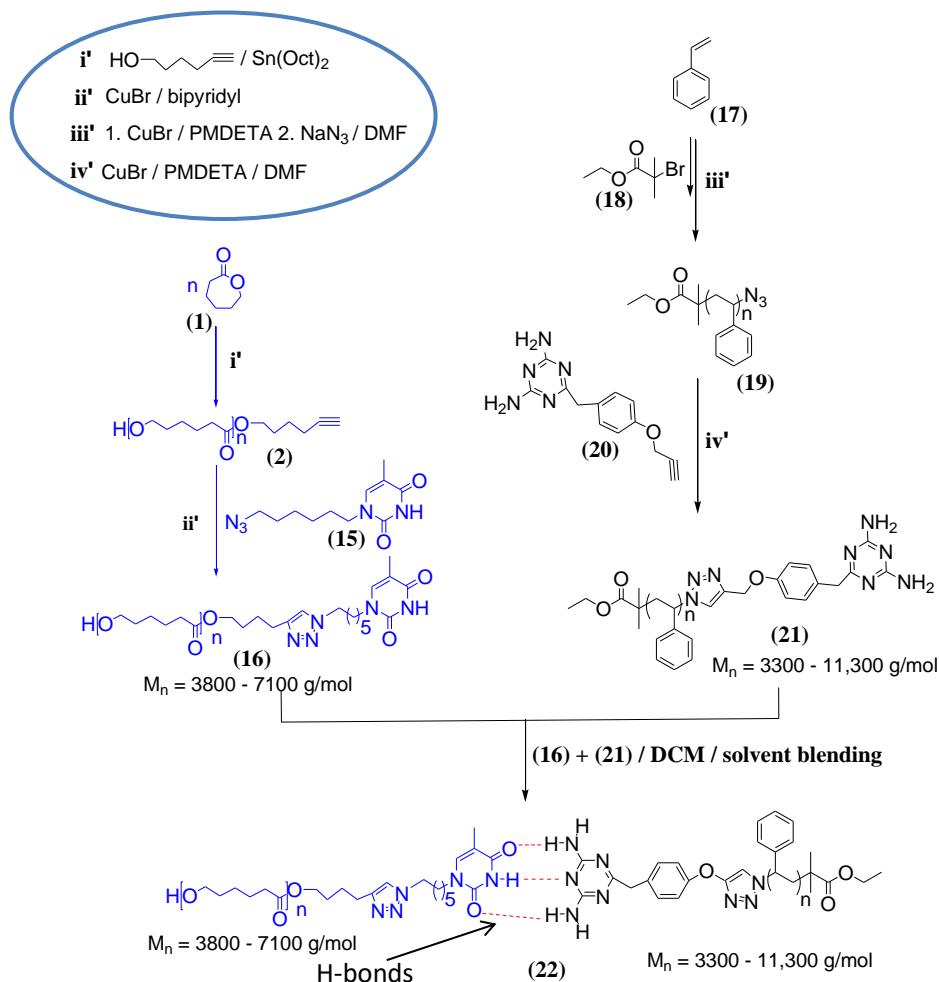


Figure 9. Hydrodynamic radius of the aggregates before (*trans*-state) and after switch (*cis* state) of the azobenzene copolymers.

Consequently, the crystallization studies in this system were done, using DSC, SSA and WAXS analysis. DSC studies revealed a decrease in the melting enthalpy of (**14**) (ΔH_m range from = 61-117 J/g) and a shift of the T_m values to high temperatures (T_m range from 141-159 °C) when compared to ADMET PE without defect ($T_m = 134$ °C, $\Delta H_m = 211$ J/g). SSA and WAXS analysis of (**14**) ($M_n = 2800$ -17000 g/mol) showed the inclusion of the azo-moieties into the PE crystal, resulting in mixed crystal structures. Accordingly, SSA did not cause a significant fractionation, as expected if defects were included within the lamellar crystal. The unsaturated azobenzene polymers (**13**) on the other hand were 100 % amorphous, recording no T_m and T_c values. A glass transition temperature, T_g in the range of 68-91 °C was observed for these unsaturated azobenzene polymers (**13**). Changing the molecular structure of the defect from o,o H/H-azobenzene to o,o F/F-azobenzene, led to an increase in the melting temperatures of about 14 °C and an increased enthalpy of about 51 J/g. This was due to the strong dipolar interactions of the F-atoms in the o,o F/F-azobenzene oligomers/polymers that stabilized the chain conformations in the crystalline state, thus enhancing the thermal stability of these oligomers and polymers.

Poly(ϵ -caprolactone)-b- poly(styrene)

[Appiah, C.; Akbarzadeh, J.; Stojanovic-Marinow, A.; Peterlik, H.; Binder, W. H., Hierarchically Mesostructured Polyisobutylene-Based Ionic Liquids. *Macromol. Rapid Commun.* 2016, 37 (14), 1175-1180].



Scheme 4.3. General synthetic pathway toward the designed of supramolecular block copolymers; poly(ϵ -caprolactone)-b-poly(styrene)

To investigate the crystallization behavior of the supramolecular block copolymers, a series of poly(ϵ -caprolactone)-b-poly(styrene) (22) were successfully synthesized. Different molecular weight supramolecular block copolymers, each having poly(ϵ -caprolactone) (PCL) as a crystallizable block which was linked to a second block poly(styrene) (PS) were synthesized. The supramolecular nature of this bond was based on a triple complementary hydrogen bond between the thymine end group incorporated into the PCL (16) and the 2,4-diaminotriazine end group shown in the second PS block (21). The synthesis of the thymine-functionalized PCL contained two steps: polymerization and subsequent functionalization. The polymerization proceeded was performed via a coordination insertion ring-opening

polymerization (ROP) using ϵ -caprolactone as monomer, 5-hexyn-1-ol as initiator and tin (II) 2-ethylhexanoate as catalyst. The amorphous PS block on the other side was prepared via atom transfer radical polymerization (ATRP) of styrene, using ethyl-2-bromoisobutyrate as an initiator and CuBr as a catalyst. Azide end groups were introduced in the subsequent step and the final functionalization of the PS-block was performed via an azide/alkyne-click reaction with 6-(4-(prop-2-yn-1-yloxy)benzyl)-1,3,5-triazine-2,4-diamine (2,4-diaminotriazine) (**20**) and PS-N₃ (**19**). The purity of the functionalized polymers was determined via NMR measurements and MALDI-ToF MS. Thymine-functionalized PCL (**16**) with molecular weights ranging from 3000 g/mol to 6000 g/mol and 2,4-diaminotriazine-functionalized PS (**21**) with molecular weights of 3000 g/mol to 11000 g/mol were subsequently blended in a low polar solvent (DCM), enhancing their supramolecular interactions via a triple complementary H-bonding reactions.

Crystallization studies of the supramolecular block copolymers were subsequently investigated using DSC studies and in-situ SAXS experiments. DSC studies revealed a partially blended microphase segregation of the supramolecular block copolymers, especially the copolymers with the higher molecular weight PS blocks (7000 g/mol and 11000 g/mol). Copolymers (**22**) ($M_n = \sim 7000$ g/mol) with nearly equal volume fraction of PCL/PS blocks showed a cold crystallization behavior with an emergence of a single endothermic peak, while samples with different block ratios showed a double endothermic peak (fractionated crystallization). In-situ temperature dependent SAXS studies of the supramolecular block copolymers based on fits using Lorentzian functions for the temperature dependent and temperature independent peaks showed that the PS blocks acted as confined space for the crystallization of the PCL (confined crystallization).

5.0 REFERENCES

1. (a) Muthukumar, M. In Progress in Understanding of Polymer Crystallization; Reiter, G., Strobl, G., Eds.; Springer-Verlag Berlin Heidelberg **2007**, p 1-18.
(b) Xue, F.; Jiang, S., Crystallization Behaviors and Structure Transitions of Biocompatible and Biodegradable Diblock Copolymers. *Polymer* **2014**, *6*, 2116-2145.
2. Wang, J.-L.; Dong, C.-M., Crystallization Behaviors and Structure Transitions of Biocompatible and Biodegradable Diblock Copolymers. *Polymer* **2006**, *47*, 3218-3228.
3. Ni, Y.; Zheng, S. J., Melting and crystallization behavior of polyhedral oligomeric silsesquioxane-capped poly(ϵ -caprolactone). *Polym. Sci., Part B: Polym. Phys.*, **2007**, *45*, 2201-2214.
4. Atanase, L. I.; Glaied, O.; Riess, G., Crystallization kinetics of PCL tagged with well-defined positional triazole defects generated by click chemistry. *Polymer* **2011**, *52*, 3074-3081.
5. Kai, W.; Hua, L.; Dong, T.; Pan, P.; Zhu, B.; Inoue, Y., Fullerene End-Capped Biodegradable Poly(ϵ -caprolactone). *Macromol. Chem. Phys.* **2008**, *209*, 104-111.
6. (a) Takizawa, K.; Tang, C.; Hawker, C. J., Molecularly Defined Caprolactone Oligomers and Polymers: Synthesis and Characterization. *J. Am. Chem. Soc.* **2008**, *130*, 1718-1726.
(b) Duran, H.; Steinhart, M.; Butt, H.-J.; Floudas, G. From Heterogeneous to Homogeneous Nucleation of Isotactic Poly(propylene) Confined to Nanoporous Alumina *Nano Lett.* **2011**, *11*, 1671-1675
7. Müller, A. J.; Balsamo, V.; Arnal, M. L.; Reiter, G.; Strobl, G., Crystallization in block copolymers with more than one crystallizable block, In: Reiter G, Strobl G, editors. Lecture notes in physics: progress in understanding of polymer crystallization. Berlin, Germany: Springer: **2007**; Vol. 714.
8. Hamley, W., Crystallization in Block Copolymers. *Adv. Polym. Sci.* **1999**, *148*, 113-137.
9. Müller, A. J.; Balsamo, V.; Arnal, M. L., Nucleation and Crystallization in Diblock and Triblock Copolymers. *Adv. Polym. Sci.* **2005**, *190*, 1-63.
10. Nandan, B.; Hsu, J. Y.; Chen, H. L., Crystallization Behavior of Crystalline-Amorphous Diblock Copolymers Consisting of a Rubbery Amorphous Block. *J. Macromol. Chem. Part C Polym. Rev.* **2006**, *46*, 143-172.
11. Sun, J.; Hong, Z.; Yang, L.; Tang, Z.; Chen, X.; Jing, X., Study on crystalline morphology of poly(l-lactide)-poly(ethylene glycol) diblock copolymer. *Polymer* **2004**, *45* (17), 5969-5977.
12. Zha, L.; Hu, W., Molecular simulations of confined crystallization in the microdomains of diblock copolymers. *Prog. Polym. Sci.* **2016**, *54-55*, 232-258.
13. Chanda, S.; Ramakrishnan, S., Controlling Interlamellar Spacing in Periodically Grafted Amphiphilic Copolymers. *Macromolecules* **2016**, *49*, 3254-3263.
14. Loo, Y.-L.; Register, R. A.; Ryan, A. J., Modes of Crystallization in Block Copolymer Microdomains: Breakout, Templated, and Confined. *Macromolecules* **2002**, *35*, 2365-2374.
15. Bendejacq, D.; Ponsinet, V.; Joanicot, M.; Loo, Y. L.; Register, R. A., Well-Ordered Microdomain Structures in Polydisperse Poly(styrene)-Poly(acrylic acid) Diblock Copolymers from Controlled Radical Polymerization. *Macromolecules* **2002**, *35*, 6645-6649.

16. Quiram, D. J.; Register, R. A.; Marchand, G. R., Crystallization of Asymmetric Diblock Copolymers from Microphase-Separated Melts. *Macromolecules* **1997**, *30*, 4551-4558.
17. Hamley, I. W.; Fairclough, J. P. A.; Bates, F. S.; Ryan, A. J., Crystallization thermodynamics and kinetics in semicrystalline diblock copolymers. *Polymer* **1998**, *39*, 1429-1437.
18. Bates, F. S.; Fredrickson, G. H., Crystallization thermodynamics and kinetics in semicrystalline diblock copolymers. *Annu. Rev. of Phys. Chem.* **1990**, *41*, 525-557.
19. He, W.-N.; Xu, J.-T., Crystallization assisted self-assembly of semicrystalline block copolymers. *Prog. Polym. Sci.* **2012**, *37*, 1350-1400.
20. Shiomi, T.; Imai, K.; Takenaka, K.; Takeshita, H.; Hayashi, H.; Tezuka, Y., Appearance of double spherulites like concentric circles for poly(ϵ -caprolactone)-block-poly(ethylene glycol)-block-poly(ϵ -caprolactone). *Polymer* **2001**, *42*, 3233-3239.
21. Nojima, S.; Fujimoto, M.; Kakihira, H.; Sasaki, S., Effects of Copolymer Composition on the Crystallization and Morphology of Poly([ϵ]-caprolactone)-block-Polystyrene. *Polym. J.* **1998**, *30*, 968-975.
22. Nojima, S.; Hashizume, K.; Rohadi, A.; Sasaki, S., Crystallization of ϵ -caprolactone blocks within a crosslinked microdomain structure of poly(ϵ -caprolactone)-block-polybutadiene. *Polymer* **1997**, *38*, 2711-2718.
23. Nojima, S.; Kato, K.; Yamamoto, S.; Ashida, T., Crystallization of block copolymers. Small-angle x-ray scattering study of an epsilon-caprolactone-butadiene diblock copolymer. *Macromolecules* **1992**, *25*(8): p. 2237-2242.
24. Nojima, S.; Kikuchi, N.; Rohadi, A.; Tanimoto, S.; Sasaki, S., Melting Behavior of Poly(ϵ -caprolactone)-block-Poly(butadiene) Copolymers. *Macromolecules* **1999**, *32* (11), 3727-3734.
25. Nojima, S.; Ohguma, Y.; Kadana, K.-i.; Ishizone, T.; Iwasaki, Y.; Yamaguchi, K., *Macromolecules* **2010**, *43*, 3916-3923.
26. Rohadi, A.; Endo, R.; Tanimoto, S.; Sasaki, S.; Nojima, S., Effects of Molecular Weight and Crystallization Temperature on the Morphology Formation in Asymmetric Diblock Copolymers with a Highly Crystalline Block. *Polym. J.* **2000**, *32*, 602-609.
27. Bogdanov, B.; Vidts, A.; Schacht, E.; Berghmans, H., Isothermal Crystallization of Poly(ϵ -caprolactone-ethylene glycol) Block Copolymers. *Macromolecules* **1999**, *33*, 726-731.
28. He, C.; Sun, J.; Deng, C.; Zhao, T.; Deng, M.; Chen, X.; Jing, X., Study of the Synthesis, Crystallization, and Morphology of Poly(ethylene glycol)-Poly(ϵ -caprolactone) Diblock Copolymers. *Biomacromolecules* **2004**, *5*, 2042-2047.
29. He, C.; Sun, J.; Ma, J.; Chen, X.; Jing, X., Composition Dependence of the Crystallization Behavior and Morphology of the Poly(ethylene oxide)-poly(ϵ -caprolactone) Diblock Copolymer. *Biomacromolecules* **2006**, *7*, 3482-3489.
30. Hamley, I. W.; Castelletto, V.; Castillo, R. V.; Müller, A. J.; Martin, C. M.; Pollet, E.; Dubois, P., Crystallization in Poly(L-lactide)-b-poly(ϵ -caprolactone) Double Crystalline Diblock Copolymers: A Study Using X-ray Scattering, Differential Scanning Calorimetry, and Polarized Optical Microscopy. *Macromolecules* **2005**, *38*, 463-472.

31. Albuérne, J.; Marquez, L.; Müller, A. J.; Raquez, J. M.; Degee, P.; Dubois, P.; Castelletto, V.; Hamley, I., Nucleation and Crystallization in Double Crystalline Poly(p-dioxanone)-b-poly(ϵ -caprolactone) Diblock Copolymers. *Macromolecules* **2003**, 36, 1633.
32. Müller, A. J.; Albuérne, J.; Esteves, L. M.; Marquez, L.; Raquez, J.-M.; Degée, P.; Dubois, P.; Collins, S.; Hamley, I. W., Confinement Effects on the Crystallization Kinetics and Self-Nucleation of Double Crystalline Poly(p-dioxanone)-b-poly(ϵ -caprolactone) Diblock Copolymers. *Macromol. Symp.* **2004**, 215, 369-382.
33. Feng, Y.; Klee, D.; Höcker, H., Biodegradable block copolymers with poly(ethylene oxide) and poly(glycolic acid-valine) blocks. *J. Appl. Polym. Sci.* **2002**, 86, 2916-2919.
34. Li, J.; Li, X.; Ni, X.; Leong, K. W., Synthesis and Characterization of New Biodegradable Amphiphilic Poly(ethylene oxide)-b-poly[(R)-3-hydroxy butyrate]-b-poly(ethylene oxide) Triblock Copolymers. *Macromolecules* **2003**, 36, 2661-2667.
35. Sun, X.; Zhang, H.; Zhang, L.; Wang, X.; Zhou, Q.-F., Synthesis of Amphiphilic Poly(ethylene oxide)-b-Poly(methyl methacrylate) Diblock Copolymers via Atom Transfer Radical Polymerization Utilizing Halide Exchange Technique. *Polym. J.* **2005**, 37, 102-108.
36. Hillmyer, M. A.; Bates, F. S., Influence of crystallinity on the morphology of poly(ethylene oxide) containing diblock copolymers. *Macromol. Symp.* **1997**, 117, 121-130.
37. Ciolino, A.; Sakellariou, G.; Pantazis, D.; Villar, M. A.; Vallés, E.; Hadjichristidis, N., Synthesis and characterization of model diblock copolymers of poly(dimethylsiloxane) with poly(1,4-butadiene) or poly(ethylene). *J. Polym. Sci. Part A: Polym. Chem.* **2006**, 44, 1579-1590.
38. Inci, B.; Wagener, K. B., ng the Alkyl Branch Frequency in Precision Polyethylene: Pushing the Limits toward Longer Run Lengths. *J. Am. Chem.Soc.* **2011**, 133 (31), 11872-11875.
39. Qiu, W.; Sworen, J.; Pyda, M.; Nowak-Pyda, E.; Habenschuss, A.; Wagener, K. B.; Wunderlich, B., Effect of the Precise Branching of Polyethylene at Each 21st CH₂ Group on Its Phase Transitions, Crystal Structure, and Morphology. *Macromolecules* **2006**, 39 (1), 204-217.
40. Rojas, G.; Inci, B.; Wei, Y.; Wagener, K. B., Precision Polyethylene: Changes in Morphology as a Function of Alkyl Branch Size. *J. Am. Chem.Soc.* **2009**, 131 (47), 17376-17386.
41. Rojas, G.; Wagener, K. B., Precisely and Irregularly Sequenced Ethylene/1-Hexene Copolymers: A Synthesis and Thermal Study. *Macromolecules* **2009**, 42 (6), 1934-1947.
42. Androsch, R.; Blackwell, J.; Chvalun, S. N.; Wunderlich, B., Wide- and Small-Angle X-ray Analysis of Poly(ethylene-co-octene). *Macromolecules* **1999**, 32 (11), 3735-3740.
43. Bassett, D. C.; Block, S.; Piermarini, G. J., A high-pressure phase of polyethylene and chain-extended growth. *J. Appl. Phy.* **1974**, 45 (10), 4146-4150.
44. Baughman, T. W.; Sworen, J. C.; Wagener, K. B., Sequenced Ethylene-Propylene Copolymers: Effects of Short Ethylene Run Lengths. *Macromolecules* **2006**, 39 (15), 5028-5036.
45. Boz, E.; Wagener, K. B.; Ghosal, A.; Fu, R.; Alamo, R. G., Synthesis and Crystallization of Precision ADMET Polyolefins Containing Halogens. *Macromolecules* **2006**, 39 (13), 4437-4447.
46. Dong, X.-H.; Van Horn, R.; Chen, Z.; Ni, B.; Yu, X.; Wurm, A.; Schick, C.; Lotz, B.; Zhang, W.-B.; Cheng, S. Z. D., Exactly Defined Half-Stemmed Polymer Lamellar Crystals with Precisely

-
- Controlled Defects' Locations. *J. Phy.Chem. Lett.* **2013**, 4 (14), 2356-2360.
47. Du, Z. X.; Xu, J. T.; Dong, Q.; Fan, Z. Q., Thermal fractionation and effect of comonomer distribution on the crystal structure of ethylene-propylene copolymers. *Polymer* **2009**, 50 (11), 2510-2515.
 48. Sworen, J. C.; Smith, J. A.; Wagener, K. B.; Baugh, L. S.; Rucker, S. P., Modeling Random Methyl Branching in Ethylene/ Propylene Copolymers Using Metathesis Chemistry: Synthesis and Thermal Behavior. *J. Am. Chem.Soc.* **2003**, 125 (8), 2228-2240.
 49. Richardson, M. J.; Flory, P. J.; Jackson, J. B., Crystallization and melting of copolymers of poly(methylene). *Polymer* **1963**, 4, 221-236.
 50. Martuscelli, E.; Pracella, M., Effects of chain defects on the thermal behaviour of polyethylene. *Polymer* **1974**, 15 (5), 306-314.
 51. Alamo, R.; Domszy, R.; Mandelkern, L., Thermodynamic and structural properties of copolymers of ethylene. *J. Phy. Chem.* **1984**, 88 (26), 6587-6595.
 52. Alamo, R. G.; Mandelkern, L., The crystallization behavior of random copolymers of ethylene. *Thermochim. Acta* **1994**, 238, 155-201.
 53. Isasi, J. R.; Haigh, J. A.; Graham, J. T.; Mandelkern, L.; Alamo, R. G., Some aspects of the crystallization of ethylene copolymers. *Polymer* **2000**, 41 (25), 8813-8823.
 54. Mandelkern, L., *Crystallization of Polymers*. 2 ed.; Cambridge University Press: Cambridge, **2004**; Vol. 2.
 55. Ortmann, P.; Trzaskowski, J.; Krumova, M.; Mecking, S., Precise Microstructure Self-Stabilized Polymer Nanocrystals. *ACS Macro. Lett.* **2013**, 2 (2), 125-127.
 56. Russell, K. E.; Hunter, B. K.; Heyding, R. D., Polyethylenes revisited: Waxes and the phase structure. *Eur. Polym. J.* **1993**, 29 (2-3), 211-217.
 57. Flory, P. J., Theory of crystallization in copolymers. *Trans. Faraday Soc.* **1955**, 51 (0), 848-857.
 58. Flory, P. J., Thermodynamics of Crystallization in High Polymers. IV. A Theory of Crystalline States and Fusion in Polymers, Copolymers, and Their Mixtures with Diluents. *J. Chem. Phy.* **1949**, 17 (3), 223-240.
 59. Baker, C. H.; Mandelkern, L., The crystallization and melting of copolymers I—The effect of the crystallization temperature upon the apparent melting temperature of polymethylene copolymers. *Polymer* **1966**, 7 (1), 7-21.
 60. Sanchez, I. C.; Eby, R. K., Thermodynamics and Crystallization of Random Copolymers. *Macromolecules* **1975**, 8 (5), 638-641.
 61. Helfand, E.; Lauritzen, J. I., Theory of Copolymer Crystallization. *Macromolecules* **1973**, 6 (4), 631-638.
 62. Passaglia, E.; DiMarzio, E. A., Estimation of the amount of nonadjacent reentry in polymer crystallization. II. Application to once folded n-paraffins. *J. Chem. Phy.* **1987**, 87 (8), 4908-4916.
 63. DiMarzio, E. A.; Passaglia, E., Estimation of the amount of adjacent reentry in polymer crystallization. I. The basic equations. *J. Chem. Phy.* **1987**, 87 (8), 4901-4907.
 64. Sanchez, I. C.; DiMarzio, E. A., Dilute Solution Theory of Polymer Crystal Growth: A Kinetic

-
- Theory of Chain Folding. *J. Chem. Phys.* **1971**, 55 (2), 893-908.
65. Lieberwirth, I.; Zhou, H., Defects in Polyethylene Single Crystals: From Precisely Branched Molecules to Defect Planes in Polyethylene Single Crystals. *Microsc. Microanal.* **2013**, 19 (S2), 1558-1559.
66. Hosoda, S.; Nozue, Y.; Kawashima, Y.; Utsumi, S.; Nagamatsu, T.; Wagener, K.; Berda, E.; Rojas, G.; Baughman, T.; Leonard, J., Perfectly Controlled Lamella Thickness and Thickness Distribution: A Morphological Study on ADMET Polyolefins. *Macromol. Symp.* **2009**, 282 (1), 50-64.
67. Buitrago, C. F.; Jenkins, J. E.; Opper, K. L.; Aitken, B. S.; Wagener, K. B.; Alam, T. M.; Winey, K. I., Room Temperature Morphologies of Precise Acid- and Ion-Containing Polyethylenes. *Macromolecules* **2013**, 46 (22), 9003-9012.
68. Song, S.-F.; Guo, Y.-T.; Wang, R.-Y.; Fu, Z.-S.; Xu, J.-T.; Fan, Z.-Q., Synthesis and Crystallization Behavior of Equisquential ADMET Polyethylene Containing Arylene Ether Defects: Remarkable Effects of Substitution Position and Arylene Size. *Macromolecules* **2016**, 49, 6001-6011.
69. Trigg, E. B.; Stevens, M. J.; Winey, K. I., Chain Folding Produces a Multilayered Morphology in a Precise Polymer: Simulations and Experiments. *J. Am. Chem. Soc.* **2017**, 139 (10), 3747-3755.
70. Roy, R. K.; Gowd, E. B.; Ramakrishnan, S., Periodically Grafted Amphiphilic Copolymers: Nonionic Analogues of Ionenes. *Macromolecules* **2012**, 45 (7), 3063-3069.
71. Brückner, S.; Phillips, P. J.; Mezghani, K.; Meille, S. V., On the crystallization of γ -isotactic polypropylene: A high pressure study. *Macromol. Rapid Commun.* **1997**, 18 (1), 1-7.
72. Feng, Y.; Hay, J. N., The characterisation of random propylene-ethylene copolymer. *Polymer* **1998**, 39 (25), 6589-6596.
73. Feng, Y.; Hay, J. N., The measurement of compositional heterogeneity in a propylene-ethylene block copolymer. *Polymer* **1998**, 39 (26), 6723-6731.
74. Zimmermann, H. J., Structural analysis of random propylene-ethylene copolymers. *J. Macromol. Sci. Phys.* **1993**, B32(2), 141-161.
75. Laihonon, S.; Gedde, U. W.; Werner, P. E.; Martinez-Salazar, J., Crystallization kinetics and morphology of poly(propylene-stat-ethylene) fractions. *Polymer* **1997**, 38 (2), 361-369.
76. Hosier, I. L.; Alamo, R. G.; Lin, J. S., Lamellar morphology of random metallocene propylene copolymers studied by atomic force microscopy. *Polymer* **2004**, 45 (10), 3441-3455.
77. Laihonon, S.; Gedde, U. W.; Werner, P. E.; Westdahl, M.; Jääskeläinen, P.; Martinez-Salazar, J., Crystal structure and morphology of melt-crystallized poly(propylene-stat-ethylene) fractions. *Polymer* **1997**, 38 (2), 371-377.
78. Alamo, R. G.; Mandelkern, L., Thermodynamic and structural properties of ethylene copolymers. *Macromolecules* **1989**, 22 (3), 1273-1277.
79. Jeon, K.; Palza, H.; Quijada, R.; Alamo, R. G., Effect of comonomer type on the crystallization kinetics and crystalline structure of random isotactic propylene 1-alkene copolymers. *Polymer* **2009**, 50 (3), 832-844.
80. Vile, J.; Hendra, P. J.; Willis, H. A.; Cudby, M. E. A.; Bunn, A., Chain branching in high pressure polymerized polyethylene: 2. *Polymer* **1984**, 25 (8), 1173-1177.

-
81. Cutler, D. J.; Hendra, P. J.; Cudby, M. E. A.; Willis, H. A., Chain branching in high pressure polymerized polyethylene. *Polymer* **1977**, 18 (10), 1005-1008.
 82. France, C.; Hendra, P. J.; Maddams, W. F.; Willis, H. A., A study of linear low-density polyethylenes: branch content, branch distribution and crystallinity. *Polymer* **1987**, 28 (5), 710-712.
 83. Glotin, M.; Mandelkern, L., A Raman spectroscopic study of the morphological structure of the polyethylenes. *Colloid Polym. Sci.* **1982**, 260 (2), 182-192.
 84. Zheng, Y.-R.; Tee, H. T.; Wei, Y.; Wu, X.-L.; Mezger, M.; Yan, S.; Landfester, K.; Wagener, K.; Wurm, F. R.; Lieberwirth, I., Morphology and Thermal Properties of Precision Polymers: The Crystallization of Butyl Branched Polyethylene and Polyphosphoesters. *Macromolecules* **2016**, 49 (4), 1321-1330.
 85. Babur, T.; Balko, J.; Budde, H.; Beiner, M., Confined relaxation dynamics in long range ordered polyesters with comb-like architecture. *Polymer* **2014**, 55 (26), 6844-6852.
 86. Holmes, D. R.; Bunn, C. W.; Smith, D. J., The crystal structure of polycapromamide: Nylon 6. *J. Polym. Sci.* **1955**, 17 (84), 159-177.
 87. Inoue, K.; Hoshino, S., Crystal structure of nylon 12. *J. Polym. Sci. Polym. Phys. Ed.* **1973**, 11 (6), 1077-1089.
 88. Kaner, P.; Ruiz-Orta, C.; Boz, E.; Wagener, K. B.; Tasaki, M.; Tashiro, K.; Alamo, R. G., Kinetic Control of Chlorine Packing in Crystals of a Precisely Substituted Polyethylene. Toward Advanced Polyolefin Materials. *Macromolecules* **2014**, 47 (1), 236-245.
 89. Lieser, G.; Wegner, G.; Smith, J. A.; Wagener, K. B., Morphology and packing behavior of model ethylene/propylene copolymers with precise methyl branch placement. *Colloid Polym. Sci.* **2004**, 282 (8), 773-781.
 90. Gaines, T. W.; Trigg, E. B.; Winey, K. I.; Wagener, K. B., High Melting Precision Sulfone Polyethylenes Synthesized by ADMET Chemistry. *Macromol. Chem. Phys.* **2016**, 217 (21), 2351-2359.
 91. Pulst, M.; Samiullah, M. H.; Baumeister, U.; Prehm, M.; Balko, J.; Thurn-Albrecht, T.; Busse, K.; Golitsyn, Y.; Reichert, D.; Kressler, J., Crystallization of Poly(ethylene oxide) with a Well-Defined Point Defect in the Middle of the Polymer Chain. *Macromolecules* **2016**, 49 (17), 6609-6620.
 92. Gadinski, M. R.; Chanthad, C.; Han, K.; Dong, L.; Wang, Q., Synthesis of poly(vinylidene fluoride-co-bromotrifluoroethylene) and effects of molecular defects on microstructure and dielectric properties. *Polym. Chem.* **2014**, 5 (20), 5957-5966.
 93. Alamo, R. G.; VanderHart, D. L.; Nyden, M. R.; Mandelkern, L., Morphological Partitioning of Ethylene Defects in Random Propylene-Ethylene Copolymers. *Macromolecules* **2000**, 33 (16), 6094-6105.
 94. Alamo, R. G.; Jeon, K.; Smith, R. L.; Boz, E.; Wagener, K. B.; Bockstaller, M. R., Crystallization of Polyethylenes Containing Chlorines: Precise vs Random Placement. *Macromolecules* **2008**, 41 (19), 7141-7151.
 95. Inci, B.; Lieberwirth, I.; Steffen, W.; Mezger, M.; Graf, R.; Landfester, K.; Wagener, K. B.,

-
- Decreasing the Alkyl Branch Frequency in Precision Polyethylene: Effect of Alkyl Branch Size on Nanoscale Morphology. *Macromolecules* **2012**, 45 (8), 3367-3376.
96. Tasaki, M.; Yamamoto, H.; Hanesaka, M.; Tashiro, K.; Boz, E.; Wagener, K. B.; Ruiz-Orta, C.; Alamo, R. G., Polymorphism and Phase Transitions of Precisely Halogen-Substituted Polyethylene. (1) Crystal Structures of Various Crystalline Modifications of Bromine-Substituted Polyethylene on Every 21st Backbone Carbon. *Macromolecules* **2014**, 47 (14), 4738-4749.
97. Campillos, E.; Marcos, M.; Serrano, J. L.; Alonso, P. J.; Martinez, J. I., Paramagnetic liquid-crystal side-chain polyacrylates containing Schiff base copper (II) complexes. *J. Mater. Chem.* **1996**, 6 (4), 533-538.
98. García-Amorós, J.; Velasco, D., Recent advances towards azobenzene-based light-driven real-time information-transmitting materials. *Beilstein J. Org. Chem.* **2012**, 8, 1003-1017.
99. Rau, H.; Rötger, D., Recent advances towards azobenzene-based light-driven real-time information-transmitting materials. *Mol. Cryst. Liq. Cryst. Sci. Tech. Sec. A. Mol. Cryst. Liq. Cryst. Sci.* **1994**, 246 (1), 143-146.
100. Hamon, F.; Djedaini-Pilard, F.; Barbot, F.; Len, C., Azobenzenes-synthesis and carbohydrate applications. *Tetrahedron* **2009**, 65, 10105-10123.
101. Mitscherlich, E., Ueber das Stickstoffbenzid. *Ann. Pharm.* **1834**, 12, 311-314.
102. Hartley, G. S., The cis-form of azobenzene and the velocity of the thermal cis[*rightward arrow*]trans-conversion of azobenzene and some derivatives. *J. Chem. Soc.* **1938**, 633-642.
103. Yager, K. G.; Barrett, C. J., Azobenzene Polymers as Photomechanical and Multifunctional Smart Materials. *RSC Adv.* **2008**, 424-446.
104. Merino, E.; Ribagorda, M., Control over molecular motion using the cis-trans photoisomerization of the azo group. *Beilstein J. Org. Chem.* **2012**, 8, 1071-1090.
105. Rau, H., *Photoisomerization of Azobenzenes*, In *Photochemistry and Photophysics*. ed. J. Rebek, CRC Press, Boca Raton, FL **1990**.
106. (a) Georgiou, D.; Muzkat, K. A.; Fisher, E., *J. Am. Chem. Soc.* **1986**, 90, 12. (b) Ciardelli, F.; Ruggeribc, G.; Pucci, A., Dye-containing polymers: methods for preparation of mechanochromic materials. *Chem. Soc. Rev.* **2013**, 42, 848-870.
107. Lewis, G. E., Photochemical Reactions of Azo Compounds. I. Spectroscopic Studies of the Conjugate Acids of cis- and trans-Azobenzene. *J. Org. Chem.* **1960**, 25 (12), 2193-2195.
108. Badger, G. M.; Drewer, R. J.; Lewis, G. E., Photochemical Reactions of Azo Compounds. II. Photochemical Cyclodehydrogenations of Methyl- and Dimethylazobenzenes. *Aust. J. Chem.* **1963**, 16, 1042.
109. Moreno, J.; Gerecke, M.; Dobryakov, A. L.; Ioffe, I. N.; Granovsky, A. A.; Bléger, D.; Hecht, S.; Kovalenko, S. A., Two-Photon-Induced versus One-Photon-Induced Isomerization Dynamics of a Bistable Azobenzene Derivative in Solution. *J. Phy. Chem. B* **2015**, 119 (37), 12281-12288.
110. Priewisch, B.; Rück-Braun, K., Efficient Preparation of Nitrosoarenes for the Synthesis of Azobenzenes. *J. Org. Chem.* **2005**, 70 (6), 2350-2352.
111. Tie, C.; Gallucci, J. C.; Parquette, J. R., Helical Conformational Dynamics and Photoisomerism of

-
- Alternating Pyridinedicarboxamide/m-(Phenylazo)azobenzene Oligomers. *J. Am. Chem. Soc.* **2006**, 128 (4), 1162-1171.
112. Saiki, Y.; Sugiura, H.; Nakamura, K.; Yamaguchi, M.; Hoshi, T.; Anzai, J.-i., [3+3]Cycloalkyne Dimers Linked by an Azo Group: A Stable cis-Azo Compound Forms Polymeric Aggregates by Nonplanar π - π Interactions. *J. Am. Chem. Soc.* **2003**, 125 (31), 9268-9269.
113. Schuster, D. I.; Li, K.; Guldi, D. M.; Palkar, A.; Echegoyen, L.; Stanisky, C.; Cross, R. J.; Niemi, M.; Tkachenko, N. V.; Lemmetyinen, H., Azobenzene-Linked Porphyrin-Fullerene Dyads. *J. Am. Chem. Soc.* **2007**, 129 (51), 15973-15982.
114. Mukherjee, P. S.; Das, N.; Kryschenko, Y. K.; Arif, A. M.; Stang, P. J., Design, Synthesis, and Crystallographic Studies of Neutral Platinum-Based Macrocycles Formed via Self-Assembly. *J. Am. Chem. Soc.* **2004**, 126 (8), 2464-2473.
115. Nihei, M.; Kurihara, M.; Mizutani, J.; Nishihara, H., Synthesis of Azo-Conjugated Metalladithiolenes and Their Photo- and Proton-Responsive Isomerization Reactions. *J. Am. Chem. Soc.* **2003**, 125 (10), 2964-2973.
116. Orito, K.; Hatakeyama, T.; Takeo, M.; Uchiito, S.; Tokuda, M.; Sugimoto, H., Dimerization of anilines and benzylamines with mercury(II) oxide-iodine reagent. *Tetrahedron* **1998**, 54 (29), 8403-8410.
117. Rojanathanes, R.; Pipoosananakaton, B.; Tuntulani, T.; Bhanthumnavin, W.; Orton, J. B.; Cole, S. J.; Hursthouse, M. B.; Grossel, M. C.; Sukwattanasinitt, M., Comparative study of azobenzene and stilbene bridged crown ether p-tert-butylcalix[4]arene. *Tetrahedron* **2005**, 61 (5), 1317-1324.
118. Peters, M. V.; Goddard, R.; Hecht, S., Synthesis and Characterization of Azobenzene-Confined Porphyrins. *J. Org. Chem.* **2006**, 71 (20), 7840-7845.
119. Davey, M. H.; Lee, V. Y.; Miller, R. D.; Marks, T. J., Synthesis of Aryl Nitroso Derivatives by tert-Butyl Hypochlorite Oxidation in Homogeneous Media. Intermediates for the Preparation of High-Hyperpolarizability Chromophore Skeletons. *J. Org. Chem.* **1999**, 64 (13), 4976-4979.
120. Standaert, R. F.; Park, S. B., Abc Amino Acids: Design, Synthesis, and Properties of New Photoelastic Amino Acids. *J. Org. Chem.* **2006**, 71 (21), 7952-7966.
121. Kim, J. Y.; Kim, G.; Kim, C. R.; Lee, S. H.; Lee, J. H.; Kim, J. S., UV Band Splitting of Chromogenic Azo-Coupled Calix[4]crown upon Cation Complexation. *J. Org. Chem.* **2003**, 68 (5), 1933-1937.
122. Roth, I.; Simon, F.; Bellmann, C.; Seifert, A.; Spange, S., Fabrication of Silica Particles Functionalized with Chromophores and Amino Groups Using Synergism of Poly(vinylamine) Adsorption and Nucleophilic Aromatic Substitution with Fluoroaromatics. *Chem. Mater.* **2006**, 18 (20), 4730-4739.
123. Lee, M. H.; Cho, B.-K.; Yoon, J.; Kim, J. S., Selectively Chemodosimetric Detection of Hg(II) in Aqueous Media. *Org. Lett.* **2007**, 9 (22), 4515-4518.
124. Lee, S. J.; Jung, J. H.; Seo, J.; Yoon, I.; Park, K.-M.; Lindoy, L. F.; Lee, S. S., A Chromogenic Macrocyclic Exhibiting Cation-Selective and Anion-Controlled Color Change: An Approach to Understanding Structure-Color Relationships. *Org. Lett.* **2006**, 8 (8), 1641-1643.

-
125. Lee, S. J.; Lee, S. S.; Lee, J. Y.; Jung, J. H., A Functionalized Inorganic Nanotube for the Selective Detection of Copper(II) Ion. *Chem. Mater.* **2006**, 18 (20), 4713-4715.
126. Corral, C.; Lissavetzky, J.; Quintanilla, G., New method for the synthesis of chloro-substituted dibenzo[b,f][1,4,5]thiadiazepines and their 5,6-dihydro derivatives. *J. Org. Chem.* **1982**, 47 (11), 2214-2215.
127. Drug, E.; Gozin, M., Catalytic Oxidation of Hydrazo Derivatives Promoted by a TiCl₃/HBr System. *J. Am. Chem. Soc.* **2007**, 129 (45), 13784-13785.
128. Barth, M.; Shah, S. T. A.; Rademann, J., High loading polymer reagents based on polycationic Ultraresins. Polymer-supported reductions and oxidations with increased efficiency. *Tetrahedron* **2004**, 60 (39), 8703-8709.
129. Yamamura, M.; Kano, N.; Kawashima, T., Systematic Study on the Structures and Reactivity of Hydrazobenzenes and Azobenzenes Bearing a Chalcogenophosphoryl Group. *Inorg. Chem.* **2006**, 45 (16), 6497-6507.
130. Alonso, F.; Radivoy, G.; Yus, M., Reduction of Hydrazines, Azo and Azoxy Compounds, and Amine N-Oxides with the NiCl₂·2H₂O–Li–DTBB (cat.) Combination. *Tetrahedron* **2000**, 56 (44), 8673-8678.
131. Aly, A. A., Photochemical synthesis of [2.2](3,8)-pyridazinophane and quinolinophane-2(1H)-one as well as synthesis of [2](5,8)-quinolinophanes and fused spiro-pyranoindanoparacyclophanes. *Tetrahedron* **2003**, 59 (10), 1739-1747.
132. Singh, S. K.; Srinivasa Reddy, M.; Mangle, M.; Ravi Ganesh, K., Cu(I)-mediated deoxygenation of N-oxides to amines. *Tetrahedron* **2007**, 63 (1), 126-130.
133. Sanz, R.; Escribano, J.; Fernandez, Y.; Aguado, R.; Pedrosa, M. R.; Arnaiz, F. J., Deoxygenation of N-Oxides with Triphenylphosphine, Catalyzed by Dichlorodioxomolybdenum(VI). *J. Synlett.* **2005**, 1389–1392.
134. Gilbert, A. M.; Failli, A.; Shumsky, J.; Yang, Y.; Severin, A.; Singh, G.; Hu, W.; Keeney, D.; Petersen, P. J.; Katz, A. H., Pyrazolidine-3,5-diones and 5-Hydroxy-1H-pyrazol-3(2H)-ones, Inhibitors of UDP-N-acetylenolpyruvyl Glucosamine Reductase. *J. Med. Chem.* **2006**, 49 (20), 6027-6036.
135. Bayly, S. R.; Humphrey, E. R.; de Chair, H.; Paredes, C. G.; Bell, Z. R.; Jeffery, J. C.; McCleverty, J. A.; Ward, M. D.; Totti, F.; Gatteschi, D.; Courric, S.; Steele, B. R.; Screttas, C. G., Electronic and magnetic metal-metal interactions in dinuclear oxomolybdenum(V) complexes across bis-phenolate bridging ligands with different spacers between the phenolate termini: ligand-centred vs. metal-centred redox activity. *J. Chem. Soc. Dalton Trans.* **2001**, 9, 1401-1414.
136. Chi, L.; Sadvoski, O.; Woolley, G. A., A Blue-Green Absorbing Cross-Linker for Rapid Photoswitching of Peptide Helix Content. *Bioconjug. Chem.* **2006**, 17 (3), 670-676.
137. Brenzovich Jr, W. E.; Houk, R. J. T.; Malubay, S. M. A.; Miranda, J. O.; Ross, K. M.; Abelt, C. J., The synthesis and properties of some carboxy-substituted analogs of butter yellow. *Dyes Pigm.* **2002**, 52 (2), 101-114.
138. Naeimi, H.; Safari, J.; Heidarneshad, A., Synthesis of Schiff base ligands derived from condensation of salicylaldehyde derivatives and synthetic diamine. *Dyes Pigm.* **2007**, 73 (2),

- 251-253.
139. Khan, A.; Hecht, S., Towards Photocontrol over the Helix–Coil Transition in Foldamers: Synthesis and Photoresponsive Behavior of Azobenzene-Core Amphiphilic Oligo(meta-phenylene ethynylene)s. *Chem. Eur. J.* **2006**, *12* (18), 4764-4774.
140. Pipoosananakaton, B.; Sukwattanasinitt, M.; Jaiboon, N.; Chaichit, N.; Tuntulani, T., Preparation of new azobenzene crown ether p-tert-butylcalix[4]arenes and their roles as switchable ionophores for Na⁺ and K⁺ ions. *Tetrahedron Lett.* **2000**, *41* (47), 9095-9100.
141. Srinivasa, G. R.; Abiraj, K.; Gowda, D. C., The synthesis of azo compounds from nitro compounds using lead and triethylammonium formate. *Tetrahedron Lett.* **2003**, *44* (31), 5835-5837.
142. Ghosh, S.; Banthia, A. K.; Chen, Z., Synthesis and photoresponsive study of azobenzene centered polyamidoamine dendrimers. *Tetrahedron* **2005**, *61* (11), 2889-2896.
143. Lee, S. J.; Lee, S. S.; Jeong, I. Y.; Lee, J. Y.; Jung, J. H., Azobenzene coupled chromogenic receptors for the selective detection of copper(II) and its application as a chemosensor kit. *Tetrahedron Lett.* **2007**, *48* (3), 393-396.
144. Lee, H. G.; Lee, J.-E.; Choi, K. S., Chromoionophoric N₂S₂ macrocycles exhibiting mercury(II) selectivity. *Inorg. Chem. Commun.* **2006**, *9* (6), 582-585.
145. Tomasulo, M.; Raymo, F. M., Colorimetric Detection of Cyanide with a Chromogenic Oxazine. *Org. Lett.* **2005**, *7* (21), 4633-4636.
146. Gopalan, P.; Katz, H. E.; McGee, D. J.; Erben, C.; Zielinski, T.; Bousquet, D.; Muller, D.; Grazul, J.; Olsson, Y., Star-Shaped Azo-Based Dipolar Chromophores: Design, Synthesis, Matrix Compatibility, and Electro-optic Activity. *J. Am. Chem. Soc.* **2004**, *126* (6), 1741-1747.
147. Campbell, V. E.; In, I.; McGee, D. J.; Woodward, N.; Caruso, A.; Gopalan, P., Chromophore Orientation Dynamics, Phase Stability, and Photorefractive Effects in Branched Azobenzene Chromophores. *Macromolecules* **2006**, *39* (3), 957-961.
148. Desroches, C.; Parola, S.; Vocanson, F.; Ehlinger, N.; Miele, P.; Lamartine, R.; Bouix, J.; Eriksson, A.; Lindgren, M.; Lopes, C., Synthesis, characterization and optical power limiting behaviour of phenylazo- and 4-nitrophenylazo-tetrahydroxytetrathiacalix[4]arene. *J. Mater. Chem.* **2001**, *11* (12), 3014-3017.
149. Lhoták, P.; Morávek, J.; Stibor, I., Diazo coupling: an alternative method for the upper rim amination of thiacalix[4]arenes. *Tetrahedron Lett.* **2002**, *43* (20), 3665-3668.
150. Kim, S. K.; Kim, S. H.; Kim, H. J.; Lee, S. H.; Lee, S. W.; Ko, J.; Bartsch, R. A.; Kim, J. S., Indium(III)-Induced Fluorescent Excimer Formation and Extinction in Calix[4]arene–Fluoroionophores. *Inorg. Chem.* **2005**, *44* (22), 7866-7875.
151. Oueslati, F.; Dumazet-Bonnamour, I.; Lamartine, R., Synthesis and extraction properties of multifunctionalized azocalix[4]arenes containing bipyridyl subunits. *New J. Chem.* **2004**, *28* (12), 1575-1578.
152. Bouoit-Montésinos, S.; Bassus, J.; Perrin, M.; Lamartine, R., Synthesis of new phenylazocalix[n]arenes (n=4, 5). *Tetrahedron Lett.* **2000**, *41* (15), 2563-2567.
153. Alder, M. J.; Bates, V. M.; Cross, W. I.; Flower, K. R.; Pritchard, R. G., The synthesis and structural

-
- characterisation of some azo-containing phosphine chalcogenides and comparison to non-phosphorus-containing analogues. *J. Chem. Soc., Perkin Trans. 1* **2001**, 20, 2669-2675.
154. Barbero, M.; Degani, I.; Dughera, S.; Fochi, R.; Perracino, P., Preparation of Diazenes by Electrophilic C-Coupling Reactions of Dry Arenediazonium o-Benzenedisulfonimides with Reagents. *Synthesis* **1998**, 1235–1237.
155. Barbero, M.; Cadamuro, S.; Dughera, S.; Giaveno, C., *Eur. Reactions of Dry Arenediazonium o-Benzenedisulfonimides with Triorganoindium Compounds. J. Org. Chem.* **2006**, 21, 4884-4890.
156. Dong, S.-L.; Löweneck, M.; Schrader, T. E.; Schreier, W. J.; Zinth, W.; Moroder, L.; Renner, C., A Photocontrolled β -Hairpin Peptide. *Chem. Eur. J.* **2006**, 12 (4), 1114-1120.
157. Badjic, J. D.; Kostic, N. M., Behavior of organic compounds confined in monoliths of sol-gel silica glass. Effects of guest-host hydrogen bonding on uptake, release, and isomerization of the guest compounds. *J. Mater. Chem.* **2001**, 11 (2), 408-418.
158. Harvey, J. H.; Butler, B. K.; Trauner, D., Functionalized azobenzenes through cross-coupling with organotrifluoroborates. *Tetrahedron Lett.* **2007**, 48 (9), 1661-1664.
159. Shee, B.; Pratihari, J. I.; Chattopadhyay, S., Synthesis and characterization of new Pt(II) and Pt(IV) orthometallated complexes incorporating 1-arylozo-2-ethyl sulfanyl benzene. *Polyhedron* **2006**, 25 (13), 2513-2518.
160. Peters, M. V.; Goddard, R.; Hecht, S., On the Illusive Nature of o-Formylazobenzenes: Exploiting the Nucleophilicity of the Azo Group for Cyclization to Indazole Derivatives. *J. Org. Chem.* **2006**, 71 (20), 7846-7849.
161. Zarwell, S.; Rück-Braun, K., Synthesis of an azobenzene-linker-conjugate with tetrahedral shape. *Tetrahedron Lett.* **2008**, 49 (25), 4020-4025.
162. Sakamoto, A.; Hirooka, A.; Namiki, K.; Kurihara, M.; Murata, M.; Sugimoto, M.; Nishihara, H., Photon-, Electron-, and Proton-Induced Isomerization Behavior of Ferrocenylazobenzenes. *Inorg. Chem.* **2005**, 44 (21), 7547-7558.
163. Wang, S.; Wang, X.; Li, L.; Advincula, R. C., Design, Synthesis, and Photochemical Behavior of Poly(benzyl ester) Dendrimers with Azobenzene Groups throughout Their Architecture. *J. Org. Chem.* **2004**, 69 (26), 9073-9084.
164. Galvan-Gonzalez, A.; Belfield, K. D.; Stegeman, G. I.; Canva, M.; Marder, S. R.; Staub, K.; Levina, G.; Twieg, R. J., Photodegradation of selected π -conjugated electro-optic chromophores. *J. Appl. Phy.* **2003**, 94 (1), 756-763.
165. Galvan-Gonzalez, A.; Belfield, K. D.; Stegeman, G. I.; Canva, M.; Chan, K.-P.; Park, K.; Sukhomlinova, L.; Twieg, R. J., Photostability enhancement of an azobenzene photonic polymer. *Appl. Phy. Lett.* **2000**, 77 (14), 2083-2085.
166. Uhrich, K. E.; Cannizzaro, S. M.; Langer, R. S.; Shakesheff, K. M., Polymeric Systems for Controlled Drug Release. *Chem. Rev.* **1999**, 99 (11), 3181-3198.
167. Li, X.; Wen, R.; Zhang, Y.; Zhu, L.; Zhang, B.; Zhang, H., Photoresponsive side-chain liquid crystalline polymers with an easily cross-linkable azobenzene mesogen. *J. Mater. Chem.* **2009**, 19 (2), 236-245.

-
168. Altomare, A.; Carlini, C.; Ciardelli, F.; Solaro, R.; Rosato, N., Photochromism of 4-acryloxyazobenzene/(-)-menthyl acrylate copolymers. *J. Polym. Sci.: Polym. Chem. Ed.* **1984**, *22* (6), 1267-1280.
169. Li, X.; Fang, L.; Hou, L.; Zhu, L.; Zhang, Y.; Zhang, B.; Zhang, H., Photoresponsive side-chain liquid crystalline polymers with amide group-substituted azobenzene mesogens: effects of hydrogen bonding, flexible spacers, and terminal tails. *Soft Matter* **2012**, *8* (20), 5532-5542.
170. Li, Z.; Zhang, Y.; Zhu, L.; Shen, T.; Zhang, H., Efficient synthesis of photoresponsive azobenzene-containing side-chain liquid crystalline polymers with high molecular weights by click chemistry. *Polym. Chem.* **2010**, *1*, 1501-1511.
171. Fang, L.; Zhang, H.; Li, Z.; Zhang, Y.; Zhang, Y.; Zhang, H., Synthesis of Reactive Azobenzene Main-Chain Liquid Crystalline Polymers via Michael Addition Polymerization and Photomechanical Effects of Their Supramolecular Hydrogen-Bonded Fibers. *Macromolecules* **2013**, *46* (19), 7650-7660.
172. Haque, H. A.; Hara, M.; Nagano, S.; Seki, T., Photoinduced In-Plane Motions of Azobenzene Mesogens Affected by the Flexibility of Underlying Amorphous Chains. *Macromolecules* **2013**, *46* (20), 8275-8283.
173. Zhao, Y.; He, J., Azobenzene-containing block copolymers: the interplay of light and morphology enables new functions. *Soft Matter* **2009**, *5* (14), 2686-2693.
174. Weber, C.; Liebig, T.; Gensler, M.; Pithan, L.; Bommel, S.; Bléger, D.; Rabe, J. P.; Hecht, S.; Kowarik, S., Light-Controlled "Molecular Zippers" Based on Azobenzene Main Chain Polymers. *Macromolecules* **2015**, *48* (5), 1531-1537.
175. Jochum, F. D.; Theato, P., Temperature- and light-responsive smart polymer materials. *Chem. Soc. Rev.* **2013**, *42*, 7468-7483.
176. Xue, X.; Zhu, J.; Zhang, Z.; Zhou, N.; Tu, Y.; Zhu, X., Soluble Main-Chain Azobenzene Polymers via Thermal 1,3-Dipolar Cycloaddition: Preparation and Photoresponsive Behavior. *Macromolecules* **2010**, *43* (6), 2704-2712.
177. Kumar, G. S.; Neckers, D. C., Photochemistry of azobenzene-containing polymers. *Chem. Rev.* **1989**, *89* (8), 1915-1925.
178. Yager, K. G.; Barrett, C. J., Novel photo-switching using azobenzene functional materials. *J. Photochem. Photobiol. Chem.* **2006**, *182*, 250-261..
179. Ding, L.; Xu, M.; Wang, J.; Liao, Y.; Qiu, J., Controlled synthesis of azobenzene functionalized homo and copolymers via direct acyclic diene metathesis polymerization. *Polymer* **2014**, *55* (7), 1681-1687.
180. Ding, L.; Zhang, L.; Han, H.; Huang, W.; Song, C.; Xie, M.; Zhang, Y., Hyperbranched Azo-Polymers Synthesized by Acyclic Diene Metathesis Polymerization of an AB₂ Monomer. *Macromolecules* **2009**, *42* (14), 5036-5042.
181. (a) Junge, D.M.; McGrath D. V., Photoresponsive Azobenzene-Containing Dendrimers with Multiple Discrete States. *J. Am. Chem. Soc.*, **1999**, *121*(20), 4912-4913. (b) Zhang, L.; Zhang, H.; Gao, F.; Peng, H.; Ruan, Y.; Xu, Y.; Weng, W., Host-guest interaction between fluoro-substituted

-
- azobenzene derivative and cyclodextrins. *RSC Adv.* **2015**, 5 (16), 12007-12014.
182. Romero, E. L.; D'Vries, R. F.; Zuluaga, F.; Chaur, M. N., Multiple Dynamics of Hydrazone Based Compounds. *J. Braz. Chem. Soc.* **2015**, 26 (6), 1265-1273.
183. Özen, A. S.; Doruker, P.; Aviyente, V., Effect of Cooperative Hydrogen Bonding in Azo-Hydrazone Tautomerism of Azo Dyes. *J. Phy. Chem. A* **2007**, 111 (51), 13506-13514.
184. Gerson, F.; Heilbronner, E., Physikalisch-chemische Eigenschaften und Elektronenstruktur der Azo-Verbindungen. Teil XI: Bemerkung zur Struktur des Azonium-Kations des p,p'-Bis-dimethylamino-azobenzols. *Helv. Chim, Acta* **1962**, 45 (1), 51-59.
185. Brown, E. V.; Granneman, G. R., Cis-trans isomerism in the pyridyl analogs of azobenzene. Kinetic and molecular orbital analysis. *J. Am. Chem.Soc.* **1975**, 97 (3), 621-627.
186. Haberfield, P.; Block, P. M.; Lux, M. S., Enthalpies of solvent transfer of the transition states in the cis-trans isomerization of azo compounds. Rotation vs. the nitrogen inversion mechanism. *J. Am. Chem.Soc.* **1975**, 97 (20), 5804-5806.
187. Garcia-Amorós, J.; Sánchez-Ferrer, A.; Massad, W. A.; Nonell, S.; Velasco, D., Kinetic study of the fast thermal cis-to-trans isomerisation of para-, ortho- and polyhydroxyazobenzenes. *Phys. Chem.* **2010**, 12, 13238-13242.
188. Garcia-Amorós, J.; Nonell, S.; Velasco, D., Photo-driven optical oscillators in the kHz range based on push-pull hydroxyazopyridines. *Chem. Commun.* **2011**, 47 (11), 4022-4024.
189. Garcia-Amorós, J.; Martínez, M.; Finkelmann, H.; Velasco, D., Kinetic-Mechanistic Study of the Thermal Cis-to-Trans Isomerization of 4,4'-Dialkoxyazoderivatives in Nematic Liquid Crystals. *J. Phys. Chem. B* **2010**, 114 (3), 1287-1293.
190. Hagen, S.; Kate, P.; Peters, M. V.; Hecht, S.; Wolf, M.; Tegeder, P., Kinetic analysis of the photochemically and thermally induced isomerization of an azobenzene derivative on Au(111) probed by two-photon photoemission. *Appl. Phys. A.* **2008**, 93 (2), 253-260.
191. Smets, G., Photochromic phenomena in the solid phase. *Adv. Polym. Sci.* **1983**, 50, 17-44.
192. Irie, M.; Schnabel, W., On the dynamics of photostimulated conformational changes of polystyrene with pendant azobenzene groups in solution. *Macromolecules* **1985**, 18 (3), 394-398.
193. Irie, M.; Schnabel, W., Photoresponsive polymers. Dynamics of conformational changes of polyamides with backbone azobenzene groups. *Macromolecules* **1981**, 14, 1246-1249.
194. Beck, G.; Kiwi, J.; Lindenau, D.; ^{Schnabel}, W., On the kinetics of polymer degradation in solution—I. Laser flash photolysis and pulse radiolysis studies using the light scattering detection method. *Eur. Polym. J.* **1974**, 10 (11), 1069-1075.
195. Kumar, G. S.; Neckers, D. C., Photochemistry of azobenzene-containing polymers. *Chem. Rev.* **1989**, 89 (8), 1915-1925.
196. Kumar, G. S.; Depra, P.; Neckers, D. C., Chelating copolymers containing photosensitive functionalities. *Macromolecules* **1984**, 17 (10), 1912- 1917.
197. Kumar, G. S.; Depra, P.; Zhang, K.; Neckers, D. C., Chelating copolymers containing photosensitive functionalities. 2. *Macromolecules* **1984**, 17 (12), 2463-2467.
198. Chen, D. T.-L.; Morawetz, H., Photoisomerization and Fluorescence of Chromophores Built into

-
- the Backbones of Flexible Polymer Chains. *Macromolecules* **1976**, 9 (3), 463-468.
199. Tabak, D.; Morawetz, H., Rate of Conformational Transitions in Solutions of Randomly Coiled Polymers. III. The cis-trans Isomerization of Azobenzene Residues in the Backbone of Polyamides. *Macromolecules* **1970**, 3 (4), 403-410.
200. Paik, C. S.; Morawetz, H., Photochemical and Thermal Isomerization of Azoaromatic Residues in the Side Chains and the Backbone of Polymers in Bulk. *Macromolecules* **1972**, 5 (2), 171-177.
201. (a) Chen, D. T.-L.; Morawetz, H., Photoisomerization and Fluorescence of Chromophores Built into the Backbones of Flexible Polymer Chains. *Macromolecules* **1976**, 9 (3), 463-468. (b) Chang, C.-W.; Lu, Y.-C.; Wang, T.-T.; Diao, E. W.-G., Photoisomerization Dynamics of Azobenzene in Solution with S1 Excitation: A Femtosecond Fluorescence Anisotropy Study. *J. Am. Chem. Soc.* **2004**, 126 (32), 10109-10118.
202. Delaire, J. A.; Nakatani, K., Linear and Nonlinear Optical Properties of Photochromic Molecules and Materials. *Chem. Rev.* **2000**, 100 (5), 1817-1846.
203. Yesodha, S. K.; Sadashiva Pillai, C. K.; Tsutsumi, N., Stable polymeric materials for nonlinear optics: a review based on azobenzene systems. *Prog. Polym. Sci.* **2004**, 29 (1), 45-74.
204. Appiah, C.; Siefermann, K. R.; Jorewitz, M.; Barqawi, H.; Binder, W. H., Synthesis and characterization of new photoswitchable azobenzene-containing poly(ϵ -caprolactones). *RSC Adv.* **2016**, 6 (8), 6358-6367.
205. Bléger, D.; Liebig, T.; Thiermann, R.; Maskos, M.; Rabe, J. P.; Hecht, S., Light-Orchestrated Macromolecular "Accordions": Reversible Photoinduced Shrinking of Rigid-Rod Polymers. *Angew. Chem. Int. Ed.* **2011**, 50 (52), 12559-12563.
206. Grebel-Koehler, D.; Liu, D.; De Feyter, S.; Enkelmann, V.; Weil, T.; Engels, C.; Samyn, C.; Müllen, K.; De Schryver, F. C., Synthesis and Photomodulation of Rigid Polyphenylene Dendrimers with an Azobenzene Core. *Macromolecules* **2003**, 36 (3), 578-590.
207. Xiang, Y.; Xue, X.; Zhu, J.; Zhang, Z.; Zhang, W.; Zhou, N.; Zhu, X., Fluorescence behavior of an azobenzene-containing amphiphilic diblock copolymer. *Polym. Chem.* **2010**, 1, 1453-1458.
208. (a) Cai-CaiZhang; Li, S.-H.; Cui-FangZhang; Liu, Y., Switchable Supramolecular Nanoparticle Based on Azobenzene Derivative within Anionic Pillar[5] arene. *Scientific Reports* **2016**. (b) Buswell, M.; Fleming, I.; Ghosh, U.; Mack, S.; Russell, M.; Clark, B. P., The extraordinary reactions of phenyldimethylsilyllithium with N,N-disubstituted amides. *Org. Biomol. Chem.* **2004**, 2, 3006-3017.
209. Concellón, A.; Blasco, E.; Martínez-Felipe, A.; Martínez, J. C.; Šics, I.; Ezquerra, T. A.; Nogales, A.; Piñol, M.; Oriol, L., Light-Responsive Self-Assembled Materials by Supramolecular Post-Functionalization via Hydrogen Bonding of Amphiphilic Block Copolymers. *Macromolecules* **2016**, 49 (20), 7825-7836.
210. Sun, Y.; Zhou, N.; Zhang, W.; Li, Y.; Cheng, Z.; Zhu, J.; Zhang, Z.; Zhu, X., Synthesis of Novel Side-Chain Triphenylamine Polymers with Azobenzene Moieties via RAFT Polymerization and Investigation on Their Photoelectric Properties. *Polym. Chem.* **2012**, 50, 3788-3796.
211. Wang, S.; Zhang, N.; Ge, X.; Wan, Y.; Li, X.; Yan, L.; Xia, Y.; Song, B., Self-assembly of an

- azobenzene-containing polymer prepared by a multi-component reaction: supramolecular nanospheres with photo-induced deformation properties. *Soft Matter* **2014**, 10 (27), 4833-4839.
212. Bléger, D.; Schwarz, J.; Brouwer, A. M.; Hecht, S., o-Fluoroazobenzenes as Readily Synthesized Photoswitches Offering Nearly Quantitative Two-Way Isomerization with Visible Light. *J. Am. Chem. Soc.* **2012**, 134 (51), 20597-20600.
213. Bléger, D., Orchestrating Molecular Motion with Light – From Single (macro)Molecules to Materials. *Macromol. Chem. Phys.* **2016**, 217 (2), 189-198.
214. Yamamoto, H.; Nishida, A.; Takimoto, T.; Nagai, A., Photoresponsive peptide and polypeptide systems. VIII. Synthesis and reversible photochromism of azo aromatic poly(L-ornithine). *J. Polym. Sci. Part A: Polym. Chem.* **1990**, 28 (1), 67-74.
215. Arai, K.; Kawabata, Y., Changes in the sol-gel transformation behavior of azobenzene moiety-containing methylcellulose irradiated with UV light. *Macromol. Rapid Commun.* **1995**, 16 (12), 875-880.
216. Mahimwalla, Z.; Yager, K. G.; Mamiya, J.-i.; Shishido, A.; Priimagi, A.; Barrett, C. J., *Polym. Bull.* **2012**, 69 (8), 967-1006.
217. Ebralidze, T. D.; Mumladze, A. N., Light-induced anisotropy in azo-dye-colored materials. *Appl. Opt.* **1990**, 29 (4), 446-447.
218. Aoki, K. i.; Nakagawa, M.; Ichimura, K., Self-Assembly of Amphoteric Azopyridine Carboxylic Acids: Organized Structures and Macroscopic Organized Morphology Influenced by Heat, pH Change, and Light. *J. Am. Chem. Soc.* **2000**, 122 (44), 10997-11004.
219. Kadota, S.; Aoki, K.; Nagano, S.; Seki, T., Photocontrolled Microphase Separation of Block Copolymers in Two Dimensions. *J. Am. Chem. Soc.* **2005**, 127 (23), 8266-8267.
220. Zhou, H.; Xue, C.; Weis, P.; Suzuki, Y.; Huang, S.; Koynov, K.; Auernhammer, G. K.; Berger, R.; Butt, H.-J.; Wu, S., Photoswitching of glass transition temperatures of azobenzene-containing polymers induces reversible solid-to-liquid transitions. *Nat. Chem.* **2016**, 1-7.
221. Baroncini, M.; d'Agostino, S.; Bergamini, G.; Ceroni, P.; Comotti, A.; Sozzani, P.; Bassanetti, I.; Grepioni, F.; Hernandez, T. M.; Silvi, S.; Venturi, M.; Credi, A., Photoinduced reversible switching of porosity in molecular crystals based on star-shaped azobenzene tetramers. *Nat. Chem.* **2015**, 7 (8), 634-640.
222. Velema, W. A.; Szymanski, W.; Feringa, B. L., Photopharmacology: Beyond Proof of Principle. *J. Am. Chem. Soc.* **2014**, 136 (6), 2178-2191.
223. Velema, W. A.; van der Berg, J. P.; Hansen, M. J.; Szymanski, W.; Driessen, A. J. M.; Feringa, B. L., Optical control of antibacterial activity. *Nat. Chem.* **2013**, 5 (11), 924-928.
224. Fehrentz, T.; Schönberger, M.; Trauner, D., Optochemical Genetics. *Angew. Chem. Int. Ed.* **2011**, 50 (51), 12156-12182.
225. Ali, A. M. J.; Al-Saigh, Z. Y., Photodecomposition of azobenzenes. *J. Chem. Technol. Biotechnol.* **1980**, 30 (1), 440-446.
226. Davis, T. W.; Jahn, F. P.; Burton, M., The Photolysis of Azomethane. III. The Effect of Nitric Oxide and the Nature of the Primary Step^{1,2}. *J. Am. Chem. Soc.* **1938**, 60 (1), 10-17.

-
227. Wu, E. C.; Rice, O. K., Photolysis of perfluoroazomethane. *J. Am. Chem. Soc.* **1968**, 72 (2), 542-546.
228. Toby, S.; Nimoy, J., Intramolecular Formation of Ethane in the Gas-Phase Photolysis of Azomethane. *J. Am. Chem. Soc.* **1966**, 70 (3), 867-870.
229. Rebbert, R. E.; Ausloos, P., The Photolysis and Radiolysis of $\text{CH}_3\text{N}_2\text{CH}_3$ and $\text{CH}_3\text{N}_2\text{CH}_3\text{-CD}_3\text{N}_2\text{CD}_3$ Mixtures. *J. Phy. Chem.* **1962**, 66 (11), 2253-2258.
230. Barrett, C.; Natansohn, A.; Rochon, P., Thermal Cis-Trans Isomerization Rates of Azobenzenes Bound in the Side Chain of Some Copolymers and Blends. *Macromolecules* **1994**, 27 (17), 4781-4786.
231. Barrett, C.; Natansohn, A.; Rochon, P., Cis-Trans Thermal Isomerization Rates of Bound and Doped Azobenzenes in a Series of Polymers. *Chem. Mater.* **1995**, 7 (5), 899-903.
232. Norikane, Y.; Kitamoto, K.; Tamaoki, N., Novel Crystal Structure, Cis-Trans Isomerization, and Host Property of Meta-Substituted Macrocyclic Azobenzenes with the Shortest Linkers. *J. Org. Chem.* **2003**, 68 (22), 8291-8304.
233. Nagamani, S. A.; Norikane, Y.; Tamaoki, N., Photoinduced Hinge-Like Molecular Motion: Studies on Xanthene-Based Cyclic Azobenzene Dimers. *J. Org. Chem.* **2005**, 70 (23), 9304-9313.
234. Lamarre, L.; Sung, C. S. P., Studies of physical aging and molecular motion by azochromophoric labels attached to the main chains of amorphous polymers. *Macromolecules* **1983**, 16 (11), 1729-1736.
235. Müri, M.; Schuermann, K. C.; De Cola, L.; Mayor, M., Shape-Switchable Azo-Macrocycles. *Eur. J. Org. Chem.* **2009**, 2009 (15), 2562-2575.
236. Norikane, Y.; Katoh, R.; Tamaoki, N., Unconventional thermodynamically stable cis isomer and trans to cis thermal isomerization in reversibly photoresponsive [0.0](3,3[prime or minute])-azobenzenophane. *Chem. Commun.* **2008**, 16, 1898-1900.
237. Rau, H.; Lueddecke, E., On the rotation-inversion controversy on photoisomerization of azobenzenes. Experimental proof of inversion. *J. Am. Chem. Soc.* **1982**, 104 (6), 1616-1620.
238. Gräf, D.; Nitsch, H.; Ufermann, D.; Sawitzki, G.; Patzelt, H.; Rau, H., Azobenzene Phanes. *Angew. Chem. Int. Ed. Engl.* **1982**, 21 (5), 373-374.
239. Röttger, D.; Rau, H., Photochemistry of azobenzenophanes with three-membered bridges. *J. Photochem. Photobiol. A: Chem.* **1996**, 101 (2-3), 205-214.
240. Siewertsen, R.; Neumann, H.; Buchheim-Stehn, B.; Herges, R.; Näther, C.; Renth, F.; Temps, F., Highly Efficient Reversible Z-E Photoisomerization of a Bridged Azobenzene with Visible Light through Resolved $\text{S}_1(\text{n}\pi^*)$ Absorption Bands. *J. Am. Chem. Soc.* **2009**, 131 (43), 15594-15595.
241. Norikane, Y.; Tamaoki, N., Light-Driven Molecular Hinge: A New Molecular Machine Showing a Light-Intensity-Dependent Photoresponse that Utilizes the Trans-Cis Isomerization of Azobenzene. *Org. Lett.* **2004**, 6 (15), 2595-2598.
242. Bassotti, E.; Carbone, P.; Credi, A.; Di Stefano, M.; Masiero, S.; Negri, F.; Orlandi, G.; Spada, G. P., Effect of Strain on the Photoisomerization and Stability of a Congested Azobenzenophane: A Combined Experimental and Computational Study. *J. Phy. Chem. A* **2006**, 110 (45), 12385-12394.

-
243. Kang, H.-M.; Jung, J.-W.; Cho, C.-G., Practical Synthesis of Azobenzenophanes. *J. Org. Chem.* **2007**, 72 (2), 679-682.
244. Tamaoki, N.; Wada, M., Dynamic Control of Racemization Rate through E-Z Photoisomerization of Azobenzene and Subsequent Partial Photoresolution under Circular Polarized Light. *J. Am. Chem. Soc.* **2006**, 128 (19), 6284-6285.
245. Knie, C.; Utecht, M.; Zhao, F.; Kulla, H.; Kovalenko, S.; Brouwer, A. M.; Saalfrank, P.; Hecht, S.; Bléger, D., ortho-Fluoroazobenzenes: Visible Light Switches with Very Long-Lived Z Isomers. *Chem. A Eur. J.* **2014**, 20 (50), 16492-16501.
246. Ostas, E.; Schröter, K.; Beiner, M.; Yan, T.; Thurn-Albrecht, T.; Binder, W. H., *J. Polym. Sci. Part A: Polym. Chem.* **2011**, 49 (15), 3404-3416.
247. Barqawi, H.; Ostas, E.; Liu, B.; Carpentier, J.-F.; Binder, W. H., Multidimensional Characterization of α,ω -Telechelic Poly(ϵ -caprolactone)s via Online Coupling of 2D Chromatographic Methods (LC/SEC) and ESI-TOF/MALDI-TOF-MS. *Macromolecules* **2012**, 45 (24), 9779-9790.
248. Barqawi, H.; Schulz, M.; Olubummo, A.; Saurland, V.; Binder, W. H., 2D-LC/SEC-(MALDI-TOF)-MS Characterization of Symmetric and Nonsymmetric Biocompatible PEOm-PIB-PEOn Block Copolymers. *Macromolecules* **2013**, 46 (19), 7638-7649.
249. Gallot, B.; Fafiotte, M.; Fissi, A.; Pieroni, O., Liquid-crystalline structure of poly(L-lysine) containing azobenzene units in the side chain. *Macromol. Rapid Commun.* **1996**, 17 (8), 493-501.
250. Barqawi, H.; Binder, W. H., Azide/alkyne-“click”-reactions on amino resin materials: An LC-ESI-TOF analysis. *J. Polym. Sci. Part A: Polym. Chem.* **2010**, 48 (21), 4855-4866.

6.0 SUPPLEMENTARY INFORMATION

6.1 Synthesis and Characterization of new Photoswitchable Azobenzene-containing poly(ϵ -caprolactones).

Synthesis of 4-azidobenzoic acid

The synthesis of 4-azidobenzoic acid was followed as described in the literature [250]. To a suspension of 4-aminobenzoic acid (4.5 g, 33 mmol) in water (25 mL) in a 2 L-round bottom flask was added concentrated HCl (5.6 mL) drop wise while the mixture was vigorously stirred. After the addition has been finished the reaction mixture was cooled down to 0 °C with an ice-salt-mixture. A solution of NaNO₂ (2.3 g, 33 mmol) in water (10 mL) was added slowly (about 30 min) via dropping funnel. The colour of the mixture changes to yellow-orange during the addition. Subsequently, a solution of NaN₃ (2.14 g, 33 mmol) in water (25 mL) was added slowly whilst the mixture was vigorously stirred, whereby an enormous foam formation could be observed. The cooling bath was removed and stirring was continued for 90 min and afterwards a 100 mL water and 125 mL ethylacetate were added. The phases were separated via a separating funnel and the water phase was extracted two times with 50 mL ethylacetate. The organic phase was washed with 1 N NaOH (40 mL). The water phase was acidified with 1 N HCl (80 mL), whereby a yellow solid precipitates. During the acidification ethylacetate (150 mL) was added in portions, which solves the yellow solid. The organic phase was separated and the unified organic phases were then dried over Na₂SO₄, filtered and concentrated via vacuum distillation at room temperature to furnish a yellow solid. Yield: 4.98 g (92 %).

¹H-NMR (400 MHz, DMSO, δ , ppm): 12.89, (s, 1H), 7.94 (d, 2H, J = 8.63 Hz), 7.19 (d, 2H, J = 8.63 Hz).
¹³C-NMR (100 MHz, DMSO, δ , ppm): 166.9, 144.4, 131.6, 127.7, 119.6.

IR: 2813, 2541, 2101, 1672, 1600, 1577, 1507, 1424, 1316, 1282, 1177, 1138, 1122, 934, 856, 765

Synthesis of 4-azidobenzoylchloride

4-Azidobenzoic acid (1 g, 6.13 mmol) was added to freshly distilled thionylchloride (22.2 mL, 306 mmol) and refluxed for 4 h at 75 °C. When the reaction has finished the excess thionylchloride was removed under vacuum. The achieved brown solid was dried using high vacuum. Yield: 1.1 g (99 %).

¹H-NMR (400 MHz, DMSO, δ , ppm): 8.10 (d, 2H, J = 8.63 Hz), 7.12 (d, 2H, J = 8.63 Hz).
¹³C-NMR (100 MHz, DMSO, δ , ppm): 167.8, 144.4, 131.6, 127.7, 119.6.

IR: 3098, 2401, 2252, 2119, 1737, 1594, 1498, 1417, 1306, 1282, 1208, 1171, 1121, 876, 837, 815, 804, 726, 696, 642.

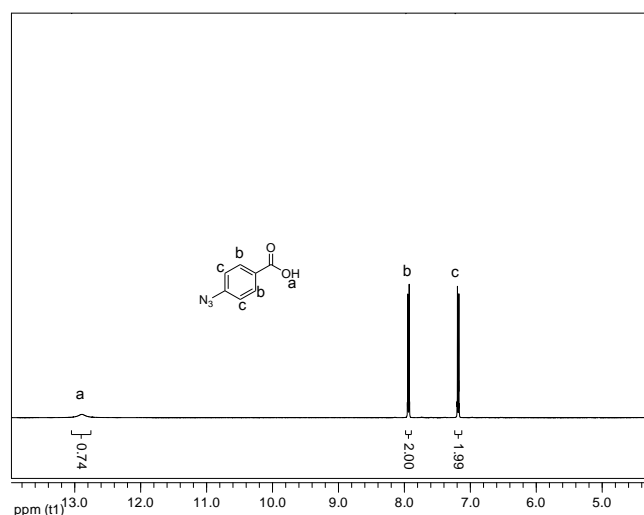


Figure S1: ¹H-NMR spectrum of compound 4-azidobenzoic acid

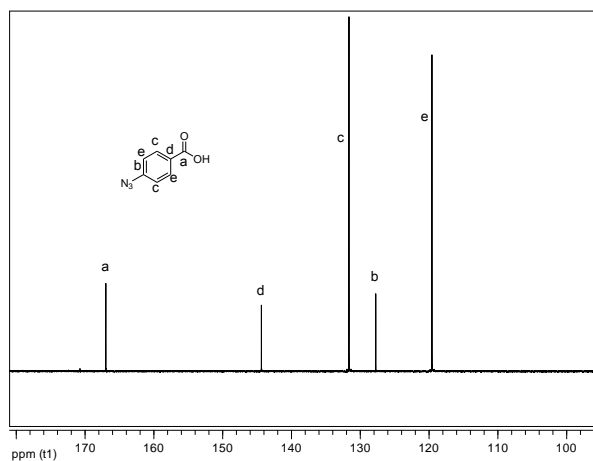


Figure S2: ^{13}C -NMR spectrum of compound 4-azidobenzoic acid

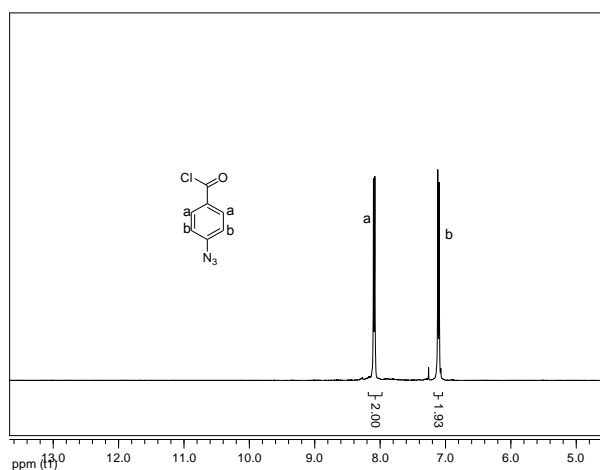


Figure S3: ^1H -NMR spectrum of compound 4-azidobenzoylchloride

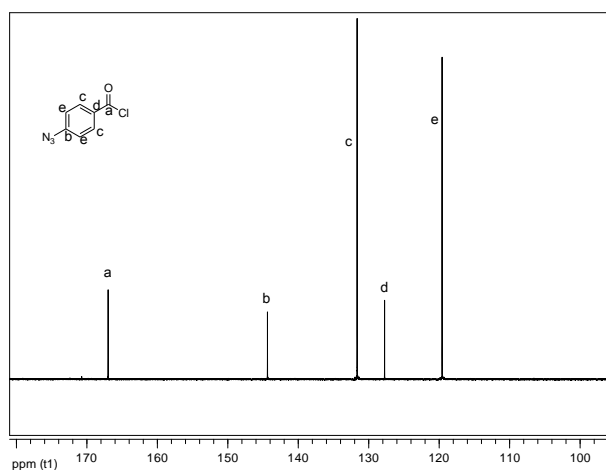


Figure S4: ^{13}C -NMR spectrum of compound 4-azidobenzoylchloride

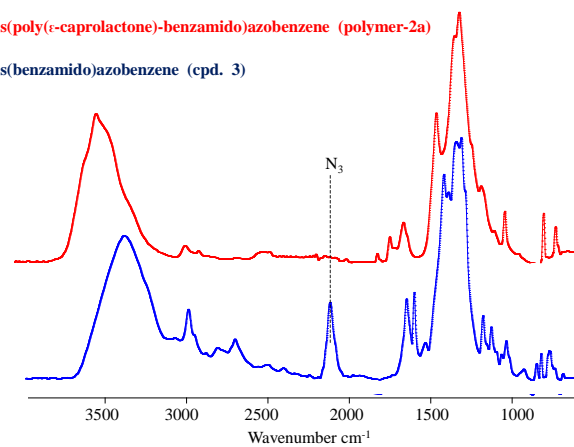


Figure S5a: FTIR spectra of compound **3** and **polymer-2b** showing the disappearance of the azide group after the click chemistry.

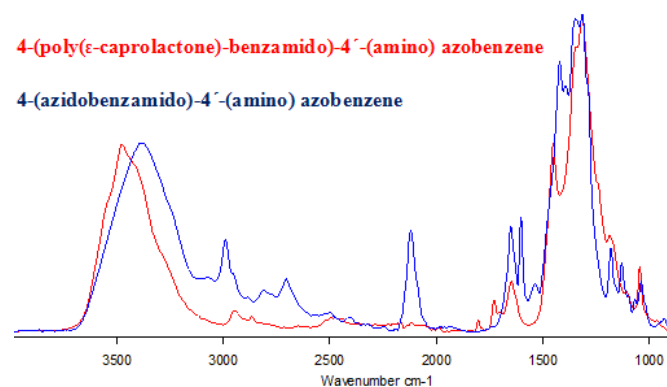


Figure S5b: FTIR spectra of compound **2** and **polymer-1b** showing the disappearance of the azide group after the click chemistry.

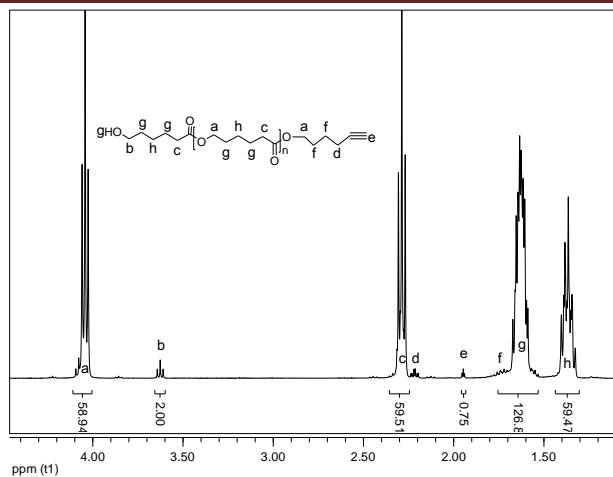


Figure S6: ^1H -NMR spectrum of PCL-alkyne3

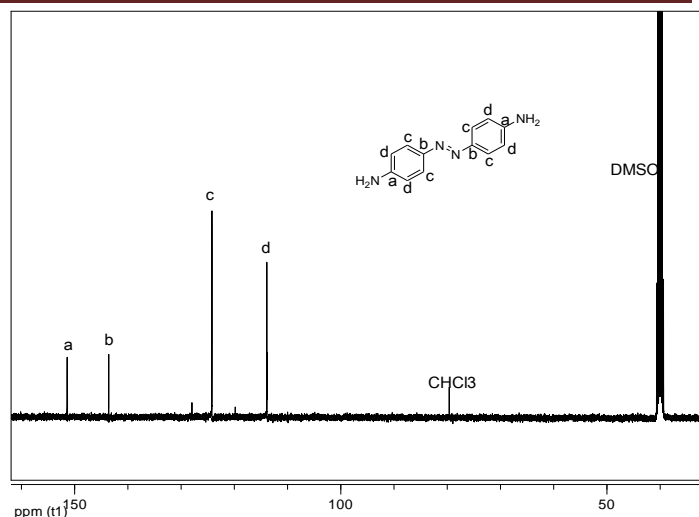


Figure S9: ^{13}C -NMR spectrum of compound 1

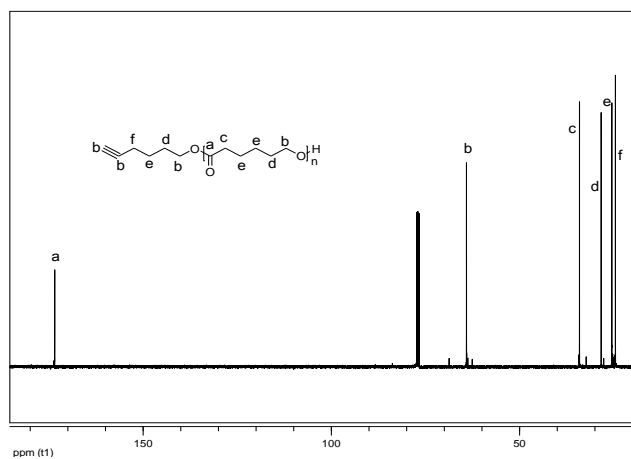


Figure S7: ^{13}C -NMR spectrum of PCL-alkyne3

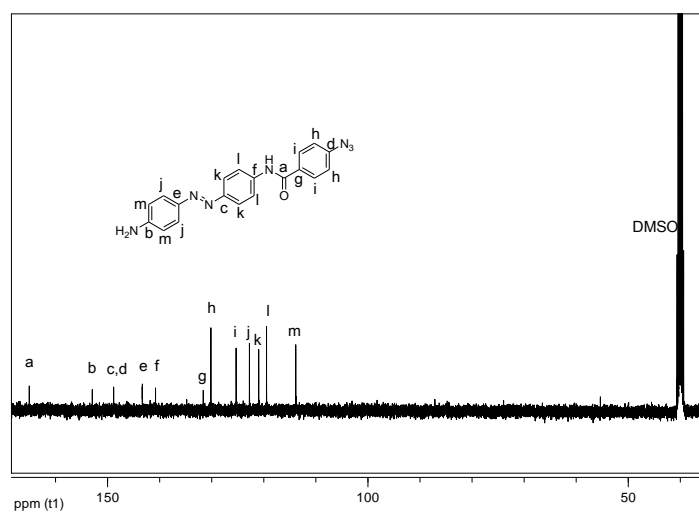


Figure S10: ^{13}C -NMR spectrum of compound 2

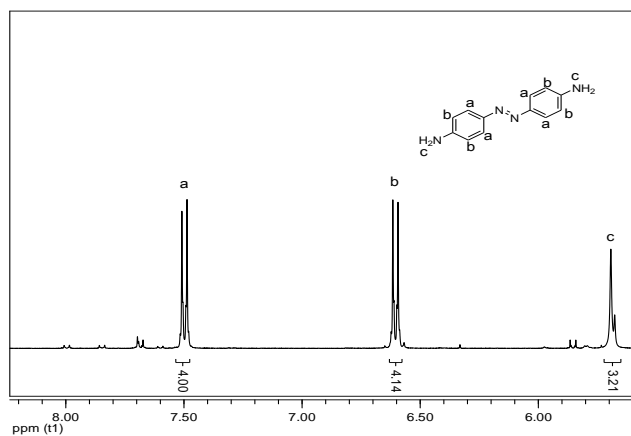


Figure S8: ^1H -NMR spectrum of compound 1

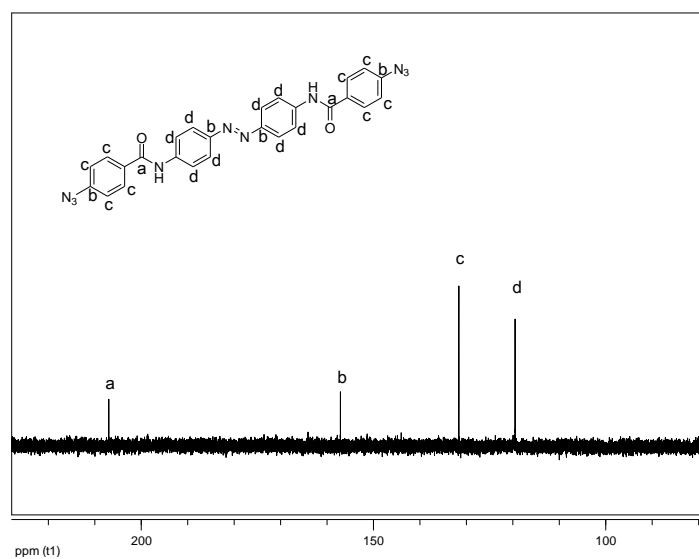
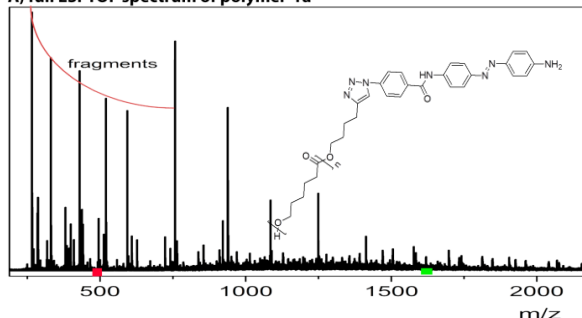


Figure S11: ^{13}C -NMR spectrum of compound 3

A) full ESI-TOF spectrum of polymer-1a



B) measured and simulated peaks for the observed signals

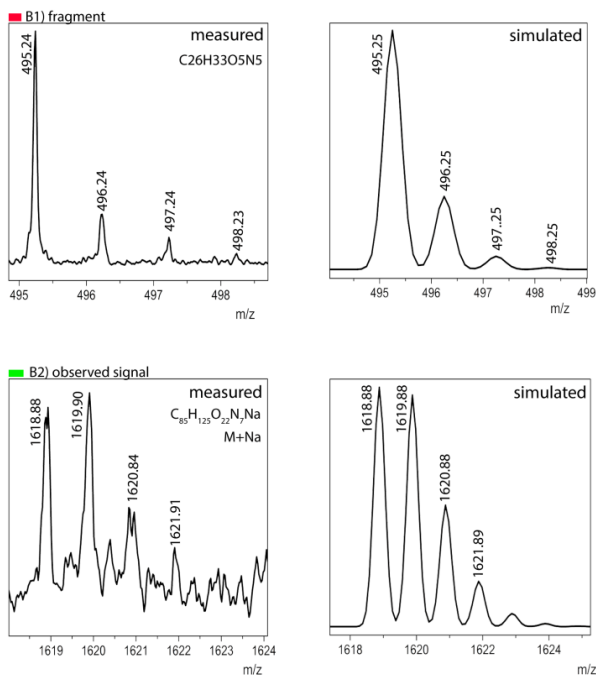


Figure S12. ESI-TOF spectra of the photoswitchable **polymer-1**, showing the observed and simulated signals.

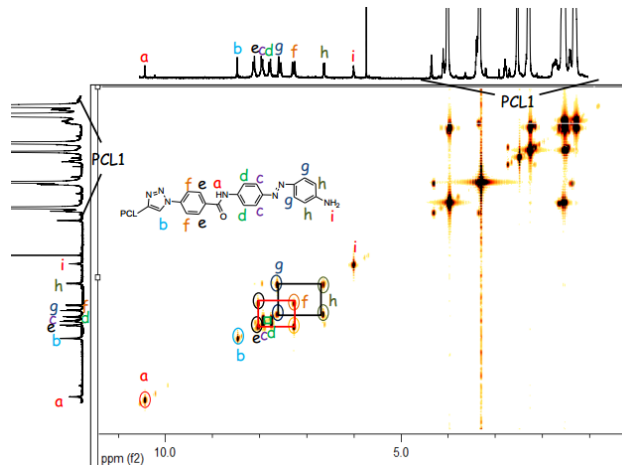


Figure S13. Proton homonuclear correlated 2-dimensional ^1H - ^1H COSY NMR of **polymer-1b**.

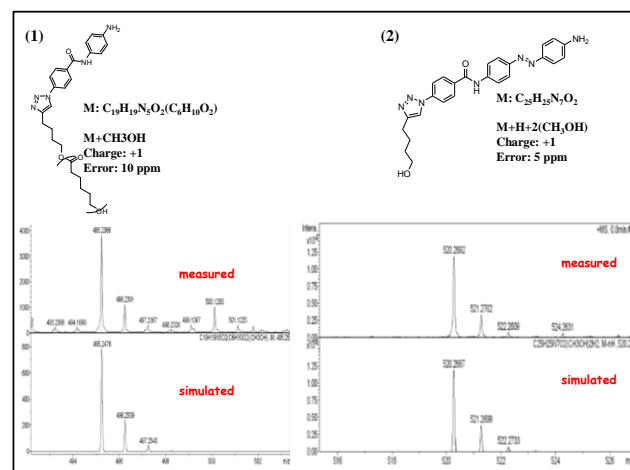


Figure S14: fragmented structures obtained from the ESI-TOF-MS analysis for **polymer-1a**

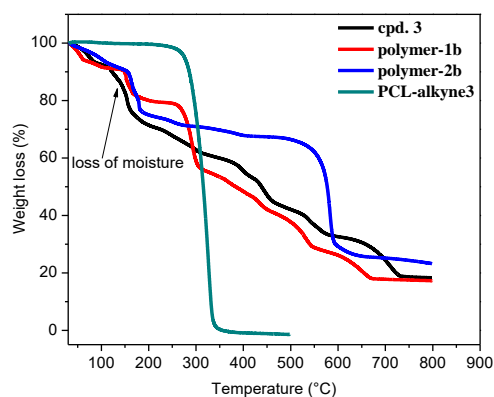
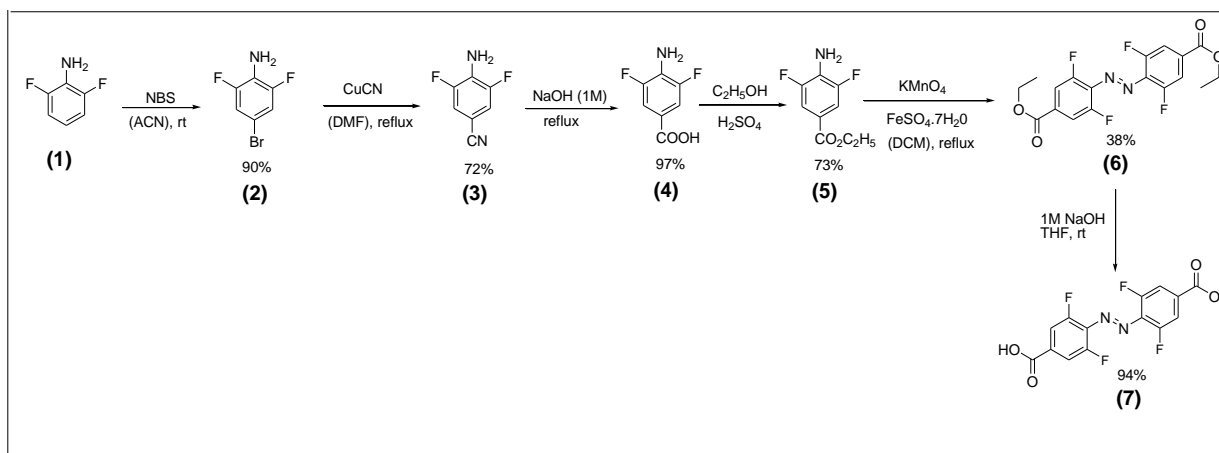


Figure S15: TGA curves of compound **3**, **polymer-1b**, **polymer-2b** and **PCL-alkyne3**.

6.2 Synthesis of Photoresponsive Main-Chain Oligomers with Azobenzene Moieties via ADMET Oligomerization and Investigation on Their Micellization Properties.

Experimental part



Scheme S1: Synthetic scheme of the fluorinated and non-fluorinated azo-monomers

Synthesis of 2,6-difluoro-4-bromoaniline (**2**)

A solution of 2,6-difluoroaniline (12.9 g, 100 mmol) in acetonitrile (200 mL) was charged with N-bromosuccinimide (17.8 g, 100 mmol). The mixture was stirred for 24 h at room temperature, and then diluted with water and hexanes. The two phases were separated and the organic phase was dried over MgSO_4 , filtered, and concentrated under reduced pressure. The crude residue was purified by column chromatography (DCM/hexanes:1/1) to give compound (**2**, 92%).

$^1\text{H-NMR}$ (**2**, CDCl_3): δ ppm 6.99 (dd, $J = 6.3$ Hz, 1.4 Hz, 2H, m-**ArH-N**), 3.73 (s, 2H, **NH**₂). $^{13}\text{C-NMR}$ (**2**, CDCl_3): δ ppm 152.7 (d, $J = 8.7$ Hz), 150.8 (d, $J = 7.7$ Hz), 123.5, 114.8, 107.1. $^{19}\text{F-NMR}$ (**2**, CDCl_3): δ ppm -132 (m). HRMS (ESI) calcd for $\text{C}_6\text{H}_5\text{BrF}_2\text{N}$ ($[\text{M}+\text{H}]^+$) 207.9568, found 207.9563

Synthesis of 4-amino-3,5-difluorobenzonitrile (**3**)

A solution of compound (**2**) (10 g, 48 mmol) in DMF (100 mL) was added CuCN (12.8 g, 144 mmol) and refluxed for 24 h. Afterwards, the mixture was poured into a NH_3 12% aqueous solution and extracted with ethyl acetate. The two phases were

separated and the organic phase was dried over MgSO_4 , filtered, and concentrated under reduced pressure. The crude residue was purified by column chromatography (DCM/hexanes:2/1) to give compound (**3**, 72%).

$^1\text{H-NMR}$ (**3**, CDCl_3): δ ppm 7.16 (dd, $J = 6.3$ Hz, 1.8 Hz, 2H, m-**ArH-N**), 4.15 (s, 2H, **NH**₂). $^{19}\text{F-NMR}$ (**3**, CDCl_3): δ ppm -130 (m). HRMS (ESI) calcd for $\text{C}_7\text{H}_3\text{F}_2\text{N}_2$ ($[\text{M}-\text{H}]^-$) 153.0439, found 153.0424

Synthesis of 4-amino-3,5-difluorobenzoic acid (**4**)

Compound (**3**) (5.3 g, 35 mmol) was suspended in NaOH 1M (160 mL) and heated to reflux for 24 h. The reaction was then cooled down to room temperature, and 1M HCl added to it, until the product precipitates as its hydrochloric salt. The salt was then dissolved in ethyl acetate, dried over MgSO_4 , filtered, concentrated under reduced pressure, to give compound (**4**, quantitative).

$^1\text{H-NMR}$ (**4**, CDCl_3): δ ppm 12.73 (s, 1H, **COOH**), 7.69 (dd, $J = 5.1$ Hz, 1.6 Hz, 2H, m-**ArH**), 3.31 (s, 2H, **NH**₂). $^{13}\text{C-NMR}$ (**4**, CDCl_3): δ ppm 165.5, 150.6 (d, $J = 9.3$ Hz), 148.4 (d, $J = 9.3$ Hz), 129.6, 117.5,

112.2. ^{19}F -NMR (**4**, CDCl_3): δ ppm -130 (m). HRMS (ESI) calcd for $\text{C}_7\text{H}_4\text{F}_2\text{NO}_2$ ($[\text{M}-\text{H}]^-$) 172.0245, found 172.0241

Synthesis of ethyl 4-amino-3,5-difluorobenzoate (**5**)

Compound (**4**) (5.3 g, 30 mmol) was dissolved in ethanol (100 mL) and H_2SO_4 (2 mL), and refluxed for 10 h. The mixture was neutralized with saturated NaHCO_3 , extracted with DCM, the two phases were separated and the organic phase was dried over MgSO_4 , filtered, and concentrated under reduced pressure to give compound (**5**, 73%).

^1H -NMR (**5**, CDCl_3): δ ppm 7.52 (dd, $J = 7.3$ Hz, 2.1 Hz, 2H, m-**ArH**), 4.18 (q, $J = 7.4$ Hz, 2H, $\text{CH}_2\text{-CH}_3$), 3.97 (s, 2H, NH_2), 1.36 (t, $J = 7.2$ Hz, 3H, $\text{CH}_2\text{-CH}_3$). ^{13}C -NMR (**5**, CDCl_3): δ ppm 169.5, 152.2 (d, $J = 8.5$ Hz), 149.3 (d, $J = 8.5$ Hz), 128.8, 118.3, 112.5, 61.4, 14.2. ^{19}F -NMR (**5**, CDCl_3): δ ppm -130 (m). HRMS (ESI) calcd for $\text{C}_9\text{H}_{10}\text{F}_2\text{NO}_2$ ($[\text{M}+\text{H}]^+$) 202.0614, found 202.0612

Synthesis of diethyl-4,4'-(2,2',6,6'-tetrafluoro)azobenzene dicarboxylate (**6**)

A one-neck flask was charged with compound (**5**) (1 g, 5 mmol) and a freshly ground mixture of KMnO_4 (8.5 g) and $\text{FeSO}_4\cdot 7\text{H}_2\text{O}$ (8.5 g) dissolved in DCM (150 mL). The solution was refluxed 24 h, filtered through celite, dried over MgSO_4 , filtered, and concentrated under reduced pressure. The crude residue was purified by column chromatography (DCM/hexanes: 1/1) to give compound (**6**, 38%).

^1H -NMR (**6**, CDCl_3): (80% *trans*-isomer) δ ppm 7.26 (m, 4H, m-**ArH-N=N-ArH**), 4.19 (q, $J = 7.2$ Hz, 4H, $\text{CH}_2\text{-CH}_3$), 1.42 (t, $J = 7.1$ Hz, 6H, $\text{CH}_2\text{-CH}_3$). ^{13}C -NMR (**6**, CDCl_3): (80% *trans*-isomer) δ ppm 164.6, 154.5 (d, $J = 5.2$ Hz), 153.2 (d, $J = 5.2$ Hz), 133.8, 113.0, 62.1, 14.0. ^{19}F -NMR (**6**, CDCl_3): δ ppm -118 (d, $J =$

6.1 Hz), -119 (d, $J = 8.5$ Hz). HRMS (ESI) calcd for $\text{C}_{18}\text{H}_{15}\text{F}_4\text{N}_2\text{O}_4$ ($[\text{M}+\text{H}]^+$) 399.0962, found 399.0966

Synthesis of 2,2',6,6'-tetrafluoro-4,4'-dicarboxyazobenzene (**7**)

Compound (**6**) (350 mg, 0.9 mmol) was dissolved in 15 mL THF and 4 mL 1 M NaOH was added, the solution was stirred for 2 h at room temperature. In the meantime, the solution was adjusted to pH = 4 with 1 M HCl, extracted with ethyl acetate and the organic phase concentrated under reduced pressure to give compound (**7**, 94%).

^1H -NMR (**7**, DMSO): (80% *trans*-isomer) δ ppm 12.75 (s, 2H, **COOH**), 7.26 (d, $J = 8.2$ Hz, 2H, m-**ArH-N=N-ArH**). ^{13}C -NMR (**7**, DMSO): (80% *trans*-isomer) δ ppm 165.9, 155.8 (d, $J = 5.2$ Hz), 153.6 (d, $J = 5.2$ Hz), 135.6, 133.4. ^{19}F -NMR (**7**, DMSO): δ ppm -118 (d, $J = 6.1$ Hz), -119 (d, $J = 8.5$ Hz). HRMS (ESI) calcd for $\text{C}_{14}\text{H}_7\text{F}_4\text{N}_2\text{O}_4$ ($[\text{M}+\text{H}]^+$) 343.0336, found 343.0333

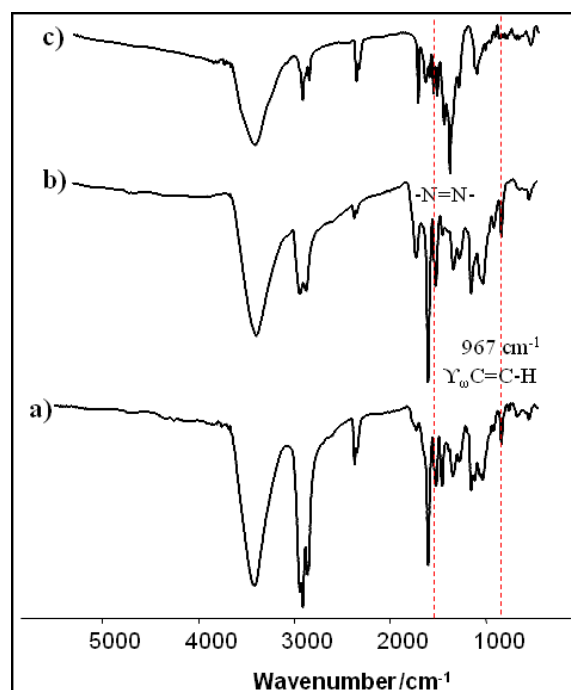


Figure S1. FTIR spectra of the non-fluorinated azobenzene compounds. (a) shows the spectrum of the azo-monomer used for the oligomerization reactions, (b) shows the spectrum of the

unsaturated oligomers and (c) Shows the spectrum of the saturated oligomers after hydrogenation

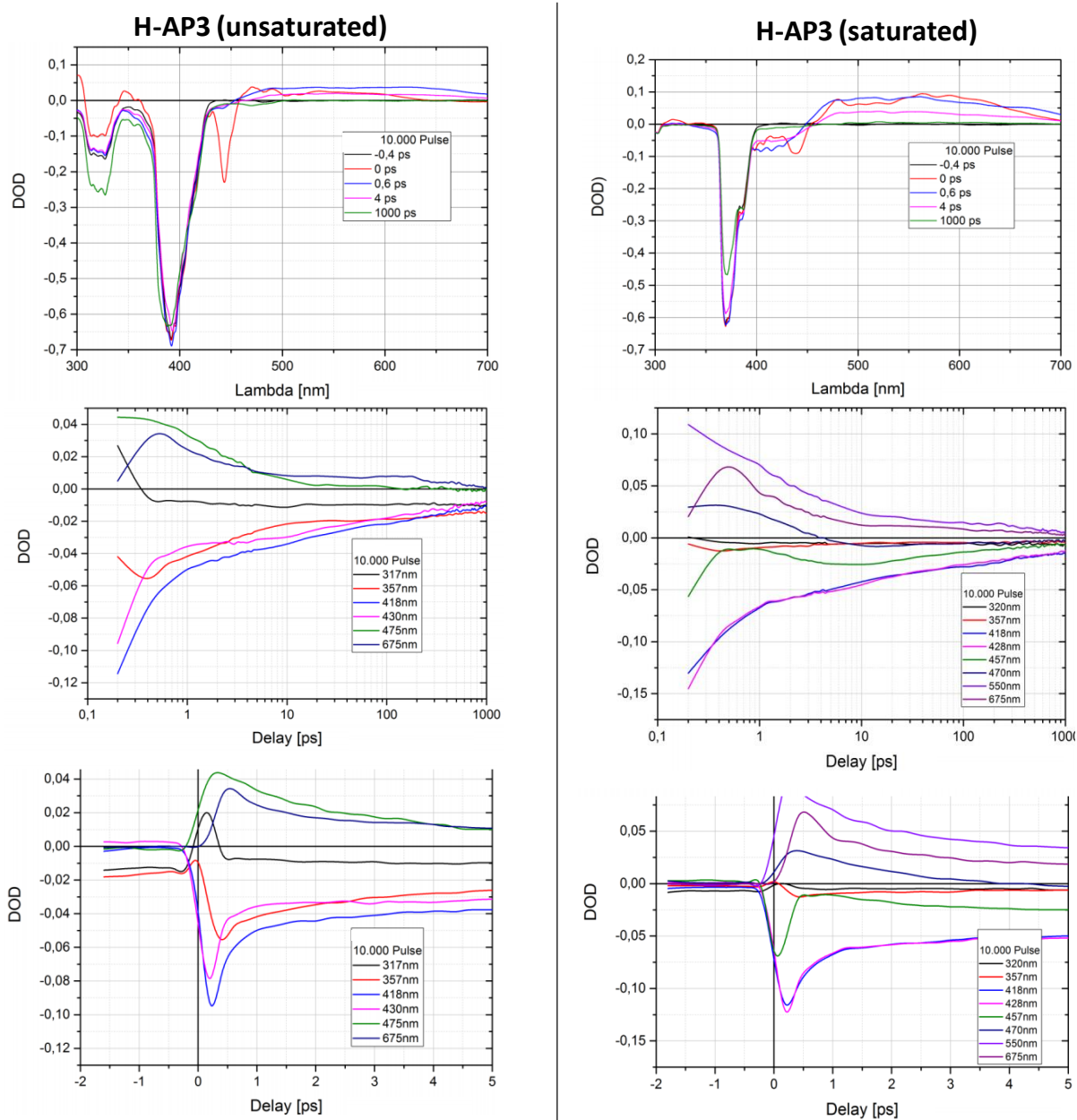


Figure S2. UV-VIS and Ultrafast dynamics measurements of the non-fluorinated azo- compounds, showing the full delay time range of transient, upon 338 nm excitation.

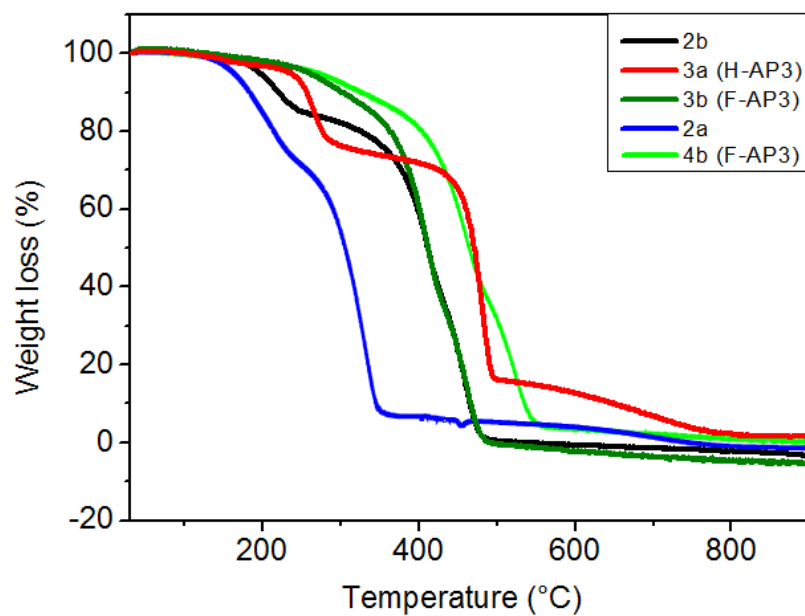


Figure S3. Thermal decomposition of the azo-monomers and oligomers

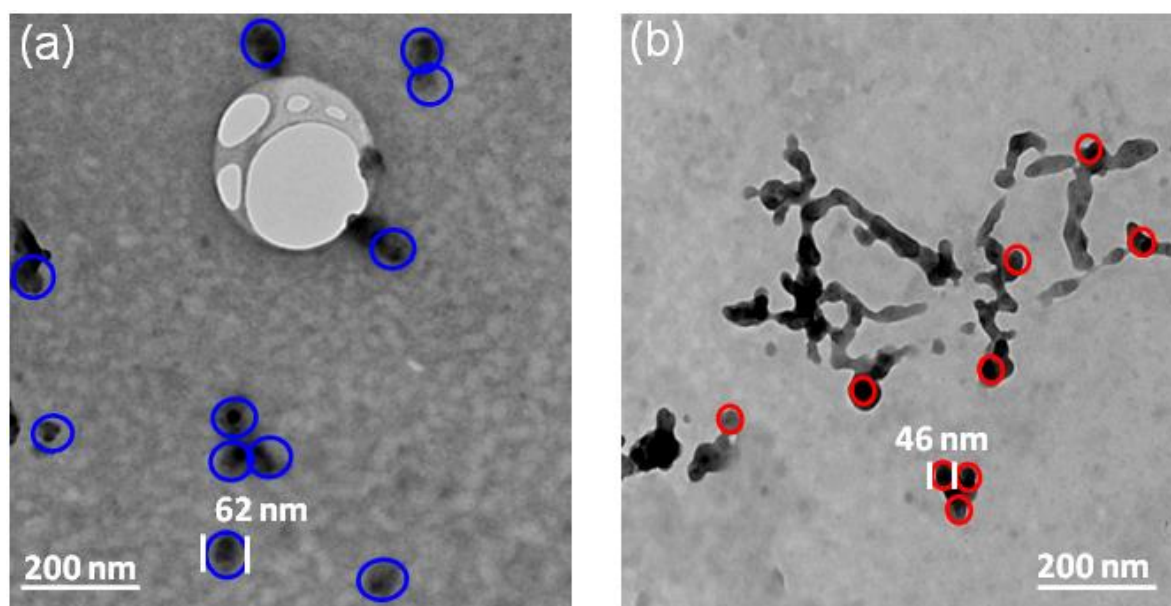


Figure S4. TEM images of the fluorinated azo-oligomers (4b) before (a) and after (b) photo-irradiation

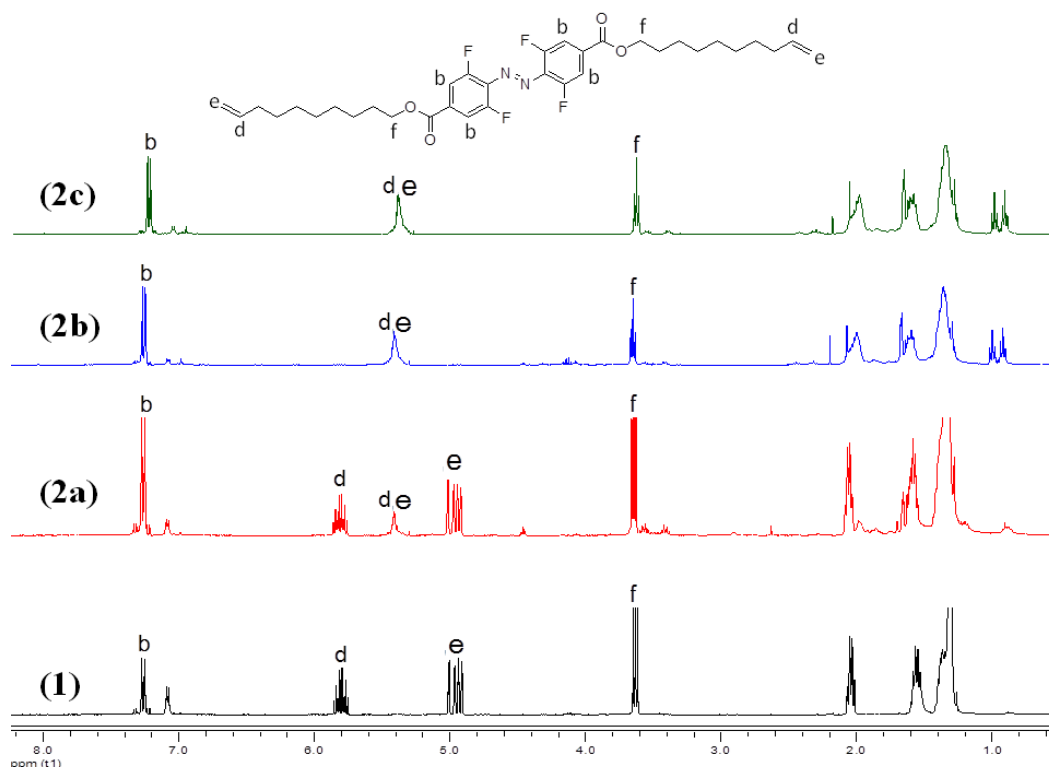


Figure S5: $^1\text{H-NMR}$ of the fluorinated azobenzenes. The numbers (1) shows the azo-monomers before oligomerization, (2) shows the azo-oligomers after oligomerization, a, b and c shows 24 h, 72 h and 120 h oligomerization time respectively.

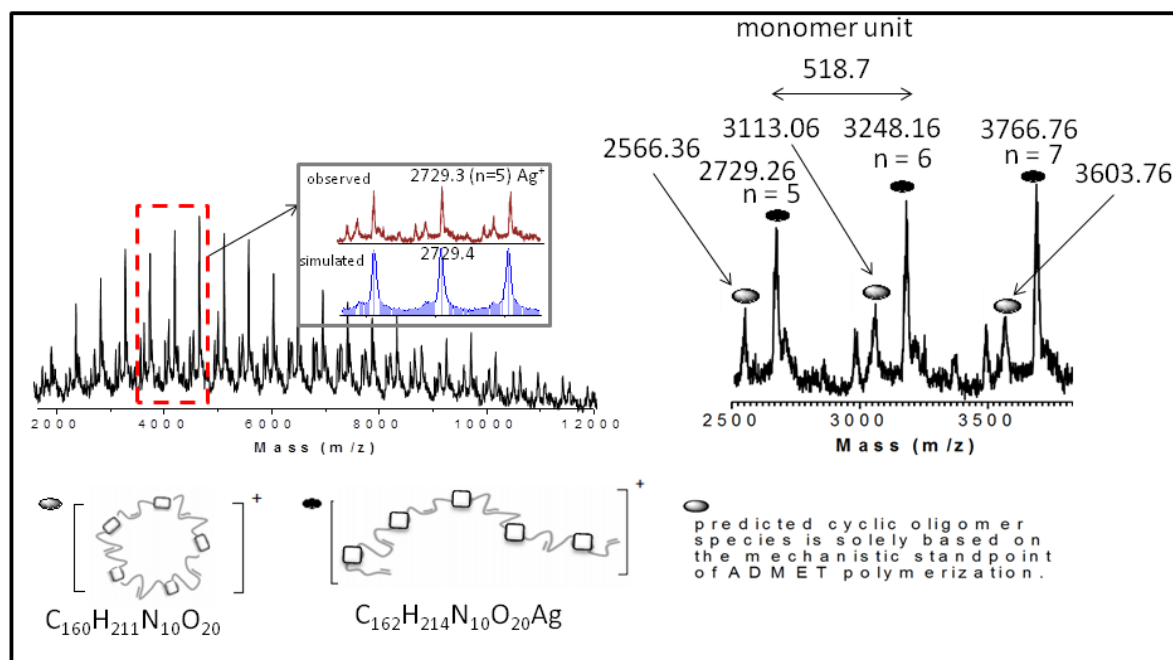


Figure S6. MALDI-ToF MS spectra of the unsaturated azo-oligomer (3a, run 4)

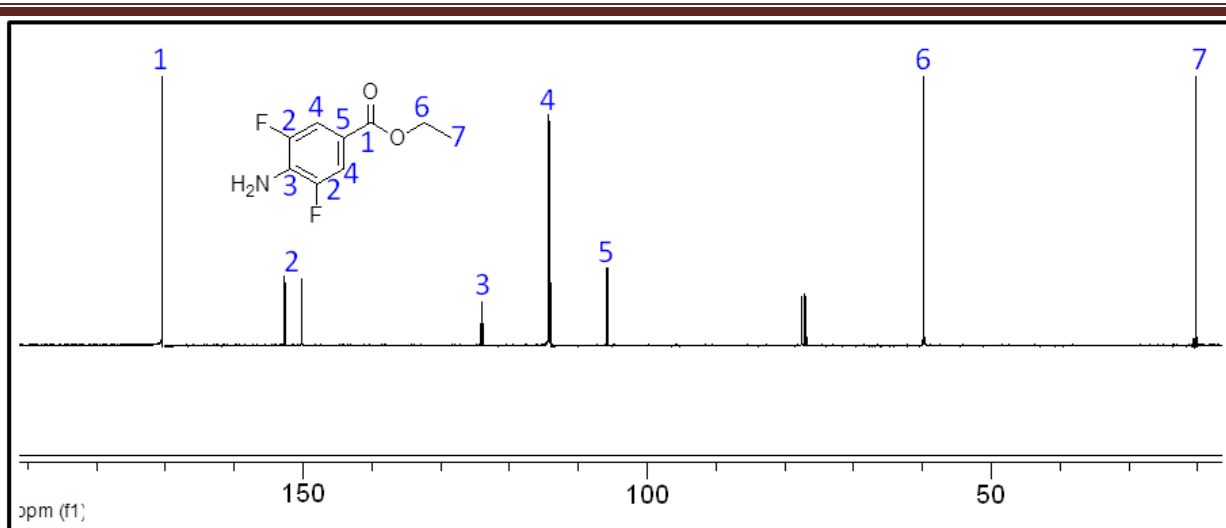


Figure S7. ^{13}C -NMR of ethyl 4-amino-3,5-difluorobenzoate (5)

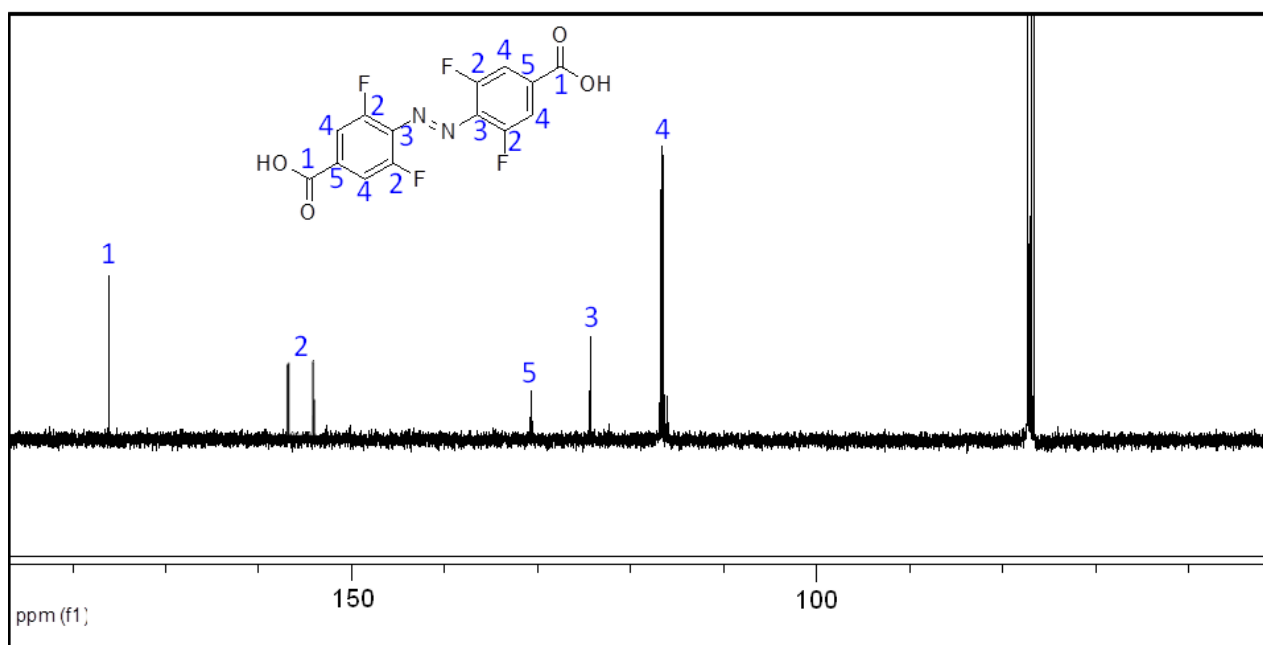


Figure S8. ^{13}C -NMR of 2,2',6,6'-tetrafluoro-4,4'-dicarboxyazobenzene (7)

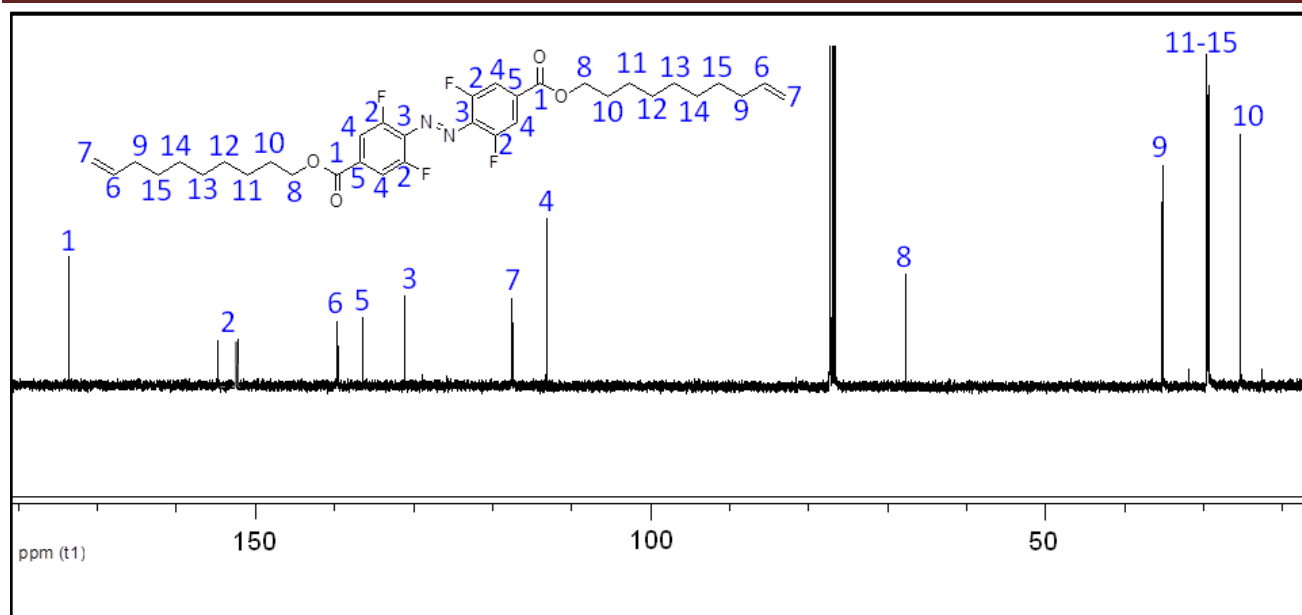


Figure S9. ^{13}C -NMR of the symmetric fluorinated azobenzene diene monomer (2b)

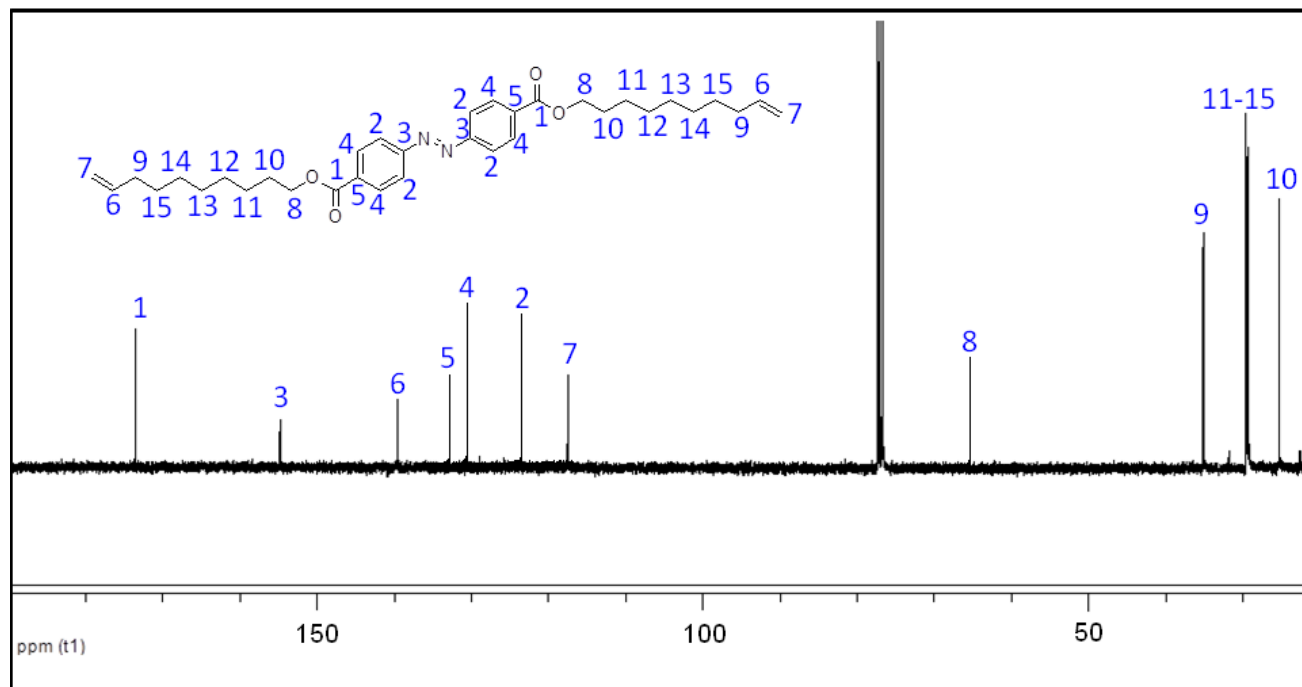


Figure S10. ^{13}C -NMR of the symmetric non-fluorinated azobenzene diene monomer (2a)

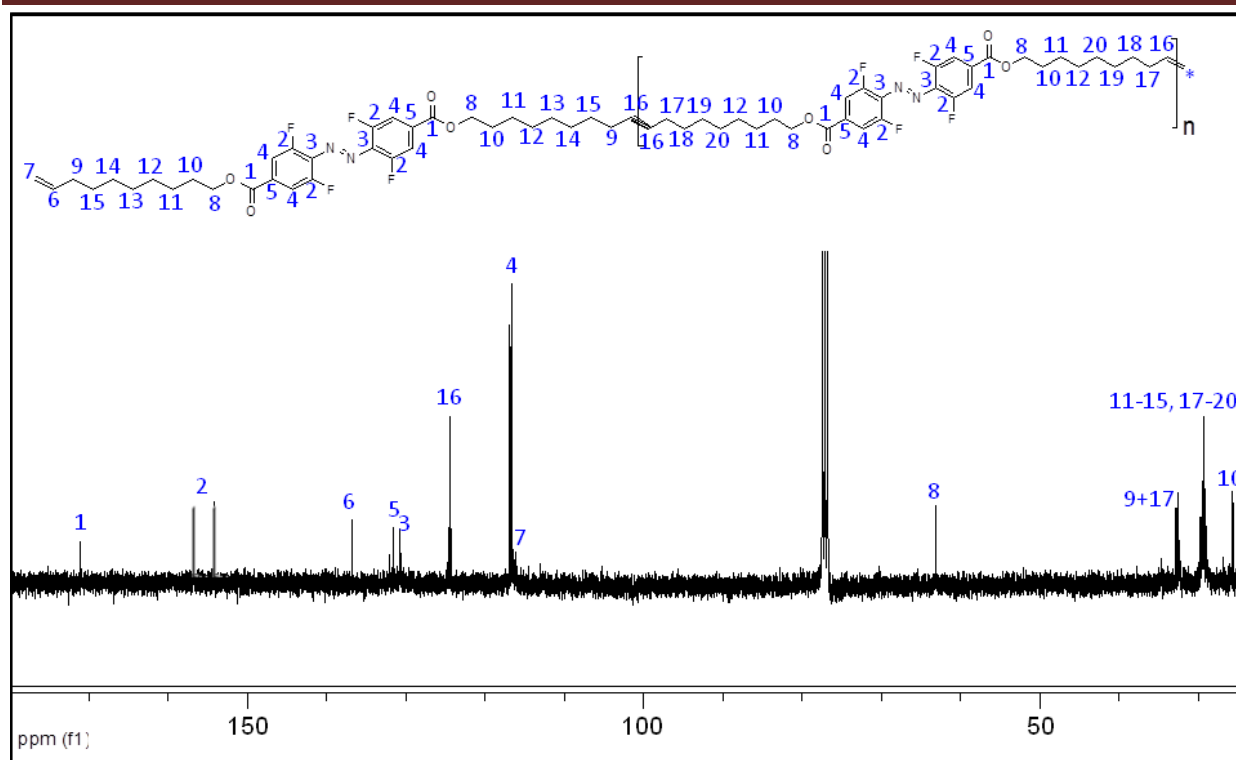


Figure S11. ^{13}C -NMR of the of the unsaturated azo-oligomer (3b)

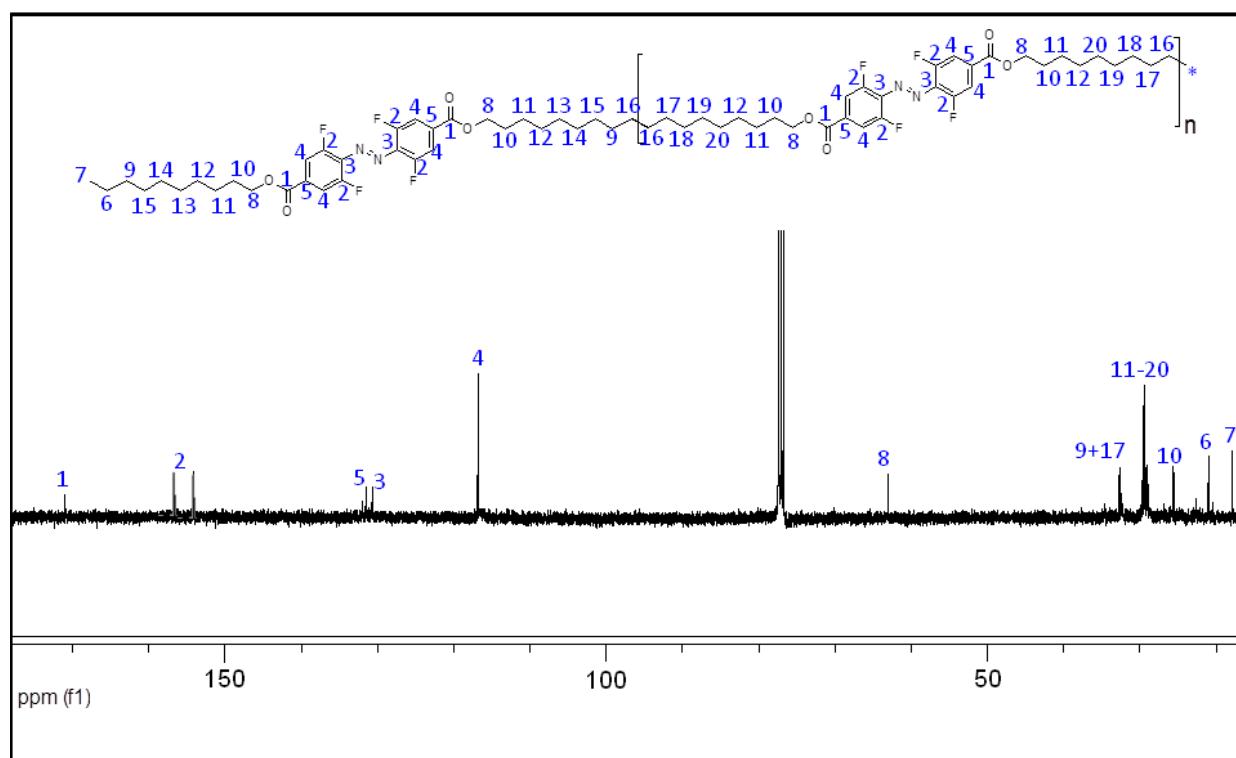


Figure S12. ^{13}C -NMR of the of the saturated azo-oligomer (4b)

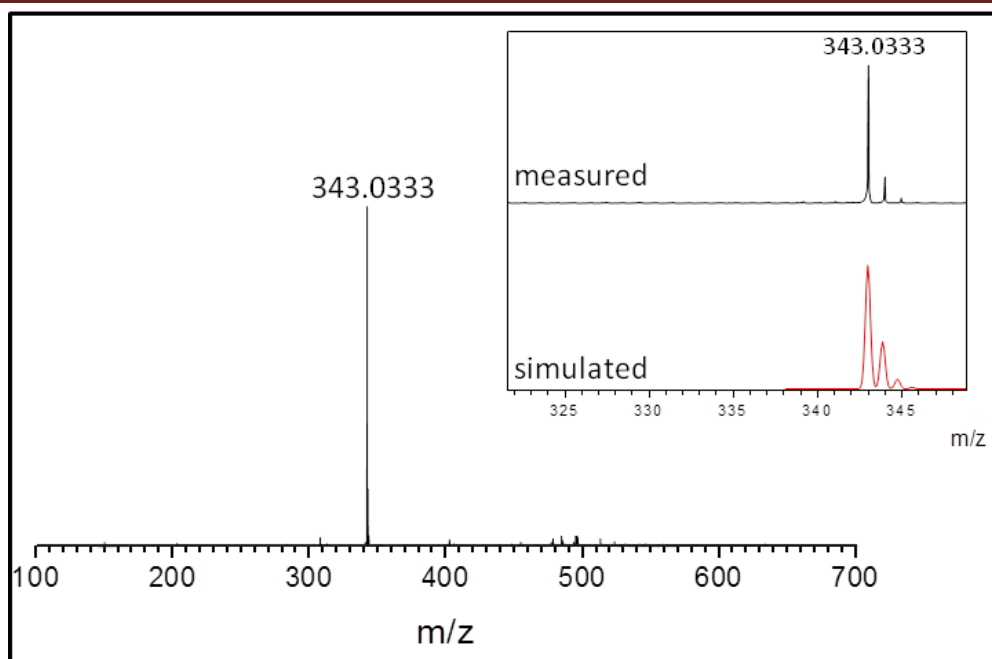


Figure S13. HRMS (ESI) of the 2,2',6,6'-tetrafluoro-4,4'-dicarboxyazobenzene (7)

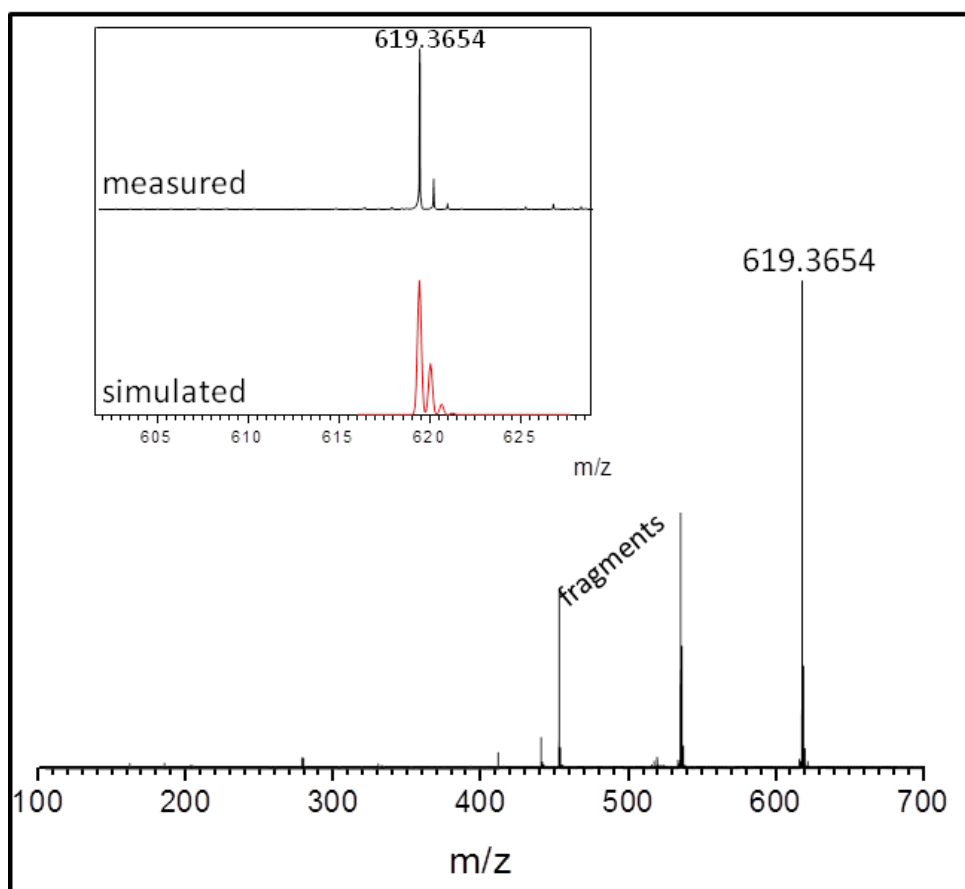


Figure S14. HRMS (ESI) of the fluorinated azo-monomer (2b)

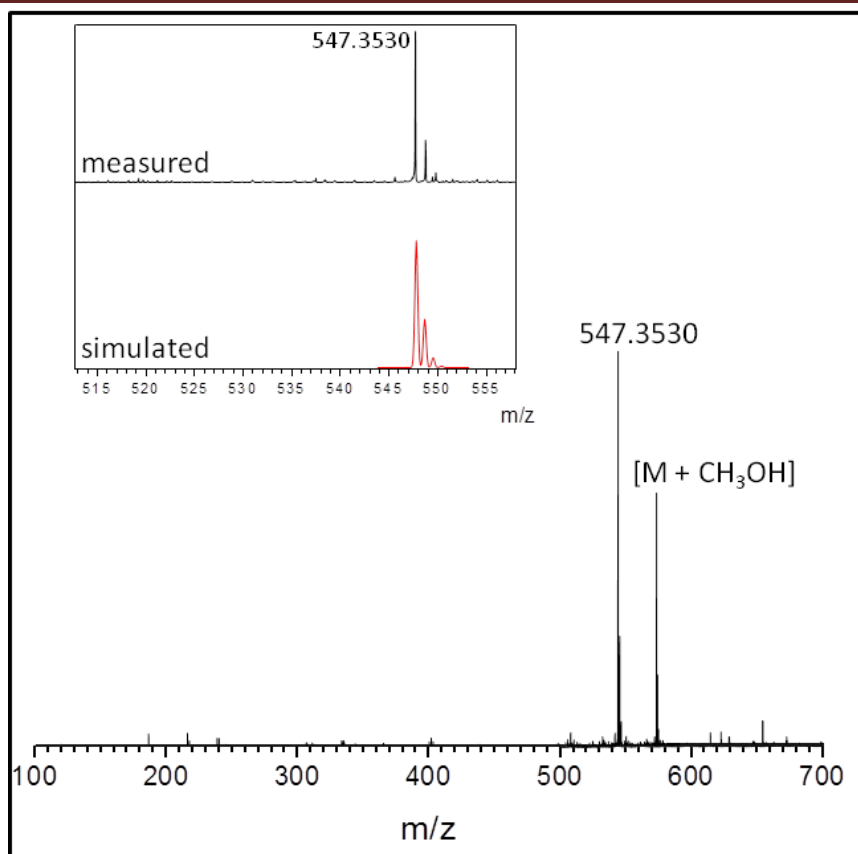


Figure S15. HRMS (ESI) of the non-fluorinated azo-monomer (2a)

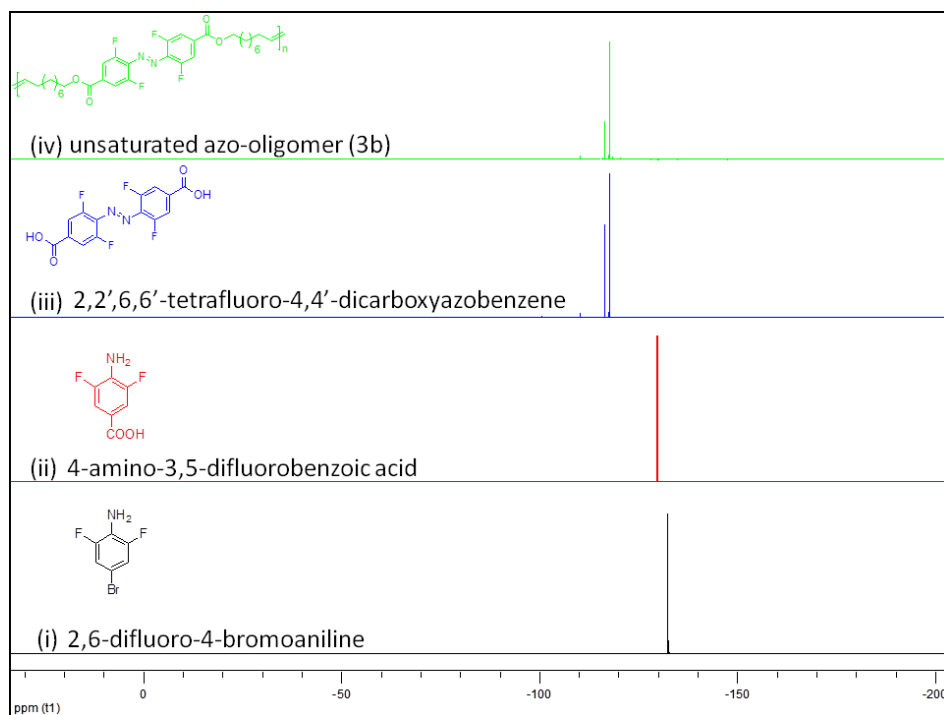


Figure S16. ^{19}F -NMR spectra of the fluorinated compounds.

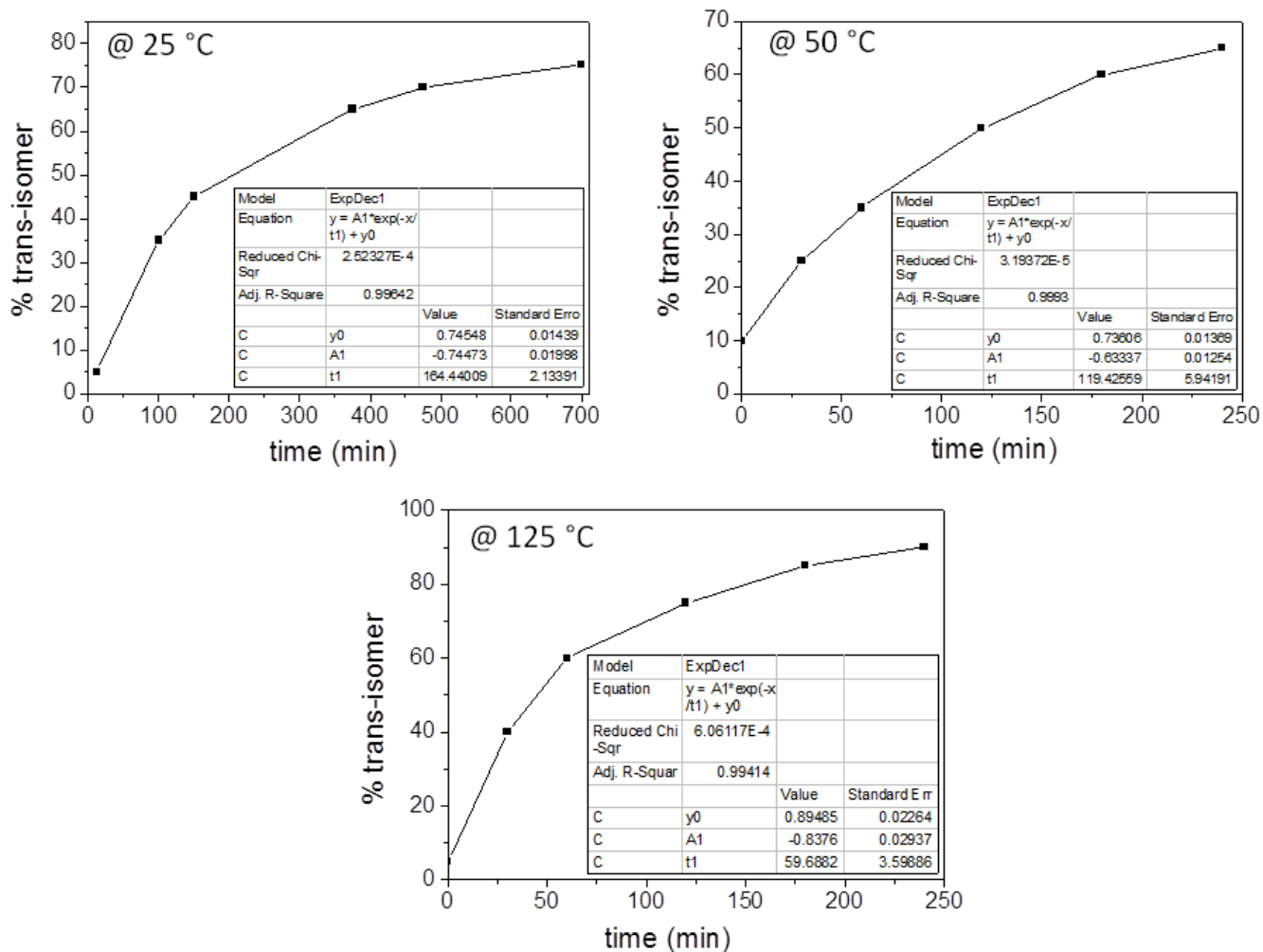


Figure S17. Estimated thermal *cis* to *trans* isomerisation kinetic studies of the fluorinated azobenzene monomer in DMSO. Plots of % *trans*-isomer (as determined by UV-VIS absorbance spectroscopy) versus time (min) at different temperatures.

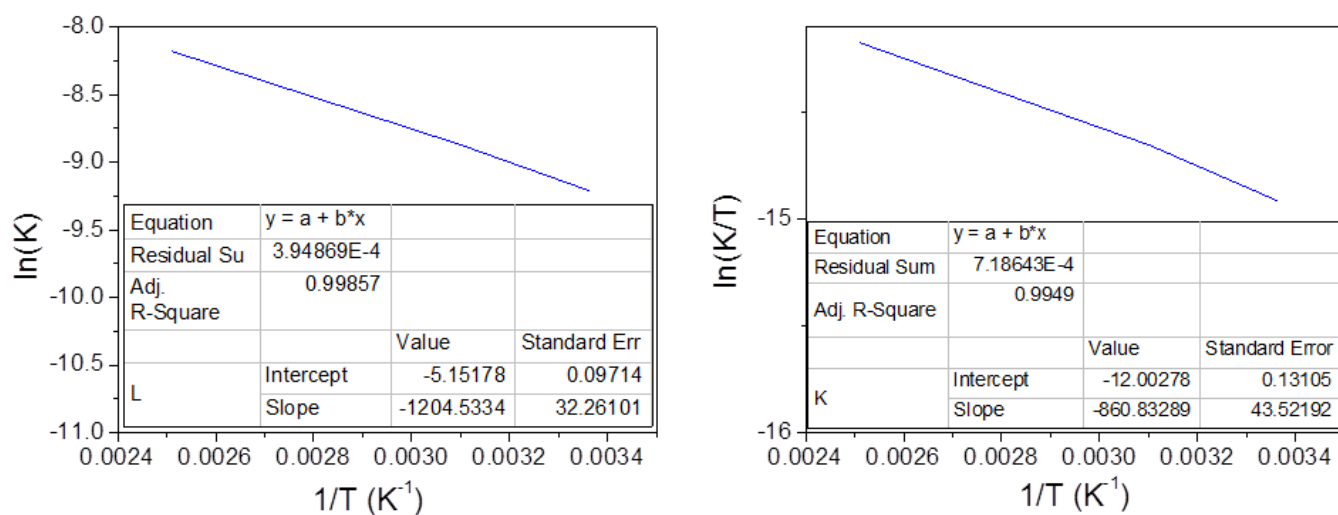


Figure S17. Arrhenius plot (left), Van't Hoff plot (right), and the corresponding kinetic data and thermodynamic parameters at 298 K as calculated using the Arrhenius and Eyring equations.

T (K)	K (s ⁻¹)	ΔH^\ddagger (kJ/mol)	ΔS^\ddagger (J/mol)	ΔG^\ddagger (kJ/mol)
298	1.02×10^{-4}	72	-297	96
323	1.40×10^{-4}			103
398	2.79×10^{-4}			190

6.3 Crystallization behavior of ADMET Polyethylene Containing Azobenzene Defects

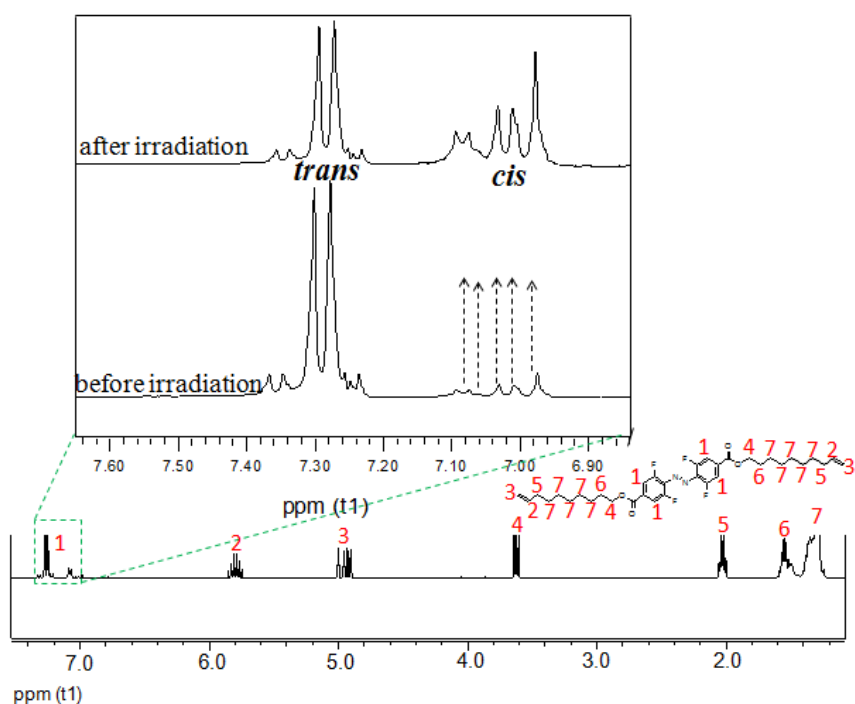


Figure S1. ^1H -NMR spectrum of the F-azo monomer. Inset shows the change in the cis/trans resonance peak after green light irradiation ($\lambda \sim 520$ nm).

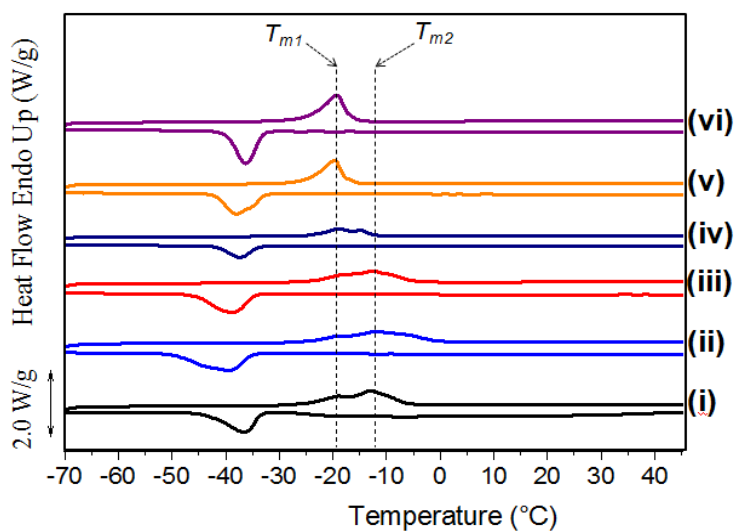


Figure S2. DSC heating/cooling scans of the F-azo monomer before green light irradiation. Measurements were conducted by annealing the samples at 10 K/min for 1h at temperatures of; (i) 75 °C (ii) 100 °C (iii) 125 °C (iv) 130 °C, (iv) 140 °C (v) 150 °C and (vi) 175 °C. Data are rescaled and shifted vertically for clarity.

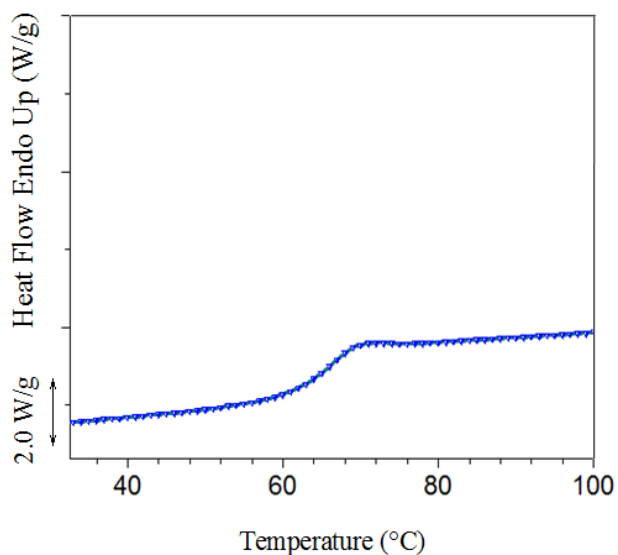


Figure S3. Glass transition temperature at 68 °C for the H-azo monomer

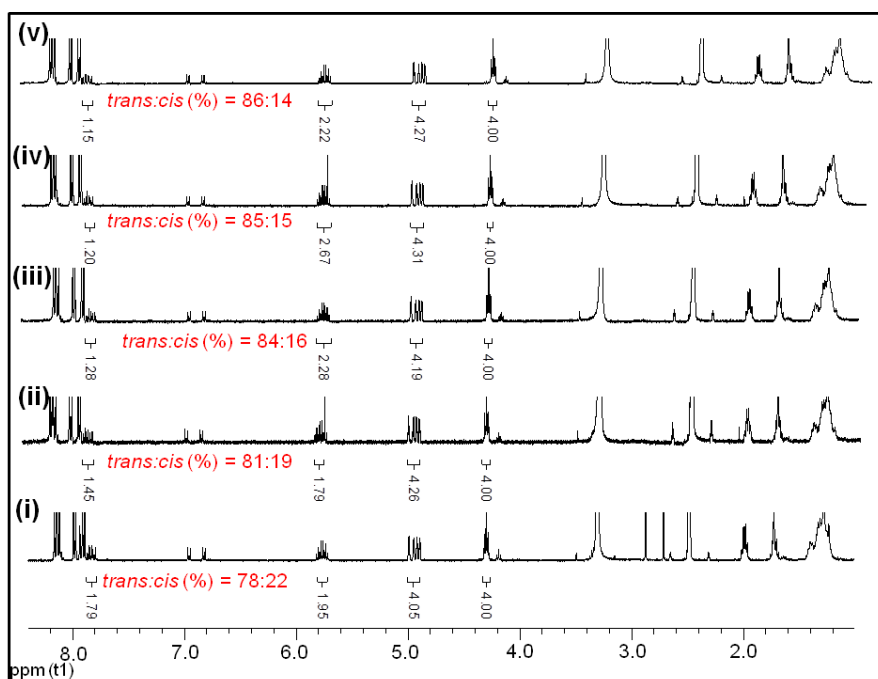


Figure S4. ¹H-NMR investigations on the temperature dependent kinetics measurements of the non-fluorinated azo-monomer before irradiation (i-v) showing the trans : cis ratio of the monomers after thermally annealing the samples in DSC at different temperatures for 1h (rate of heating is 10 K/min, trans : cis ratio before start of experiment is ~78:22 respectively). Experiment (i) was conducted at 50 °C, (ii) was conducted at 75 °C, (iii) was conducted at 100 °C, (iv) was conducted at 125 °C and (v) was conducted at 150 °C.

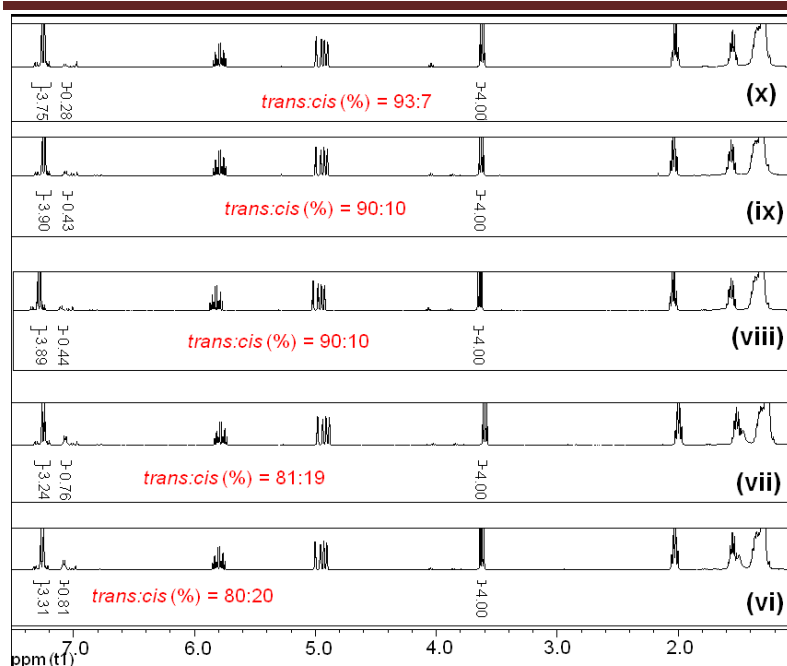


Figure S5. $^1\text{H-NMR}$ investigations on the temperature dependent kinetics measurements of the fluorinated azo-monomer before irradiation (vi-x), showing the trans : cis ratio of the monomers after thermally annealing the samples in DSC at different temperatures for 1h (rate of heating is 10 K/min, trans : cis ratio before start of experiment is $\sim 80:20$ respectively). Experiment (vi) was conducted at 50 $^\circ\text{C}$, (vii) was conducted at 75 $^\circ\text{C}$, (viii) was conducted at 100 $^\circ\text{C}$, (ix) was conducted at 125 $^\circ\text{C}$ and (x) was conducted at 150 $^\circ\text{C}$.

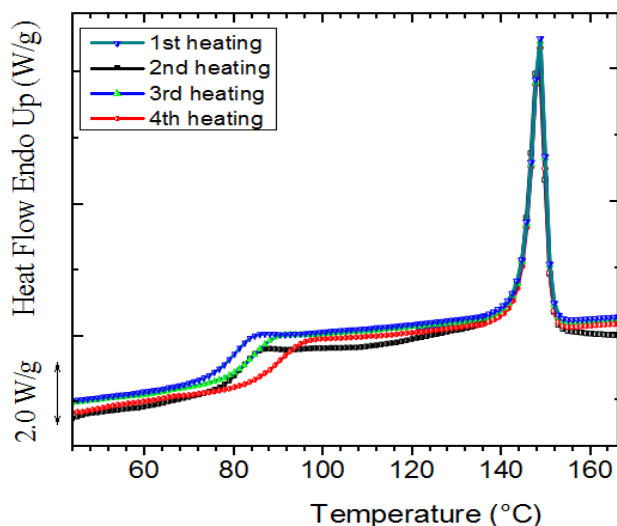


Figure S6. Four cycle DSC heating scans of the H-azo polymer showing apparently no change in the melting enthalpy. The glass transition ($T_g = 84$ $^\circ\text{C}$) on the other hand remains constant until the 4th heating scan, where a slight shift to higher temperature results ($T_g = 91$ $^\circ\text{C}$).

6.4 Crystallization in Segregated Supramolecular Pseudoblock Copolymers

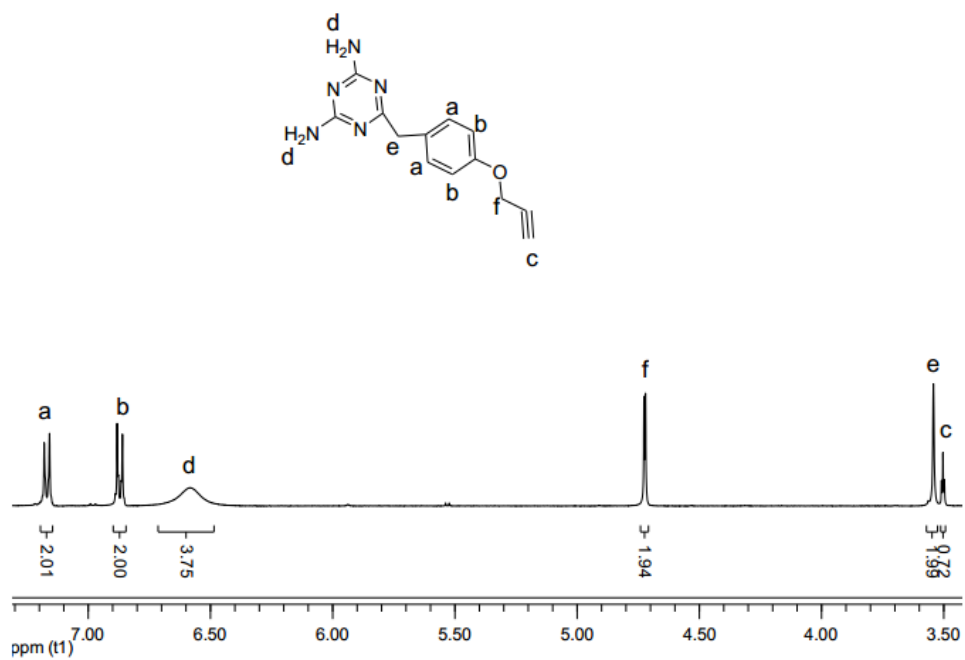


Figure S1: ¹H-NMR spectrum of 6-(4-(prop-2-yn-1-yloxy)benzyl)-1,3,5-triazine-2,4-diamine (Tr).

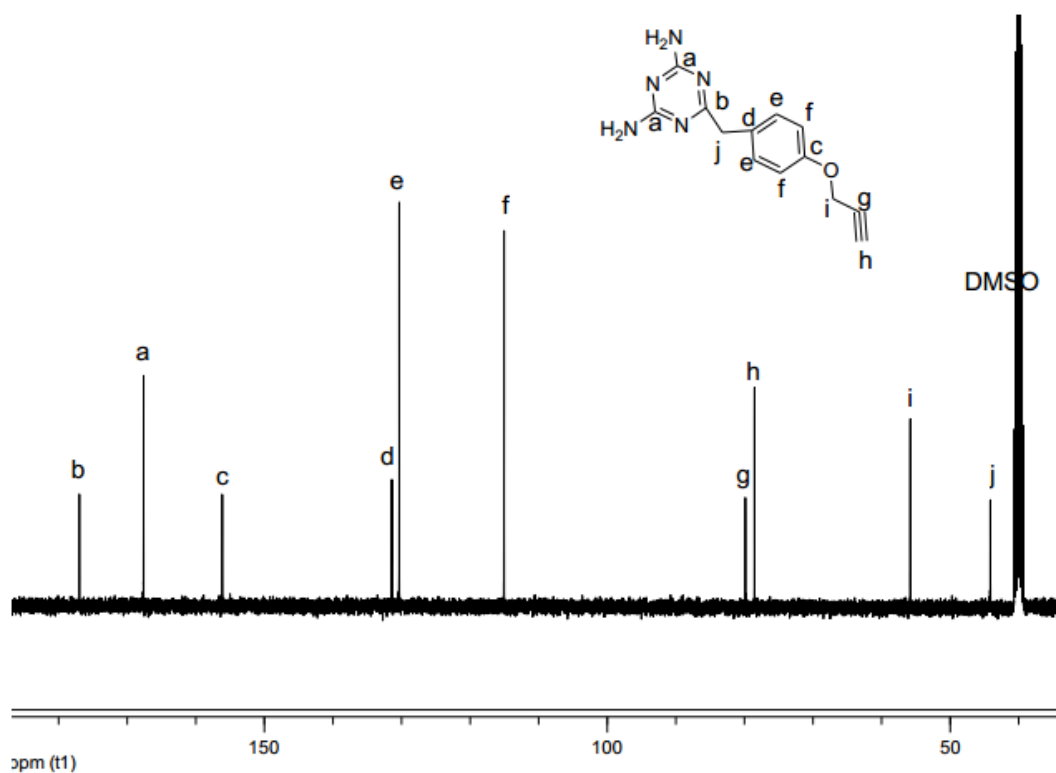


Figure S2: ¹³C-NMR spectrum of 6-(4-(prop-2-yn-1-yloxy)benzyl)-1,3,5-triazine-2,4-diamine (Tr).

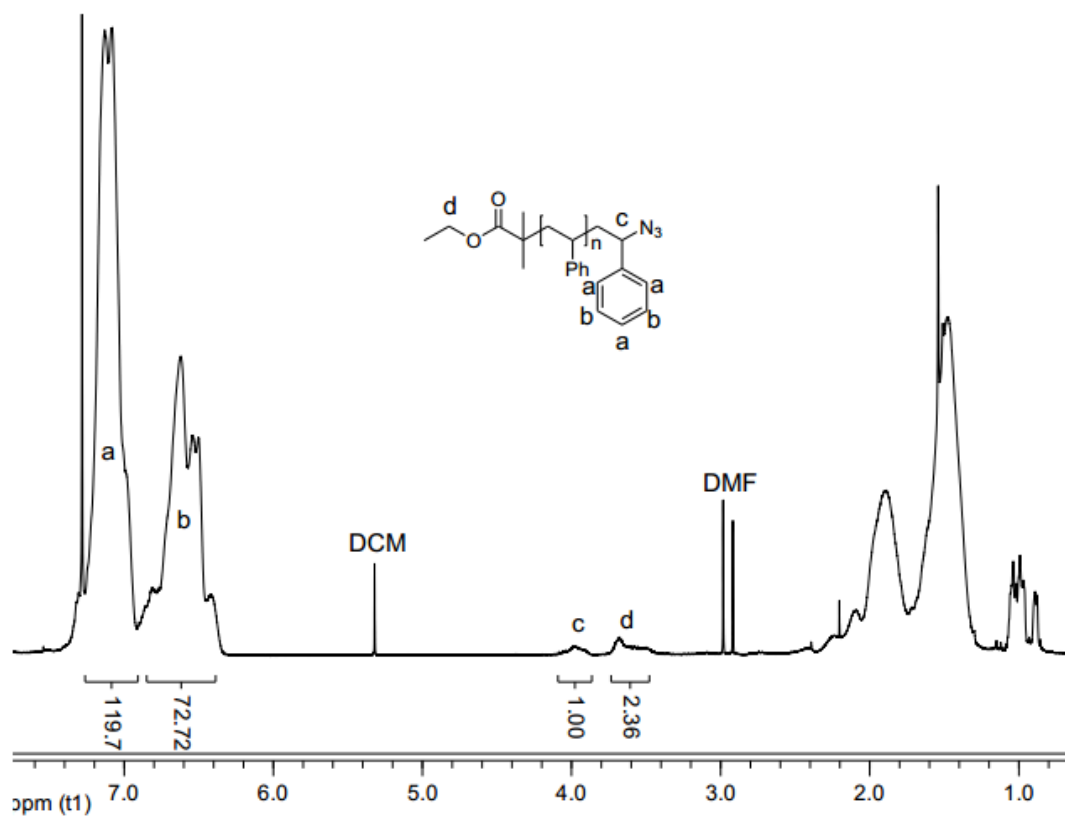


Figure S3: ^1H -NMR spectrum of azido functionalized poly(styrene) (**PS3-N₃**).

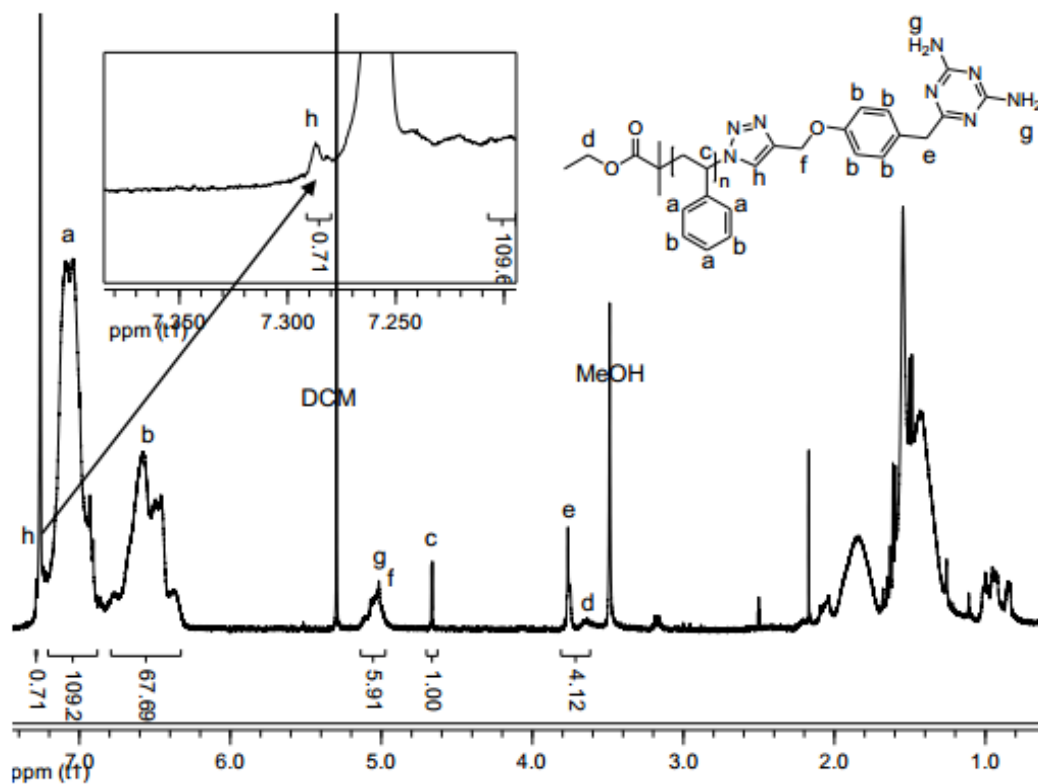


Figure S4: ^1H -NMR spectrum of 2,4-diaminotriazine-telechelic poly(styrene) (**PS3-Tr**).

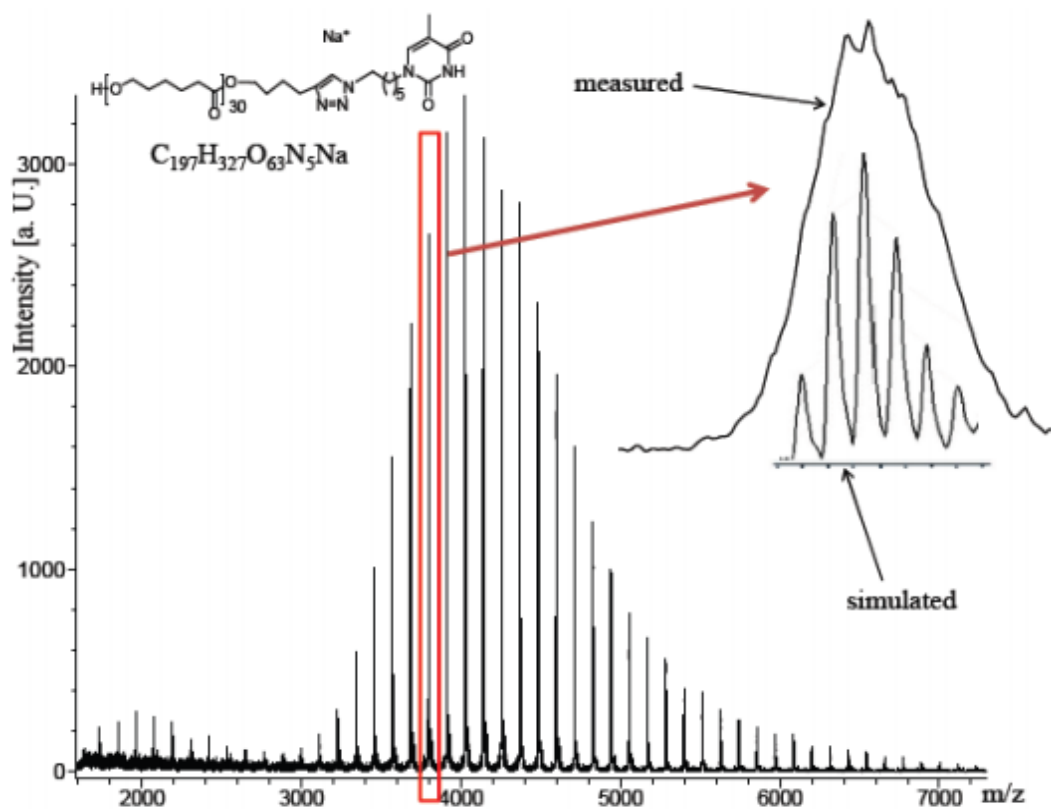


Figure S5: MALDI-TOF-MS spectrum of thymine functionalized PCL (PCL3-Thy).

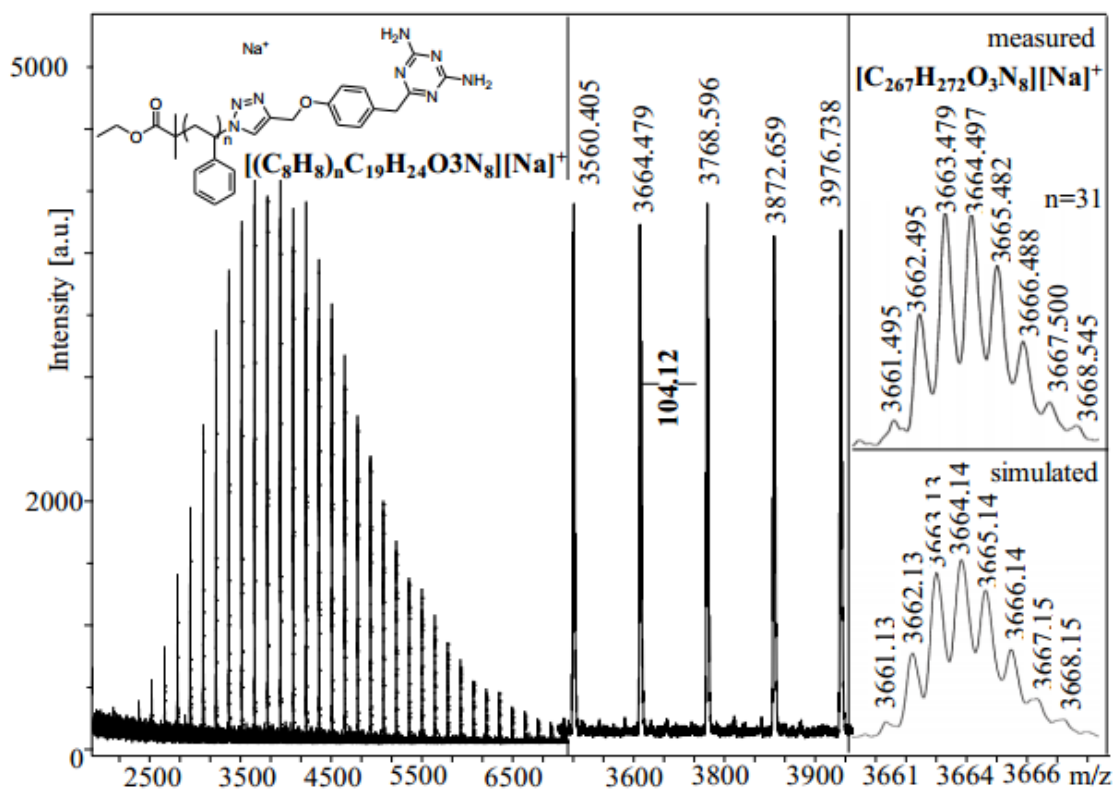


Figure S6: MALDI-TOF-MS spectrum of the 2,4-diaminotriazine-telechelic poly(styrene) (PS3-Tr)

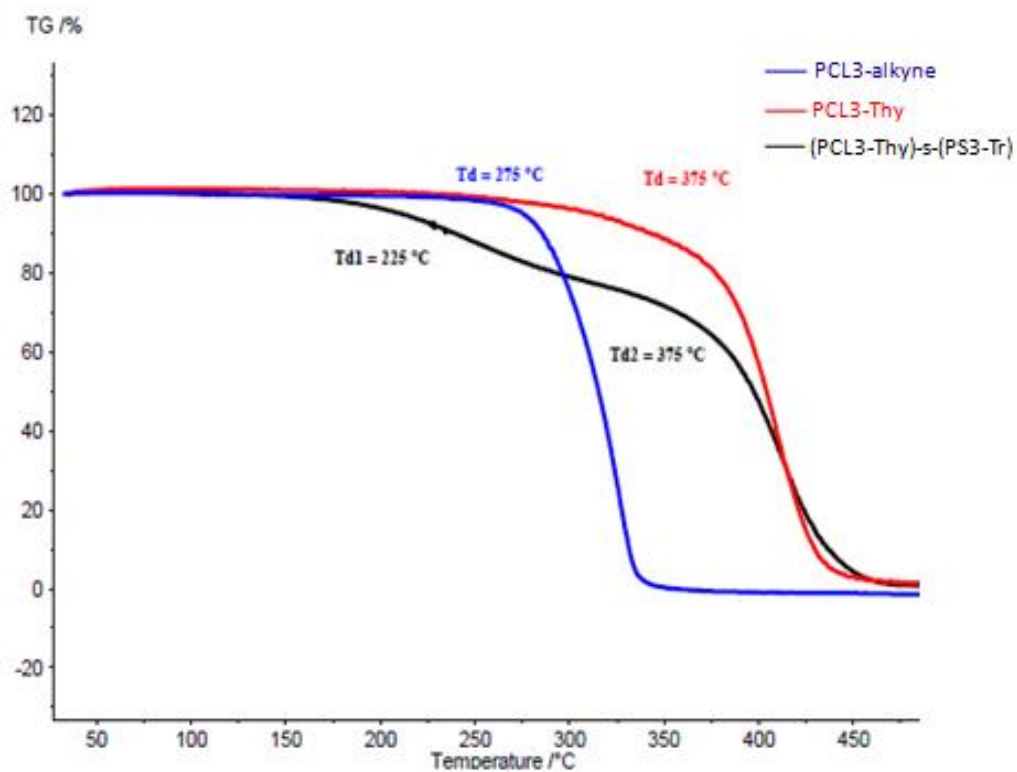


Figure S7: TGA curves for **(PCL3-Thy)-s-(PS3-Tr)** pseudoblock copolymer, **PCL3-Thy** and **PCL3-alkyne**, showing the thermal decomposition temperatures.

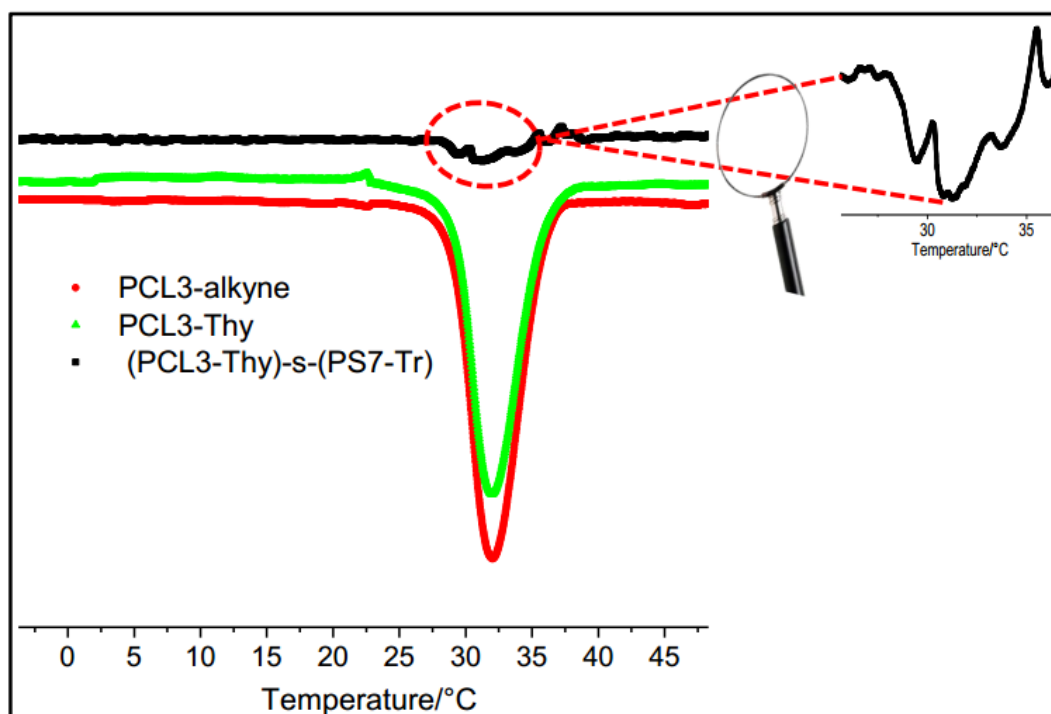


Figure S8: Cooling DSC thermograms (10 K/min) for **PCL3-alkyne**, **PCL3-Thy** and **(PCL3-Thy)-s-(PS7-Tr)**.

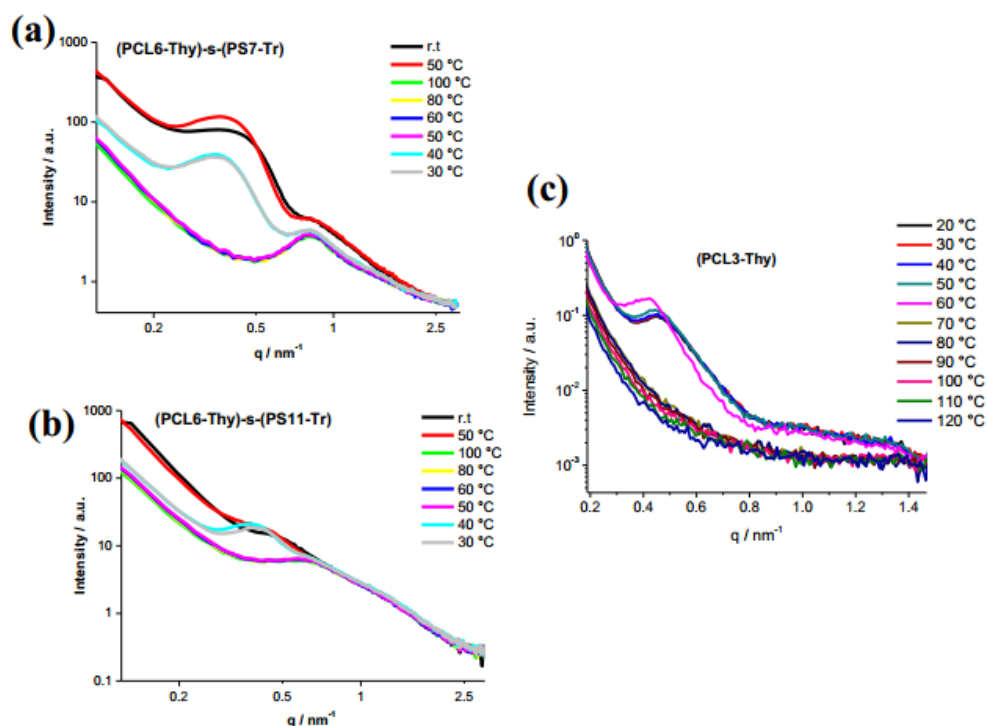


Figure S9: In-situ temperature dependent SAXS measurements for (a) **(PCL6-Thy)-s-(PS7-Tr)** (b) **(PCL6-Thy)-s-(PS11-Tr)** pseudoblock copolymers and (c) **PCL3-Thy** homopolymers.

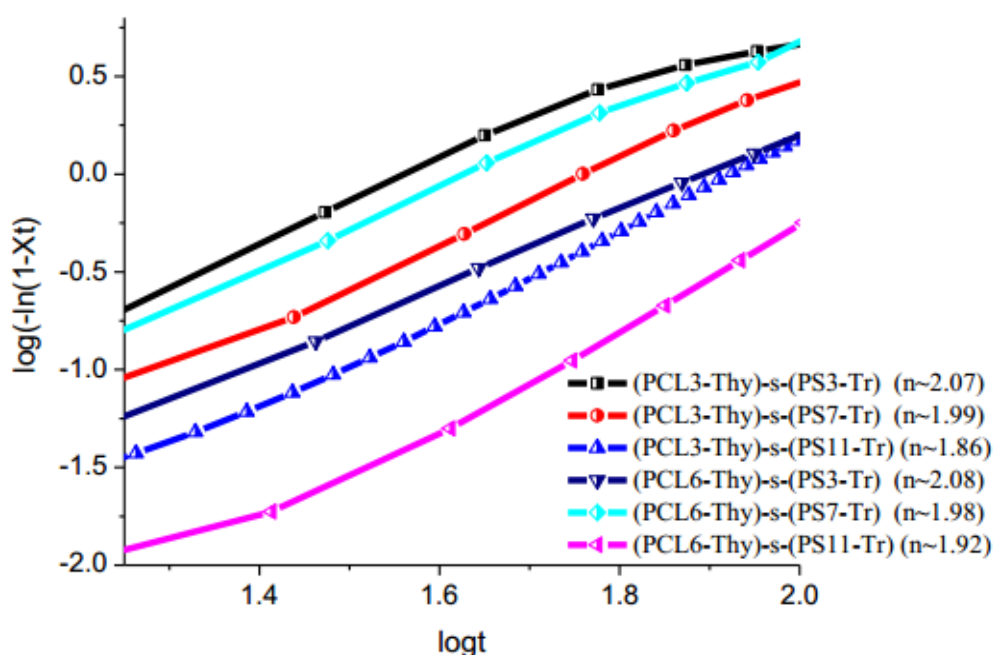


Figure S10. Avrami plots for the supramolecular pseudoblock copolymers, consisting of **PCL-Thy** and **PS-Tr** with different molecular weights. The values in parenthesis are the Avrami indexes obtained from the slope, upon linear fitting of the graphs.

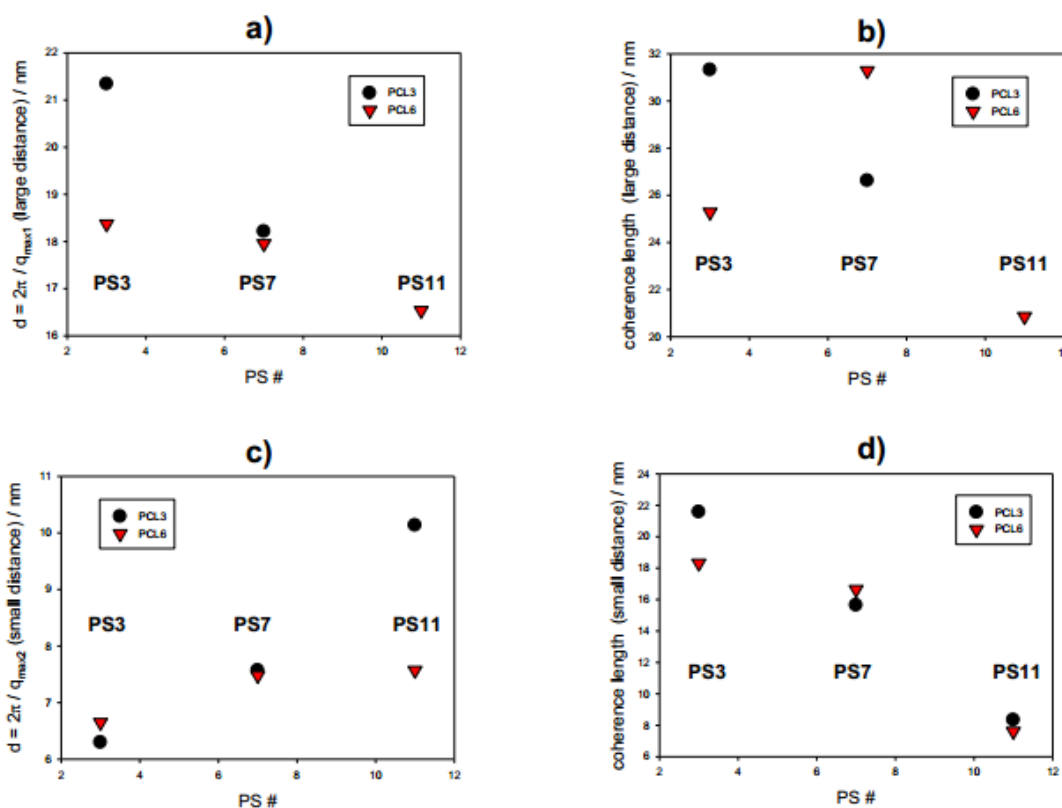


Figure S11: Distance of units: large distance from peak maximum $q_{\max1}$ at small q -values (a) and small distance from peak maximum $q_{\max2}$ at high q -values (c). Coherence length evaluated from Scherrer formula ($L=K 2\pi/\Delta q$) with Δq the full-width at half-maximum and $K=0.94$ the shape factor: Large distance peak (c), small distance peak (d).

The higher the molecular weight of the component **PS**, the larger the distance (Fig. S11c) and the lower the degree of order (lower coherence length, Fig. S11d) of the temperature-independent peak at high q -values (small distance peak). Differently, the temperature dependent crystallization peak (large distance peak) decreases in size with increasing molecular weight of **PS** (no crystallization was observed for the **(PCL6-Thy)-s-(PS11-Tr)** pseudoblock copolymer).

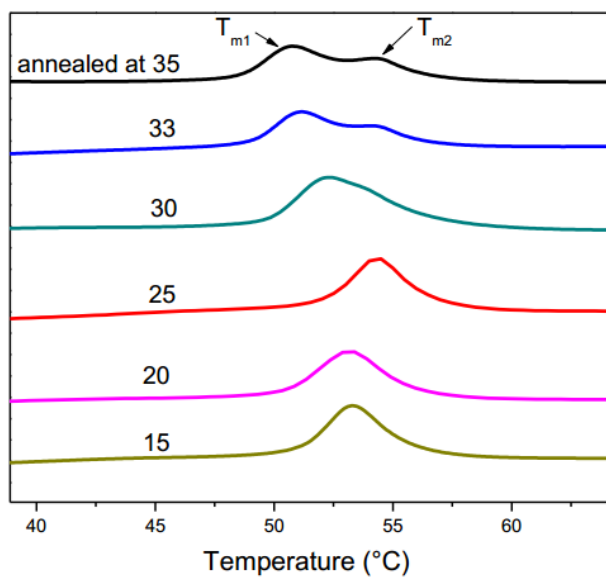


Figure S12: Annealing temperature effect on the melting behavior of **(PCL3-Thy)-s-(PS7-Tr)**. The two clearly observable endotherms (T_{m1} and T_{m2}) at 33 °C and 35 °C gets closer to each at 30 °C annealing temperature, making it difficult to clearly resolve them separately. Further decrease from 25 °C to 15 °C results in a total disappearance of the T_{m1} peak, and a shift of the T_{m2} peak towards lower temperatures.

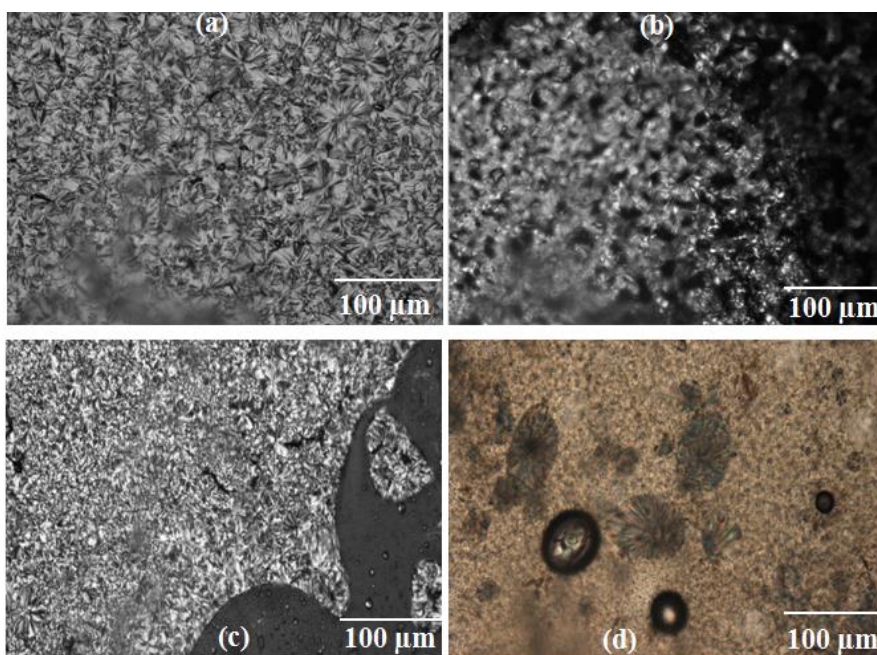


Figure S13: POM images of (a) **(PCL3-alkyne)** (b) **(PCL3-Thy)** (c) **(PCL3-Thy)/PS3-N₃** blend and (d) **(PCL3-Thy)-s-(PS3-Tr)** in the crystalline state at 30 °C

Thermal Analysis Techniques

Differential scanning calorimetry (DSC), Isothermal titration calorimetry (ITC), TGA

Spectroscopic Techniques

NMR, FTIR, UV-vis, MALDI-TOF MS, ESI-TOF MS, SAXS, HPLC-coupled-to-ESITOF/MALDI_TOF MS, WAXD, DMA, Rheology, GPC, Dynamic light scattering (DLS), Atomic force microscopy (AFM), Scanning Electron Microscopy (SEM), Surface tension & adsorption kinetics of polymers at air/water interface (Langmuir films)

ADDITIONAL INFORMATION

Interests:	Football playing - Played 3 years as midfielder in the university football team. Member of PhD student's social club and SFB research group
Languages:	English, Akan Twi, German, French
Driving licence	Driving licence class "B"
Professional Memberships:	Member of the American Chemical Society (ACS) Member of the European Chemical Society Member of the Royal Society of Chemistry (RSC)
Honours and Awards:	Best International Student (2011/2012) Martin Luther University, Halle-Wittenberg Germany
Presentation & Publications:	See https://www.linkedin.com/in/clement-appiah-81597044 for full list of publications and notable presenting/conference experience

PUBLICATION LIST

- Stojanovic, A.; Appiah, C.; Dohler, D.; Akbarzadeh, J.; Zare, P.; Peterlik, H.; Binder, W. H., Designing melt flow of poly(isobutylene)-based ionic liquids. *Journal of Materials Chemistry A* 2013, 1 (39), 12159-12169.
- Appiah, C.; Akbarzadeh, J.; Peterlik, H.; Binder, W. H., Crystallization in segregated supramolecular pseudoblock copolymers. *European Polymer Journal* 2015, 64 (0), 138-146.
- Chen, S.; Schulz, M.; Lechner, B.-D.; Appiah, C.; Binder, W. H., One-pot synthesis and self-assembly of supramolecular dendritic polymers. *Polymer Chemistry* 2015, 6 (46), 7988-7994.
- Appiah, C.; Akbarzadeh, J.; Stojanovic-Marinow, A.; Peterlik, H.; Binder, W. H., Hierarchically Mesostructured Polyisobutylene-Based Ionic Liquids. *Macromolecular Rapid Communications* 2016, 37 (14), 1175-1180.
- Appiah, C.; Siefermann, K. R.; Jorewitz, M.; Barqawi, H.; Binder, W. H., Synthesis and characterization of new photoswitchable azobenzene-containing poly(ϵ -caprolactones). *RSC Advances* 2016, 6 (8), 6358-6367.
- Appiah, C.; Woltersdorf, G.; Binder, W. H., Synthesis of photoresponsive main-chain oligomers with azobenzene moieties via ADMET oligomerization and their micellization properties. *Polymer Chemistry* 2017, 8, 2752-2763.
- Appiah, C.; Woltersdorf, G.; Pérez-Camargo R. A.; Müller A. J.; Binder, W. H., Crystallization behavior of ADMET Polyethylene Containing Azobenzene Defects. *European Polymer Journal* 2017, *accepted*.

EIGENSTÄNDIGKEITSERKLÄRUNG

Ich erkläre an Eides statt, dass ich die vorliegende Dissertation mit dem Titel "Synthesis and Crystallization Studies of Azobenzene Defect polymers and Supramolecular Block Copolymers" selbstständig und ohne fremde Hilfe verfasst, keine anderen als die von mir angegebenen Quellen und Hilfsmittel benutzt und die den zitierten Werken wörtlich oder inhaltlich entnommenen Stellen als solche kenntlich gemacht habe.

Außerdem erkläre ich, dass ich die vorliegende Dissertation an keiner anderen wissenschaftlichen Einrichtung zur Erlangung eines akademischen Grades eingereicht zu haben.

Halle (Saale), den 07.11.2017

Appiah Clement